CONF

MSNW

CONF-821124--

DE85 000450

Proceedings of the Fifth Symposium on the Physics and Technology of Compact Toroids

MATHEMATICAL SCIENCES NORTHWEST, INC.

November 16–18, 1982

MASTER

A.L. Hoffman
R.D. Milroy

January 1983

CONTENTS

SPHEROMAK EQUILIBRIUM, STABILITY AND LIFETIME

PARTICLE RINGS"

Fifth Symposium on
Physics and Technology of Compact Toroids in the
Magnetic Fusion Energy Program
November 16-18, 1982

Hosted by MSNW, Bellevue, Washington

Agenda

Tuesday, November 16, CT Formation and Heating
(Marymoor Room)

Morning Session: Co-chairmen: R. Milroy and G. Goldenbaum

Introduction - W. Dove, A. Hoffman	9:00-9:30 am
FRC Formation - T. Armstrong	9:30-10:15 am
BREAK	10:15-10:30 am
Spheromak Formation - S. Paul	10:30-11:15 am
Relativistic Ring Formation - H. Fleischmann	11:15-11:45 am
LUNCH (cost included in registration) (Bellefield Room)	11:45 am-12:30 pm
Poster Session	12:30-2:30 pm
FRC Formation	
Spheromak Formation	
Particle Rings	
Afternoon Session	
Workshop on FRC Formation: R. Milroy	2:30-3:45 pm
Workshop on Spheromak Formation: G. Goldenbaum	3:45-5:00 pm
Reception at MSNW	5:30

Wednesday, November 17, CT Equilibrium, Stability and Transport
(Marymoor Room)

Morning Session: Co-chairmen: R. Siemon and M. Yamada

Introduction - Comparison of Approaches G. Vlases	9:00-9:30 am
FRC Equilibrium Stability and Lifetime L. Steinhauer	9:30-10:15 am
BREAK	10:15-10:30 am

Spheromak Equilibrium, Stability and Lifetime T. Jarboe	10:30–11:15 am
Stability Enhancement by Relativistic Rings R. Sudan	11:15–11:45 am
LUNCH	11:45 am–12:30 pm
Poster Session FRC Equilibrium, Transport and Stability Spheromak Equilibrium, Transport and Stability	12:30–2:30 pm
Afternoon Session	
Workshop on FRC Equilibrium, Stability and Lifetimes: R. Siemon	2:30–3:45 pm
Workshop on Spheromak Equilibrium, Stability, and Lifetimes: M. Yamada	3:45–5:00 pm
Banquet (cost included in registration) (Factoria Room)	7:00 pm

Thursday, November 18
(Bellefield Room)

Breakfast	8:00 am
Reactor Scenarios for CT's – R. Hagenson	9:00–10:00 am
Summary Panel Session: G. Vlases, R. Milroy G. Goldenbaum, R. Siemon, M. Yamada	10:00 am–12:00 pm

REVIEW OF THE FIFTH SYMPOSIUM ON THE PHYSICS AND TECHNOLOGY OF COMPACT TOROIDS

Alan L. Hoffman and Richard D. Milroy

The Fifth Symposium On The Physics And Technology of Compact Toroids was hosted by Mathematical Sciences Northwest, Inc. in Bellevue, Washington, November 16-18, 1982. The symposium was conducted in a workshop format divided into the two sections of a) formation of field-reversed-configurations (FRC) and spheromaks, and b) equilibrium, lifetime, and stability of FRCs and spheromaks. The Formation Workshop was chaired by Drs. Richard Milroy (FRC) and George Goldenbaum (Spheromak). The Equilibrium, Lifetime, and Stability Workshop was chaired by Drs. Richard Siemon (FRC) and Masaki Yamada (Spheromak). Review talks on the four subjects were given by Drs. Tom Armstrong, Stephen Paul, Loren Steinhauer, and Tom Jarboe, respectively. Additional review talks on particle ring formation, stability enhancement, FRC/spheromak comparisons, and reactor considerations were given by Drs. Hans Fleishmann, Ravi Sudan, George Vlases, and Randy Hagenson. There were an additional 39 poster papers presented to the 70 registrants.

The formation workshop primarily addressed the questions of slower generation methods and scaling to large sizes. For FRCs, the principal emphasis was on the achievement of gentler density gradients through increasing $x_s = r_s/r_c$ (where r_s is the separatrix radius and r_c is the coil radius). Methods were proposed to increase x_s either by increasing the poloidal flux through better formation methods, or by reducing the external flux through translation into a smaller flux conserver. Present theta pinch generation methods are limited to operating at relatively low bias fluxes due to triggering destructively violent axial implosions if the trapped flux is too high. A strong interest was also expressed in developing slower formation techniques that would allow high poloidal fluxes to be obtained, and that would be compatible with reactor engineering requirements. It has recently been demonstrated on the TRX experiment at MSNW that reversed flux loss rates can occur on a diffusive timescale rather than the shorter radial Alfven time. However, during field reversal, the plasma rests on the wall, is unconfined at the ends, and is thus relatively cold. Although methods were suggested to alleviate these problems and the technique may still be acceptable for reactors, there was still a strong consensus to explore truly equilibrium formation techniques where the plasma can be hotter, the diffusive timescale longer,

and strong axial implosions can be avoided. The coaxial theta pinch was proposed as part of such a formation scheme. Since slow formation schemes may not produce sufficient plasma heating, the need was also expressed to investigate auxiliary heating techniques. The reactor desirability of translation and translation with adiabatic compression was also stressed.

The primary formation issue for spheromaks was the reduction of impurities and the attainment of higher electron temperatures. Slow formation has been demonstrated in the CTX coaxial gun at LANL and in the purely inductive proto S1 devices at PPPL. Spheromaks have also been formed in combination z-θ pinches and conical theta pinches. However, the temperatures have in all cases been limited to under 40 eV. There is a strong indication that the LANL gun produced spheromaks may be beta limited. In order to raise the plasma temperature of beta limited spheromaks, it is necessary to increase the BR product, which means operating at higher currents. This scaling will be tested on the S1 device, and also on the LANL gun if the impurity level can be held down as the current is raised.

The ability to form spheromaks using a wide variety of methods was taken as good evidence for the universality of the principal of relaxation to a nearly force free "Taylor" state. In a manner similar to reverse field pinch (RFP) formation, where helicity is added through the supply of poloidal flux, spheromaks can be formed with primarily toroidal flux addition. This raises the possibility of steady state operation through purely toroidal flux (and helicity) addition using external electrodes. A method was proposed based on the slow formation techniques applied to CTX. However, no detailed calculations were presented on the effects of the electrodes on impurity generation or thermal energy loss.

Some discussion was also held on the formation techniques for energetic particle rings. These rings were thought of mainly as having applications to stabilizing otherwise unstable compact toroids, and a principal formation issue will thus involve the merging of these rings with previously formed CTs. While energetic, field reversing rings have been formed in a number of experiments, no work has been attempted on merging them with compact toroid plasmas.

In the Equilibrium, Stability, and Lifetime Workshop, the large difference between FRC and spheromak physics was apparent. Spheromaks have more physics commonality with RFPs than with FRCs, and FRCs are rather a unique plasma entity whose stability and transport may be

governed by the high beta equilibrium ($\langle\beta\rangle = 1 - x_s^2/2$) imposed by present elongated, low x_s geometries. Common attractive features of the compact toroids are the simply connected geometry, the natural diverter action and, at least for FRCs, the ability to translate the configuration from a generation point to a burner location. Since FRCs will have configuration lifetimes, set by flux loss, which may only exceed the particle lifetime by a factor of several, and they will be difficult to reflux, they were mainly considered for pulsed reactors such as of the moving ring type. The observed inherent stability, high density, and flux conserver geometry make them ideal plasma configurations for such applications. Spheromaks, on the other hand, are lower beta and thus will have configuration lifetimes at least an order of magnitude longer than their plasma energy lifetimes. Because of the Taylor relaxation process, there is also a possibility of refluxing them through the addition of toroidal flux alone. Based on this refluxing posibility, and on perceived difficulties in maintaining stability while translating, spheromaks were thus considered primarily for long burn time or steady state applications.

One of the most significant accomplishments in FRC physics this last year has been the stabilization of the n=2 rotational instability using multipole barrier fields. This has been demonstrated using octopole fields on TRX and quadrupole fields on PIACE at Osaka and preliminarily on FRX-C at LANL. The critical multipole field required for stability is accurately predicted using an MHD analysis, so that this solution should remain effective as the FRC size is scaled up. MHD calculations of the tilt mode have for some time indicated rapidly growing instability. Recent calculations were made for improved equilibria (racetrack like flux surfaces) which better represent experimental plasmas. It was thought that these might exhibit MHD stability in contrast to the earlier calculations. However, the predicted growth rates are even faster for racetrack equilibria. This discrepancy between MHD theory and experimental observations is believed to be due to kinetic effects of large orbit ions. Thus, it is possible that larger, lower average beta plasmas may not have the favorable stability characteristics of present FRCs, and it is desirable to extend the present experimental results to lower beta, larger FRCs.

Another important FRC result is the quadrupling of particle lifetime due to a doubling of plasma radius on the 40-cm diameter FRX-C device. This tends to confirm the expected R^2 scaling predicted by transport calculations based on lower-hybrid-drift (LHD) anomalous resistivity. There was considerable discussion over the exact form of the scaling, the

true anomalous collision mechanism, and the expected behavior at lower beta and larger sizes when the internal plasma becomes more highly magnetized. Transport for present sized FRCs is dominated by the high density gradient near the separatrix, and the average diffusion coefficient is not predicted to decrease as the FRC radius increases, even though the drift velocity for the majority of the plasma inside the separatrix is decreasing. There is some hope that the particle loss rate will more closely approach classical as the device size increases to the point where the diffusion timescale for the inside plasma dominates the endflow rate of the plasma outside the separatrix. Present theory also predicts that the particle loss rate will decrease rapidly if x_s can be increased and the average plasma beta lowered. Both effects will reduce the pressure at the separatrix and tend to make the open field line loss processes less significant.

One other method proposed to lower the density gradients was to alter the equilibrium to make the FRC less prolate. However, this may result in the tilting or shifting instabilities endemic to spheromaks. It was suggested that energetic particle rings might be useful in promoting stability for these less elongated, more fluid like FRCs.

One other potential problem with FRCs is a high electron thermal loss rate. All present experiments produce FRCs with electron temperatures between 75 eV and 175 eV, while the ion temperatures may be several times higher. Although impurities may be a contributing factor, the present electron energy loss rates are on the order of the Bohm rate. The open field line plasma will always be cold since it is in contact with material walls, and the closed field line loss times must exceed Bohm diffusion times by over a factor of 100 for reasonable reactor energy gains to be realized.

It was apparent in the symposium that there is a strong need for more theoretical work, especially work encompassing kinetic ion effects, on the physics of the extremely high beta FRC transport. The analytical modeling using localized LHD transport has been extremely effective in predicting particle loss rates, but cannot explain the measured flux decay rates, which are several times classical, nor the rapid electron thermal loss rates.

The discussion on spheromak equilibrium, lifetime, and stability was focused on stability issues since, in most experiments, the lifetime is governed by impurities and very little information is available on the

relevant transport mechanisms. There is some evidence that the CTX gun produced spheromaks are beta limited, rather than radiation limited, and that this is reflected by a particle pumpout to low, 3×10^{13} cm^{-3} densities. The present spheromak energy loss rates are very high, with significantly lower $n\tau$ products than for smaller sized FRC plasmas. However, one might expect more favorable size and temperature scaling, similar to that seen on RFPs, where the density and temperature scale proportionatly with the total current. In the regime where the beta limit applies, the energy lifetime increases as $T_e^{3/2}$. This is in contrast to the lack of a strong temperature dependence seen on FRCs. Thus, spheromaks might eventually be expected to have lower transport loss rates than FRCs, which would compensate in part for their lower densities. Considerable work remains to be done, however, to even begin to realistically estimate transport losses in the presence of the yet undefined relaxation processes which maintain the near minimum energy configuration.

The most important recent spheromak results relate to stability. The gun produced spheromaks in CTX exhibit MHD stability against all modes for a lifetime (1 msec) which is determined by energy loss rates. However, this is accomplished with a close fitting flux conserver such that the separatrix rests against the metal wall. Rapid plasma terminations have been observed in the similar Osaka CCTX gun produced spheromak when Ti gettering clean up procedures were followed to extend the lifetime. Both the CTX and CTXX flux conservers are oblate but have some geometric differences, so that the exact shape may be important. Great strides have been taken in the PS-2 z-θ pinch spheromak device at the University of Maryland, and in the proto S1 devices to achieve stability of spheromaks without closely fitted walls. The presence of the open field line flux needed for equilibrium makes these spheromaks naturally unstable to tilt modes. Combinations of figure eight coils, saddle coils and, in the case of the Maryland experiment, close fitting conducting walls, are effective in simulating the image currents produced by a close fitting flux conserver. However, at least in the proto S1 devices, these mechanisms only delayed the onset of tilting, but did not prevent it. An internal conductor was found necesary to fully stabilize the tilt mode, which some would say violates the spirit of the compact toroid designation. However, reactor scenarios were presented which encompassed translation along a conducting core to a closely fitting burn chamber. One of the most important unresolved spheromak questions is how close this wall must fit to avoid tilting, and whether this close fit makes reactor applications impractical.

A general feeling of the compact toroid researchers attending this symposium was that the CT program has made great progress in the past year in both experimental results, and in an understanding of the remaining physics questions. The achievement of long lifetime and the demonstration of slow formation techniques for spheromaks, and the attainment of rotational stability and $n\tau$ products several times 10^{11} cm^{-3} sec for FRCs is truely impressive. We look forward in the next year to results from the Princeton S1 device, which should begin operation in the Spring of 1983, and to continued progress in all present compact toroid experiments.

FRC Formation

NUMERICAL MODELING OF FRC TRANSLATION ON FRX-C

W. T. Armstrong, Los Alamos National Laboratory
R. D. Milroy, Mathematical Sciences Northwest

INTRODUCTION

Translation of Field-Reversed Configurations (FRCs) is important as a technique for increasing x_s, the ratio of the separatrix radius r_s to conducting wall radius r_w, and thereby improving FRC confinement.[1] By axially translating the FRC from the formation region into a co-linear region where r_w and the open flux are properly decreased, an increase in x_s from the present value on FRX-C of ~ 0.4 to $\geq$ 0.8 should be possible. The associated change in the volume-averaged beta $\langle\beta\rangle$ would be from ~ 0.9 to $\leq$ 0.7 with a commensurate decrease in the density and particle transport at the plasma separatrix boundary.[2,3] Increasing x_s through translation allows maintaining r_s, n, T and R/ρ_{io} approximately constant, in contrast to in-situ techniques for increasing x_s (where n is the density, T is the total temperature and R/ρ_{io} is the ratio of the major radius to ion gyro-radius indexed to the external field). We numerically model FRC formation and translation initiation on FRX-C with a 2-D MHD code which utilizes a continuously-rezoned Lagrangian mesh.[4] Simulation results are presented which indicate adverse effects of DC translation fields on translation initiation. Successful FRC translation appears possible with these effects present. Translation enhancement is examined through "passive" techniques which require no additional powered coils. In particular, simulation results for the inclusion of a high permeability field "divertor" to overcome the DC field effects are also presented.

SIMULATION OF TRANSLATION WITHOUT PASSIVE AIDS

Translation initiation is possible either through axially-asymmetric internal fields (due to asymmetric reconnection during FRC formation) or by imposing an axially-asymmetric external field (vacuum mirror field). Asymmetric reconnection may be achieved by internal asymmetries in the plasma parameters or through controlled external field switching.[5,6] In the present FRX-C design geometry, indicated in the first frame of Fig. 1, a DC translation field opposes the reverse bias field in a transition region beween the FRC formation and translation regions. As a result of this field configuration during FRC formation, early reconnection occurs at this end of the FRC (left end) which gives an axial force on the FRC away from the translation region. Furthermore, penetration of the DC translation field into the theta-pinch formation coil results in an extraneous mirror field between the formation and translation regions, further inhibiting translation. The simulation presented in Fig. 1 incorporates an initial axial density profile which approximately symmetrizes reconnection, and a strong passive mirror at the FRCs right end to overcome the extraneous DC field mirror and initiate translation into the DC field region.

The assumed density profile has a uniform level (equivalent to a 20 mtorr D_2 fill pressure) in the center region of the theta-pinch formation coil which decreases linearly to 10 % of this value over the last 20 cm of the coils right end. This profile represents an approximation to density distributions achievable with rapid gas-puff filling in the experiment. A conducting plate is modeled between the DC coils and theta-pinch coil which would prevent inductive coupling of the high-voltage theta-pinch coil and low-voltage DC coils. The theta-pinch coil geometry consists of a 25 cm

radius over the left 100 cm and a 21.5 cm radius over the right 100 cm. The resulting 1.35 vacuum mirror ratio at the coils right end results in an acceleration of the FRC to the left, past the extraneous mirror due to the DC fields. The translation velocity achieved in the simulation is $\geq$ 6 cm/μs. This velocity is adequate for successful translation of the FRC into the smaller wall radius in the translation region during the initial FRC stable period of ~ 80 μs.[1] Simulations of the FRC passing through the transition region are in progress.

SIMULATION OF TRANSLATION WITH PASSIVE AIDS

A divertor plate (simulating a soft-iron ferromagnetic plate) replaces the conducting plate between the DC coils and theta-pinch coil incorporated in the simulation of Fig. 1. This divertor plate serves to further isolate the DC and pulsed field regions from each other. In isolating the DC and pulsed field regions, the extraneous mirror field resulting from DC field penetration into the theta-pinch coil is eliminated and an overall field geometry more conducive to FRC translation is obtained. The resulting FRC formation displayed in Fig. 2 shows immediate FRC acceleration to the left, in contrast to Fig. 1. This acceleration is due to the weak field region under the divertor plate preventing the initial inward contraction of the FRCs left end. However, the maximum velocity achieved is dominated by the energy gain of the FRC exiting the right end mirror.[7] Hence, even though the FRC accelerates earlier, the maximum velocity is still ~ 6 cm/μs. In addition, a passive conducting ring outside the coils right end is employed to insure approximately symmetric reconnection, independent of the initial axial density profile.

DISCUSSION

These simulations indicate that the required drift velocity for successful FRC translation may be achieved within the constraints of existing FRX-C hardware. Though troublesome, the penetration of the DC fields into the theta-pinch coil does not appear to prohibit successful FRC translation. Simple passive techniques are available for enhancing FRC formation and translation initiation, as indicated in the simulation of Fig. 2. Additional techniques to be simulated in the future include a larger radius coil region on the left end of the theta-pinch coil to compensate the DC field extraneous mirror. Alternatively, an additional active coil may replace the divertor plate in isolating the DC and theta-pinch fields and improving the field geometry for FRC translation. This coil could be driven early in time so as to form a cusp field and provide slow reconnection on the FRC left end. The coils field could then be reversed and adjusted to provide a more uniform external field during FRC transit.

Near term simulations will address the FRC passage through the decreasing wall radius transition region. The change in wall radius and open flux along the axis has been designed to allow a linear change in x_s while maintaining a constant plasma pressure (where a high-flux sharp boundary profile, a long transition region, and constant closed-flux is assumed).[1] The simulations will be used to develop more realistic criteria for obtaining a final wall/flux design that minimizes plasma distortions and changes in plasma pressure.

REFERENCES

1. K. F. McKenna, et. al., FRC Confinement Studies in FRX-C, these proceedings.
2. D. C. Barnes and C. E. Seyler, Proceedings of the US-Japan Joint Symposium on Compact Toruses and Energetic Particle Injection (Dec. 1979, Princeton, N.J.) P. 110.
3. M. Tuszewski and R. K. Linford, Phys. Fl. 25, 765 (1982).
4. R. D. Milroy and J. U. Brackbill, Phys. Fl. 25, 775 (1982).
5. P. Greve, et. al., Phys. Fl. 25, 452 (1982).
6. S. G. Alikhanov, et. al., Proceedings of the Ninth Int. Conf. on Contr. Nuc. Fus. Res. (Sept. 1982, Baltimore, Md.), IAEA-CN-41/V-3.
7. W. T. Armstrong and R. D. Milroy, Bull. A.P.S. 27, 929 (1982).

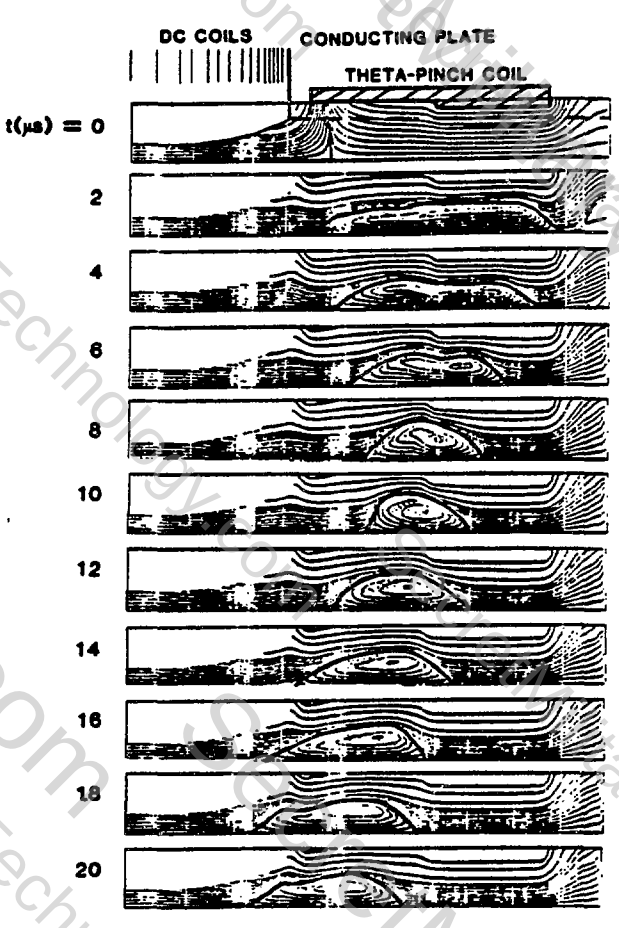

Fig. 1. Simulation of FRC formation and translation initiation with a conducting plate separating the DC coils and theta-pinch coil. Flux contours are shown with the separatrix indicated by a bold line.

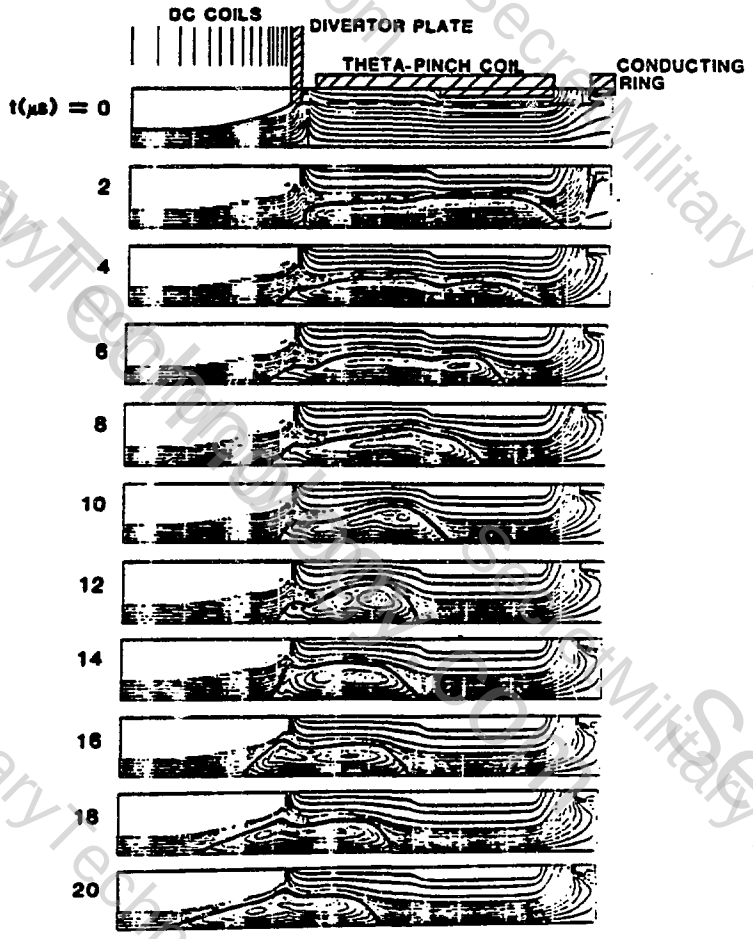

Fig. 2. Simulation of FRC formation and translation initiation with a "divertor" plate separating the DC coils and theta-pinch coil, and a conducting ring outside the right end of the theta-pinch coil.

Laser Heating of Field-Reversed Configurations

R.S. Carson and G.C. Vlases
University of Washington
Seattle, Washington 98195, U.S.A.

I. Introduction and Description

Field-reversed configurations are being formed in a small, high-density, high-field facility to investigate the effects of supplemental laser heating on flux trapping and plasma equilibrium, flux trapping for slow reversal (relative to the inertial loss time), and the scaling of FRC's with $S(=R/\rho_{i0})$ in the range of 20-50 and its effects on transport and stability.

The experimental facility is a 21-cm-long solenoid with a 5.5-cm bore. The 4-cm ID quartz tube is filled with slowly flowing H_2 to 0.5-3.0 torr. Fields up to 6.5 T in 3.7 μsec are produced, with reverse-bias fields up -1.9 T. Preionization is by 40 kA axial discharge 4.5 μsec before field-reversal is begun. The CO_2 laser used produces 300-400 J in 2 μsec, in an annular beam that can be defocused for preheating the outer edges of the plasma, or focused tightly for central-column heating and beam propagation during formation. The focusing system is displayed in Figure 1, and includes a return mirror for multiple passing of the laser energy. Diagnostics include compensated, diamagnetic flux loops, internal field probes, cross-tube and axial interferometers, fast photography, and spectroscopy.

II. Experimental Results

The trapping of reversed flux is measured at the time of field zero-crossing using the diamagnetic flux loops. Between 50% and 100% of the initial bias field can be trapped at this time, with higher trapping for lower p_0. The "Green-Newton limit"[1] is calculated to be 0.8T, but 60% of initial flux can be trapped for B_0 = 1.5T. Virtually all of the initial flux can be trapped when CO_2 laser heating is begun one-half to 1.5 μsec before t_0 (main bank start) and the laser beam is focused ahead of the plasma so that it is expanding when it goes through the plasma. Results are displayed in Figure 2. Using the laser, then, it is possible to start with a smaller bias field and end up with the same reversed flux, while having more net forward field.

Reconnection occurs spontaneously at the ends 1.2-1.5 μsec after t_0 whenever reversed flux is not fully dissipated by this time. From holograms taken at this time, the FRC has $R/a \sim 1.5$-2, and a density depression consistent with trapped flux is clearly visible (Figure 3). There is little radial bouncing, and the plasma moves through successive quasi-radial-equilibrium stages during compression. Peak densities are measured to be $2\text{-}3\cdot10^{17}cm^{-3}$ (from interferometers) and observation of an emission line from CV has indicated $T_e \approx 70$ eV in

some cases, with laser preionization. Also, energy line densities are up to 40 J/cm, which is consistent with an average temperature of 66 eV for a filling pressure of 1.5 torr when B = 3.3T.

Laser heating after reversal (rather than during preionization) extends plasma lifetime by up to 0.5 μsec, causes the plasma to bounce substantially more, and also produces 40 J/cm plasmas. The return mirror allows the beam to traverse the plasma for up to 4 round trips, and results in additional heating.

After reconnection the plasma contracts axially until it reaches an equilibrium length that depends on the amount of trapped flux, plasma pressure, and radial distance to a flux conserving wall (r_w). This has been observed using an axial array of internal probes to note the motion of the separatrix, and also using the array of flux loops to observe decreases in $\Delta\phi$ as the plasma moves past the loop position. There is no observed axial rebound of plasma after contraction, and, in fact, midplane loop signals begin to decay at approximately the time that the plasma shrinks to a length comparable to the tube diameter. From this we have inferred that there is no 2-D equilibrium possible in a simple solenoid, due to a lack of restoring force from increasing B_z when flux is conserved. We have conducted some experiments, however, in which a metal shell with a slot along its length is placed immediately outside the tube and loops. With this in place we have observed reconnected plasmas that have much slower axial contractions.

Several modes of plasma decay are inferred from the diagnostics. For larger values of trapped flux, rapid axial contraction results in a short plasma that tilts, resulting in wall contact and energetic end-loss. Low bias levels result in resistive flux loss that annihilates bias field before or shortly after reconnection occurs, because of low T_e. We have observed the development of fluting instabilities (Figure 3, with n=2) that result in wall contact and rapid loss of reversed flux and energy, even when the slotted metal shell is used to support the axial equilibrium. Rotational n=2 instabilities leading to wall contact have been observed only once, during "second-half-cycle" operation. In all cases, plasma energy is nearly zero by t = 4 μsec.

III. Discussion

Several features of this experiment make it different from other experiments in significant ways, the most obvious being the small size. The ion Larmor radius is between 0.2 mm and 0.4 mm in the external field. The major radius, R, is observed from holograms to be ~1 cm. Therefore, $S = R/\rho_{i0}$ varies from 25-50, putting this experiment in a range similar to FRX-C^2, and also putting it in the MHD limit. The plasma, however, is moderately collisional, with $\omega_{ci}\tau_i \approx 1$-3.

Because of the small plasma radius flux trapping during reversal appears to be limited by the electrical conductivity of the reversal plasma, not the Green-Newton limit (which is ≈0.8 T, the lower limit for flux trapping). In this plasma the bias field acts as a source of energy during reversal. These observations have been verified using a 1-D MHD code, DYNASOR.[3] The code also shows that 10-20 μsec radial lifetimes are possible with sufficient trapped flux and T_e.

The reconnection and contraction phases have been modeled by Richard Milroy of MSNW, using a code developed by Milroy & Brackbill.[4] A comparison of diamagnetic signals in Figure 4 for similar initial conditions shows good agreement until the axial contraction reaches the midplane, then larger code-predicted signals than are observed in the experiment, because the solenoid does not act as a flux conserver. The decay of the code signal is due to axial expansion after the contraction.

The stabilizing effect of the slotted metal shell around the tube observed in some experiments is due to the change in the apparent coil radius, which affects the global equilibrium.[5] It is obviously not as good as having a true flux conserver, since the shell can only conserve flux locally by having currents run axially along the slot. Therefore, deduced changes in r_s from more flux or additional (laser) heating are difficult to relate to x_s, as r_w is ambiguous.

The MHD fluting instabilities observed are consistent with ideal MHD theory and its predictions of instability growth times of $\tau = \sqrt{R\ell/2}/V_A \cong 0.5$ μsec.[6] Because of large S, only dissipative mechanisms appear to be able to damp the growth of these modes. In our parameter regime, the viscosity scales as $T_i^{5/2}$, so modest increases in T_i may result in plasmas more stable to fluting.

IV. Conclusions

We have produced very dense FRC's with large S in a small solenoid. Equilibrium constraints require a flux conserving wall to provide an elongated equilibrium and to stabilize against tilting in a solenoid. Initial flux trapping is much higher than that given by the Green-Newton model, and can be significantly enhanced by CO_2 laser preheating. When equilibrium is achieved MHD instabilities appear to terminate the FRC, and further work may be needed on producing hotter plasmas. If this is successful, it will allow further study of $\langle\beta\rangle$, x_s, and profile steepness of equilibrium FRC's.

Acknowledgments

The authors wish to thank Z.A. Pietrzyk, R.D. Brooks and D.E. Lotz for their contributions to this work. The support of the U.S. Department of Energy, Office of Magnetic Fusion Energy is gratefully acknowledged.

References

1. T.S. Green and A.A. Newton, Phys. Fluids 9, 1386 (1966).
2. R.E. Siemon, Los Alamos National Laboratory, private communication.
3. D.C. Quimby and L.C. Steinhauer, Phys. Fluids 23, 1426 (1980).
4. R.D. Milroy and J.U. Brackbill, Phys. Fluids 25, 775 (1982).
5. W.T. Armstrong, et al., Phys. Fluids 24, 2068 (1981).
6. D.C. Barnes and C.E. Seyler, Los Alamos National Laboratory Report LA-UR-79-13 (1979).

Figure 1.

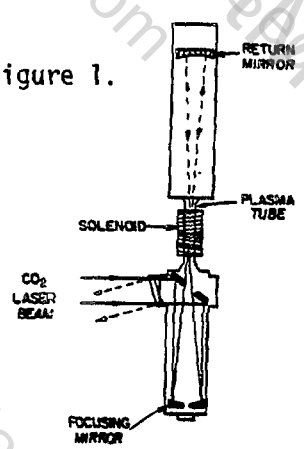

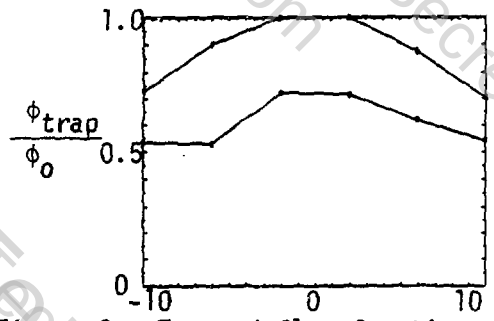

Figure 2. Trapped flux fraction vs. axial position with (top) and without(bottom) laser preheating.

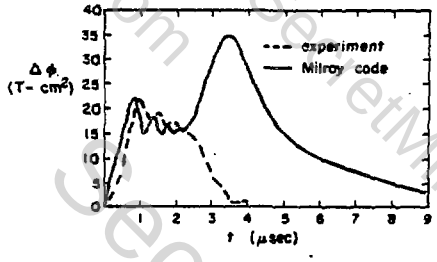

Figure 4. Near-midplane flux loop signals for code and experiment.

Figure 3. Axial hologram and density profiles.

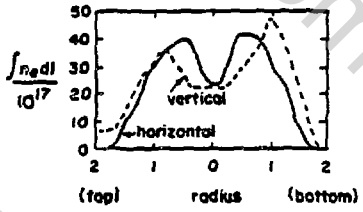

Flux Trapping During Field Reversal in a Field Reversed Theta Pinch

R.D. Milroy, A.L. Hoffman, J.T. Slough, and D.G. Harding

Mathematical Sciences Northwest, Inc.
Bellevue, Washington 98004-1495

I. Introduction

In a reversed field theta-pinch a significant fraction of the initial reverse bias magnetic flux is lost during field reversal. Green and Newton[1] studied this problem with a model where flux convection is tied to the plasma motion, and both particles and flux are assumed to be lost as plasma comes in contact with the wall. This leads to a prediction that very little reverse bias flux can be trapped when the reverse bias field, B_o, exceeds a critical value,

$$B_{GN}(kG) = 2.24\, E_\theta^{1/2}(kV/cm)\, P_o^{1/4}(mTorr).$$

Measurements of flux trapping on the TRX-1 device[2] operated at high bias fields show that much more flux can be trapped than predicted by the model of Green and Newton. Armstrong et al.[2] showed that the experimental results can be explained by postulating the formation of a conducting sheath near the tube wall which hinders the rapid loss of flux. M.I. Kutuzov et al.[3] have analytically studied the flux loss through a sheath using an equilibrium model and assuming a fully ionized plasma. They showed that a conducting sheath, which significantly retards flux loss, should form during field reversal.

In this paper we present new results from both numerical and experimental studies of the formation of the conducting sheath near the tube wall and its effectiveness in trapping bias flux during field reversal.

II. Numerical Model

Sheath formation has been studied numerically with the 1-D (r-t) Lagrangian MHD code DYNASOR[4]. The code assumes quasineutrality, separate electron and ion temperatures, and diffusive transport of heat and magnetic flux. A time dependant ionization package is used to calculate the ionization level of the deuterium gas. Transport coeficients (thermal conductivity and electrical resistivity) which encompass both the low

temperature (low $\omega\tau$) and high temperature collisionless conditions are used. In a partially ionized plasma the transport coeficients are corrected to include collisions with neutrals. Neutrals and ions are assumed to have the same temperature but the neutrals and plasma can flow with different fluid velocities. The velocities equilibriate in time due to ion-neutral collisions and charge exchange. The code is capable of assuming pressure balance (i.e. inertialess ions and neutrals) or calculating the full dynamics of both the neutral fluid and the plasma. In the calculations reported here the calculation is initiallized with a uniform density, N_o, preionization level, S_o, reverse bias field, B_o, and temperature, T_o. The external field is then specified to rise approximately linearly in time from the initial negative bias field B_o. The plasma and neutral fluid velocities are assumed to vanish at the wall and the temperature is held cold (0.1 eV).

III. Experimental Description

The trapping of reverse bias flux during field reversal was studied experimentally on the TRX-1 device. An annular z-pinch preionizer with an axial discharge current of 35 kA was employed. The forward field produced by the main bank can be altered both in magnitude and rise time by varying the number of capacitors connected to the theta-pinch coil. Since the external inductance is increased and the maximum forward field is decreased by reducing the number of capacitors, the time from firing the main bank to the plasma lift-off time, t_L, can be increased from 0.7 μsec to as long as 2.5 μsec. (t_L is defined as the time at which the magnitude of the forward external field is equal to the magnitude of the average internal field; $B_{ext} = -\phi/(\pi R_w^2)$.) This corresponds to varying $t_{1/4}$ from 3 μsec to 10 μsec. The fill pressure can be varied from 30 mTorr to as low as 7 mTorr, however the effectiveness of the preionization discharge at the lowest pressures is uncertain.

Measurement of the external magnetic field, B_{ext}, and the excluded flux, $\Delta\phi$ is sufficient to accurately determine the flux inside the discharge tube wall;

$$\phi_w = B_{ext}\pi R_w^2 - \Delta\phi \quad .$$

Until the external field reverses, the trapped flux and the flux inside the discharge tube wall are identically defined. After this time these two quantities remain approximately the same if there is negligible forward bias flux between the magnetic null and the the discharge tube wall. As will be seen in the next section, numerical simulations suggest that this is true for $t<t_L$.

IV. Results

Calculated profiles of relevant variables for typical conditions (B_o=3.6 kG, n_o=10^{15}cm^{-3}, t_L = 1.4 μsec, and S_o = 0.5) are shown on Figure 1 near the time when the external magnetic field reverses. A high-density, thin, conducting sheath forms near the discharge tube wall. This sheath supports the plasma pressure and limits the rate of magnetic field diffusion. The electrons are strongly joule heated but their temperature is limited by electron-ion equipartition of energy as well as electron thermal conduction to the wall. The ion temperature is limited by strong ion thermal conduction. The magnetic field is seen to rise from a uniform internal value of -2 kG to the external value of 0.5 kG in the thin (0.4 cm) sheath. The time dependence of the experimentally measured flux at the wall, ϕ_w, and the external magnetic field are shown in Figure 2. The numerically calculated values of ϕ_w and trapped flux, ϕ, are superimposed. This figure shows excellent agreement between theory and experiment and supports the interpretation that ϕ_w is a correct measure of trapped flux until lift-off time, t_L. After this time the flux measured at the wall drops rapidly as the forward field pushes inward.

The experimentally measured trapped flux at time t_L is plotted as a function of t_L, for several different initial bias fields in Figure 3. A numerically calculated curve assuming an initial bias field of -3.6 kG is superimposed and shows good agreement with the corresponding experimental curve. This figure shows that good flux trapping can be achieved, even when the forward field rises relatively slowly. Figure 4 shows experimentally measured and numerically calculated values of trapped flux as a function of initial fill pressure. The experimental values are seen to drop off at low fill pressures much more rapidly than predicted numerically. This may be due to the efficiency of the axial discharge preionization dropping as the fill pressure is lowered, or it may be a consequence of high sheath temperatures and unaccounted for impurity generation at low fill pressures.

VI. References

1. T.S. Green and A.A. Newton, Phys. Fluids 9, 1386 (1966)
2. W.T. Armstrong, D.G. Harding, E.A. Crawford, and A.L. Hoffman, "Flux-Trapping During the Formation of Field-Reversed Configurations", Submitted to Phys. Fluids.
3. M.I. Kutuzov, V.N. Semenov, and V.F. Strizhov, Sov. J. Plasma Phys. 7(4), 520 (1981)
4. D.C. Quimby and L.C. Steinhauer, Phys. Fluids 7, 1426 (1980)

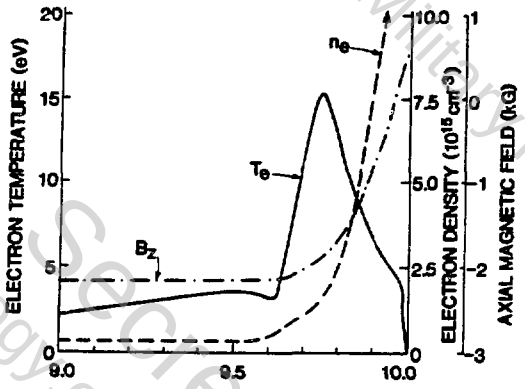

Fig. 1. Calculated wall sheath profiles near the time that the external magnetic field reverses.
B_o = -3.6 kG, p_o = 15 mTorr and t_L = 1.4 μsec.

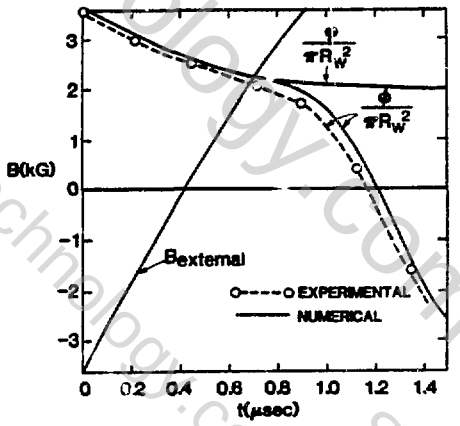

Fig. 2. A comparison of the experimentally measured flux at the discharge tube wall, ϕ_w, with the numerically derived ϕ_w and trapped flux, ϕ.
p_o = 15 mTorr, B_o = -3.6 kG, and t_L = 0.7 μsec.

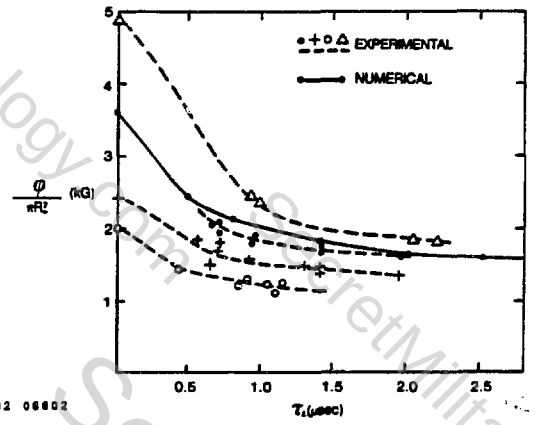

Fig. 3. Dependence of trapped flux at lift-off time on lift-off time, t_L, for several initial bias fields.
p_o = 15 mTorr

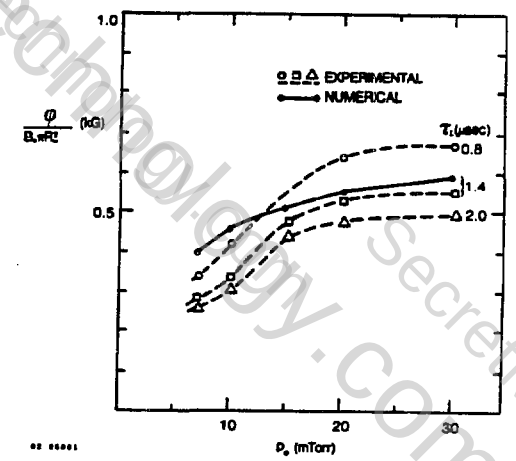

Fig. 4. Dependence of trapped flux at lift-off time on filling pressure for several values of lift-off time.
B_o = -3.6 kG

Driven-Mirror Formation of a Two-Cell Field-Reversed Configuration

E. Sevillano, H. Meuth and F.L. Ribe
Aerospace and Energetics Research Program
University of Washington
Seattle, WA 98195

Introduction

Improved plasma confinement on open field lines in field reversed configurations (FRC's) may prove to be of importance, as suggested by recent experiments[1,2] on the control of the n=2 rotational instability. Multiple mirrors have been suggested[3] as one way to accomplish this improved confinement. To study the formation of multiple-cell FRC's, driven magnetic mirrors have been added to the High Beta Q Machine[4,5] (HBQM) at three axial positions along the theta pinch coil. We report here on measurements of the reconnection process in the region between the cells and also at one end of the coil.

Experiment

The HBQM has been described elsewhere,[4] and only a brief description will be given here. The 2-m-long, 22-cm ID coil is segmented to allow for radio frequency heating experiments (33% void). The magnetic field rises to about 5 kG in 400 nsec and it is passively crowbarred. It decays with an L/R time of about 40 μsec. The preionization is a ringing theta pinch discharge with a frequency of 330 kHz. The initial bias field B_b is -560 G for the experiments reported here. Filling pressures p_o = 4-7 mTorr are used. The magnetic mirrors have a rise time of 1.7 μsec and are crowbarred at peak field. They are triggered so that they peak at the initiation of the main discharge. Their peak field is approximately 900 G, providing a 1.2 mirror ratio.

Diagnostic measurements include both axial (λ = 632.8 nm) and radial (λ = 3.39 μm), He-Ne quadrature interferometers for line integrated density measurements, axial arrays of internal and external magnetic field probes and a one-turn loop around the discharge tube measuring the total flux ϕ. A CAMAC based digital data acquisition system is also available. Ten external probes used in conjunction with the ϕ loop give the excluded flux radius $r_{\Delta\phi}$ as a function of axial position. An axial array of 4 internal field probes are enclosed in a 6 mm OD quartz sheath that is inserted from one end of the coil. The sheath can be rotated to any radial position or moved axially for $z \geq 0$ cm. (z=0 is the center of the coil.) The presence of the internal probes has some effect on the discharges obtained. The measured excluded-flux radii with and without probes are different after about 15 μsec have elapsed. This gives an estimate for the probes "belief time."

The z-component of the magnetic field is measured at 0.5-1.5 cm intervals in the radial direction and 5 cm intervals in the axial direction. The radial profiles at each axial position are fitted with a high order polynomial; the constant flux surfaces (and at the same time magnetic field line contours) are then generated with a contour-plotting routine. Reproducibility between discharges is good (less than 10% difference except near the magnetic axis). A polynomial fit was chosen so that fluctuations between discharges are smoothed out.

Results

Earlier experiments[6] without magnetic mirrors showed that configurations longer than the coil persisted for several microseconds at the higher values of the filling pressure. Magnetic mirrors were added in order to increase the parameter regime at which FRC formation was possible. A filling pressure p_o = 7 mTorr and bias field B_b = -560 G were chosen to compare the reconnection processes with and without driven mirrors. The measured flux contours at selected times during the discharges are shown in Fig. 1 for spontaneous reconnection and Fig. 2 for driven reconnection. The separatrix (ϕ=0 surface) is shown

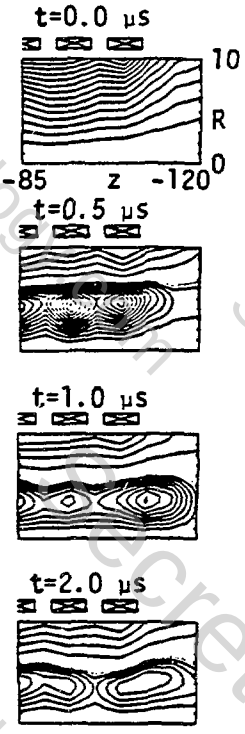

Figure 1. Spontaneous reconnection.

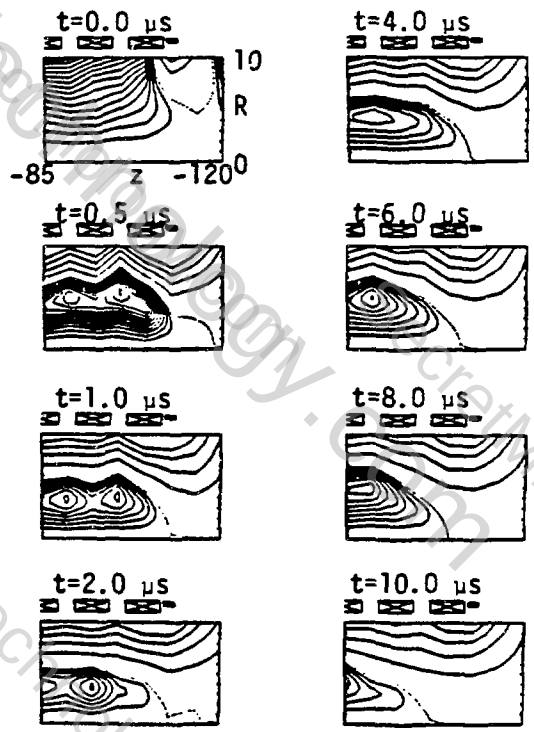

Figure 2. Driven reconnection.

as a dashed line, and the contours are drawn every 10 kG/cm^2 inside the separatrix and for every 60 kG-cm^2 outside. The coil segments are also shown so that their effect on the formation can be seen. Magnetic islands that coalesce in time are observed to form early in the discharge. For the spontaneous reconnection case a section of the plasma is ejected at the ends, the separatrix extends outside the coil for the times shown as indicated by excluded flux measurements. In the driven reconnection case, the separatrix closes on axis inside the coil at t~1 μsec; the configuration formed occupies the whole coil and remains stationary for about 7 μsec. After this time it starts to move axially inward. Measurements of the excluded flux also showed that a large fraction of the coil was occupied by the FRC. Figures 3 and 4 show the reconnection process in the region between cells for two filling pressures, 5 and 7 mTorr. Complete separatrix closure on axis is delayed for the 7 mTorr case for about 12 μsec but occurs faster for the 5 mTorr case. From previous observations for the single-cell case the plasma does not contract axially so that the cells remain connected. When the filling pressure is reduced the length of the plasmoids is also reduced, thus vacating the region between cells and allowing the separatrix to close on axis. Measurements at the University of Maryland[8] similar to ours showed island structures during the implosion phase of a reversed field theta pinch. However, in our

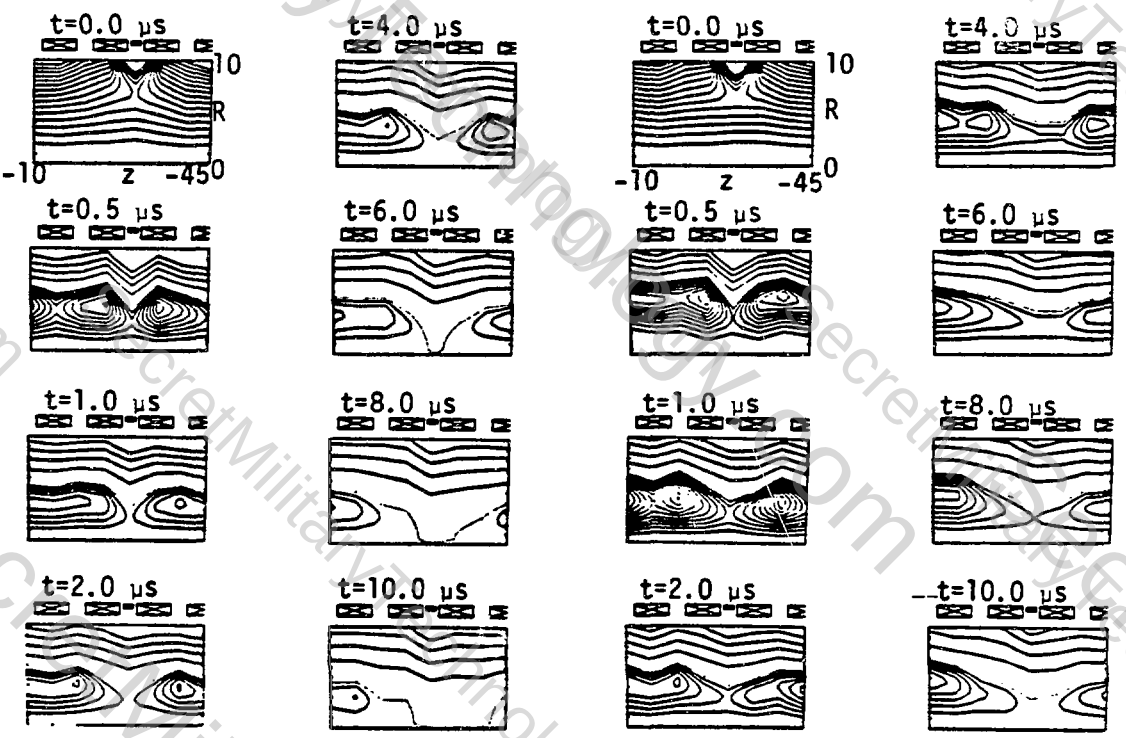

Figure 3. Two-cell formation. Filling pressure 5 mTorr.

Figure 4. Two-cell formation. Filling pressure 7 mTorr.

case there is an additional effect of the slotted coil as can be seen at t = 0.5 μsec. (t=0 is the initiation of the main discharge.)

Conclusions

Measurements of the internal fields in FRC's have been performed to study the reconnection processes near the ends and in the region between cells. Observations of formation and re-coalescence of multiple-magnetic islands may be related to the segmented coil structure. Measurements of $r_{\Delta\phi}$ give FRC lengths in good agreement with those observed with the internal probes. Formation of a double-cell FRC has been accomplished; complete separation into two cells takes about 12 μsec for the case of 7 mTorr but is more rapidly accomplished at 5 mTorr.

The configurations formed are not observed to rotate; they occupy the full length of the coil, and have separatrix-to-coil ratios $x_s \sim 0.64$.

Acknowledgments

We would like to thank G. Harper, E. Hedin and C. Greenfield for help in running the experiments and R. Milroy for providing the contour-plotting routine.

References

1. T. Minato, et al., 9th Int. Conf. on Plasma Physics and Controlled Nuclear Fusion Research (Baltimore, MD, 1982).
2. A.L. Hoffman, private communication.
3. C.E. Seyler, W. Grossmann and L.C. Steinhauer, Comments on Plasma Physics and Controlled Fusion 4, 21 (1978).
4. S.O. Knox, et al., Proc. 3rd IEEE Int. Pulsed Power Conf. (Albuquerque, NM, 1981).
5. S.O. Knox, et al., Phys. Fluids 25, 262 (1982).
6. E. Sevillano, F.L. Ribe and H. Meuth, Proc. 4th Symp. on the Physics and Technology of Compact Toroids (Livermore, CA, 1981).
7. J.H Irby, J.F. Drake and H.R. Griem, Phys. Rev. Lett. 42, 228 (1979).

GENERATION OF FIELD-REVERSED-CONFIGURATIONS WITH HIGH BIAS FLUX USING CONTROLLED RECONNECTION

John T. Slough, Dennis G. Harding, and Alan L. Hoffman
Mathematical Sciences Northwest Inc., Bellevue, Washington

ABSTRACT

The magnitude of poloidal flux and the ultimate size of field-reversed-configurations formed in field-reversed-theta-pinches depends on the amount of initial bias flux which can be trapped. Operation at high bias fluxes results in violent axial contractions and severe flux loss, thus preventing the attainment of high poloidal flux toroids. The use of controlled reconnection techniques permits stable generation at higher bias fluxes, and thus the generation of more energetic field-reversed-configurations.

I. INTRODUCTION

The ultimate poloidal flux of a field-reversed-configuration (FRC) formed in a field-reversed-theta-pinch depends on the amount of reverse bias flux that can be trapped, reconnected with the external flux, and maintained during a strong axial implosion and plasma readjustment to a two-dimensional equilibrium distribution.[1-4] High flux trapping has been demonstrated in the TRX-1 theta pinch, where 50 percent of an initial reverse bias flux of 1200 kG-cm^2 (4 kG in a 20 cm diameter plasma tube) can be trapped in an antiparallel field configuration at the time the plasma is lifted off the tube wall.[5] However, in order to form a stable FRC, reconnection must be delayed until the reverse flux has decayed to a far lower value. Reconnection at high reverse fluxes always results in immediate plasma destruction, most likely due to a tilting instability observed on TRX-1 when the resultant axial contraction was too strong. Theta-pinches with passive end mirrors must be operated at low bias fields to avoid this instability.[6] The TRX-1 theta-pinch, which has independently triggerable active end mirrors, can be operated at far higher bias fields, but reconnection triggering must be delayed. Operation in this high bias field, delayed reconnection mode has been claimed by Kurtmullaev to allow the "neutral" plasma sheath to diffuse and to lead to more stable axial implosions.[1] On TRX-1 we notice that higher x_s values can be obtained in this mode than for equal dimension theta pinches with passive mirrors, such as FRX-B at Los Alamos National Laboratory.[2] A significant portion of the plasma heating also derives from dissipation of the reverse bias flux remaining when the plasma is first removed from the wall, and the delayed reconnection technique can thus lead to higher plasma temperatures.

II. EXPERIMENT DESCRIPTION

A schematic of the TRX-1 theta-pinch is shown on Figure 1. It is similar to the 20-cm diameter BN experiment at the Kurchatov Institute where the controlled reconnection technique was first developed.[1] The main coil is composed of five 20-cm long, 23-cm diameter single turn coils. Individual

collector plate lead inductances add an additional 2 cm to the effective flux conserving diameter. The mirror coils are 7.5-cm long and have the same diameter as the main coils. Quasi-steady coils are located outside the mirror coils in order to produce an initial mirror field which aids in directing the axial preionization discharge. After field reversal, the quasi-steady coil current produces a cusp configuration which delays the reconnection that tends to occur spontaneously before mirror triggering.[7] Octopole barrier fields are used on TRX-1 to improve flux trapping[5] and have also been observed to help delay spontaneous reconnection.

Fig. 1 Schematic of TRX-1 Field-Reversed-Theta-Pinch. Field lines are shown during reverse bias phase just prior to main field initiation.

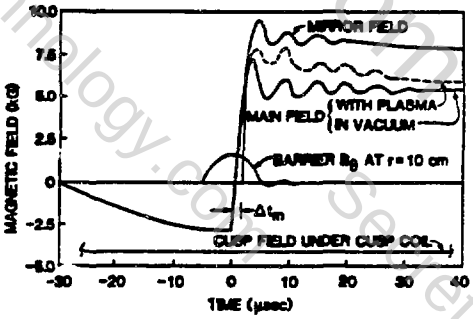

Fig. 2 Typical First Half Cycle Timing Sequence. Axial discharge preionization occurs at -15μsec.

The timing sequence between the various magnetic fields is shown on Figure 2. The delay Δt_m between firing the main coils and the mirror coils has been used to characterize the reconnection process. Generally this delay ranges between 0 and 2 μsec. Negative delays always result in overly violent axial implosions and immediate plasma destruction, and longer delays are sometimes accompanied by internal tearing or assymetrical spontaneous reconnection.

III. FLUX LOSS DURING THE AXIAL IMPLOSION

The complete FRC generation process can be best considered in terms of the inventory of reverse flux. This inventory, along with the external field and centerplane diamagnetism, $\Delta\phi$, time histories are shown schematically on Figure 3. A finite amount of flux (generally about 50 percent) is lost during the flux reversal process[5] as indicated by regions 0 and 1 of the figure. When the plasma is first removed from the tube wall, it is contained in a narrow annulus by an open, antiparallel field configuration. The inserts on Figure 3 indicate the end-on visual appearance and assumed magnetic field profiles at various times. The rate of flux loss decreases once the plasma is removed from the wall, but it is still fairly rapid due to the steep density gradients in the narrow plasma annulus. The delay in mirror initiation determines the amount of flux remaining when reconnection is triggered. Examples of a short, and a longer delay are indicated by the dashed and dotted lines, respectively. The most significant, but incompletely understood, aspect of this reconnection process is a large loss of internal flux occurring during the axial implosion and readjustment from an axially unconfined pressure distribution to a toroidally confined one. The higher the initial flux and the stronger the axial implosion (as indicated by the dynamic overshoot in the diamagnetic signal), the greater the flux loss.

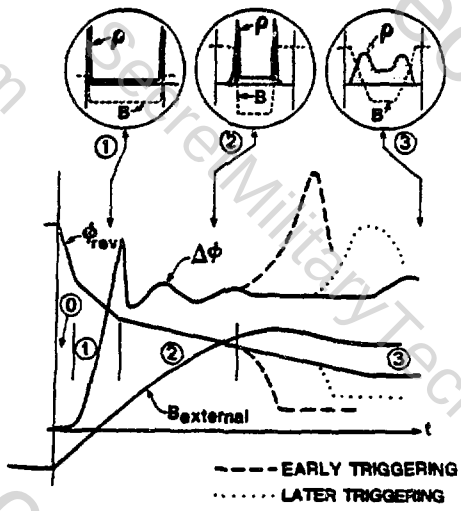

⓪ UNINHIBITED FLUX ESCAPE
① WALL SHEATH LIMITED FLUX DIFFUSION
② SHARP GRADIENT NON RECONNECTED CONFIGURATION
③ EQUILIBRIUM FIELD REVERSED CONFIGURATION

Fig. 3 Schematic of Field Reversed Configuration Formation Process

Examples of this effect can be seen from the experimental plots on Figures 4 and 5 of the midplane diamagnetic signal for gentle and moderately strong axial implosions. Both first half cycle and second half cycle results are shown. The diamagnetic signal before reconnection is indicative of the amount of trapped flux, and the cases on Figure 4 with low diamagnetism before reconnection were run with low initial bias fluxes. Reconnection in these examples could be triggered at $\Delta t_m = 0$ with no dire effects. With higher initial bias fields and greater trapped flux in the antiparallel configuration, reconnection had to be delayed by $\Delta t_m \approx 1.5$ μsec in order to produce the results shown on Figure 4. When the initial bias field was even higher or reconnection was triggered earlier ($\Delta t_m = 0.5$ μsec), the results were as shown on Figure 5. The diamagnetic signal after reconnection was lower than that measured prior to reconnection, indicating a substantial flux loss since axial compression should increase the midplane diamagnetism. This flux loss is not predicted by the magnetohydrodynamic modeling and must be due to unstable three-dimensional behavior. Even though the diamagnetic signals measured on Figure 5 during the peak of the axial implosion do not represent excluded flux radii $r_{\Delta\phi} = (\Delta\phi/\pi B_z)^{1/2}$ (separatrix radius $r_s \approx r_{\Delta\phi}$) contacting the tube walls, a bright flash of light is seen at that

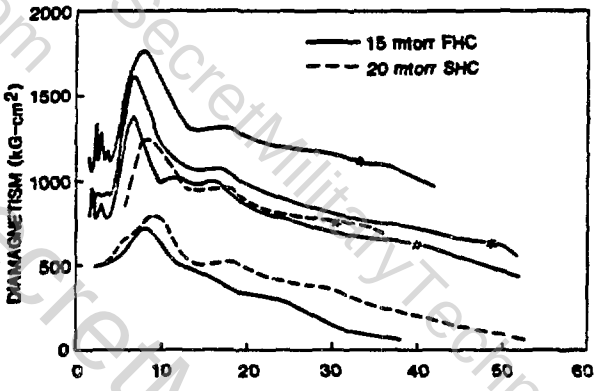

Fig. 4 Midplane Diamagnetic Loop Measurements for Gentle Axial Implosions (asterisk indicates the beginning of a rotational instability).

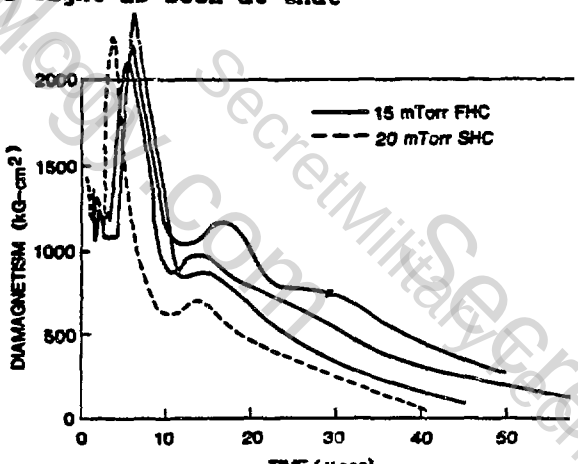

Fig. 5 Midplane Diamagnetic Loop Measurements for Moderately Strong Axial Implosions

time. This may be due to plasma tilting or fluting and, although a FRC is still successfully formed, the eventual diamagnetism decay rate is higher than experienced after gentle axial implosions. For even more violent axial implosions, no FRC was formed. When internal probes were inserted to investigate the cause of the plasma destruction, a distinct tilting instability was seen.

Once an equilibrium configuration is obtained, the poloidal flux can be determined from the two-dimensional equilibrium relationship,[1]

$$\phi_p \approx 0.3\left[r_{\Delta\phi}/r_c\right]\Delta\phi$$

where r_c is the coil radius. The magnetic field during the equilibrium phase of these experiments ranged from 6 to 9 kG, yielding peak poloidal flux values of about 200 kG-cm^2. The largest separatrix radii obtained were 7 cm, corresponding to $x_s = r_s/r_c$ values of 0.6. This is considerably higher than the separatrix radii which could be obtained at lower bias fields with immediate reconnection, or the separatrix radii which were obtained on experiments with passive mirrors.[2]

Since the numerical modeling does not predict the measured reconnection flux loss, it is unclear exactly what role controlled reconnection plays in obtaining larger x_s values. Both plasma diffusion across field lines before reconnection and axial density smoothing due to end loss may be contributing factors. One predictable benefit of controlled reconnection is the additional field energy available for plasma heating after the first plasma removal from the tube walls. Some of this energy is dissipated due to ohmic heating in the sharp density gradient plasma existing before reconnection, and additional energy is added to the plasma by the dynamic axial reconnection process.[3] The measured total plasma temperatures, based on pressure balance and interferometry, are shown on Figure 6 as a function of the final external magnetic field. These temperatures have been

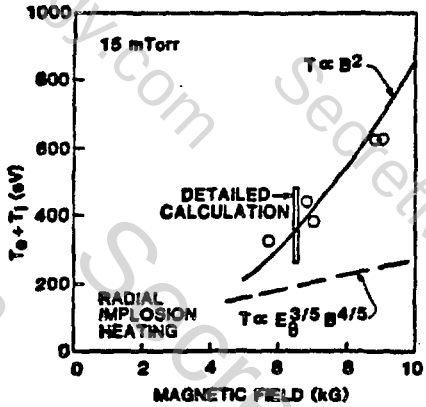

Fig. 6 Comparison of Measured and Calculated Plasma Temperatures.

confirmed by spectroscopic and Doppler broadening measurements. A curve (dashed line) based on radial implosion heating and adiabatic compression is shown for comparison. The measured plasma temperatures are far higher than those that would be achieved through this "standard" theta pinch process. In fact, the FRC temperatures appear to scale as B^2 rather than in accordance with an adiabatic relationship.

Since so much internal field energy is available for plasma heating, it is not surprising that higher temperatures can be achieved in reverse-field-theta-pinches. The approximate B^2 scaling is also reasonable since the initial bias field was generally increased as the main field was raised. The vertical bar on Figure 6 represents the range of temperatures calculated with a simple ohmic heating/axial shock model assuming either half or all the initial bias flux is still present after plasma removal from the wall.[8] This range of flux trapping agrees with detailed measurements,[5] and the resultant plasma temperature is seen to agree with the calculations. The observed efficiency of the ohmic heating/axial shock process is extremely encouraging since it permits operation with low voltage theta-pinches.

IV. CONCLUSIONS

It has been shown that, within certain limits set by spontaneous reconnection, the reconnection process can be controlled, and that this control provides certain advantages with respect to plasma heating and high flux trapping. However, it has still not been possible to produce field-reversed-configurations with separatrix radius to coil radius ratios greater than 0.6. Methods have recently been found to control the primary rotational n=2 FRC instability,[9,10] and the principal impetus of future FRC research should be directed toward increasing x_s and reducing anomalous transport rates across the separatrix.

* This work was funded by DOE contract #DE-AC06-80ER53096.

REFERENCES

1. A.G. Es'kov, et al., "Features of Plasma Heating and Confinement in a Compact Toroidal Configuration," in Proceedings of the Seventh International Conference on Plasma Physics and Controlled Nuclear Fusion Research, Innsbruck, Austria, 1978 (IAEA, Vienna, 1979).

2. W.T. Armstrong, R.K. Linford, J. Lipson, D.A. Platts, and E.G. Sherwood, Phys. Fluids 24: 2068 (1981).

3. A.L. Hoffman, R.D. Milroy and L.C. Steinhauer, Appl. Phys. Lett. 41: 31 (1982).

4. Y. Nogi et al., Proceedings of the Fourth Symposium on the Physics and Technology of Compact Toroids, (Lawrence Livermore National Laboratory, 1982), p. 65.

5. W.T. Armstrong, D.G. Harding, E.A. Crawford, and A.L. Hoffman, "Flux-Trapping During the Formation of Field-Reversed Configurations," to be published in Phys. Fluids.

6. Richard E. Siemon - private communication.

7. A.L. Hoffman and W.T. Armstrong, "Compact Toroid Formation Using Barrier Fields and Controlled Reconnection in the TRX-1 Field-Reversed Theta-Pinch," Proceedings of the Fourth Symposium on the Physics and Technology of Compact Toroids, (Lawrence Livermore National Laboratory, 1982), p. 61.

8. L.C. Steinhauer, "Axial Shock Wave Heating of Reversed-Field-Theta-Pinch Plasmas," to be published.

9. A.L. Hoffman, J.T. Slough, and D.G. Harding, "Suppression of the n=2 Rotational Instability in Field-Reversed-Configurations," to be published.

10. T. Minato et al., "Experimental Studies on Confinement of FRC Plasma," in Proceedings of the Ninth International Conference on Plasma Physics and Controlled Nuclear Fusion Research, Baltimore, Maryland, 1982 (IAEA, Vienna, to be published).

Spheromak Formation

SPHEROMAK HEATING WITH MHD WAVES

S. O. Knox, Los Alamos National Laboratory;
J. A. Tataronis and C. E. Kieras, Univ. of Wisconsin-Madison

The spheromak configuration posseses several properties which are desirable in magnetic confinement schemes; unfortunately, most present day spheromak experiments appear to have high power losses due to impurity line radiation, which clamps the electron temperature below 100-eV. A possible exception is the Los Alamos spheromak experiment CTX, where operation in a mode not dominated by radiation has been demonstrated. However, an additional source of energy might be needed in order to burn through the low-Z impurity radiation barrier. In addition, a spatially-selective rf heating pulse can be used to study transport locally in a spheromak. We propose to add this energy via radio-frequency (rf) waves imposed by an external antenna structure. The wave coupling to the plasma is via the fast(compressional) magnetosonic wave, which propagates isotropically across the inhomogeneous, helical magnetic fields of a spheromak. The compressional mode gives rise to finite particle displacements with respect to the magnetic field, thus establishing a perpendicular electric field $E_\perp$. This field, coupled with the resonance condition for the shear Alfven wave ($\omega/k_\parallel = V_A$ on a magnetic surface) can lead to strong wave absorption and damping within the plasma.

We take for analysis the minimum energy, constant helicity, force-free equilibrium discussed by Taylor[1]. In cylindrical coordinates the fields have the form[2,3]

$$B_r = -B_o \frac{k_z}{k_r} J_1(k_r r)\cos(k_z z) \qquad (1)$$

$$B_\phi = B_o\left[1+\left(\frac{k_z}{k_r}\right)^2\right]^{1/2} J_1(k_r r)\sin(k_z z) \qquad (2)$$

$$B_z = B_o J_o(k_r r)\sin(k_z z) \qquad (3)$$

where $k_r = 3.83/R$, $k_z=\pi/L$, and $k_r^2 + k_z^2 = \lambda^2 =$ constant. In the proposed heating scheme, the poloidal field B_p ($B_p^2 = B_r^2 + B_z^2$) is modulated at a frequency ω, exciting the compressional wave.

The reduced set of equations which describes modes in the continuous spectrum of ideal magnetohydrodynamics (MHD) in the limit of low beta for axisymmetric toroidal equilibria should provide a good description of the continuum and heating rates for the low frequency RF heating experiment on CTX. When the equilibrium pressure is set equal to zero in the linearized ideal MHD equations, the cusp continuum is reduced to a single point $\omega=0$ in the spectrum, and a single second-order differential equation which describes the shear Alfven

continuum survives in this limit. The structure of the system of equations in the zero beta limit has been established by Kieras and Tataronis[4]. The fundamental variables are the perturbed velocity across flux surfaces, $v^1 = \underline{v}\cdot\nabla\psi$, and the total perturbed pressure in the zero beta limit, $p^* = \underline{B}\cdot\underline{b}/\mu_o$. The spatial structure of v^1 and p^* is obtained for a given ω by specifying appropriate boundary values for them on the magnetic axis and then integrating across flux surfaces using the following equations:

$$\frac{\partial v^1}{\partial \psi} = a_{11}v^1 + a_{12}p^* + c_1 v_3 \qquad (4)$$

$$\mu_o \frac{\partial p^*}{\partial \psi} = a_{21}v^1 + a_{22}p^* + c_2 v_3 \qquad (5)$$

$$Lv_3 \equiv \mu_o \rho \omega^2 v_3 + \underline{B}\cdot\nabla\left[\frac{R^2B_p^2}{B^2}\underline{B}\cdot\nabla\left(\frac{B^2}{R^2B_p^2}v_3\right)\right] = k_1 v^1 + k_2 p^* \qquad (6)$$

where $v_3 = R\underline{v}\cdot\nabla\phi$. The coefficients a_{ij}, c_{ij}, k_i are functions of the equilibrium which may contain differential operators with respect to the poloidal and toroidal angles, θ and ϕ, but not with respect to ψ. To perform the integration one must first invert Eq.(6) to eliminate v_3 in favor of v^1 and p^* in Eqs.(4)-(5). However, if a nontrivial solution exists to the equation $Lv_3=0$ subject to the boundary conditions that v_3 be periodic in θ and ϕ then the inverse of the operator L does not exist. The set of frequencies which satisfies $Lv_3=0$ defines the shear Alfven continuum for the system. Analytic solutions for v^1, p^* and v_3 may be obtained using a generalized method of Frobenius about the region where $Lv_3=0$. The behavior of v^1, p^* and v_3 in the remainder of the discharge may be obtained through numerical integration of Eqs.(4)-(6). Heating rates (via antenna loading resistances) are estimated in this report for CTX using a code based on the cylindrical model of these equations[5] and the zero pressure model for the equilibrium[3]. A new code which utilizes eqs.(4)-(6) directly to calculate heating rates is currently under development.

An axisymmetric 2-D code to determine general spheromak equilibria[6] has been used here to calculate flux surfaces in an oblate cylindrical flux conserver (cf. Fig. 1); flux surfaces determined from this numerical calculation are used as the input to a fully toroidal code (toroidal variation as $e^{in\phi}$) which then calculates the Alfven wave resonances as a function of frequency. The numerical results are given in Fig. 2, where the normalized resonance frequency $(\omega/\omega_o)^2$ ($\omega_o = V_A/2a$, where a=plasma radius) is plotted versus the equilibrium flux surface of Fig. 1. Results are given for the n=2, m=2 mode, where m=2 is the dominate poloidal mode number for the noncircular flux surfaces. This mode also displays the highest loading resistance (and, hence, energy absorption) in the ideal MHD calculation. The antenna loading resistance as a function of frequency for the n=2, m=2 mode is given in Fig. 3. It should

be noted that the total theoretical loading resistance is actually higher, since more than one mode can exist simultaneously in the plasma, and the resultant loading resistance is the sum of the contributions from more than one mode. Also, the results of Fig. 3 are for the ideal MHD situation, where the nature of the singularity might give resistances in excess of that for a plasma with finite conductivity. However, Fig. 3 does demonstrate that large antenna loading resistances are available for rf energy deposition within the spheromak plasma. For example, we take two points in time during a CTX spheromak to determine the Alfven speed V_A and hence ω_o:

TABLE 1

ω_o ($\times 10^6$)	n_e ($\times 10^{14}$)	B_o (kG)
1.7	0.2	2
1.4	2.0	5

In order to deposit the energy well within the spheromak, we choose an inner flux surface from Fig. 1 and take $(\omega/\omega_o)^2 = 4$ in Fig. 2. Thus, the resulting excitation frequencies for the parameters of Table 1 are .54 and .45 MHz respectively. These frequencies are readily accessible to ringing capacitor technology where very high rf powers are available for short times[7]. Referring to Fig. 3, a loading resistance of ~1 ohm can be expected for an antenna of length 1-m. Using this value of resistance (which is significantly greater than any circuit resistance), we can expect to dissipate a nominal 1-kJ of capacitor energy in ~50-μs for an average power of 20-MW.

REFERENCES

1. J. B. Taylor, Phys. Rev. Lett. 33, 1139 (1974).
2. J. M. Finn and W. M. Manheimer, Phys. Fluids 24, 1336 (1981).
3. A. Bondeson, et. al., Phys. Fluids 24, 1682 (1981).
4. C. E. Kieras and J. A. Tataronis, Phys. Fluids 25, 1228 (1982).
5. J. A. Tataronis and W. Grossmann, Nucl. Fusion 16, 667 (1976).
6. R. L. Spencer, private communication.
7. S. O. Knox and B. L. Wright, Proc. Fourth Symp. Physics and Tech. of Compact Toroids, LLNL Report CONF-811087, p. 145 (1981).

Figure Captions

Figure 1. Flux surface plots for cylindrical flux conserver. The innermost surface is T and the outermost surface is A.

Figure 2. Plot of normalized resonance frequency for n=2, m~2 mode vs. flux surface of Fig. 1.

Figure 3. Antenna loading resistance vs. frequency for the n=2, m=2 mode.

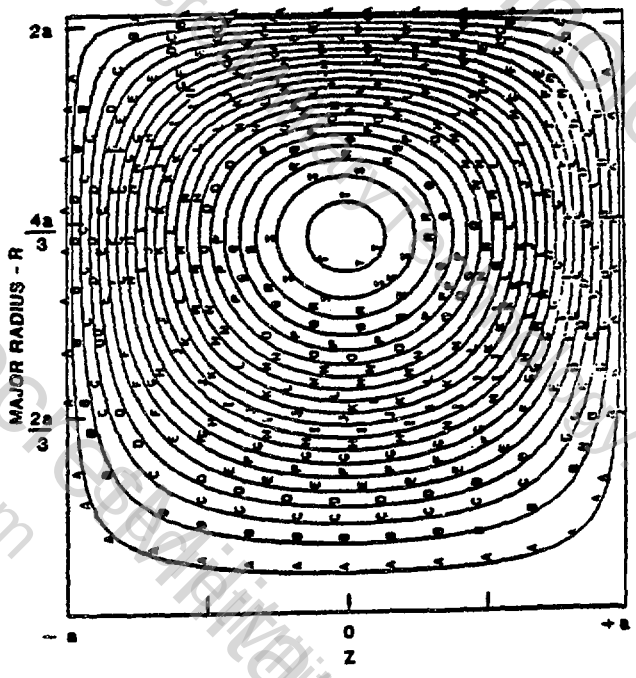

Figure 1.

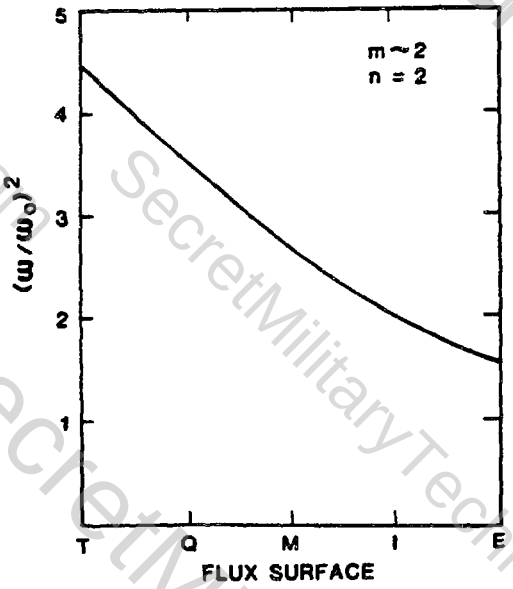

Figure 2.

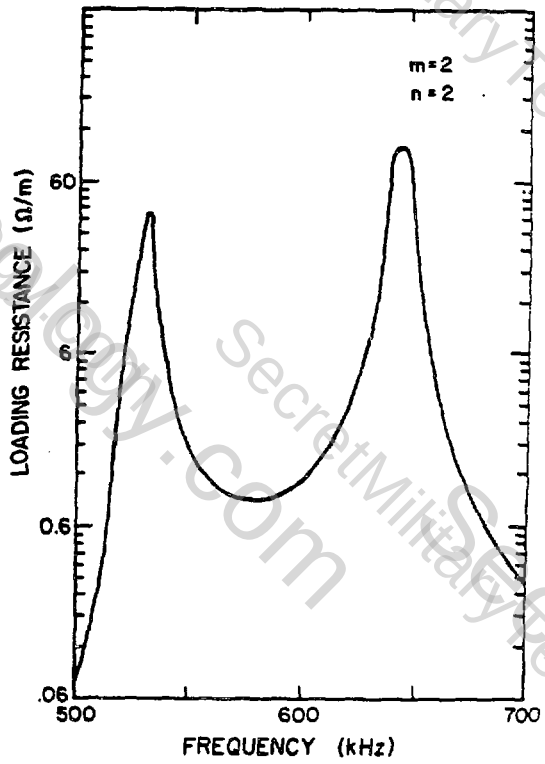

Figure 3.

Merging Spheromaks Produced by the CθP Machine

K. Kawai, Z.A. Pietrzyk and R.D. Brooks
University of Washington
Seattle, Washington 98195, U.S.A.

Previous experiments by Wells,[1,2] Jones and Miller,[3] and T.K. Allen, et al.[4] show that a conical θ-pinch discharge can produce plasmoids of a spheromak magnetic field structure (poloidal and toroidal field of the same magnitude). We have reported similar results at previous meetings.[5] Here we report experiments on the collision of two spheromaks within a flux conserver.

The experimental setup, which consists of two identical conical theta pinches facing each other, is shown in Fig. 1. The pinches produce spheromaks moving with a velocity of 3-5 cm/μs. Though the current in the pinches is not crowbarred, the magnetic field on axis within the merged spheromaks lies in one direction. The fill pressure for stable operation can be varied from 5-200 mT. Diagnostics include: internal magnetic probes, diamagnetic probes, spectroscopy, Thomson scattering and visual photography.

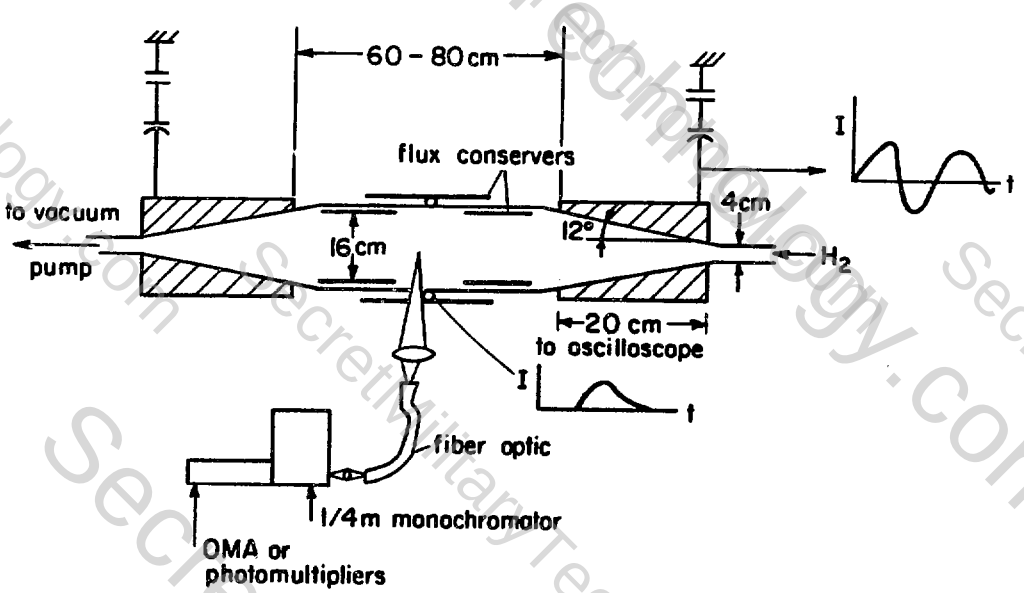

Fig. 1. The Conical θ-Pinch Experimental Apparatus Showing the Flux Conserver Configuration Most Often Used.

Figure 2 shows the time dependence of the diamagnetic signal measured by a single loop outside of the vacuum tube but inside the flux conserver. A slowly decaying signal should be seen for a stable spheromak while unstable spheromak usually show oscillating signals. The time decay of the diamagnetic signal for various initial pressures is shown in Fig. 3 together with the theoretical field diffusion time into a cylindrical conductor for T_e = 5 and 10 eV plasmas. The decay rate is consistent with the measured temperatures discussed later.

We observed a great influence both of the flux conserver shape and the base pressure on the stability and reproducibility of the diamagnetic signal. A stable merged spheromak could not be achieved with a straight solid or perforated flux conserver. But for a flux conserver wider in the center than at the ends a stable collision was attainable.

Only for a base pressure (while pumping) below $2 \cdot 10^{-6}$Torr was a stable spheromak collision reproducibly realizable, while for a base pressure above $8 \cdot 10^{-6}$Torr a stable collision was only rarely observed.

Spectroscopic measurements were used to estimate plasma parameters and to study the impurity content of the plasmoids. The electron density was determined by H_β line broadening where it should be pointed out that most of the H_β radiation comes from the colder regions of the

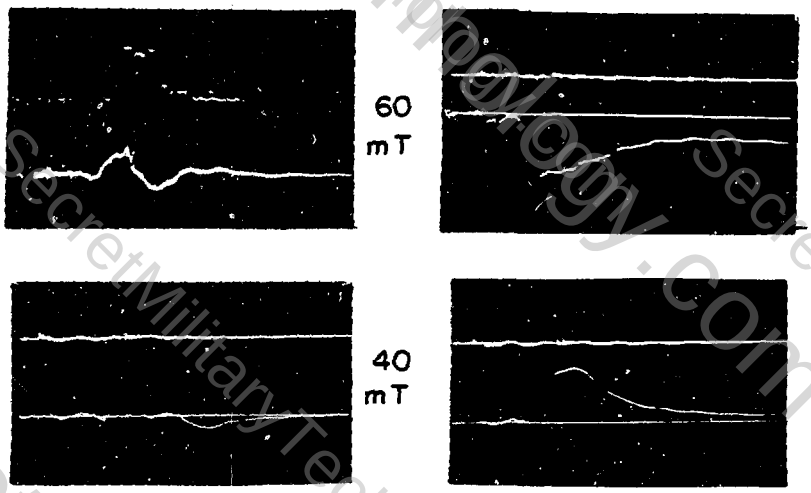

Fig. 2. Diamagnetic Signals for Stable and Unstable Spheromak Collisions.

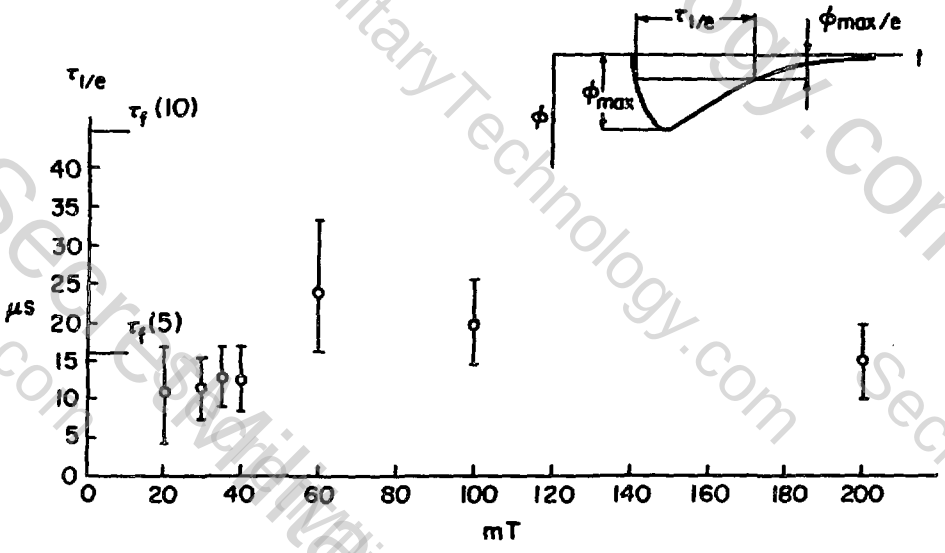

Fig. 3. Time of Decay of the Diamagnetic Signal After the Spheromaks Collide as a Function of Fill Pressure. The theoretical field diffusion times for 5 and 10 eV plasmas are indicated.

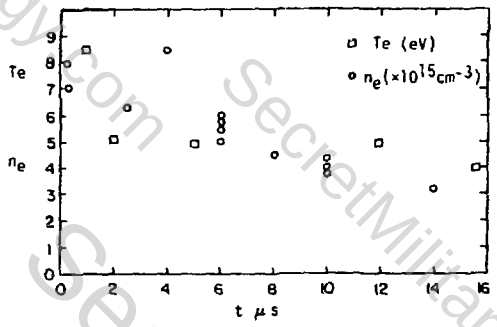

Fig. 4. Electron Density and Temperature vs. Time after Spheromak Collision as Determined by the Hβ Profile for a Fill Pressure of 60 mTorr.

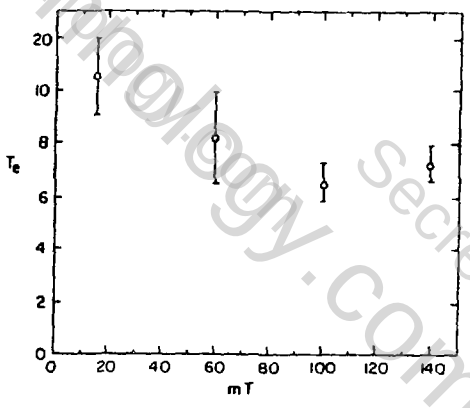

Fig. 5. Maximum Electron Temperature after Spheromak Collision as Determined by Thomson Scattering.

plasma. A plot of the density determined in this way for a 60 mT fill is shown in Fig. 4. It shows that the merged spheromaks have a density of about 2 times the filling density which is also the approximate density before the collision.

Carbon lines were observed to determine the temperature range. Lines up to C_{IV} were found, while C_V lines were not visible at any time. This suggests a temperature below 60 eV which is consistent with the temperature later determined by Thomson scattering.

An analysis of the impurity lines shows mainly oxygen and silicon to be present though an estimate of their concentration is not yet available.

The temperature at the center of the colliding spheromaks was measured by ruby laser Thomson scattering. The time dependence of the temperature is shown in Fig. 4 for a 60 mT fill. Figure 5 shows the maximum temperature after the spheromaks collide as a function of the fill pressure. The measured temperature is consistent with spectroscopic observations. A comparison of the measured temperature, density, and magnetic field, assuming they are average values, indicates an average poloidal β above 5.

In conclusion, a simple conical θ-pinch can generate the spheromak structure with translational motion. The spheromak can be transported distances up to 1 m in a copper flux conserver. Colliding spheromaks are stable in a flux conserver if the flux conserver has a larger diameter in the collision region and the base pressure is below 10^{-6}Torr. Decay of flux is consistent with the measured temperature and a high β suggests that the plasma is resting against the wall.

The authors wish to thank Hamilton Hunter and Dan Lotz for their valuable contributions to this research. This work was supported by the U.S. Department of Energy, Office of Magnetic Fusion Energy.

REFERENCES

1. D.R. Wells, Phys. Fluids 7, 826 (1964).
2. D.R. Wells, J. Davidson, L.G. Phodke, J.G. Hirschberg and S. Tunstall, Phys. Rev. Lett. 41, 166 (1978).
3. W.B. Jones and R.D. Miller, Phys. Fluids 11, 1550 (1968).
4. T.K. Allen, K. Doble, T.J.L. Jones, R.M. Payne and I.J. Spalding, Phys. Fluids 9, 1394 (1966).
5. K. Kawai and Z.A. Pietrzyk, Bull. Am. Phys. Soc. 26, 905 (1981).

SPHEROMAK ICRF HEATING STUDIES AT LOW POWER

B. L. Wright
Los Alamos National Laboratory, Los Alamos, New Mexico 87545

At the Fourth Compact Toroid Symposium we outlined plans for studying rf heating possibilities in the spheromak plasmas produced at Los Alamos. Heating at the ion-cyclotron range of frequencies (including shear Alfvén wave heating) showed the best prospects because large power levels are more readily achieved at lower frequencies and because ICRF requirements lead naturally to global coupling schemes that are compatible with spheromak symmetry. At the same time, the relatively high densities and low magnetic fields of our configurations make them inaccessible to conventional rf heating methods at higher frequencies (lower hybrid, ECRH). Our experimental activity has proceeded on two fronts: the initiation of studies at low power to investigate plasma response in the ICRF regime and the development of a high-power generator (initially to be based on ringing capacitors) for actual plasma heating. A facility for testing components for the latter system is currently under construction. We report below on the status of low power studies.

The antenna configuration that we envisage consists of a toroidal strap (or straps) encircling the spheromak near its midplane that drives an rf poloidal magnetic field at the wall of the flux conserver. For test purposes, we have used a #10 copper wire that follows the spheromak equator at a distance of 1 cm from the wall. A segmented quartz tube provides insulation but not electrostatic shielding for the wire. In work done to date, rf magnetic fields have been monitored with high-frequency (20 Mhz) surface magnetic probes whose location relative to the antenna is shown in Fig. 1. An additional probe is located at 90 degrees to the plane of the figure. Each probe has coils to detect both poloidal and toroidal components of the field. Conventional axial probes are also available but have not been used pending further calibration. The signal from a surface probe may also be integrated in the usual manner to monitor the plasma magnetic field. Such a trace is shown in Fig. 2 for a poloidal field component. At this point it is important to note that all rf studies have been performed in our prototype facility. In this facility, unlike CTX, no attempts have been made at impurity control. The configuration is radiation dominated and supports a magnetic field for about 250 μs.

Low power studies involve both the detection of rf activity within the plasma and the measurement of antenna loading i.e., the resistive part of the antenna impedance due to the absorption of rf energy by the plasma. To investigate the latter topic, the antenna is configured as the inductance in an LC tank circuit. The Q is sufficient that several cycles are required for oscillations to damp when the excitation of the circuit ceases. The damping rate increases noticeably (see Fig. 3) in the presence of plasma. Using this technique we plot the antenna loading as a function of time (Fig. 4). We find a substantial contribution to the resistance extending to times well beyond the nominal termination of the shot. It is reasonable to suppose that absortion at the later times is due to the

presence of a weakly-ionized afterglow plasma in the flux conserver. The time scale of a millisecond seen in the data is consistent with the diffusion rate of room-temperature ions. The data shown here for antenna loading were taken at 0.96 MHz. Plans for additional work at other frequencies must await further protection of the solid-state generator used.

An induction heater rated at 1 kW has been used at 0.58 MHz to look at the response of the surface magnetic probes. Bandpass filters transmitting from 0.2 to 1.3 MHz are used to reduce the noise (mostly below the band) caused by spontaneous variations in the plasma magnetic field. These fluctuations are particularly strong during the first 60 μs after the source is fired. An example of digitized probe data from 100 to 200 μs is shown in Fig. 5 along with the antenna current waveform. This trace illustrates two features consistently seen during that time interval. First there is a burst that definitely matches the frequency of the oscillator. It is followed by an approximately periodic fluctuation of lesser amplitude whose center frequency is obviously unrelated. These features are borne out by the spectrum of the entire trace shown in Fig. 6.

The case illustrated here exemplifies phenomena seen on other shots during the interval that the spheromak is in place. In the absence of a driven rf field, narrow-band signals are observed in the frequency range of interest. Often the apparent period of these fluctuations shows a lengthening with time. When an rf field is applied, clear bursts of activity at the rf frequency are detected by individual probe coils on the "roof" that last for an interval of roughly 20 μs. The impression given by the data is that the character of the oscillations driven by the antenna is identical to that of the spontaneous fluctuations--with the driving field serving to lock them in frequency and enhance them in amplitude. Of obvious concern is the spatial extent of this phenomenon and whether it can, for example, be taken as evidence for the excitation of global eigenmodes. A crude estimate of the frequency of the lowest driven fast-magnetosonic eigenmode under these conditions gives around 0.23 MHz, so one may expect that the frequencies of such modes can sweep through the oscillator frequency during a shot. Indeed the observed period lengthening of spontaneous fluctuations during a shot is consistent with the decrease of the Alfvén speed as the magnetic field decays. However, the lack of shot-to-shot reproducibility and the absence of an unmistakable concurrence among raw probe signals means that a conclusion on the eigenmode issue must await the development of additional software tools for a proper correlation analysis. (Though the single probe on the end face of the flux conserver should have a significant bearing on this issue, it exhibits a higher level of spontaneous fluctuations than the other probes and has been used in only a few shots to date.)

Probe signals observed during the late afterglow phase (>300 μs) show a linear, reproducible response to the antenna rf current that is easily monitored. Figs. 7 and 8 show the time dependence of the amplitude and phase of the rf signal seen by one of the poloidal coils on the "roof". The amplitude is represented as the ratio of the probe signal (mv) to the antenna current (amps). The phase is likewise determined relative to the antenna current with zero phase corresponding to the vacuum case. For an rms antenna current of 24 amps, the rms vacuum rf field at the probe is

0.05 G. Also included in these figures are the amplitudes and phases of rf bursts monitored by the coil at earlier times.

The data reported above are quite recent and are only partly analysed. The analyses that have been made suggest further avenues of investigation both in the development of techniques that treat the issue of global activity and in the establishment of a more comprehensive data base in support of those techniques. A further need is for a reasonably realistic physical model of allowed modes (including surface waves) and their damping in the collisional regime of the present experiment. The damping problem is clouded by the fact that deuterium ion-cyclotron reasonance layers (B = 760 G at 0.58 MHz) are located within the plasma during the greater portion of each shot under current operating conditions.

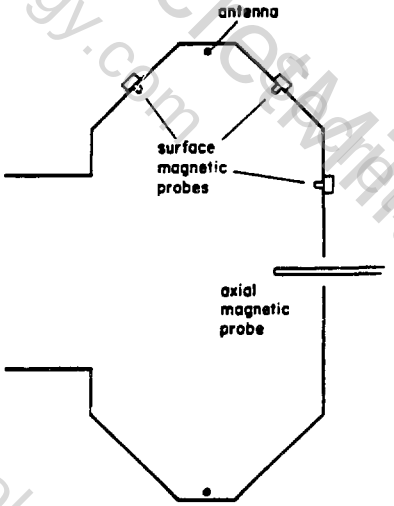

Fig. 1. Flux conserver geometry.

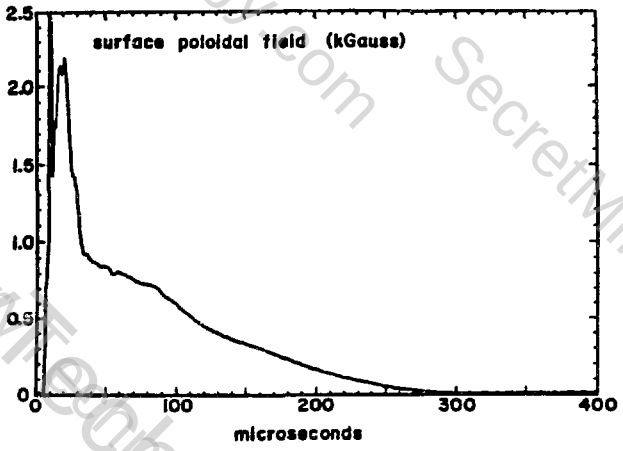

Fig. 2. Surface poloidal magnetic field.

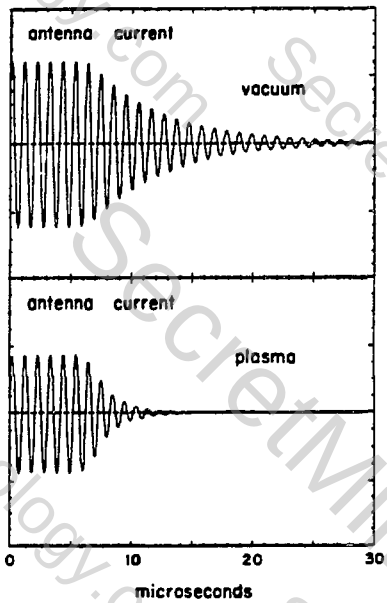

Fig. 3. Technique for measurement of antenna loading.

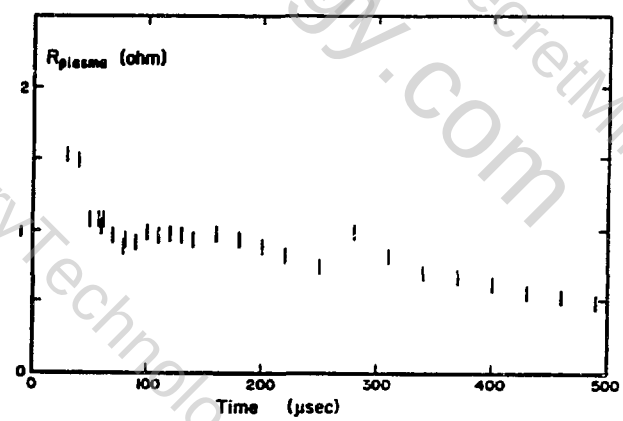

Fig. 4. Antenna loading.

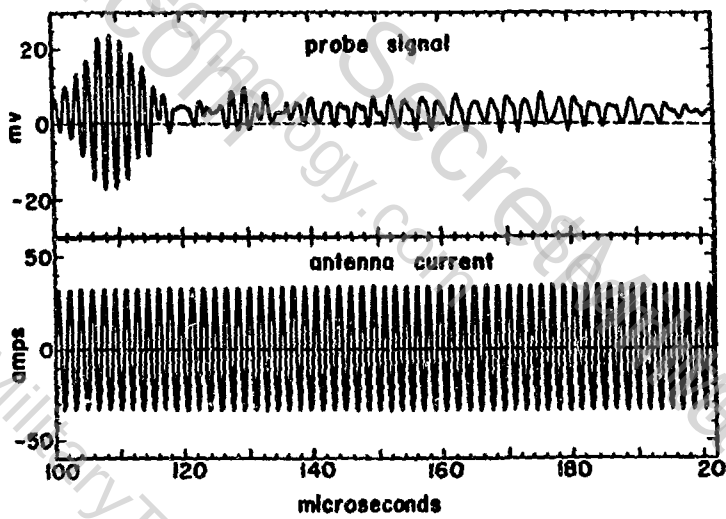

Fig. 5. Magnetic probe signal.

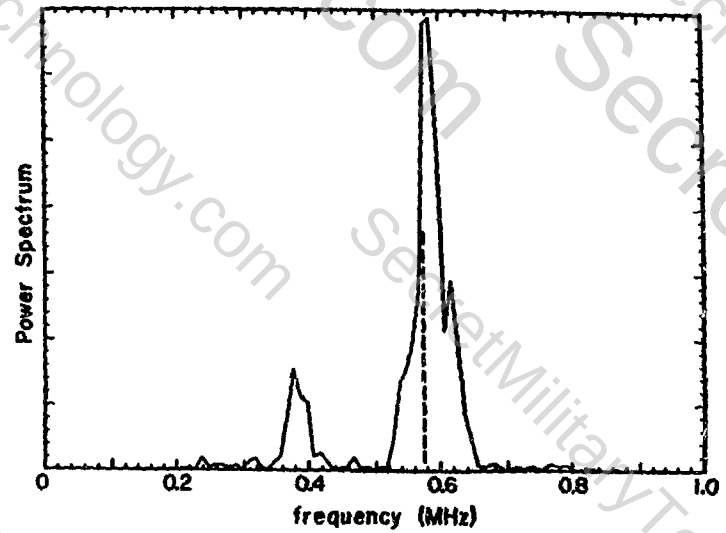

Fig. 6. Spectrum of magnetic probe signal (dashed line shows oscillator frequency).

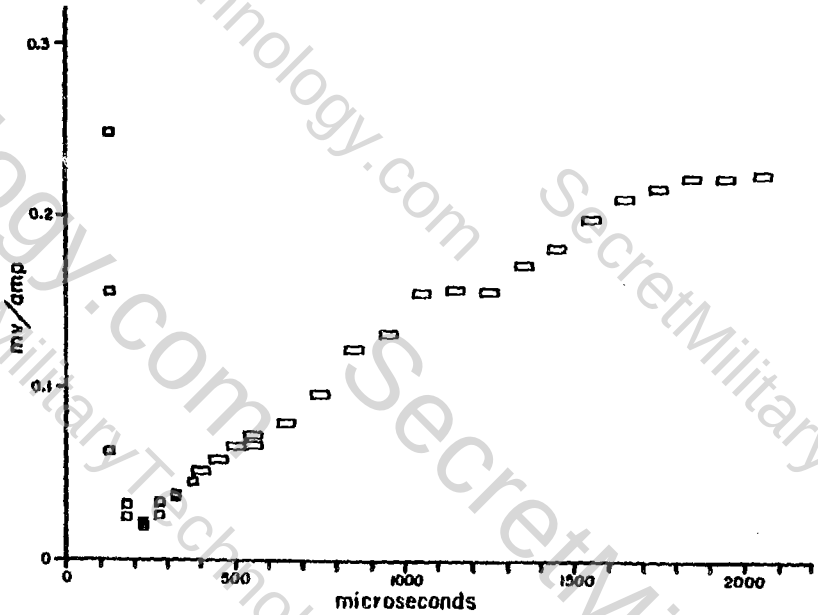

Fig. 7. Amplitude of poloidal rf component.

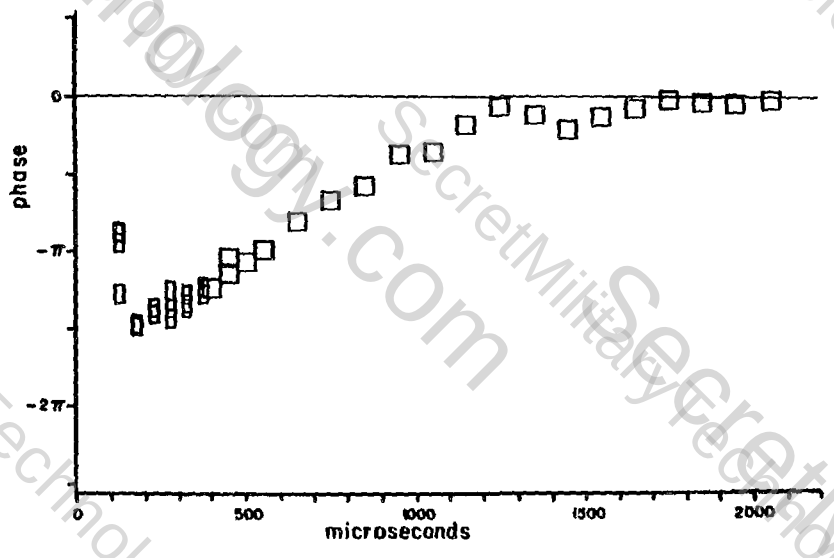

Fig. 8. Phase of poloidal rf component.

COMPUTATIONAL SIMULATION OF SPHEROMAK PLASMA HEATING

R. E. Olson and G. H. Miley
Fusion Studies Laboratory
University of Illinois
103 S. Goodwin Avenue
Urbana, Illinois 61801

Recent conceptual design studies in the U.S. and Japan underline the inherent attractive features of compact tori (CT) reactor systems. At the same time, considerable progress has been made in both experimental and computational demonstrations of the formation and gross stability of compact tori (especially spheromak) plasmas.

A general assumption involved in the conceptual reactor studies has been that a compact toroid can achieve thermonuclear-level temperatures without the use of auxiliary heating methods. Laboratory CT plasmas are still quite cold so heating has yet to be studied experimentally. The purpose of the present study is to help fill this "gap" by identifying some of the important questions connected with the heating of a spheromak plasma.

Computational simulations of the spheromak formation phase have taken advantage of a reduced set of one-fluid equations in which the pressure gradient and convective derivative terms in the momentum equation are dropped.[1] These assumptions are, of course, well justified for the formation of a cold, very low β plasma. In the heating phase, however, we are interested primarily in effects that are intimately related to cross surface convection, a significant pressure gradient, and a two-fluid (i.e., electron-ion) interaction. Hence, our approach in the heating study has been to develop and utilize a 1 1/2-D model[2] in which poloidal flux profiles of electron and ion pressure are advanced independently (together with the

equations for particle and toroidal flux conservation). This code (named SPTR for spheromak transport) makes use of arbitrary aspect ratio, integral transform solutions of Grad-Shafranov equilibrium equation to determine the 2-D spacial positioning of the poloidal flux surfaces within the plasma separatrix. These solutions are then coupled with a computational package that solves the 1-D ψ-dependent flux surface averaged moment equations for advancing the electron and ion temperatures and densities with time. The moment equations are self-consistently solved via a 4x4 block tridiagonal setup and the results are utilized in a 2-D repositioning of the poloidal flux surfaces.

From a heating standpoint, there are two features of the spheromak equlibrium solution that are quite noticeable--first, that current densities are ~10x greater than in a comparable tokamak equilibrium; and second, that the lack of hardware in the center of the plasma "doughnut" makes it possible to compress the plasma in the toroidal direction. Consequently, the computational model has been set up in a fashion that will allow simulation of both ohmic decay with a static applied field and/or adiabatic compression via a rapid buildup of the applied equilibrium field.

We have begun the study with an attempt to computationally simulate two of the small experimental plasmas presently under study (the PS-1c at Princeton[3] and the Beta-II at Livermore[4]), and, particularly, to explain the observed clamping of electron temperature and rapid decay of the poloidal flux surfaces. Computational simulation of these experiments with a purely classical transport model and static applied fields predicts that the plasma should exist for times exceeding 100 μs with temperatures approaching the 100

eV level--a behavior quite different from what is actually observed. To explain this discrepancy, we have considered several models that could account for enhanced losses. The first model, and the most likely candidate for explaining the early PS-1c and Beta-II results, includes heavy impurity radiation. With a modest (.5% Fe, 1.5% O) impurity level we observe an electron temperature that is clamped at levels below 20 eV with complete poloidal flux surface decay occurring on a ~30μs timescale. This is in line with actual experimental results. Plasma cleanup, of course, could remove such barriers.

With an eye towards future developments, we have also pursued two additional enhanced energy loss mechanisms--soft beta limit losses and resistive interchange transport. The soft beta limit model anomalously dumps energy from a flux surface region in which the increase in pressure gradient leads to a local violation of the ideal Mercier criterion. The resistive interchange model depicts a random walk transport across a locally braided magnetic field.

The ability to simulate a time dependent applied equilibrium field allows us to propose and study a combined heating scenario in which time-stepped adiabatic heating and ohmic heating are used to overcome enhanced losses of the type described above. Preliminary studies, for example, indicate that any of the above three temperature clamps could be overcome in a S-1 size plasma by means of a staged adiabatic and ohmic heating scenario. In fact, our earlier global studies of heating in a reactor-size spheromak indicated that an ohmic heating to ~1 keV followed by an adiabatic compression could tolerate significantly enhanced loss rates ($\propto 1/100\tau_{E\ Bohm}$) and still lead to thermonuclear-level temperatures.[5]

In summary the examination of spheromak plasma heating provides a logical bridge between the present-day experimental studies of compact torus formation and the futuristic conceptual studies of the spheromak and moving ring reactors. In the near term, the work helps in understanding the temperature clamping in experiments and provides some insight into how to overcome this obstacle (e.g., via impurity cleanup). In the longer term, the work also provides some insight into other possible temperature clamping problems (i.e., soft beta limit and resistive interchange) and allows us to propose and study methods for overcoming them.

References

1. S. C. Jardin and W. Park, Phys. Fluids, 24, 679 (1981).
2. H. Grad, "Survey of 1-1/2 D Transport Codes," U.S. ERDA Rpt COO-3077-154, (1978).
3. M. Yamada, et al., Phys. Rev. Lett., 46, 188 (1981).
4. W. C. Turner, et al., Proc. Third Symp. on Compact Toroids in the Magnetic Fusion Program, Los Alamos, NM, LA-8700 (1980).
5. R. Olson, J. Gilligan, G. Miley, Proceedings Third Compact Tori Symposium, Los Alamos, NM (1980), LA-8700-C.

Status of Fabrication of the S-1 Spheromak Device*

R. Ellis, Jr., A. Janos, J. Joyce, M. Yamada

Plasma Physics Laboratory, Princeton University

Princeton, New Jersey 08544

The S-1 Spheromak is nearing completion and the first plasma operation is scheduled for March, 1983. The design started in 1980. A budget adjustment forced postponement of completion from December 1982 to August 1983.

The quasistatic inductive transfer of flux has been tested in prototype devices at the Princeton University Plasma Physics Laboratory. This method of producing a spheromak employs poloidal (PF) and toroidal (TF) windings in a "flux core" first to produce a plasma surrounding the flux core that subsequently forms a spheromak by a reconnection process. The equilibrium is maintained by a steady field (EF) supplied by a coil system that is mounted on the vacuum vessel. The state of construction of the principal elements of the S-1 device are described.

The flux core is the most challenging component. The location of the poloidal and toroidal field windings in the flux core is shown in Figure 1. The flux core has a major radius of 1m and a minor radius of 0.19m. There is also an equilibrium field winding in the flux core. Figure 2 shows the flux core with the toroidal windings in place. The Inconel cover of the flux core which prevents outgassing of the flux core into the plasma space must be thin enough to allow the flux to penetrate in a short time. This created a difficult fabrication problem because the average thickness must be less than 0.5mm. The first flux core liner for S-1 has an average thickness of 0.25mm. Inconel sheets about 2.25mm thick were formed on a mandrel to "half-toroids" and chemical milling was used to reduce the liner halves to the final thickness. After machining to size, the liner halves were welded in place on the flux core and the space between the liner and the core was filled with urethane. The completed flux core mounted in the vacuum vessel center section is shown in Figure 3.

The quasisteady equilibrium field is produced by a set of coils that is mounted on the vacuum vessel domes and two turns located inside the flux core. These coils can be connected in different combinations that yield the following values of the field index: - 0.33, + 0.060, + 0.124, and + 0.354. The EF coils are powered by two large DC generators.

The vacuum vessel consists of two domes and a center section, all of stainless steel. The domes are commercially available pressure vessel components that were machined at PPPL. The flux core is mounted in a short center section. Figure 4 shows the completed vacuum vessel mounted on the support structure with the external EF coils in place.

The pumping system is a conventional turbomolecular system consisting of two 1500 liter/sec pumps backed by blowers. The base pressure expected is about 8×10^{-8} torr. All seals are metal except the large diameter Viton seal between the domes and the center section.

*Work supported by the U.S. Department of Energy
Contract DE-AC02-76-CHO-3073

Capacitor banks are used for energy storage for the PF and TF circuits. Simplified circuit diagrams are shown in Figures 5 and 6. A photograph of the capacitor banks is shown in Figure 7 and a photograph of the switching tubes is shown in Figure 8.

The digital control system is based on an LSI11 computer. A serial highway links the control computer and the various subsystem CAMAC crates. Control system timer is an adaptation of the TFTR encoded dock timer system. Fiber optic transmission lines connect the CAMAC crates and distribute the clock signals. The control room is shielded to reduce electromagnetic interference. A photograph of the control room is shown in Figure 9. A block diagram of the control system is shown in Figure 10.

The schedule for fabrication of S-1 calls for first plasma in the Mode D configuration in March, 1983 and completion of the Engineering Handbook device in August, 1983. At the time this is written, it appears that these milestones can be accomplished. The control system is on the critical path and there is no slack. In order to have first plasma on schedule, the control system must support system testing by the end of 1982.

If there are no unforeseen problems, we should have spheromak plasmas in S-1 during FY83.

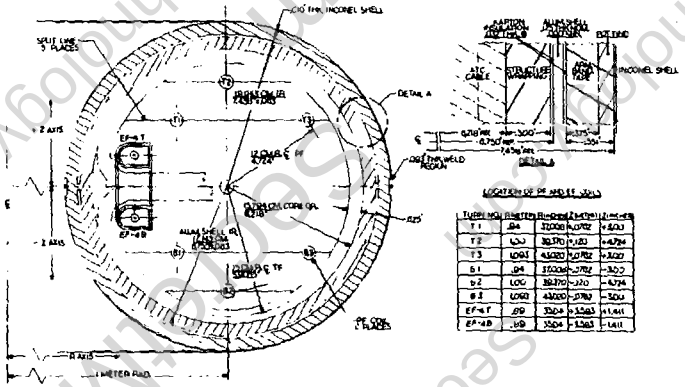

FIG. 1

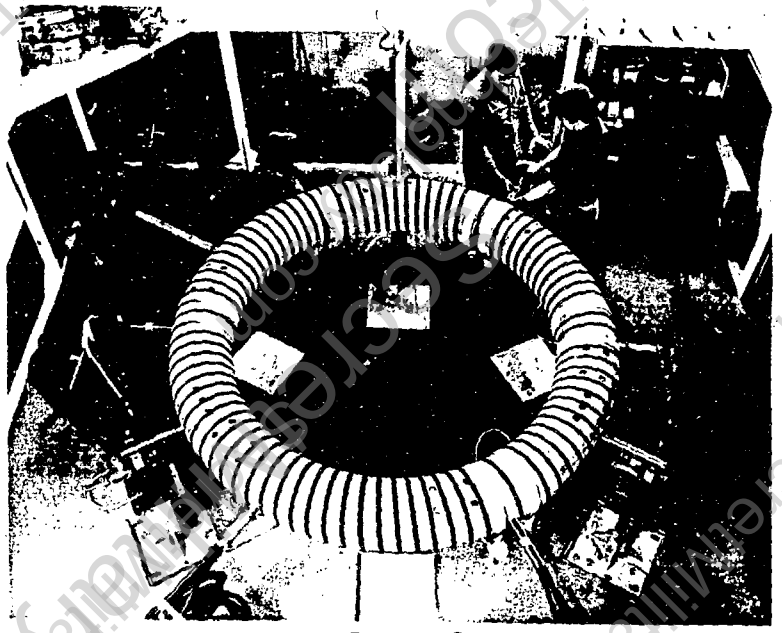

FIG. 2

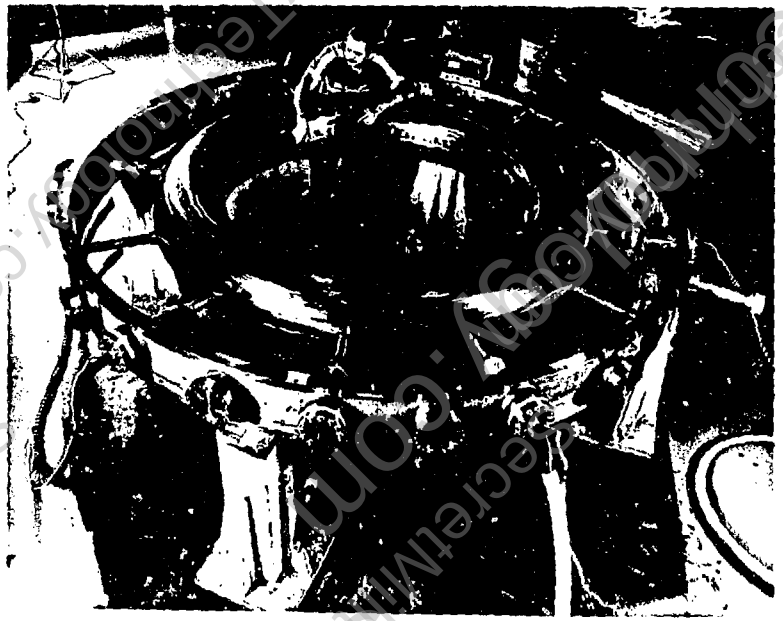

FIG. 3

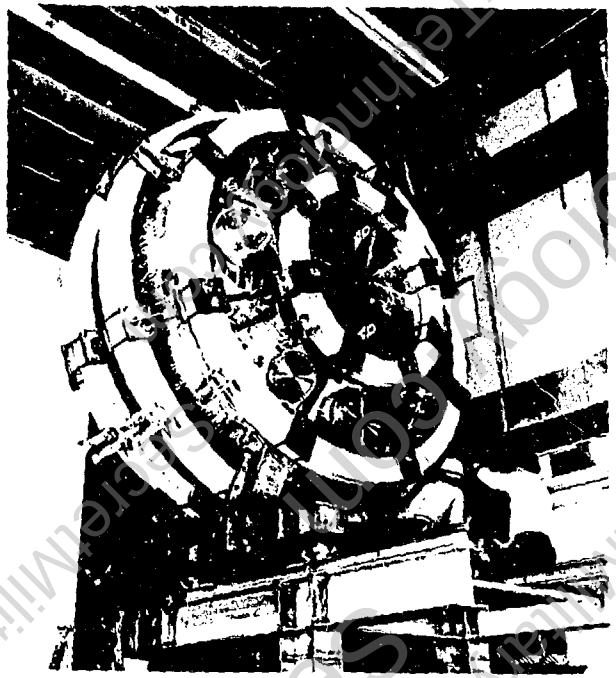

FIG. 4

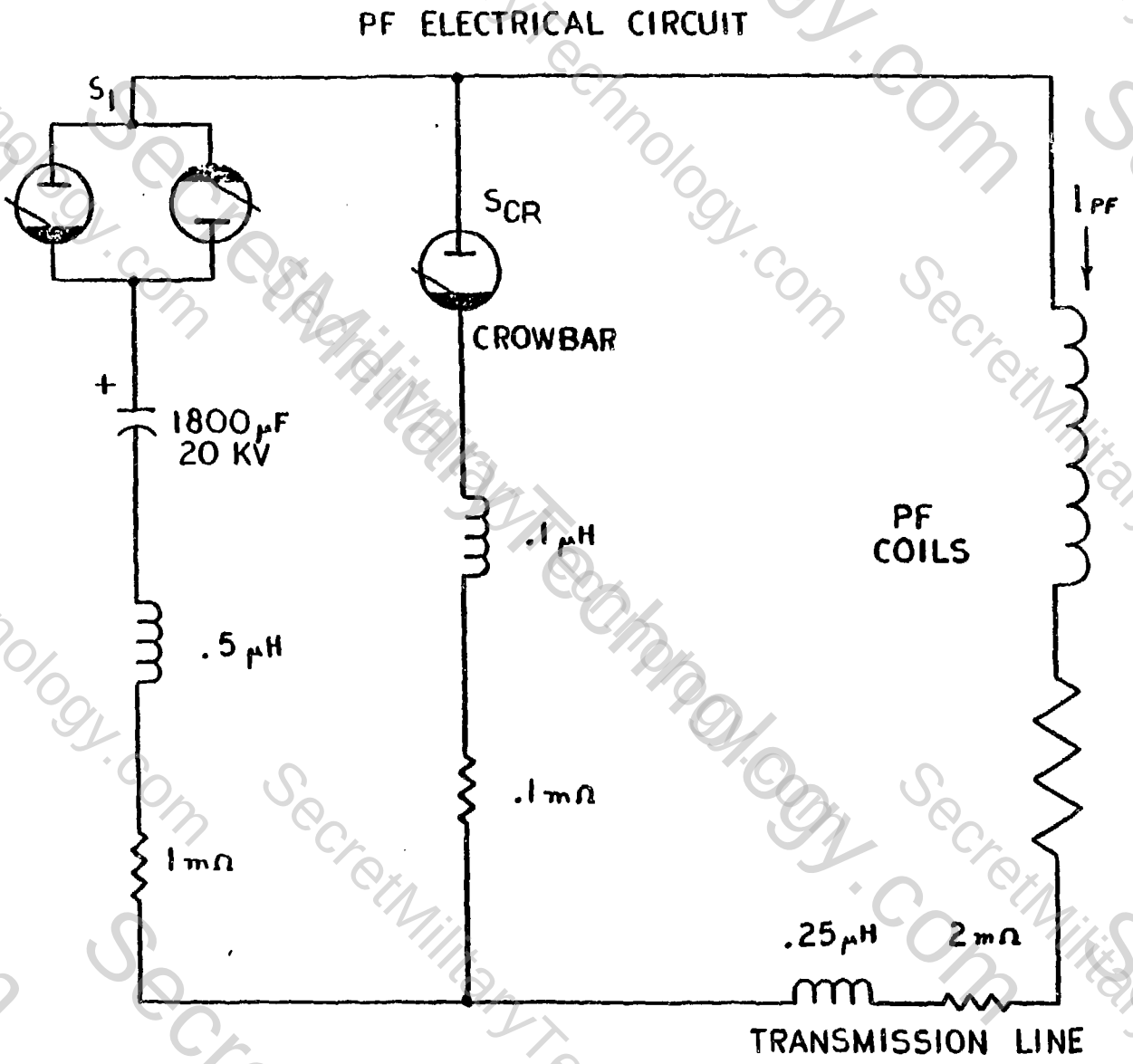

PF CIRCUIT

Figure 5

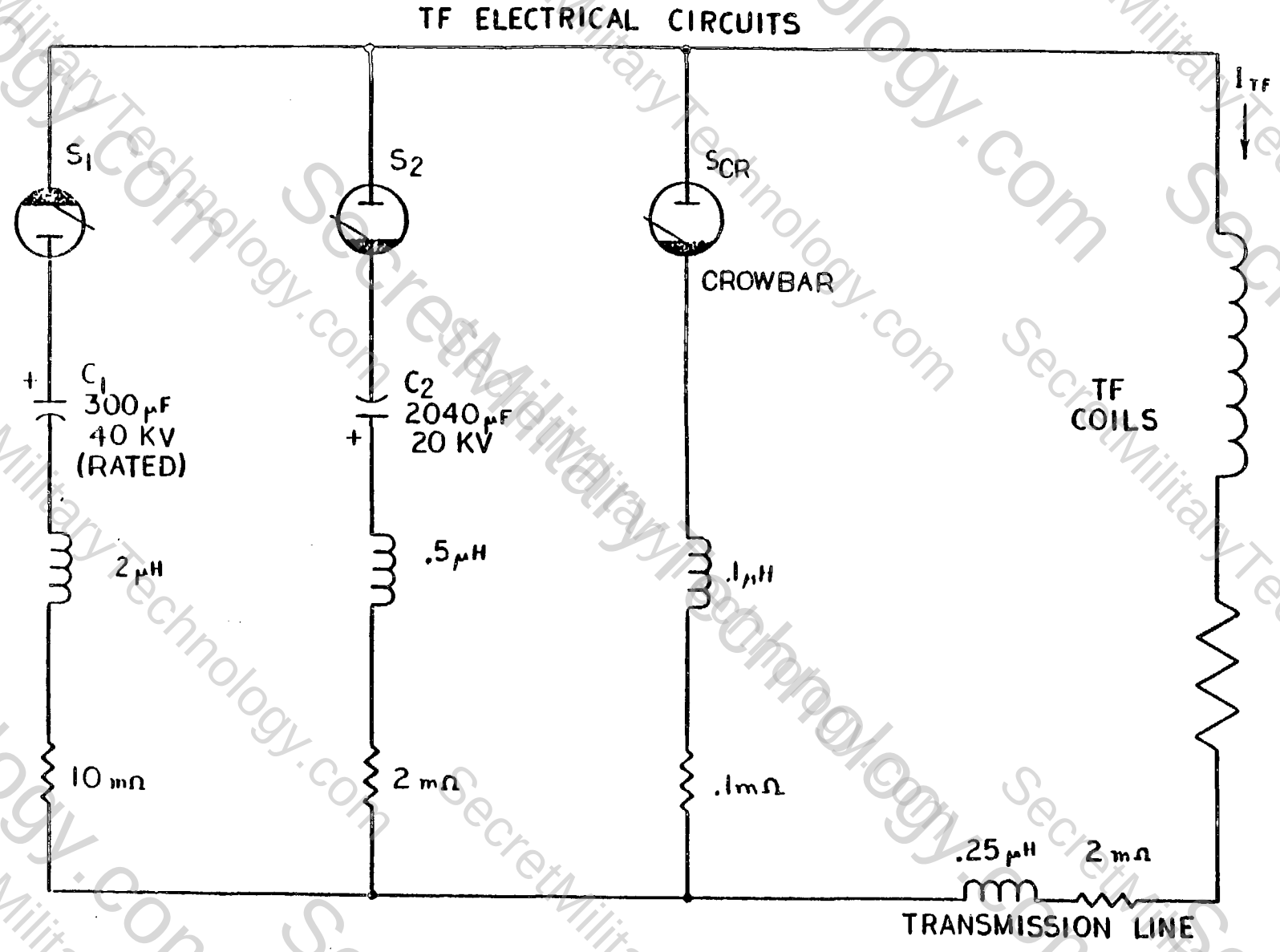

TF CIRCUIT

Figure 6

FIG.7

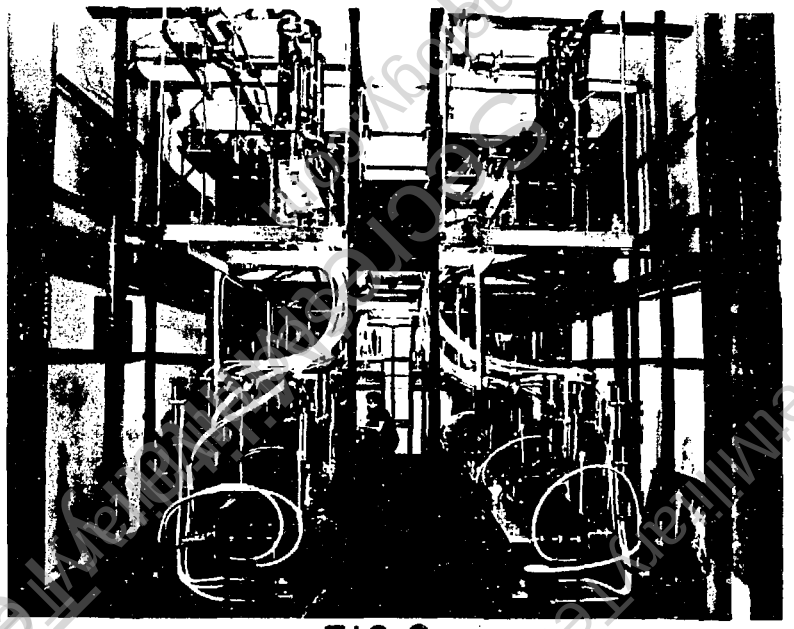

FIG.8

FIG.9

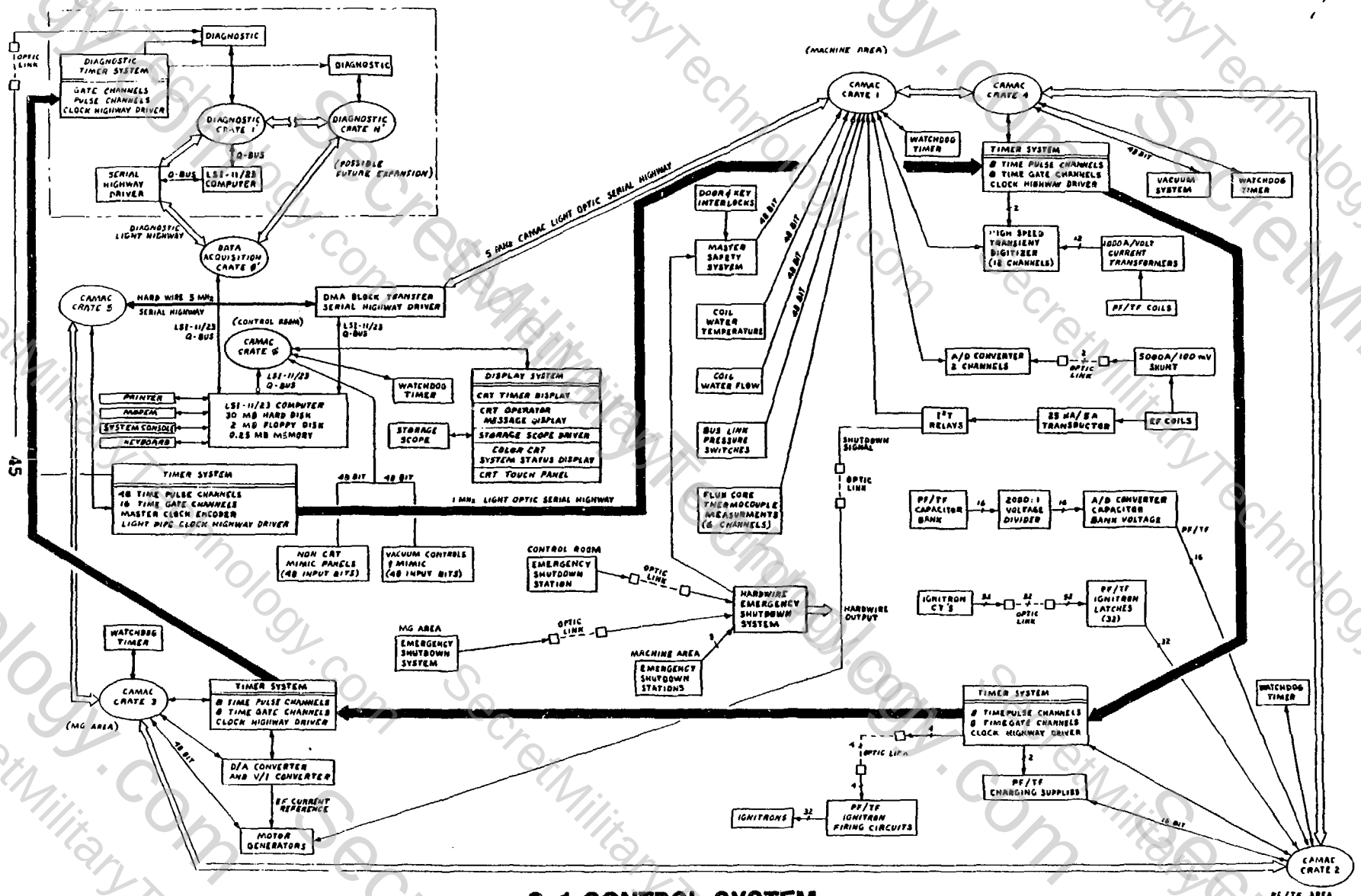

S-1 CONTROL SYSTEM

Spheromak Formation with Divertors

by

Y.C. Sun, S.C. Jardin and M. Yamada
Plasma Physics Laboratory, Princeton University
Princeton, NJ 08544

It has recently been suggested [1] that a set of divertor coils could be used as a "socket" on which the spheromak plasma can be attached to keep it from tilting or shifting, or can be turned loose to move to a different "socket" in a new location. It is the intent of this work to investigate the feasibility of this idea for the Proto S-1C device and to find the optimum coil location and current combinations to produce the desired divertor plasma configuration.

The tool we used for this investigation is a previously reported simulation code [2,3]. It is a one fluid, two-dimensional, resistive MHD code with coupled circuit equations to compute the inductive transfer of current from the poloidal and toroidal coils to the plasma. A coronal non-equilibrium atomic physics model is used to compute the impurity radiation losses. We have added internal divertor coils to the code for our present study.

The formation process without divertor coils is described in detail in Ref. 4 and 5. We follow the same procedure in the formation with divertor coils. Fig. 1 is a schematic diagram of the Proto S-1C spheromak with divertor coils. Initially, constant currents in the EF coil and divertor coils are applied and kept constant during the formation process. The currents of the PF coil inside the flux core and the TF coil around the flux core are shown in Fig. 2. We present four test cases with coil locations and currents shown in Table 1.

The final poloidal flux distribution of each case is shown in Fig. 3. In case 1, a divertor plasma configuration was formed for a short time. Because the coils are too close to the center axis, the configuration starts to deform after 51 μsec as shown in Fig. 3(a). The coils were then moved away from the axis by 9cm in case 2. Fig. 3(b) is the results at $t = 48$ μsec. Reconnection on the lefthand side of the coils indicates that the coils B and C are too close together or the current in coil B is too weak. On subsequent test runs in which we moved coils B and C further apart a better result was obtained. Case 3 is another coil locations and currents combination. Results in Fig. 3(c) show that the coils are too far from the plasma or the current in coil B is too strong. After moving the coils down by 4cm, we got a final perfect configuration as shown in Fig. 3(d). The time evolution of poloidal flux during the formation of this case is shown in Fig. 4.

In conclusion we demonstrated by simulation that a divertor spheromak plasma configuration is achievable. Its stability and the

control of plasma position by divertors are the subjects of future investigations.

Acknowledgement

This work was supported by DOE Contract No. DE-AC02-CHO-3073

References

1. H. P. Furth, private communication.
2. S. C. Jardin and W. Park, Phys. Fluids 24, 679 (1981).
3. Y. C. Sun and S. C. Jardin, Bull. Am. Phys. Soc. 25, 1023 (1980).
4. M. Yamada, et al, Phys. Rev. Lett. 46, 188 (1981).
5. A. Janos, et al, 137, Proc. of the 4th Sym. on Phys. and Tech. of Compact Toroids (1981).

Case No.	Divertor coil locations						Currents		
	A		B		C		A	B	C
	R(M)	Z(M)	R(M)	Z(M)	R(M)	Z(M)	(KA)	(KA)	(KA)
1	.09	.21	.04	.14	.14	.14	40.	-20.	-10.
2	.15	.21	.11	.14	.19	.14	40.	-10.	-10.
3	.11	.21	.06	.14	.16	.14	40.	-20.	-10.
4	.11	.17	.06	.10	.16	.10	40.	-20	-10.

Table 1. Location and current of the divertor coils.

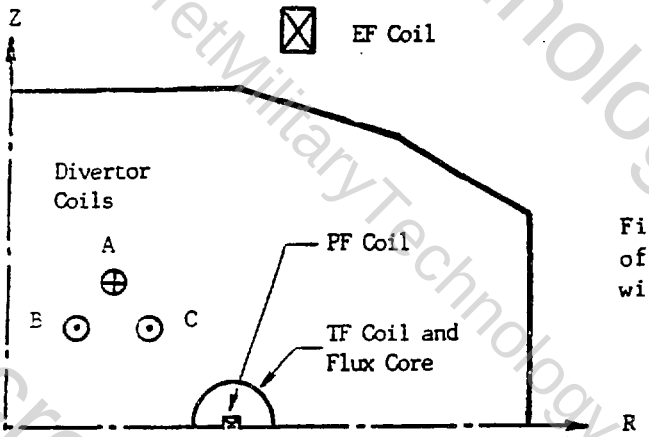

Figure 1. Schematic diagram of the Proto S-1C device with divertors.

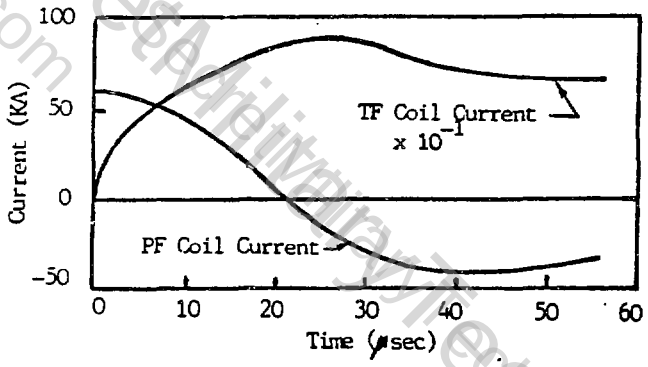

Figure 2. Time evolution of currents of the PF and TF coils during formation.

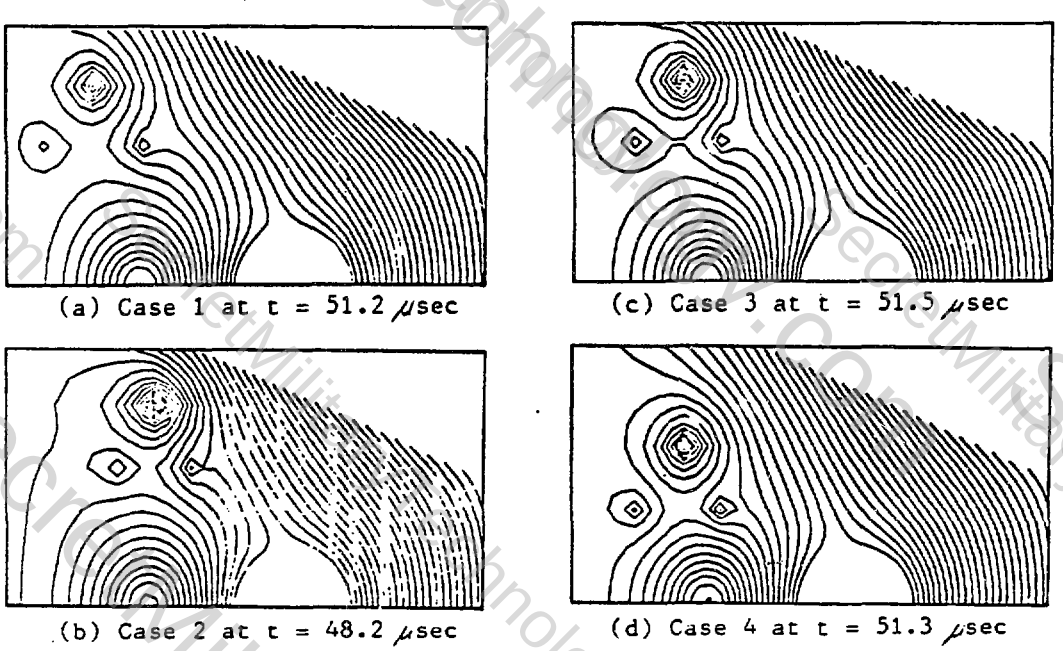

Figure 3. Poloidal flux of case 1 - 4.

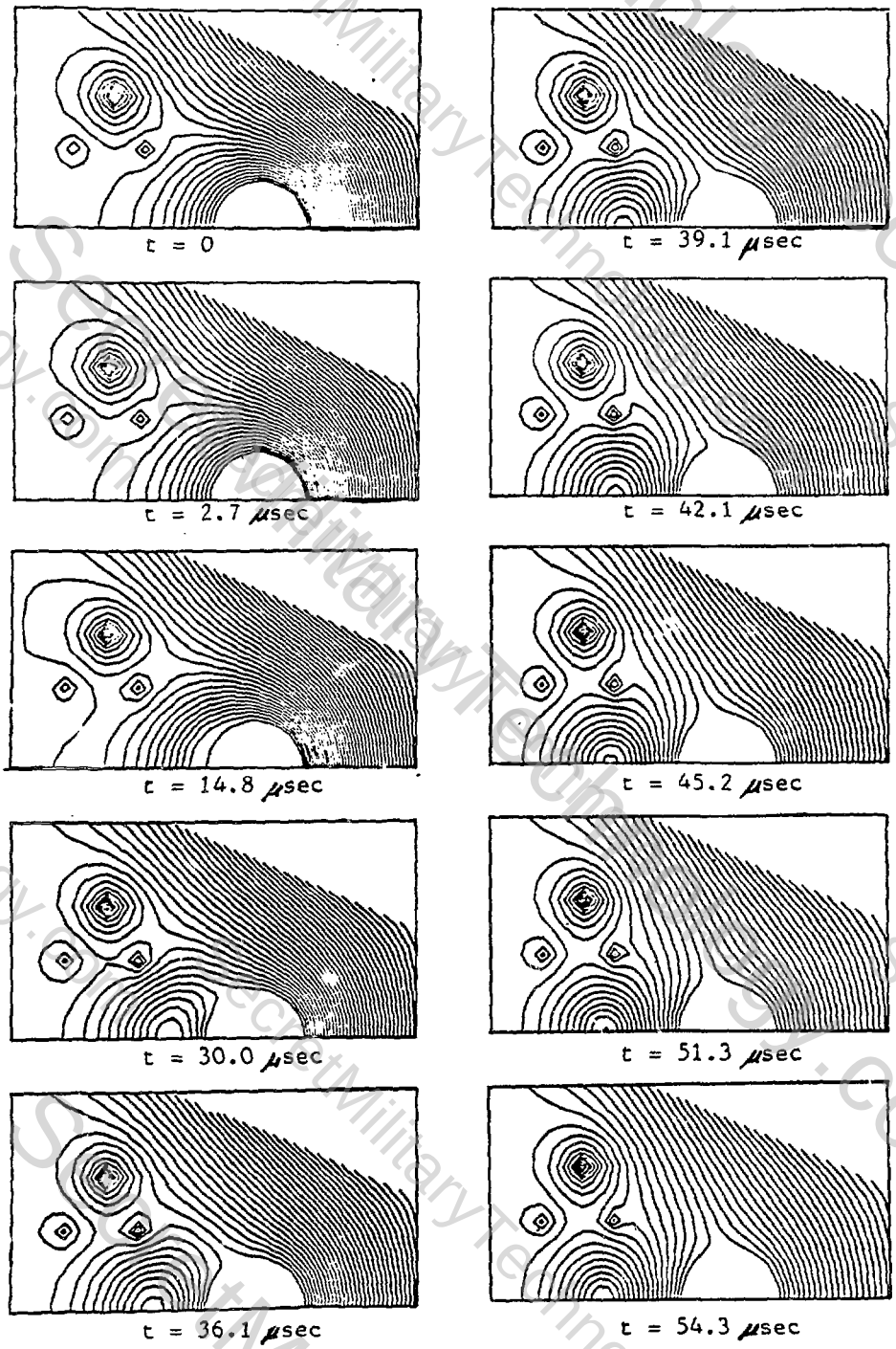

Figure 4. Time evolution of the poloidal flux of case 4.

FRC Equilibrium, Stability and Lifetime

SUPPRESSION OF THE n=2 ROTATIONAL INSTABILITY IN FIELD-REVERSED-CONFIGURATIONS

Alan L. Hoffman, John T. Slough, and Dennis G. Harding
Mathematical Sciences Northwest Inc., Bellevue, Washington

ABSTRACT

Compact toroid plasmas formed in field-reversed-theta-pinches are generally destroyed after 30-50 μsec by a rotating n=2 instability. This instability has been controlled, and the plasma destruction avoided in the TRX-1 theta-pinch through the application of octopole magnetic fields. The decay times for loss of poloidal flux and particles are unaffected by the octopole fields. These decay times are about 100 μs based on inferences from interferometry and excluded flux measurements. The weak, rotating elliptical disturbance (controlled n=2 mode) also made possible a novel determination of the density profile near the separatrix using single-chord interferometry. The local density gradient scale length in this region was found to be about one ion gyrodiameter.

I. INTRODUCTION

During the last decade many laboratories have successfully generated compact toroids in field-reversed-theta-pinches. These plasmas contain no toroidal magnetic field and have been called field-reversed-configurations (FRC). Excepting only the BN experiments at the Kurchatov Institute,[1] it has been universally reported that an FRC spins up and develops a rotating n=2 instability, resulting in destruction of the plasma.[2-6] The TRX-1 experiment at Mathematical Sciences Northwest[4] has been constructed with the same unique features used on the Kurchatov BN experiments, namely fast, independently triggered mirrors to control reconnection, and pulsed octopole "barrier" fields designed to reduce plasma wall contact during the field reversal phase. Compact toroids generated in TRX-1, in a mode nearly identical to that used in the BN devices, still develop the rotational n=2 instability. However, a method has been found to control this instability through the application of the octopole fields throughout the equilibrium phase.

TRX-1 is a 1-m long, 23-cm diameter theta-pinch with a 20-cm internal diameter quartz plasma tube.[4] It employs axial discharge preionization and has been operated on both first and second half cycles. Optimal FRC formation for each operational mode requires a different preionization level and field timing sequence, but the ultimate stability and lifetime properties of a well formed FRC appears to be independent of the generation method. Figure 1 illustrates the time history of the various magnetic fields for second half cycle operation, which was used in the Kurchatov experiments. The octopole barrier fields were normally timed to peak during the field reversal phase and were then shut off (Fig. 1, solid line). Although influencing the amount of

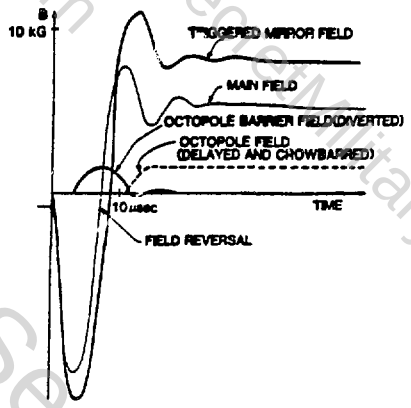

Fig. 1 Second Half Cycle Timing Sequence Indicating Use of Barrier Fields for Enhanced Flux Trapping or Instability Suppression

flux trapped, this method of barrier field employment had absolutely no effect on the toroid stability. In order to separate the barrier field's strong influence on flux trapping from its latter influence on stability, the barrier field timing shown by the dashed line was adopted for the stability experiments. The barrier fields were activated after the field reversal phase and kept on.

II. ROTATION AND DECAY RATES ON THE STABILIZED TRX-1

The excluded flux $\Delta\phi$, the external magnetic field B_e, and the cross tube integrated density $\int n_e d\ell$ were monitored at the center of the theta pinch. A 3.39μ interferometer viewing along a tube diameter was used for the density measurements. A comparison of the excluded flux radius $r_{\Delta\phi} = (\Delta\phi/\pi B_e)^{1/2}$ and interferometer data with and without the octopole barrier fields is shown on Fig. 2. The rotating n=2 distortion is apparent from the sinusoidal variation in the interferometer signal, and its amplitude can be characterized by the excursion of the interferometer reading about an average value. This is seen to be reduced from about 70 percent to 20 percent when the barrier fields are applied. The reduced n=2 distortion agrees qualitatively with observations on a smaller field-reversed-theta-pinch experiment at Osaka University employing quadrapole fields for stabilization.[7]

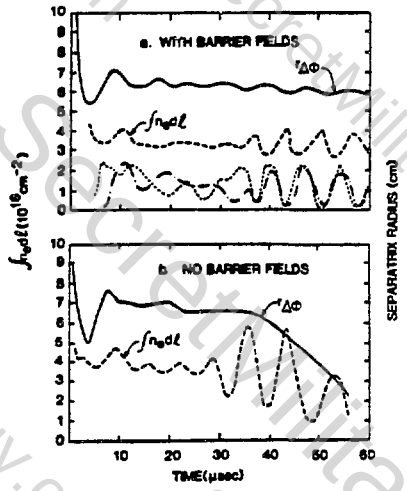

Fig. 2 Suppression of Rotating n=2 Instability by Octopole Preionization
(dotted and dash-dotted interferometer traces were obtained simultaneously on chords 6 cm below and above the tube axis)

The Osaka experimenters found that the quadrapole fields reduced the amplitude of the distortion, and eliminated it entirely when the magnitude of the quadrapole field pressure at the toroid separatrix equaled the centrifugal pressure of the rotating plasma. In particular, a detailed stability analysis by Ishimura[8] shows a critical vacuum multipole magnetic field for stability to an n=2 distortion of

$$B_c = \left[\mu_o \rho\right]^{1/2} \Omega r_s / 2(m-1)^{1/2} \qquad [1]$$

where ρ is the plasma density, Ω is the plasma rotational speed which is taken from the analysis to be twice the observed real mode frequency, ω_r, r_s is the separatrix radius, and m=2 for quadrapole fields and m=4 for octopole fields. For our plasma with $\rho = 8.7 \times 10^{-9}$ g/cm^3, $\Omega = 0.9 \times 10^6$ sec^{-1}, $r_s = 6.3$ cm, and m=4, this critical field strenth is 0.6 kG. The vacuum octopole magnetic field at the separatrix in the TRX-1 experiments is 0.4 kG.

The Osaka and TRX-1 results indicate that barrier fields do not prevent plasma rotation, but that they limit or prevent the instability that ordinarily accompanies rotation. The onset time of the instability also does not appear to be affected by the barrier fields. However, the reduction in amplitude delays the plasma termination (marked by a rapid decay in $r_{\Delta\phi}$) from about 33 μsec without barrier fields to over 60 μsec with barrier fields. The longer time is consistent with a lifetime determined by cross field transport.

It is important to determine the influence of the stabilizing barrier fields on the decay of particles and poloidal flux. Steady multipole fields are believed to open up otherwise closed field lines, leading potentially to enhanced loss rates. The total particle and poloidal flux loss rates for typical examples are plotted on Fig. 3 for operation at various D_2 fill pressures. The poloidal flux is calculated from the elongated equilibrium formula[3]

$$\phi_p = 0.3\, x_s\, \Delta\phi, \qquad [2]$$

and the total number of particles from the interferometer signal and the relationship

$$N = \pi r_s \ell \int n_e d\ell / 2, \qquad [3]$$

where $x_s = r_s/r_c$. The separatrix radius r_s is assumed equal to $r_{\Delta\phi}$ near the coil midplane, r_c is the effective flux conserving radius of 12.5 cm, and ℓ is the nominal plasma length taken to be the distance between the axial locations where the excluded flux falls to one half its peak value. Both the loss of particles and loss of flux seem to be characterized by constant rates of 2×10^{15} particles/μsec-cm of original column length, and 1.5 kG-cm^2/μsec. At the 20 mTorr fill pressure, where the unstabilized plasma lifetimes were long enough to measure decay rates, there does not appear to be any difference in particle or flux loss rate due to the octopole fields. For the present TRX-1 operating conditions, the loss rates increase rapidly at fill pressures above 20 mTorr, most likely due to insufficient plasma temperature. At fill pressures below 7 mTorr, the flux trapping is too inefficient to generate much poloidal flux.

III. DENSITY PROFILE NEAR THE SEPARATRIX

The loss rates shown on Fig. 3 are consistent with measured loss rates (before the onset of instability) on the Los Alamos National Laboratory FRX-B[3] and FRX-C[6] experiments. They are characteristic of an anomalous resistivity equal to about 5 times the classical value at the measured 100-150 eV electron temperatures. The anomalous resistivity undoubtably arises from turbulence driven by steep density gradients and the consequently high drift speeds near the separatrix. We can accurately determine the density profile in this region by positioning cross tube interferometer beams near the undistorted separatrix radius, and observing the small cyclic distortion present when weak barrier fields are used. Traces from two such interferometer beams positioned at locations 6 cm above and below the tube axis are included on Fig. 2a. All three interferometer traces were obtained simultaneously with a three chord interferometer, and the symmetry indicates that the instability is indeed n=2 with very little n=1 wobble. (A noticeable n=1 wobble is present when barrier fields are not used.)

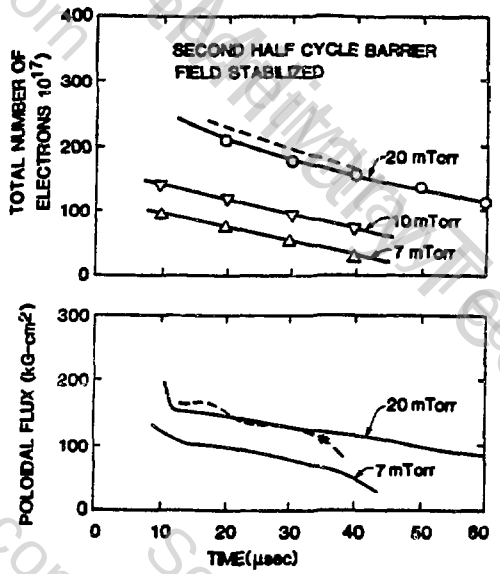

Fig. 3 Illustration of Constant Rates of Total Particle and Poloidal Flux Loss. (dashed line without barrier fields, asterisk indicates onset of n=2 mode)

The density gradient at the separatrix was calculated by graphically inverting the +6 cm interferometer trace between 38 and 44 μsec. The separatrix radius was assumed to have a cyclic variation of the form

$$r_s = r_{so} + \Delta r_s \sin\left[2\omega_r t\right]. \qquad [4]$$

The density was assumed to be a function of r/r_s only. The result of the interferometer signal inversion is shown on Fig. 4. This calculation assumed $\Delta r_s/r_{so} = 0.2$ based on the oscillation amplitude of the signal through the axis. Also shown is the excluded flux radius at 41 μs. For this example, the ion gyroradius based on the ion temperature inferred from pressure balance (220 eV) is about 0.35 cm. Thus, the density gradient scale length is about one gyrodiameter.

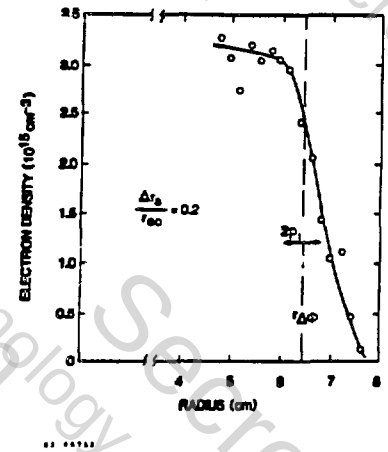

Fig. 4 Density Profile Near the Separatrix Inferred from Unfolded Interferometer Signal (38μs < t < 44μs) on a Chord 6 cm Off the Axis. (20 mTorr fill pressure, second half cycle operation)

The density between the field null at R ≈ 4.5 cm and the separatrix at $r_s \approx 6.4$ cm appears to be nearly uniform, in agreement with MHD calculations[9,10] based on the 2-dimensional MHD relationship for average plasma beta

$$\bar{\beta} = 1 - x_s^2/2 \qquad [5]$$

and lower hybrid drift[11] governed transport. The high average β value of 0.74 implies a relatively flat density profile inside the separatrix (assuming that the temperature profile is relatively flat[3]) which is confirmed by the measurements. The calculated open field line density profile in an MHD model is determined by the competition between radial diffusion and axial streaming loss, and is also in agreement with the measurements.

It has been assumed by most researchers that high density values and steep density gradients near the separatrix are the cause of the anomalously fast measured particle loss rates. The TRX-1 measurements shown on Fig. 4 confirm the density profiles predicted for the low x_s values of only about 0.5. Now that the rotational n=2 instability appears controllable, increasing x_s and reducing the density gradient near the separatrix should be the next goal for field-reversed-configuration research.

Acknowledgements

The authors would like to acknowledge suggestions made some time ago by W. Grossmann and W.P. Dove that steady barrier fields might influence the rotational instability.

This work was supported by DOE Contract #DE AC06-80ER53096.

References

1. A.G. Es'kov, R.Kh. Kurtmullaev, A.P. Kreshchuk. Ya.N. Laukhin, A.I. Malyutin, A.I. Markin, Yu.S. Martyushov, B.N. Mironov, M.M. Orlov, A.P. Proshletsov, V.N. Semyenov, Yu.S. Sosunov, "Features of Plasma Heating and Confinement in a Compact Toroidal Configuration," in Proceedings of the Seventh International Conference on Plasma Physics and Controlled Nuclear Fusion Research, Innsbruck, Austria, 1978 (IAEA, Vienna 1979).

2. A. Eberhagen and W. Grossmann, Z. Physic 248, 130 (1971).

3. W.T. Armstrong, R.K. Linford, J. Lipson, D.A. Platts and E.G. Sherwood, Phys. Fluids 24, 2068 (1981).

4. A.L. Hoffman and W.T. Armstrong, Proceedings of the Fourth Symposium on the Physics and Technology of Compact Toroids, Oct. 27-29, 1981 (Lawrence Livermore National Laboratory, 1982), p. 61.

5. Y. Nogi, et al., Proceedings of the Fourth Symposium on the Physics and Technology of Compact Toroids, Oct. 27-29, 1981 (Lawrence Livermore National Laboratory, 1982), p. 65.

6. M. Tuszewski, et al., "Flux Loss During the Equilibrium Phase of Field-Reversed Configurations," to be published in Phys. Fluids.

7. T. Minato, et al., "Experimental Studies on Confinement of FRC Plasma," in Proceedings of the Ninth International Conference on Plasma Physics and Controlled Nuclear Fusion Research, Baltimore, Md., 1982 (IAEA, Vienna, to be published).

8. T. Ishimura - private communication

9. M. Tuszewski and R.K. Linford, Phys. Fluids 25, 765 (1982).

10. L.C. Steinhauer, R.D. Milroy and A.L. Hoffman, Proceedings of the Fourth Symposium on the Physics and Technology of Compact Toroids, Oct. 27-29, 1981 (Lawrence Livermore National Laboratory, 1982), p. 47.

11. R.C. Davidson and N.A. Krall, Nucl. Fusion 17, 1313 (1977).

Stability Model for One-Dimensional FRCs

J. L. Schwarzmeier, T. Hewitt, H. R. Lewis, C. E. Seyler* and K. R. Symon**
Los Alamos National Laboratory; Los Alamos, NM 87545

The subject of transport near the separatrix in FRC devices is important for determining the performance to be expected from an FRC reactor or from FRC experiments. We are constructing a computer code for studying the micro-stability properties of FRCs near the separatrix as a first step in obtaining quasilinear transport coefficients that can be used in a transport code. We expect to use the code to study instabilities in the frequency range corresponding to the lower-hybrid-drift instability. We consider collisionless ions and electrons, without an expansion in powers of a parameter, like the electron or ion gyroradius, and we approximate the equilibrium with an infinitely long axially and translationally symmetric equilibrium. Thus, in our equilibria, there are only an axial magnetic field and a radial electric field. Our equilibria are collisionless, two-species, diffuse-profile, one-dimensional, θ-pinch equilibria. We allow the possibility that there be a magnetic field null in order to be able to model FRC devices more realistically. The basis for the micro-stability computer code is the formulation of Lewis, Seyler and Symon[1-3] for linearized Vlasov systems with spatially nonuniform equilibria.

*Permanent address: Cornell University; Department of Electrical Engineering; Ithaca, NY 14853
**Permanent address: University of Wisconsin; Department of Physics; Madison, WI 53706

In our model, the distribution function for each particle species satisfies the Vlasov equation and the electromagnetic field satisfies the full Maxwell equations. Our formulation allows the equilibrium distribution functions to be arbitrary functions of the constants of the motion. Our initial choice of the equilibrium distribution function for species s is

$$f_{0s} = c_s e^{-[\alpha_s H_{0s} - \beta_s p_\theta + \gamma_s p_\theta^2]} , \tag{1}$$

where H_{0s} is the equilibrium Hamiltonian for species s, and c_s, α_s, β_s, and γ_s are constants. In position and velocity space, this distribution function is a local drifting Maxwellian. All equilibrium quantities are assumed to depend only on the radial variable of a cylindrical coordinate system. The equilibrium electric and magnetic fields are computed self-consistently. The perturbation distribution functions and electromagnetic potentials satisfy linearized Vlasov and Maxwell equations.

The eigenfrequencies and eigenfunctions for the linearized problem are determined by the properties of a dispersion matrix $D_{\ell\ell'}(\omega)$, where the indicies ℓ and ℓ' refer to an expansion of the perturbation potentials in terms of a set of basis functions. If $\hat{\Phi}_1$ is a column vector of the Laplace-transformed perturbation scalar and vector potentials, then we express $\hat{\Phi}_1$ in terms of basis functions η_ℓ by

$$\hat{\Phi}_1 = \sum_\ell \alpha_\ell \eta_\ell . \tag{2}$$

The coefficients α_ℓ corresponding to a normal mode are determined by the eigenvalue equation

$$\sum_{\ell'} D_{\ell\ell'}(\omega)a_{\ell'} = 0 \ , \tag{3}$$

and the eigenfrequency ω is determined by the condition

$$\det D_{\ell\ell'}(\omega) = 0 \ . \tag{4}$$

The elements of the dispersion matrix are expressed in terms of orbit integrals involving the basis functions η_ℓ and Liouville eigenfunctions w_{sr}, and in terms of particle resonances involving Liouville eigenvalues μ_{sr}. The Liouville eigenfunctions and eigenvalues are defined by

$$L_{s0}w_{sr} = i\mu_{sr}w_{sr} \ , \tag{5}$$

where the index r stands for a list of indices needed to specify a unique eigenfunction. The equilibrium Liouville operator L_{s0} is anti-Hermitian and the eigenfunctions may be taken to be orthonormal. For equilibria of the sort that we are considering, for which there is only one nonignorable coordinate, the functions w_{sr} and the eigenvalues μ_{sr} can be written explicitly.[3]

For our stability code, we are using the expressions appropriate to the dispersion matrix for one nonignorable coordinate that are given in Ref. 3. Our choice of gauge for the electromagnetic potentials is that the radial component of the vector potential vanish. This gauge can always be chosen and does not impose a restriction on the physical problems that can be examined.

References

1) K. R. Symon, C. E. Seyler and H. R. Lewis, J. Plasma Phys. 27, 13 (1982).

2) H. R. Lewis and C. E. Seyler, J. Plasma Phys. 27, 25 (1982).

3) C. E. Seyler and H. R. Lewis, J. Plasma Phys. 27, 37 (1982).

FRC Confinement Studies in FRX-C

K. F. McKenna, W. T. Armstrong, R. R. Bartsch, R. E. Chrien, J. C. Cochrane, Jr., R. W. Kewish, Jr., P. Klingner, R. K. Linford, D. J. Rej, E. G. Sherwood, and M. Tuszewski

Los Alamos National Laboratory
Los Alamos, New Mexico 87545

The measured particle containment times of up to 190 μs in FRX-C correspond to R^2 scaling and agree with predictions based on lower-hybrid cross-field diffusion. Further improvement in confinement may be possible by translating a field-reversed configuration (FRC) in such a way as to increase x_s.

I. Introduction

The particle confinement in FRC plasmas has been experimentally investigated in the FRX-C device over a significant range of parameters. The results from this study, and data from the smaller FRX-B machine, confirm the approximate scaling of particle containment time with R^2/ρ_{i0}. In addition, these results are in excellent agreement with predictions by Tuszewski and Linford[2] based on a model that assumes lower-hybrid cross-field transport driven by the sharp density gradients that are characteristic of the high-beta FRC equilibrium. The model also predicts that reduced density gradients resulting from increased x_s (the ratio of FRC separatrix radius to conducting wall radius) should result in substantial increases in particle confinement time. The ratio x_s can be increased by axially translating an already formed FRC out of the theta-pinch coil (formation region) into an appropriately shaped and magnetically biased flux conserver. Experiments in the next two years will involve translating FRCs, increasing x_s, and testing the predicted increase of particle confinement time.

II. Description of Experiment

The FRX-C device is a field-reversed theta pinch. The coil is 2 m long and 0.5 m in diameter; passive mirrors 0.20 m in axial extent and 0.44 m in diameter provide an on-axis mirror ratio of 1.17 at each end. The quartz discharge tube has an inner diameter of 0.4 m. The bias field is variable to about 4 kG. The main field rises in 4.5 μs to about 10 kG and has a crowbarred decay time of 300 μs.

An axial array of magnetic field probes is used to determine the excluded flux radius $r_{\Delta\phi}$. In regions of straight field lines the separatrix radius can be approximated as $r_s = r_{\Delta\phi}$ and the major radius is $R = r_s/\sqrt{2}$. A side-on 3.39-μm double-pass interferometer is used to measure $\int n d\ell$ through a diameter of the FRC near the coil midplane. Measurements of T_e by Thomson scattering are taken with the scattering volume located 5 cm off the coil axis and 10 cm from the coil midplane. Neutron emission is measured with a scintillator and an activation counter. An end-viewing, double-pass, ruby-laser holographic interferometer is used to measure particle inventory and radial density profile. Visible and VUV spectroscopy are used for line intensities and line broadening measurements.

III. FRC Formation Phase

The process of FRC formation in a theta pinch has been described elsewhere.[1] To form long-lived FRCs it is necessary to adjust empirically the initial fill pressure, bias field level, passive magnetic mirror ratio, and preionization conditions. The mirror ratio appears to have a strong influence on the field-line reconnection at the plasma ends. When first operated, FRX-C had a mirror ratio of 1.05. With an initial pressure of 20 mtorr of deuterium, the FRC shape as deduced from the magnetic probe array often lacked symmetry and indicated an axial movement of the FRC out of the coil. According to MHD code simulations, reconnection proceeds more rapidly if the mirror strength is increased, thus reducing the likelihood of reconnection asymmetry. A larger mirror ratio (1.17) was installed on FRX-C and the result was improved symmetry of the $r_{\Delta\phi}$ profiles and a reduced tendency for axial motion.

IV. Typical Plasma Parameters

Data obtained on a typical discharge at 20 mtorr fill pressure and 1.7 kG bias field are shown in Fig. 1 as a function of time. The external magnetic field waveform, B, is recorded near the coil midplane. The FRC length, $\ell_{\Delta\phi}$, is defined as the distance between the axial positions where $r_{\Delta\phi}$ decreases to 65% of its maximum value. The average density is defined as $\bar{n} = \int n d\ell / 4 r_{\Delta\phi}$. The value of $\bar{n}$ differs little from the volume-averaged density. The electron temperature measured by Thomson scattering on similar discharges is $T_e = 100 \pm 20$ eV. The total temperature, $T_e + T_i$ is deduced from pressure balance. The quiescent plasma confinement phase is terminated by a rotational n = 2 instability that begins at about 100 μs. The growth of the n = 2 distortion can be identified by the modulation of the side-on interferometer density data. End-on holograms also show the n = 2 nature of the instability.

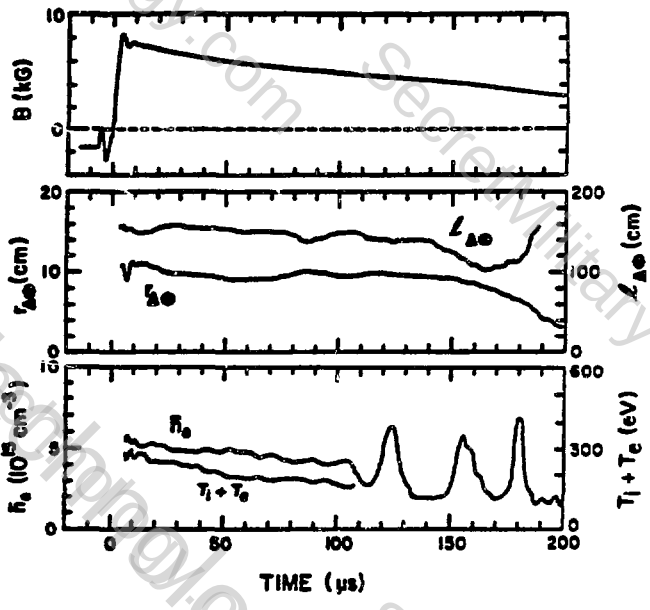

Figure 1.

Data obtained at 5 mtorr fill pressure display higher temperatures, measurable neutron emission, and shorter quiescent periods. Assuming a Maxwellian ion velocity distribution, the measured neutron emission, combined with density and volume measurements, corresponds to a peak ion temperature of about 1.0 keV at 10 μs. Line broadening of CV, if interpreted as thermal Doppler broadening, corresponds to T_i of about 3 keV at 10 μs, or about five times the pressure balance temperature, dropping to a factor of two at 30 μs. The pressure balance temperature of about 0.5 keV is considered the most reliable, but further study of this issue is needed. Electron temperature from

Thomson scattering is 175 ± 25 eV.

V. Scaling of Particle Confinement

It was reported for FRX-B at 17 mtorr filling pressure that the particle confinement time was $\tau_N = 39 \pm 15$ μs.[1] The magnetic field, temperature, and density were similar to the FRX-C parameters at 20 mtorr. The particle inventory in FRX-C at 5 and 20 mtorr has been measured by the end-viewing holographic interferometer, and independently estimated from the density measured by the side-on interferometer and volume measured by the magnetic probe data. A least-squares fit of an exponential to the more definitive holography data gives for the e-folding decay time $\tau_N = 68 \pm 25$ μs at 5 mtorr and $\tau_N = 187 \pm 25$ μs at 20 mtorr. Figure 2 presents the particle containment time as a function of the scaling parameter R^2/ρ_{io} (ρ_{io} = ion gyro radius). The solid dots are predictions of the Tuszewski-Linford lower-hybrid transport model. The open circles are the particle confinement times determined from holography. The half-open circles are from the side-on interferometer and magnetic probe data. Although the particle confinement time scales approximately linearly with R^2/ρ_{io}, as originally suggested by Hamasaki[3], it is also clear from the Tuszewski-Linford model that other factors such as x_s, open-field-line confinement, temperature, etc., are important. It is clear that the predictions of the lower-hybrid transport model and the experimental results are in good agreement, and confirm the R^2 scaling of particle confinement in an FRC.

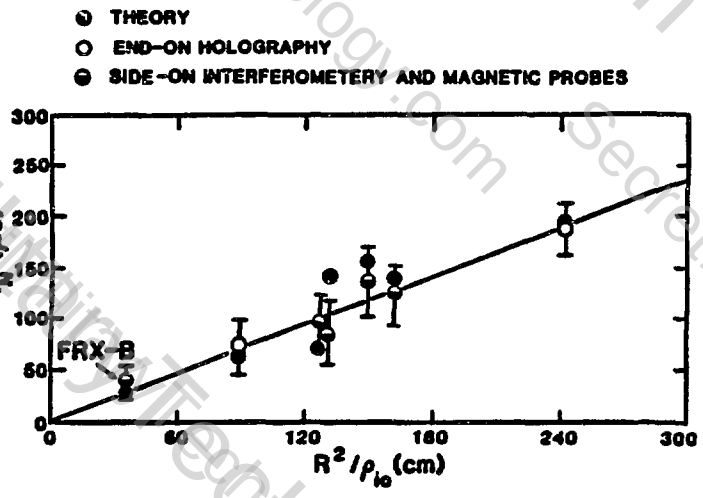

Figure 2.

The FRC stable period, defined as the duration of the quiescent phase before the onset of the n = 2 rotational mode, is observed to increase as the containment time increases. However, neither the experimental data nor the theoretical understanding of the n = 2 mode is sufficient to define the appropriate scaling of the stable period. It was recently reported by Ohi at Osaka that the n = 2 can be suppressed by application of quadrupole fields following FRC formation.[4] A quadrupole system has recently been added to FRX-C and preliminary results also demonstrate stabilization of the n = 2 mode. Presuming that quadrupole stabilization has no detrimental effect on confinement, the most important concerns for FRC research become transport scaling and MHD stability as the ratio of density gradient length to ion gyro radius is further increased.

VI. Translation Plans

Axial translation of an FRC without excessive losses of particles, flux, or energy leads to a variety of attractive fusion reactor possibilities. The process of translation should permit increased values of x_s and corresponding increases in the particle confinement time. The particle confinement can be improved because the density gradient is reduced when x_s is increased. In Fig. 3 the predicted radial beta profiles are compared for $x_s = 0.5$ and $x_s = 0.9$. Beta is defined here as local nT relative to external $B^2/8\pi$. Thus, for uniform temperature, β and density are proportional. The reduced density gradient seen for $x_s = 0.9$ is mostly a result of the average beta condition for an FRC, $\langle\beta\rangle = 1 - x_s^2/2$ where $\langle\beta\rangle$ is the volume-averaged beta inside the separatrix.[1] The predicted particle confinement time is increased by a factor of five for conditions that are similar to FRX-C.

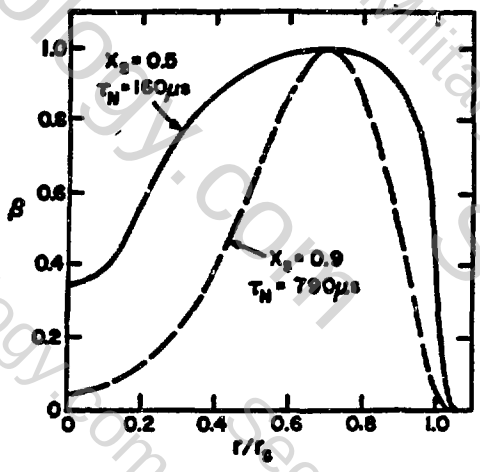

Figure 3.

The design for the transition region where the FRC enters a close-fitting flux conserver is still evolving. For a first approximation, it may be assumed that the FRC undergoes a completely adiabatic process with no losses of magnetic flux, energy, or particles. By assuming a particular uniform pressure profile, $\beta = \langle\beta\rangle$ that contains the maximum flux for a given x_s, analytic calculations are easily carried out. However, as discussed in these proceedings, more refined calculations are underway that take into account dynamic effects by use of a 2-D MHD code.[5] In addition, an analysis of the effects of diffuse profiles has also been carried out.[6]

References

1. W. T. Armstrong, R. K. Linford, J. Lipson, D. A. Platts, and E. G. Sherwood, Phys. Fluids 24, 2068 (1981).
2. M. Tuszewski and R. K. Linford, Phys. Fluids 25, 765 (1982).
3. S. Hamasaki and N. A. Krall, Conference Record IEEE International Conference on Plasma Science, Montreal, 5E10 (IEEE, New York, 1979).
4. T. Minato et al, Paper M-3, Proc. of the 9th International Conference on Plasma Physics and Controlled Nuclear Fusion Research, Baltimore, Md., (1982).
5. W. T. Armstrong and R. D. Milroy, these proceedings.
6. M. Tuszewski, R. Spencer, and R. K. Linford, these proceedings.

Velocity-Space Particle Loss in Field-Reversed Configurations

Ming-Yuan Hsiao and George H. Miley
Fusion Studies Laboratory
University of Illinois
103 S. Goodwin Avenue
Urbana, IL 61801

The particle confinement criteria for axisymmetric field-reversed configurations (FRCs) are obtained from the two constants of motion, H and P_θ [1-3]. Here, H and P_θ are the total energy and canonical angular momentum of a particle. It is found that only part of (H,P_θ) space is available for particle confinement. As with the loss in velocity space for a simple mirror, a loss region in (H,P_θ) space, or equivalently in velocity space, have a significant influence on plasma behavior in FRCs. In present work we study the effect of this loss region on particle loss.

For simplicity, approximate particle confinement criteria[1] are used. Furthermore, the lower bound on P_θ/q, which represents a constraint for particle confinement and reduces the confinement region in (H,P_θ) space[1], consequently in $(\underset{\sim}{r},\underset{\sim}{v})$ space, is neglected. The particle confinement criteria then become:

$$\left.\begin{aligned} \frac{(P_\theta - \frac{q}{c}\psi)^2}{2mr^2} \leq H < -\frac{qB_o}{mc} P_\theta \ , \\ P_\theta/q < 0 \ . \end{aligned}\right\} \tag{1}$$

With a fast loss of unconfined particles the constraints on the particle distribution function, f, are f = 0 on the loss boundary and f finite for all $\underset{\sim}{v}$. In present case, after shifting the origin of (v_r,v_θ,v_z) space from (0,0,0) to $(0, -qB_0r/mc, 0)$, this condition becomes $f(\underset{\sim}{r},\underset{\sim}{v},t) = 0$ for $|\underset{\sim}{v}| = v = v_c(r,z)$, where $v_c(r,z) = |q|B_0r(1-2\psi/B_0r^2)^{1/2}/mc$, and all other notations follow convention. This represents a spatially dependent

but isotropic boundary condition in velocity space for f.

Let us consider the particle loss due to like-particle collisions. Making use of the assumption that the spatial gradient is relatively small and the fact that $\underset{\sim}{v} \times \underset{\sim}{B} \cdot \nabla_{\underset{\sim}{v}} f$ vanishes for an isotropic f, the Fokker-Planck kinetic equation in spherical velocity coordinates, (v,θ_v,ψ_v), reduces to $\partial f(r,z,v,t)/\partial t = (\partial f/\partial t)_c$. By using a model distribution function, f_o, for f in evaluating the Rosenbluth potentials, g and h, where

$$f_o(\underset{\sim}{r},\underset{\sim}{v}) = n(r,z)\, C_1(r,z)\left(1 - \frac{v^2}{v_c^2}\right) \exp\left(-\frac{v^2}{v_c^2}\right) U\left(1 - \frac{v}{v_c}\right) , \tag{2}$$

$$C_1(r,z) = \left\{ \int_0^{v_c(r,z)} 4\pi v^2 \left(1 - \frac{v^2}{v_c^2}\right) \exp\left(-\frac{v^2}{v_c^2}\right) dv \right\}^{-1} ,$$

U(x) and n being the heavy-side unit step function and particle number density, respectively, and changing variable $\underset{\sim}{v} = \underset{\sim}{v}' v_c$, the kinetic equation becomes

$$\frac{\partial F(r,z,v',t)}{\partial t} = \frac{\Gamma n}{v_c^3} D\{F\} , \quad 0 \leq v' \leq 1 , \tag{3}$$

with

$$\left.\begin{aligned} &F(r,z,v',t) = 0 \text{ for } v' = 1 , \\ &F(r,z,v',t) \text{ finite for all } v'. \end{aligned}\right\} \tag{4}$$

Here D is a second order differential operator depending on v' only, $F(r,z,v',t) \equiv f(r,z,v \equiv v'v_c,t)$ and $\Gamma = 4\, q^2 \ell n \Lambda / m^2$. Equation (3) is linear in F and separable in $\underset{\sim}{r}$ and v'.

In solving the boundary-value problem, defined by Eqs. (3-4), it is useful to solve the following eigenvalue problem first:

$$D\{V(v')\} = \alpha V , \quad 0 \leq v' \leq 1 , \tag{5}$$

with V(1) = 0 and finiteness of V. This is done numerically. As evident from Eq. (3), the i-th mode decays exponentially with time constant $v_c^3/|\alpha_i|\Gamma n$; the larger $|\alpha_i|$, the faster decay. Therefore, near collisional equilibrium the only dominant mode is the fundamental mode. Figure 1 compares the

fundamental mode, $V_1(v')$, with the model distribution function, $V_0(v')$. The comparison is favorable and demonstrates that: (1) the linearization of the Fokker-Planck collisional term by using the model distribution function, Eq. (2), is valid, (2) the model distribution function is a good analytic representation of the actual distribution near collisional equilibrium, i.e. between V_0 and V_1.

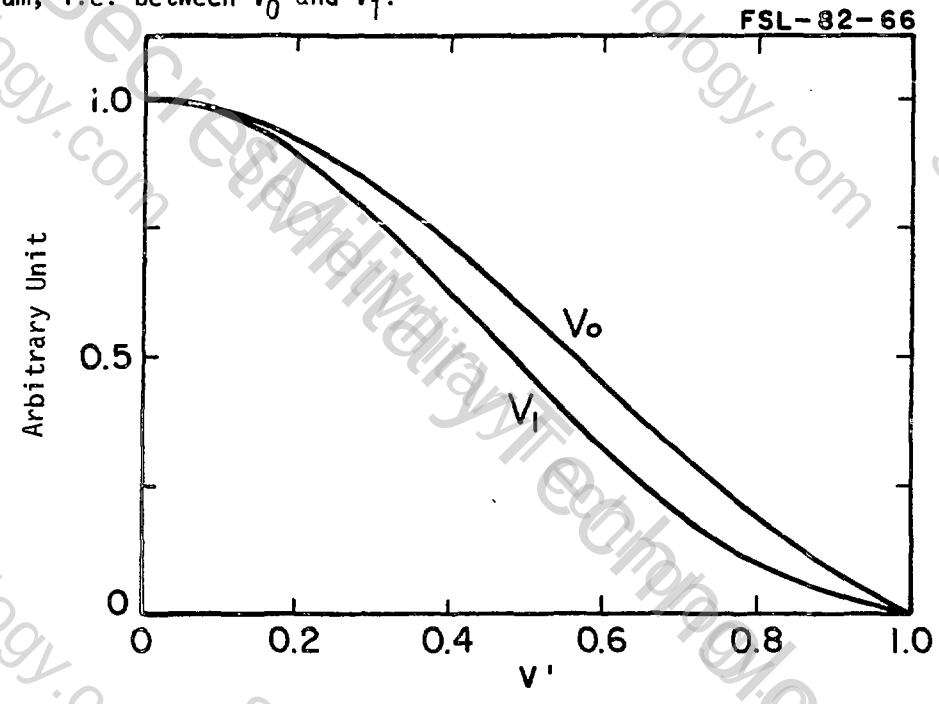

Figure 1. Comparison between $V_0(v')$ and $V_1(v')$.

Based on Eq. (3), the local particle confinement time, τ_p, defined by $-n/(\partial n/\partial t)$, is given by

$$\tau_p(r,z) = v_c^3/C_3\Gamma n \ , \qquad (6)$$

where $C_3 = 0.51$ for $V(v') = V_1(v')$, 0.97 for $V(v') = V_0(v')$. Since the equilibrium distribution lies between V_0 and V_1, for the FRX-A experiment[4] data the τ_p at field null is between 350-700 μs. Assuming rigid-rotor equilibrium density profile and magnetic field, i.e., $n(r) = n_m \mathrm{sech}(K(r^2/R^2-1))$, $B(r) = B_0 \tanh(K(r^2/R^2-1))$, the $\langle\tau_p\rangle$ (averaged over $0 \le r \le R_s = \sqrt{2}\,R_0$) for the FRX-A data is between 3.6-7.2 μs. This is shorter than the observed

value, 58 μs measured at 10 μs after implosion, probably due to the assumption of a fast loss. Still, this shows that the velocity-space particle loss, more precisely, the particle loss due to the existence of the loss region in velocity space, is very important and can be large enough to account for the observed short particle confinement time.

In conclusion, near collisional equilibrium, the particle distribution subjected to a loss boundary in velocity space is obtained. A simple analytic expression is found to be a good approximation for the distribution function. The velocity-space particle loss rate and the corresponding particle confinement time due to like-particle collisions are calculated. The important of this mechanism is demonstrated by the relatively short $<\tau_p>$ prediction.

References

1. M.-Y. Hsiao and G. H. Miley, "Particle Confinement Criteria for Axisymmetric Field-Reversed Magnetic Configurations," Internal Report COO-2218-214, Fusion Studies Laboratory, University of Illinois, April 1981.
2. M. Y. Wang and G. H. Miley, Nuclear Fusion, 19, 39 (1979).
3. R. V. Lovelace, et al., Phys. Fluids, 22, 701 (1979).
4. W. T. Armstrong, et al., Phys. Fluids, 24, 2068 (1981).

A BURN DYNAMIC EXPERIMENT BASED ON THE FIELD REVERSED THETA PINCH

George H. Miley
Fusion Studies Laboratory
University of Illinois
103 S. Goodwin Avenue
Urbana, IL 61801 USA

ABSTRACT

A D-T burn dynamic experiment using a scaled-up field-reversed theta-pinch device is proposed as a first step towards demonstration of a D-^{3}He burn. The feasibility of such an experiment is based on a loss-cone-like confinement scaling plus the use of combined pellet and neutral-beam injection to heat the plasma, build-up its density, and damp the m=2 instability.

Introduction

Advanced-fuel fusion offers many potential advantages: the elimination of tritium breeding; reduced neutron fluxes, i.e., reduced materials damage; and improved energy conversion efficiency (see Ref. 1 and refs. therein). Fuels such as p-^{11}B are long range goals. Still many advantages are offered by nearer-term deuterium-based fuels; especially, catalyzed-deuterium (Cat-D), semicatalyzed-deuterium (SCD), and D-^{3}He, all of which are independent of tritium breeding. A particularly interesting scenario would be to extract ^{3}He from the exhaust plasma from a SCD plant for use in satellite D-^{3}He units[2].

These thoughts seem quite idealistic as we are still struggling to demonstrate scientific feasibility with D-T fuel. However, once a D-T burn is achieved, thermal run-away to the temperatures required for SCD or D-^{3}He operation (~40-50 keV) may be straightforward. (In fact, control systems appear necessary to prevent run-away for D-T operation).

For eventual use as an advanced-fuel reactor, the confinement scheme selected must have a high β and favorable $n\tau$-T scaling. Both features are characteristic of compact tori concepts such as the Spheromak, Field Reversed Mirror (FRM) and Field Reversed Theta Pinch (FRTP).[3]

An essential element in the development of advanced fuels would appear to be the timely development of an experimental compact tori facility capable of burn dynamic studies, starting with D-T and eventually extending to D-^{3}He. In the present discussion we consider the possibility of using a FRTP for such a facility since: 1) FRX experiments at LANL are encouraging[4], 2) the loss-cone scaling relations proposed by Fang and Miley [5] predict favorable scale-up 3) and as proposed here, the use of neutral-beam and pellet injection would allow a rapid scale-up from present experiments.

Loss-Cone-Scattering Transport (LCST) Theory

Available experimental data is too limited to predict confinement scaling for the FRTP over the range desired. Nor is there any basis to justify use of other scaling laws, e.g., Alcator scaling. Consequently, a key aspect of the present study is the formulation of the LCST scaling law briefly outlined below.

The physical basis for LCST theory is that in the reversed-field geometry, particles having a prescribed range of energy and canonical angular momentum will be absolutely confined, but particles falling out of this range can escape along open-field lines. Then LCST theory assumes that particle losses are dominated by collisions that result in confined particles changing their energy-momentum such that they escape.

By definition the particle confinement time for species α, (α = ions, electrons), designated by $\tau_{p\alpha}$, is

$$\tau_{p\alpha} = - N_\alpha/(dN_\alpha/dt) = N_\alpha \left[\int dV \sum_\beta \oint_{S_V} \underset{\sim}{j}^{\alpha/\beta} \cdot d\underset{\sim}{S} \right]^{-1} , \qquad (1)$$

where N_α is the total number of particles present in the plasma volume V, S_V is the boundary surface for losses in velocity space, $d\underset{\sim}{S}$ is a surface element on this boundary, and $\underset{\sim}{j}^{\alpha/\beta}$ is the particle current in velocity space due to collision of species α with species β. In the present case, the loss boundary in (v_r, v_θ, v_z) space can be shown [6,7] to be a sphere of radius v* centered at $v_\theta = -r\,\omega_o$ where:

$$v^* = \left[(-2q_\alpha(\omega_o\psi + \phi) + m_\alpha r^2 \omega_o^2)/m_\alpha \right]^{1/2} , \qquad (2)$$

Here $\omega_o \equiv q_\alpha B_o/m_\alpha$ where B_o is the magnetic field in the end throat region and q_α and m_α are the particle charges and mass, respectively, ψ and ϕ are the magnetic flux function and electric potential at position r, respectively.

The current $\underset{\sim}{j}^{\alpha/\beta}$ required in Eq. (1) is given by

$$j_\ell^{\alpha/\beta} = \frac{F_\ell^{\alpha/\beta}}{m_\alpha} f_\alpha - \sum_k D_{\ell k}^{\alpha/\beta} \frac{\partial f_\alpha}{\partial v_k} , \qquad (3)$$

where ℓ indicates the velocity coordinate $F_\ell^{\alpha/\beta}$ and $D_{\ell k}^{\alpha/\beta}$ are the dynamic friction and diffusion tensors, respectively, and f_α is the distribution function for species α. The LCST approximation assumes that f_α can be represented as an exponential rigid rotor modified to vanish on the boundary S_V. These relations are used to calculate $\tau_{p\alpha}$ using the equilibrium density profile $n(r)$, magnetic flux function $\psi(r)$, and electric potential profiles $\Phi(r)$ consistent with the modified rigid rotor assumption for f_α.

Scaling Predictions

The numerical results from τ_p calculations have been correlated as a function of five key parameters: the ion temperature T_i, external field B_{ext}, peak density n_m, field coil radius r_c, and reversal factor K. The relation is:

$$\tau_p \sim T_i^{0.2} K^{2.7} r_c^{1.8} B_{ext}^{2.5} n_m^{-1} \quad . \tag{4}$$

A test of this scaling is shown in Table I where predicted confinement times are compared with reported τ_p's (or, alternately, the "stable" time τ_s). Reasonable agreement is seen for cases other than for the experiment by Eskov, et al. which appears to have been limited by the magnetic field decay time.

In addition to being consistent with experiments covering a wide range of parameters, the LCST model also predicts the plasma rotation observed in FRTP experiments reasonably well.[15]

Burn Dynamic Pilot Unit

A key aspect of the present concept is the use of neutral beam and pellet injection. In addition to heating and refueling, with proper orientation, the momentum associated with the injected neutral beam can help suppress the m=2 rotational instability[5] Likewise, pellet injection can be designed to maintain the plasma pressure profile near its equilibrium, providing diamagnetic currents that aid in maintenance of field reversal[12].

The design parameters for the proposed FRTP device are summarized in Table II and are compared with TRACT [11] (a conceptual FRTP reactor by Mathematical Sciences NW). The present device would use a 24-KG external field, a 0.29-m plasma with density $\sim 3 \times 10^{20} m^{-3}$. Neutral-beam injection plus the start-up implosion energy would provide 36-MW input power (P_{in}) and result in a fusion power of ~100 MW over the burn time of 4.5 sec. In addition to the beam/pellet injection, a major difference compared with TRACT is that the lower neutron wall-loading (P_{NW}) of ~2MW/m^2 (vs 15 MW/m^2 for TRACT).

With the 100-keV neutral-beam injection-energy selected (cf 15 MW of heating power), a beam current of 150 A is indicated. With a current density limit of 0.2 A/cm^2 for the neutral beam, a cross section of 730 cm^2 is required, (cf ~15% of the plasma end surface area). Despite the complex implosion coil structure, space of this magnitude appears to be available.

The neutral-beam current of 150 A provides ~12% of the required refueling rate, the remainder being supplied by pellet injection. Still the angular momentum carried by the neutral beam is about 40-60% of the background ions, providing a significant control over excessive spin-up.

Burn Dynamics Experiments

The pilot unit described in the preceding section would mainly be used to establish $n\tau_E$ scaling up to temperatures of order of 30-40 keV. This would be done with a programmed decrease in density (largely controlled by pellet injection) in order to maintain pressure balance without excessive plasma expansion.

Once high temperature experience is obtained with D-T excursions, an extension to D-^{3}He (i.e., replace tritium as it fuses with ^{3}He) could be attempted. $n\tau_E$ requirements for D-^{3}He are about an order of magnitude higher than for D-T. However, successful operation with a larger reversal factor, e.g., $K \sim 2.5$ vs the K=1 assumed in the design, could make up this deficit. ^{3}He fueling could be obtained by designing the neutral-beam injectors to handle both tritium and ^{3}He (see Ref. 13 for design considerations related to a ^{3}He neutral-beam injector). Pellet fueling with ^{3}He offers higher fueling rates, but this requires developing appropriate ^{3}He pellets, e.g., a deuterium-shell type noted in Ref. 14. Gas puffing could provide an alternative approach, but then maintenance of the desired pressure profile would have to rely on deuterium pellet injection.

Summary

The main point to be made from this study is that, based on present understanding of FRTP scaling, a high-β compact tori ignition (or burn) experiment appears feasible. A key aspect of the present design is the use of neutral-beam and pellet injection to supplement the implosion heating. Additional experiments and theoretical studies are obviously necessary. However, due to the relative small size of the device, experiments could be done with minimum cost and time. If successful, the high β of the device should open the door to attractive reactors including advanced-fuel Cat-D and D-^{3}He devices.

References

1. G. H. Miley, "Advanced Fuel Concepts and Applications" Proceedings, Third IAEA Technical Committee Meeting and Workshop on Fusion Reactor Design and Technology, Tokyo, Japan (October 1981).

2. E. Greenspan and G. H. Miley, Nuclear Technology/Fusion 2 (1982) 590.

3. G. H. Miley, et al., "Confinement Approaches for Burning AFs," Fourth ANS Topical Meeting on Fusion, King of Prussia, PA, Vol.II, (1980) 932.

4. W. T. Armstrong, et al., "Field Reversed Experiments (FRX) on Compact Toroids," Los Alamos Nat. Lab. Rept. LA-UR-80-1585 (1980); also see Phys. of Fluids 24 (1981) 2068.

5. Q.T. Fang and G. H. Miley, "Particle Confinement in FRTP with Loss-Cone-Like Scattering," Proceedings, Third Symp. on Plasma and Tech. of Compact Toroids in the Magnetic Fusion Energy Program, Los Alamos, NM, (Dec 1980) 144. Also Bult. Am. Phys. Soc. 26 (1981) 946.

6. M. Y. Wang and G. H. Miley, Nucl. Fusion, 19 (1979) 39.

7. M.-Y. Hsiao and G. H. Miley, "Particle Confinement Criteria for Axisymmetric Field-Reversed Magnetic Configurations," Report COO-2218-214, Fusion Studies Lab., University of Illinois, April, 1981,

8. A. C. Kolb, et al., Plasma Phys. and Contr. Nucl. Fusion Res. 1 (1966) 261.

9. A. Eberhagen and W. Grossman, Z. Phys. 248 (1971) 130.

10. A. G. Es'kov, et al., "Features of Plasma Heating and Confinement in a Compact Toroidal Configuration," Int'l Conf. on Plasma Phys. and Contr. Nucl. Fusion Res. II (1978) 187.

11. A. L. Hoffman, "CT-TRX: A Triggered-Reconnection Compact Toroid Experiment," Rept. 80-1144-3, Math Sciences Northwest, Bellevue, Washington, (May 1980).

12. G. H. Miley and J. G. Gilligan, Energy 4 (1979) 163.

13. A. S. Blum and R. W. Moir, "120-keV Helium-3 Neutral Beam Injector: Design Considerations," in EPRI ER-919, Exploratory Studies of High-Efficiency Advanced-Fuel Fusion Reactors, Electric Power Research Institute (Dec. 1978).

14. C. K. Choi, J. Gilligan and G. H. Miley, Exploratory Studies of High-Efficiency Advanced-Fuel Fusion Reactors, Electric Power Research Institute (Dec. 1978), EPRI AP-1437, (July 1980).

15. Q. T. Fang and G. H. Miley "Rotation Model for the FRTP," Proceedings, Sherwood Mtg. on Theoretical Aspects of Research, Tuscon, Arizona Paper 2B 47, (April 1980).

Table I Operating Parameters and Predicted Confinement Times

Parameters	Kolb, et al. Ref. 8	Eberhagen & Grossman Ref. 9.	A.G. Es'kov, et al. Ref. 10	FRX-B Ref. 4	TRX-1 Ref. 11
External Field, B_{ext} (T)	6.3	1.4	1.0	0.75	0.55
Peak density, n_m ($10^{15}cm^3$)	50	44	8.3	4.1	2.5
Ion temp., T_i(eV)	1000	60	100	240	200
Radius, R(cm); length, L(cm)	0.7;180	1.4;40	11.0;150	4.0;36	4.95;80
Field coil radius, r_c(cm)	7*	7*	23*	12.5	12.0
Obs. stable time, τ_s(μs)	15	7-13	100+	20-40	40-50
Measured τ_p (μs)	**	**	**	40-80	50
LCST Prediction, τ_p (μs)	13	5	450	53	78

+ B_{ext} decay time ~200μs
* Estimated
** Not reported

Table II Comparison of the Proposed FRTP with TRACT

Parameters	RFTP Concept Present	TRACT Ref. 11
R (m); L(m); r_w(m)	0.29; 10.0; 0.45	0.24; 2.1; 0.5
T_i (keV)	15.0	15.0
B_{ext} (kG)	24.0	70.0
$\bar{n}$ ($10^{21}m^{-3}$)	0.3	2.0
P_{in}(MW); P_F(MW)	36; 106	(80)†; (550)
P_{NW} (MW/m^2)	2.0	15.0
$<\beta>$	0.76	(0.5)
τ_{burn} (s)	4.5	0.5
τ_E scaling	0.8 τ_p(LCST)	1/30 τ_{class}
Q	2.4	-
P (MW)	26	90

† magnetic compression energy
( ) estimated values

ADIABATIC COMPRESSION OF ELONGATED FIELD-REVERSED CONFIGURATIONS*

R. L. Spencer, M. Tuszewski, and R. K. Linford
Los Alamos National Laboratory
University of California
Los Alamos, NM 87545

I. INTRODUCTION

The simplest model of plasma dynamics is the adiabatic model. In this model the plasma is assumed to be in MHD equilibrium at each instant of time. The equilibria are connected by the requirement that they all have the same entropy per unit flux, i.e., the equilibria form a sequence generated by adiabatic changes. The standard way of computing such a sequence of equilibria was developed by Grad[1], but its practical use requires a fairly complicated code. It would be helpful if approximately the same results could be gotten either with a much simpler code or by analytical techniques. In Sec. II a one-dimensional equilibrium code is described and its results are checked against a two-dimensional equilibrium code; in Sec. III an even simpler analytic calculation is presented.

II. ONE-DIMENSIONAL ADIABATIC MODEL

Elongated FRC equilibria can very nearly be described as two regions with straight field lines connected by a short transition region with curved field lines (see Fig. 1). This property makes it possible to extract two-dimensional information from one-dimensional calculations. It will be exploited here to obtain an approximate model for adiabatically changing FRC equilibria.

Consider an elongated FRC in a conducting cylinder of radius r_w, as shown in Fig. 1. It has magnetic flux $2\pi\psi_o$ outside of the separatrix and magnetic flux $2\pi\psi_t$ inside the separatrix. It has pressure profile $p(\psi)$, where ψ is the poloidal flux function, and separatrix length ℓ. We restrict our discussion to the case where the pressure vanishes on and outside the separatrix; the pressure is also assumed to rise monotonically from the separatrix to its maximum value, p_m, at the equilibrium vortex point. Imagine now that an initial equilibrium is adiabatically changed by slowly varying either r_w or ψ_o. Note that reversibility of adiabatic changes makes it possible to consider these two different kinds of changes separately. Under adiabatic changes ψ_t is conserved and the magnetofluid is tied to the field lines. Hence, the condition that entropy per unit flux be conserved reduces to the condition $\mu_f(\psi) = \mu_i(\psi)$ where the subscripts "i" and "f" refer to equilibria before and after the adiabatic change, respectively, and where

$$\mu(\psi) = p(\psi)\left(2\pi\oint \frac{d\ell}{B}\right)^{\gamma} \tag{1}$$

where γ is the adiabatic exponent. We now make the one-dimensional approximation by writing

$$\oint \frac{d\ell}{B} \simeq \frac{2\ell}{B} = \frac{2\ell}{[2(p_m - p(\psi))]^{1/2}} \tag{2}$$

This approximation eliminates the transition region where the field lines are

*This work was performed under the auspices of USDOE.

curved and represents the magnetofluid by a cylinder of straight field lines of length ℓ. In general this is a terrible approximation, but for highly elongated FRCs it is not too bad.

If the pressure profile is written in the form $p(\psi) = p_m\beta(\phi)$, where $\phi = \psi/\psi_t$, then entropy conservation becomes a condition relating initial and final β profiles.

$$\frac{\beta_f(\phi)}{[1-\beta_f(\phi)]^{\gamma/2}} = A\frac{\beta_i(\phi)}{[1-\beta_i(\phi)]^{\gamma/2}} \qquad (3)$$

where $A = (\ell_i/\ell_f)^{\gamma}(p_{mi}/p_{mf})^{1-\gamma/2}$. In the case of wall compression, $A = 1$ and the pressure profile does not change shape. The variation of ℓ during wall compression in this approximation is given in Table I. In the case of flux compression $A \neq 1$ and a one-dimensional equilibrium code is needed to vary A until a new equilibrium is found that satisfies radial pressure balance, the average-beta condition, and trapped flux conservation. A modification of the code described in the appendix of Ref. 2 was used here.

To test the accuracy of the one-dimensional approximation, the pressure profiles and separatrix lengths from the one-dimensional code were used in Hewett's two-dimensional FRC equilibrium code.[2] The correct entropy functions were then computed on the two-dimensional mesh and compared with each other to see if entropy was indeed conserved. We found that if the equilibria had $\ell/r_s > 10$, the one-dimensional results were accurate to about 10%. These requirements on the elongation are satisfied by most experiments.

III. ANALYTICAL MODEL

We consider an elongated FRC equilibrium inside a straight cylindrical flux conserver, as shown in Fig. 1. As in Sec. II, the separatrix is modeled as a cylinder of length ℓ and radius r_s and we consider the adiabatic compression of the FRC by changes in r_w and ψ_o (e.g. wall and flux compressions, respectively). The energy balance within the separatrix can be written as $dE = dW$, where $E = \int (p/(\gamma-1) + B^2/2\mu_o)dV$ is the total energy within the separatrix volume V and where dW is the work done on the separatrix by the external magnetic field pressure. With the above assumptions and using the average beta condition, we obtain $E = p_m V[1-(2-\gamma)x_s^2/2]/(\gamma-1)$ and, therefore,

$$dE = E\left[\frac{2dr_w}{r_w} + 2\frac{dx_s}{x_s} + \frac{d\ell}{\ell} + \frac{dp_m}{p_m} - \frac{x_s dx_s(2-\gamma)}{1-(2-\gamma)x_s^2/2}\right] . \qquad (4)$$

To obtain dW, we write $dW = F_r dr_s + F_z d\ell$, where F_r and F_z are the radial and axial forces exerted on the separatrix. By neglecting the curved field line region near $z = \ell/2$, as shown in Fig. 1, we obtain $F_r = -2\pi r_s p_m$. By using the control surfaces S_{1-5} indicated in Fig. 1, and by expressing the forces on each surface by means of the Maxwell stress tensor, the axial equilibrium relation reduces to $F_z = -F_{z1} - F_{z2}$. With $F_{z1} = p_m\pi(r_w^2-r_s^2)$ and $F_{z2} = -p_m\pi r_w^2(1-x_s^2)^2$, we obtain $F_z = -p_m\pi r_s^2(1-x_s^2)$. Combining these expressions for F_r and F_z with the definition of dW yields

$$dW = -p_m V\left[2\frac{dr_w}{r_w} + 2\frac{dx_s}{x_s} + (1-x_s^2)\frac{d\ell}{\ell}\right] . \qquad (5)$$

The trapped magnetic flux inside the separatrix can be written as $2\pi\psi_t = \pi r_w^2 B_w x_s^3/2f$ with $f = x_s/\int_0^1 (1-\beta)^{1/2}\,du$, where $u = 2r^2/r_s^2 - 1$. We assume

that f is only a function of x_s, or equivalently, that the change in pressure profile $\beta(u)$ only comes from varying x_s. Then, the relations ψ_t = constant and $p_m \propto B_w^2$ can be used to obtain

$$\frac{dp_m}{p_m} = -2(3-\varepsilon)\frac{dx_s}{x_s} - 4\frac{dr_w}{r_w} \qquad (6)$$

where $\varepsilon = (x_s/f)(df/dx_s)$. The relation dE = dW with Eqs. (4)-(6) gives

$$\frac{d\ell}{\ell} = \frac{(4-2\gamma)}{\gamma}\frac{dr_w}{r_w} + \frac{2(3-\gamma-\varepsilon)}{\gamma}\frac{dx_s}{x_s} - \frac{(1+\varepsilon-\gamma\varepsilon)}{\gamma}\frac{d\langle\beta\rangle}{\langle\beta\rangle} . \qquad (7)$$

where $\langle\beta\rangle = 1-x_s^2/2$.

For wall compression, x_s is constant and integrating Eq. (7) with $\gamma = 5/3$ gives the ℓ scaling in Table I. Assuming that the plasma is isothermal within the separatrix, using the constancy of the particle inventory $N = \langle\beta\rangle n_m \pi r_s^2 \ell$ with $p_m = n_m T_m$, and using radial pressure balance and magnetic flux conservation, we obtain the rest of Table I. These scaling laws are independent of the pressure profile, as was also obtained in Sec. II.

For flux compression, r_w is constant but Eq. (7) cannot be readily integrated unless ε is a constant as x_s varies. It has been shown[3] that two limiting cases of elongated FRC equilibria are given by sharp-boundary pressure profiles that contain the largest and smallest amount of ψ_t. These are the high-flux sharp-boundary and low-flux sharp-boundary models. For these, the values of ε are 0 and -1, respectively, and Eq. (7) can be integrated to recover known results[3] for $\gamma = 5/3$. For arbitrary diffuse pressure profiles, it can be shown that $\sqrt{2} < f < 2/x_s$, where the upper and lower limits correspond to the low flux and high flux sharp-boundary models, respectively. From this inequality, we obtain $-1 < \varepsilon < 0$, which indicates that the scaling laws of flux compression for diffuse profiles are bounded by the two sharp-boundary models. The numerical results of Sec. II show that ε is approximately a constant as x_s varies for a given initial $\beta(\phi)$. Even with different initial β profiles, we find that ε nearly always lies between -0.2 and -0.3. Therefore, most diffuse profiles scale in flux compression in a way similar to the high-flux sharp-boundary profile for which $\varepsilon = 0$. We approximate ε by the constant value -0.25 for diffuse profiles and neglect the small variations of less than 10% in the coefficients of Eq. (7) due to departures of ε from this value. This approximation is well justified within the one-dimensional model of this work. Then integrating Eq. (7) with the relations N = const., ψ_t = const., $p_m \propto B_w^2$, $V \propto x_s^2 \ell$, and $\gamma = 5/3$ we obtain Table II. Figure 2 shows the comparison between the analytic scaling for ℓ and that obtained by the calculation in Sec. II in the case of a typical diffuse profile. The adiabatic compression of diffuse profile FRCs can thus be quite accurately described by simple formulae.

REFERENCES

1. H. Grad, P. N. Hu, and D. C. Stevens, Proc. Nat. Acad. Sci. USA 72, 3789 (1975).
2. D. W. Hewett and R. L. Spencer, submitted to Phys. Fluids, Los Alamos report LA-UR-82-2520.
3. W. T. Armstrong, et. al., in Plasma Physics and Controlled Nuclear Fusion Research (International Atomic Energy Agency, Vienna, 1981), Vol. I, p. 481.

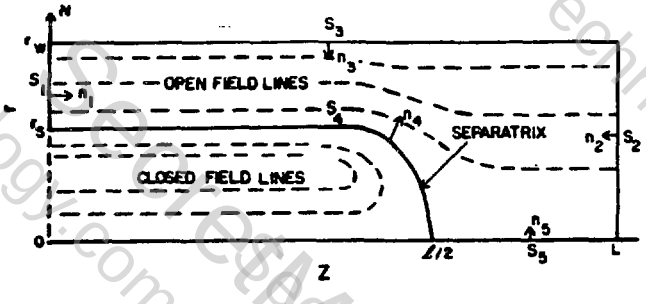

Figure 1: A field-reversed configuration inside a cylindrical flux conserver.

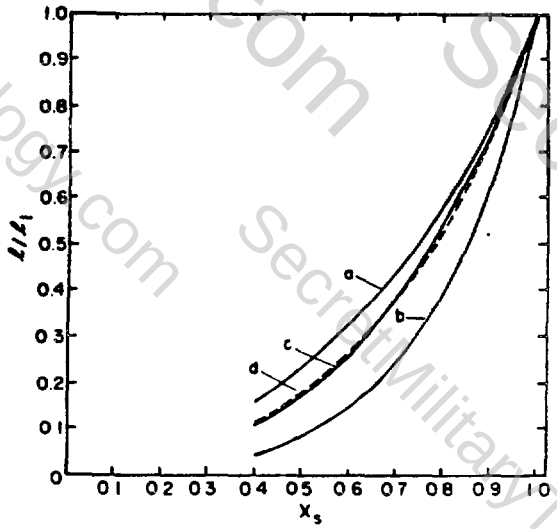

Figure 2: FRC length as a function of x_s for flux compression. (a) High flux sharp-boundary. (b) Low flux sharp-boundary. (c) One-dimensional compression code. (d) Typical diffuse profile formula from Table II.

TABLE I

Adiabatic Wall Compression Scaling Laws for $\gamma = 5/3$

$\frac{\ell}{r_w^{2/5}}$	$\frac{T_m}{r_w^{-8/5}}$	$\frac{n_m}{r_w^{-12/5}}$	$\frac{B_w}{r_w^{-2}}$

TABLE II

Adiabatic Flux Compression Scaling Laws for $\gamma = 5/3$

	High-flux Sharp Boundary	Typical Diffuse Profile	Low-flux Sharp Boundary
ℓ	$x_s^{8/5}\langle\beta\rangle^{-3/5}$	$x_s^{19/10}\langle\beta\rangle^{-7/10}$	$x_s^{14/5}\langle\beta\rangle^{-1}$
T_m	$x_s^{-12/5}\langle\beta\rangle^{2/5}$	$x_s^{-13/5}\langle\beta\rangle^{3/10}$	$x_s^{-16/5}$
n_m	$x_s^{-18/5}\langle\beta\rangle^{-2/5}$	$x_s^{-39/10}\langle\beta\rangle^{-3/10}$	$x_s^{-24/5}$
B_w	x_s^{-3}	$x_s^{-13/4}$	x_s^{-4}

A ZERO-DIMENSIONAL MODEL FOR FIELD-REVERSED CONFIGURATIONS

D. J. Rej and M. Tuszewski
Los Alamos National Laboratory, Los Alamos, N.M., 87545

I. Introduction: A 0-D model has been developed to study energy, particle, and internal flux confinement during the equilibrium phase in field-reversed configurations (FRC's). Earlier work[1] has been extended to include: (1) a 1-D radial equilibrium pressure profile consistent with particle transport calculations[2]; (2) a time-dependent treatment of impurity radiation losses; (3) a more consistent treatment of ohmic power. The 0-D model is described in Sec. II. Example numerical solutions are presented in Sec. III, modeling data from the FRX-C experiment.[3]

II. Basic Equations: We consider an elongated FRC in equilibrium inside cylindrical flux conserver. The plasma is assumed to be isothermal within the separatrix, as observed experimentally,[4] and the plasma pressure on open field lines is neglected. The basis for the power balance in our model is the adiabatic formalism of Spencer, Tuszewski, and Linford,[5] which is valid for arbitrary diffuse pressure profiles with the above assumptions. When loss terms are included in this model, one obtains

$$\dot{E}_p = -p_m V[2\dot{x}_s/x_s + (1-x_s^2)\dot{\ell}/\ell] - \dot{E}_B - P_{losses} \qquad (1)$$

where p_m is the external field pressure $B_{ext}^2/8\pi$, $x_s=r_s/r_w$ is the ratio of separatrix to coil radii, ℓ is the FRC length, E_p and E_B are the plasma and and magnetic field energies, respectively, within the separatrix volume V. The sum of the first two terms on the right-hand side of Eq. (1) is the total input power to the plasma from compression P_c and ohmic dissipation P_Ω. It is assumed that the compressional power on the separatrix volume (first term on the right-hand side of Eq. 1) is the same as in the adiabatic case.[5] One obtains $P_c=(-2/3)E_B\{\dot{V}/V+[x_s^2/(1-x_s^2/2)]\dot{f}/f\}$ and $P_\Omega=-2E_B(3\dot{x}_s/x_s+\dot{B}_{ext}/B_{ext}-\dot{f}/f)$ where $f = x_s B_{ext}/\int_0^1 B\,du$ with $u=r^2/R^2-1$. Then, Eq. (1) can be split into electron and ion power balances

$$\dot{T}_e/T_e = P_c/E_p + (1-\varepsilon)(1+T_i/T_e)/\tau_\Omega + [T_i/T_e - 1]/\tau_{eq} - 1/\tau_r - 1/\tau_{Ee} \qquad (2)$$

$$\dot{T}_i/T_i = P_c/E_p + \varepsilon(1+T_e/T_i)/\tau_\Omega + [T_e/T_i-1]/\tau_{eq} - 1/\tau_{Ei} \qquad (3)$$

where τ_{eq} is the classical ion-electron energy equilibration time,[6] $\tau_\Omega=E_p/P_\Omega$ is the ohmic time, τ_r is an impurity radiation energy loss time and $\tau_{Ee,i}$ are thermal conduction times. The quantity ε is the fraction of the ohmic power deposited into the ions. Three additional equations are obtained from particle inventory, radial pressure balance and internal flux decay

$$\dot{V}/V = -\dot{n}/n - 1/\tau_N \qquad (4)$$

$$\dot{n}/n = -(\dot{T}_e+\dot{T}_i)/(T_e+T_i) + 2\dot{B}_{ext}/B_{ext} - (\dot{R}/R)x_s^2/(1-x_s^2/2) \qquad (5)$$

$$\dot{R}/R = (-\dot{B}_{ext}/B_{ext} - 1/\tau_\phi + \dot{f}/f)/3 \qquad (6)$$

where n is the average density over V, $R = r_s/\sqrt{2}$ is the major radius, $\tau_N = -N/\dot{N}$ and $\tau_\phi = -\phi/\dot{\phi}$ are particle inventory and internal flux $\phi = \pi R^2 \int_0^1 B du$ decay times, respectively. The last term in Eq. (5) comes from the average beta condition[4] $\langle\beta\rangle = n/n_{max} = 1 - x_s^2/2$. For a given choice of radial pressure profile, the times τ_{eq}, τ_Ω, τ_r, $\tau_{Ee,i}$, τ_N, τ_ϕ can be calculated. With $B_{ext}(t)$ as an input, Eqs. (2)-(6) can then be solved for 5 unknowns T_e, T_i, n, V, R, given initial conditions.

The energy confinement time τ_E for an FRC is defined as $\tau_E = E_p/(P_c + P_\Omega - \dot{E}_p)$ which in terms of Eqs. (2)-(6) can be expressed in a variety of forms:

$$1/\tau_E = 1/\tau_N + [1/(1+T_i/T_e)][1/\tau_r + 1/\tau_{Ee}] + 1/[(1+T_e/T_i)\tau_{Ei}] \tag{7a}$$

$$1/\tau_E = 2/3\tau_V + 1/\tau_\Omega + 1/\tau_N + 1/\tau_T \tag{7b}$$

$$1/\tau_E = 5/3\tau_V + 2/\tau_B + [2(1-\langle\beta\rangle)/\langle\beta\rangle][1/\tau_R + 2/3\tau_B] \tag{7c}$$

where we define $\tau_T = -(T_e+T_i)/(\dot{T}_e+\dot{T}_i)$, $\tau_B = -B_{ext}/\dot{B}_{ext}$, $\tau_R = -R/\dot{R}$, and $\tau_V = -V/\dot{V}$. The last equation is particularly useful since τ_E can be inferred exclusively from external magnetic probe data.

We choose as a pressure profile a truncated rigid-rotor

$$\beta(u) = n(u)/n_{max}(u) = [1 - \tanh^2 \kappa u(1+\mu u^{10})] \tag{8}$$

where the time-dependent coefficients κ and μ are determined from the average beta condition and the boundary condition at the separatrix from particle transport.[2] This choice is based on the fact that viscosity tends to relax the bulk of pressure profile towards the rigid-rotor while a truncation occurs in the vicinity of the separatrix because of radial transport to the near-vacuum open field lines. The truncation power of 10 used in Eq. (8) allows easy computation of κ, μ, τ_N and τ_ϕ. Variation of this truncation power does not significantly change the computed τ_ϕ and τ_N values. For this choice of pressure profile, the term $\dot{f}/f$ used in Eq. (6) and in calculating P_c and P_Ω can be neglected for values of x_s in the range of interest, from 0.3 to 0.7. One obtains

$$\tau_\phi = 7.4\times10^{-10} r_s^2/\eta_\perp(0) \tag{9}$$

where the resistivity $\eta_\perp(0)$ at r=R is in units of Ω-cm. Unless otherwise specified, all dimensions are in cm, temperatures in eV, times in sec and B in gauss. We also obtain from the definition of τ_Ω and Eq. (6)

$$\tau_\Omega = \frac{3\langle\beta\rangle}{4(1-\langle\beta\rangle)}\,\tau_\phi \tag{10}$$

The particle loss time τ_N is calculated from the lower-hybrid-drift transport theory.[2] Estimates of impurity line radiation can not be usually obtained from steady-state coronal equilibrium calculations[7] because of the relatively short time scales of FRC experiments. Instead, we calculate τ_r for each impurity species with the Jahoda model[8]

$$\tau_{rZ} = \frac{T_e}{\sum_{m=1,Z} n_{Zm} h_{Zm}(T_e)} \frac{\langle\beta\rangle}{(1-\langle\beta\rangle^2\kappa^2/3)} \tag{11}$$

where Z is the impurity atomic number, n_{Zm} is the average density of charge state m-1, and $h_{Zm}(T_e)$ can be inferred from Ref. 8. We assume the identical

radial distribution Eq. (8) for the impurity and electron densities. The n_{Zm} values using the ionization and recombination rates σ_m and α_m, respectively, are computed as

$$\dot{n}_{Z1} = -n_e n_{Z1}\sigma_{Z1} + n_e n_{Z2}\alpha_{Z2}$$

$$\dot{n}_{Zm} = n_e n_{Zm-1}\sigma_{Zm-1} - n_e n_{Zm}\sigma_{Zm} - n_e n_{Zm}\alpha_{Zm} + n_e n_{Zm+1}\alpha_{Zm+1} \qquad (2<m<Z) \qquad (12)$$

$$\dot{n}_{ZZ+1} = n_e n_{ZZ}\sigma_{ZZ} - n_e n_{ZZ+1}\alpha_{ZZ+1} \quad .$$

III. Solutions: The numerical solutions of Eqs. (2)-(6) modeling data measured in the FRX-C experiment[3] are indicated by the dashed-lines in Fig. 1. All solid-lines are data collected from five typical 20 mTorr D_2 discharges. The main capacitor bank is discharged at time t=0. The parameters r_s, V, n, N, T_e, and T_i (where $T_e \simeq T_i$) are determined from excluded flux and side-on interferometer measurements. The N(t) data points are from independent particle inventory measurements using end-on holographic interferometry. The initial conditions are taken at t=20 μs, allowing time for FRC equilibrium formation. The modeling ends at t=100 μs, prior to the onset of the n=2 rotational instability. The external magnetic field is an input to the calculation and for this example it is modeled as $B_{ext}(KG) = 7.7\times\exp\{-t(\mu s)/230\}$. Agreement with the experimental results is obtained using the adjustable parameters ε, $n_{Zm}(t=20\,\mu s)$, τ_{Ee}, τ_{Ei}, and k_η where we define k_η as the ratio of $\eta_\perp(0)$ to the classical resistivity with $Z_{eff}=1$. For these examples we assume ε=0. The theoretically predicted average particle confinement time $\tau_N=181$ μs is in very good agreement with the 187 μs experimental values. At t = 50 μs one calculates $\tau_\phi \simeq 155$ μs (corresponding to $k_\eta=4$) and $\tau_E \simeq 80$ μs, the latter value indicating non-negligible losses from thermal conduction and/or radiation. Since the electron and ion energies are almost fully equilibrated, it is difficult to determine the fractional energy loss through each species; however, the relationship, $[\tau_r^{-1} + \tau_{Ee}^{-1} + \tau_{Ei}^{-1}]^{-1} \simeq 70$ μs, can be obtained. In the limit $\tau_{Ee,i} = \infty$, these losses can be explained with a 6% oxygen impurity concentration (to date, the only impurity investigated). A global energy confinement parameter $n\tau_E \simeq 4\times10^{11}$ cm^{-3}s is found.

Modeling 5 mTorr FRX-C data ($n\simeq2\times10^{15}$cm^{-3}, T_i=450-700 eV, $T_e\simeq$150-200 eV) results in $\tau_N\simeq70$ μs, $\tau_\phi\simeq150$ μs (with $k_\eta\simeq8$), $\tau_{Ei}\simeq150$ μs, $[\tau_{Ee}^{-1}+\tau_r^{-1}]^{-1} \simeq 25$ μs, and $\tau_E\simeq35$ μs. The energy lost by thermal conduction and/or radiation in the electron channel is comparable to the energy lost through particle transport. Reasonable oxygen concentrations (<10%) can not solely explain these results, suggesting losses due to the presence of higher Z impurities (e.g., Si) and/or anomalous electron thermal conduction due to microinstabilities. These effects are under investigation. From these data, τ_ϕ is longer than both τ_N and τ_E, indicating that flux loss is not a dominant mechanism controlling either particle or energy confinement. This was already observed in earlier 5 mTorr data.[9]

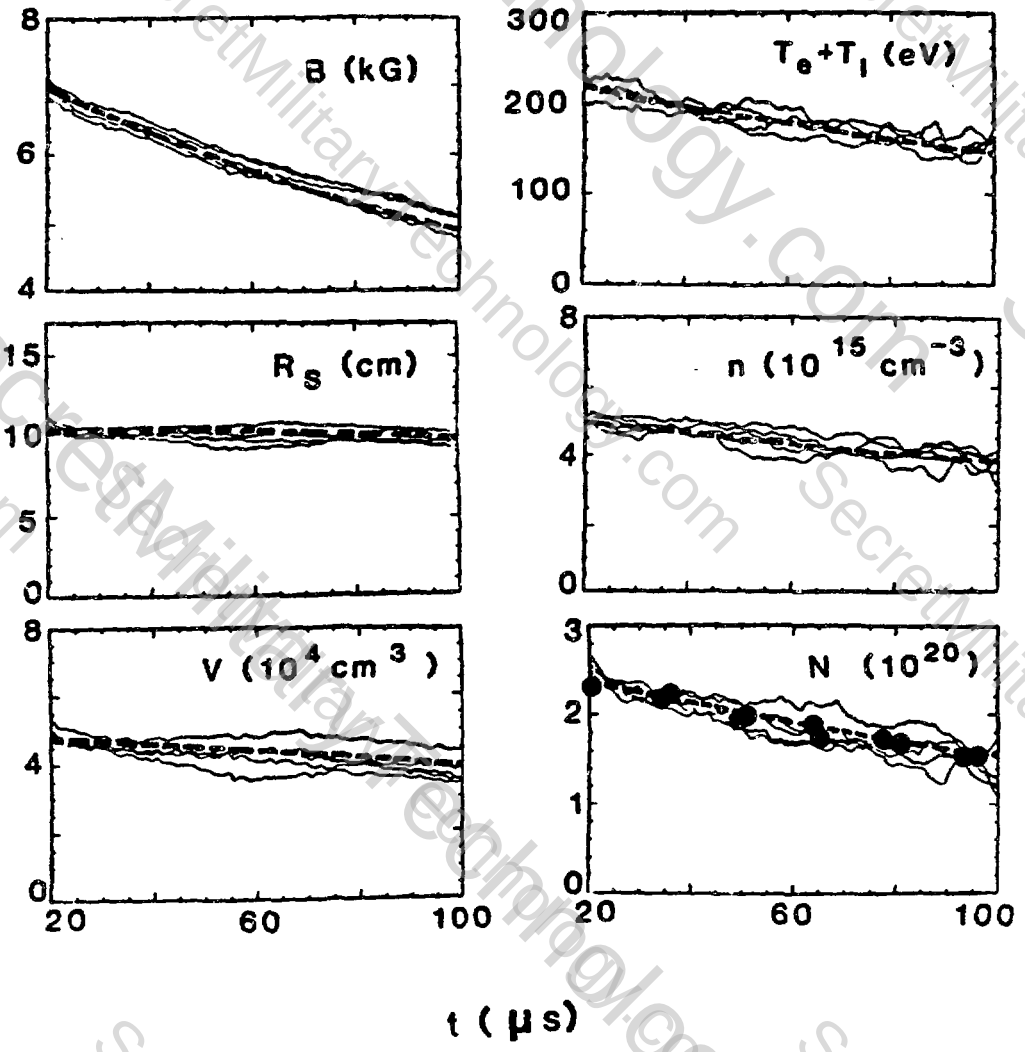

Figure 1: Numerical solutions of Eqs. (2)-(6) (dashed-lines) and 20 mTorr data (points and solid-lines) obtained from FRX-C.

REFERENCES:

1. E. H. Klevans, in Proc. of the US-Japan Joint Symp. on Compact Toruses and Energetic Particle Injection (Princeton, 1979), p. 135.
2. M. Tuszewski and R. K. Linford, Phys. Fluids 25, 765 (1982).
3. K. F. McKenna, et. al., these proceedings.
4. W. T. Armstrong, et. al., Phys. Fluids 24, 2068 (1981).
5. R. Spencer, M. Tuszewski and R. K. Linford, to be published.
6. L. Spitzer, Physics of Fully Ionized Gases, (Interscience Publ. Inc., New York, 1956).
7. D. E. Post, et. al., At. Data and Nucl. Data Tables 20, 397 (1977).
8. F. Jahoda in S. Ortolani, Los Alamos Nat. Lab. Rep. LA-8261-MS (1980).
9. M. Tuszewski, et. al., Phys. Fluids 25, 1696 (1982).

ADIABATIC INVARIANTS FOR FIELD REVERSED CONFIGURATIONS

J. L. Schwarzmeier, H. R. Lewis, and C. E. Seyler[a)]

Los Alamos National Laboratory, Los Alamos, NM 87545
[a)]Department of Electrical Engineering, Cornell University, Ithaca, NY 14853

Field reversed configurations (FRCs) are characterized by azimuthal symmetry, so two exact constants of the particle motion are the total particle energy E and the canonical angular momentum p_θ. For many purposes it is desirable to construct a third (adiabatic) constant of the motion if this is possible. It is shown that for parameters characteristic of current FRCs that the magnetic moment μ is a poor adiabatic invariant, while the radial action J is conserved rather well.

The magnetic moment of a particle at position $\vec{r}$ is

$$\mu(\vec{r}) = \frac{mv_\perp^2(\vec{r})}{2B(\vec{r}_{gc})}, \qquad (1)$$

where $\vec{r}_{gc}$ is the position of the particle's guiding center. $B(\vec{r}_{gc})$ can be estimated from $B(\vec{r})$ by Taylor expanding B about $\vec{r}_{gc} = \vec{r}$. For μ to be conserved it is necessary that a particle see little change in B during a radial oscillation. In Fig. 1 we show trajectories of thermal particles in the fields of the FRX-B equilibrium as calculated by Spencer and Hewett.[1,2] This equilibrium has T_i = 340eV, $n_{max} = 3\times10^{15}cm^{-3}$, B_w = 6.5kG, r_w = 12.5cm, x_s = .46, and P_{sep}/P_{max} = .44. For these parameters

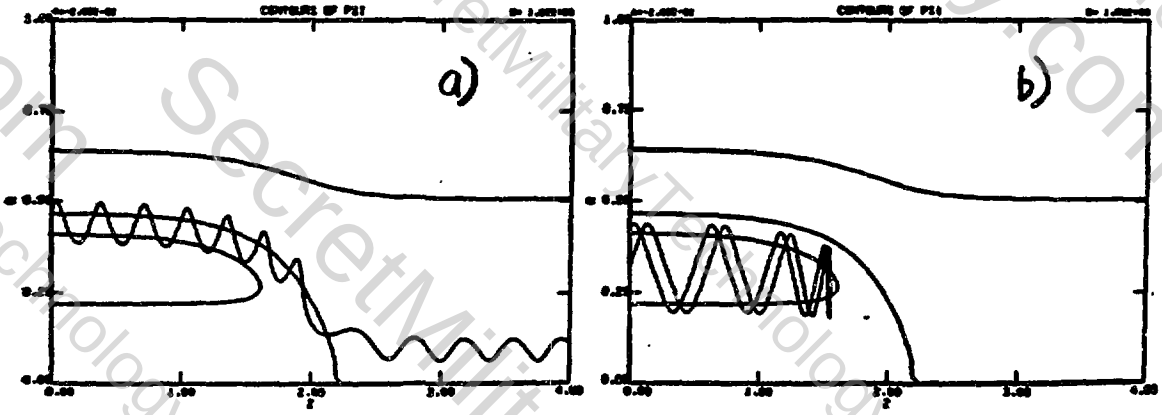

Figure 1. Particle trajectories and flux surfaces for a) cycloidal particle, and b) betatron particle, using FRX-B parameters.

the radial gradient in B in the midplane of the device is sufficiently steep that the particle sees a large variation in B during one radial oscillation. By the time the (cycloidal) particle has reached z = 1 in Fig. 1a it has experienced a variation in μ of $\Delta\mu \sim \pm 65\%$, which surely is unacceptable for μ to be considered conserved; for the betatron particle in Fig. 1b μ is meaningless. The conclusion is that μ is not a suitable invariant for any class of particles in the FRC. This suggests that not only is MHD an invalid model, but the guiding center model also is not applicable.

Fortunately there remains a small parameter of FRCs that can be exploited to derive a new adiabatic invariant to replace μ. That small parameter is the elongation of the configuration, ε, which typically is in the range $.15 \leq \varepsilon \leq .25$. We now show that the radial action J is an invariant for elongated FRCs.

The equilibrium single particle Hamiltonian is (p_θ is a parameter throughout)

$$H(r,p_r,z,p_z) = \frac{p_r^2}{2m} + \frac{p_z^2}{2m} + U(r,z), \tag{2}$$

where the two dimensional potential is

$$U(r,z) = \frac{[p_\theta - e\psi(r,z)/c]^2}{2mr^2} + e\Phi(\psi), \tag{3}$$

and Φ is the electric potential determined from ion pressure balance. The highly elongated nature of FRCs manifests itself in that the potential variation in z is much "slower" than it is in r. (This is true except for a highly racetrack equilibrium, where all the axial variation occurs at the tip of the flux surface on the same spatial scale length as the radial variation.) Thus to do the perturbation theory for slow z variation we replace

$$U(r,z) \to U(r,\varepsilon z), \tag{4}$$

treat ε as small in the analysis, and then at the end let $\varepsilon \to 1$. Mynick[3] used the slow-z approximation (4) and made some analytical approximations

to obtain a Hamiltonian as an explicit function of J that determines the radial and axial motions of a particle through order ε^2. Here we present a simple derivation of the lowest order Hamiltonian, without seeking to make approximations of the integrals involved, and we present numerical tests of the constancy of J for realistic equilibria. Define the radial action J as

$$J(E_0,\varepsilon z) \equiv \frac{1}{2\pi} \oint dr\ p_r(r,E_0,\varepsilon z). \tag{5}$$

The p_r in Eq. (5) is

$$p_r(r,E_0,\varepsilon z) = \{2m[E_0 - U(r,\varepsilon z)]\}^{1/2}, \tag{6}$$

where E_0 is a constant value of the radial Hamiltonian H_0

$$H_0(r,p_r,\varepsilon z) = \frac{p_r^2}{2m} + U(r,\varepsilon z) = \text{constant} \equiv E_0. \tag{7}$$

For each z in Eq. (7), E_0 varies over a range of values. For each z and E_0 in Eq. (5), J has a certain value. The relation $J = J(E_0,\varepsilon z)$ can be inverted to give E_0 as a function of J and εz:

$$E_0 = H_0(r,p_r,\varepsilon z) = K_0(J,\varepsilon z). \tag{8}$$

That is, we have transformed from (r,p_r) to action-angle variables (ϕ,J).

Since ε is a parameter in the potential U, a perturbation solution for $z(t)$ will depend on ε,

$$z(t;\varepsilon) = z_0(t) + \varepsilon z_1(t) + \varepsilon^2 z_2(t) + \ldots. \tag{9}$$

(It is well known that a straightforward perturbation expansion as in (9) leads to secular growth of $z(t)$, so that the solution soon becomes invalid as t becomes large.[4] These secularities can be removed from the solution by allowing $z(t)$ to depend on ε through various time scales T_0, T_1, ..., T_n, defined by $T_n = \varepsilon^n t$, $n = 0,1,2,\ldots$. However, in this

calculation we do not actually need the multiple time scale formalism.) When the expansion (9) is substituted into $U(r,\varepsilon z)$ we have

$$U(r,\varepsilon z) = U(r,\varepsilon(z_0+\varepsilon z_1+\ldots))$$

$$= U(r,\varepsilon z_0+\varepsilon^2 z_1+\ldots)$$

$$= U(r,\varepsilon z_0) + \varepsilon^2 z_1 \frac{\partial U(r,\varepsilon z_0)}{\partial(\varepsilon z_0)} + \ldots = U(r,\varepsilon z_0) + O(\varepsilon^2). \quad (10)$$

Therefore the Hamiltonian that determines to lowest order in ε the radial and axial motion of a particle is obtained by substituting Eqs. (10,7,8) into Eq. (2) (letting $z_0 \to z$):

$$K(J,\varepsilon z,p_z) = K_0(J,\varepsilon z) + \frac{p_z^2}{2m} + O(\varepsilon^2). \quad (11)$$

From Eq. (11) we conclude that J is an adiabatic invariant:

$$\frac{dJ}{dt} = -\frac{\partial K}{\partial \phi} = 0 + O(\varepsilon^2).$$

For the cylcoidal particle in Fig. 1a, by the time the particle reaches $z = 1$ the variation in J has been $\Delta J \sim \pm 11\%$. For the betatron particle in Fig. 1b the variation in J is $\Delta J \sim \pm 8\%$ during an axial bounce time. (For FRX-C parameters the variations in μ and J are about 50% of what they are for FRX-B parameters.) By solving Eq. (11) for p_z and using the equation $dz/dt = p_z/m$, the axial time of a particle's position is (letting $\varepsilon \to 1$)

$$\tau(z) = \int_{z_1}^{z} \frac{dz'}{\{\frac{2}{m}[E - K_0(J,z')]\}^{1/2}}, \quad (12)$$

where E is a constant value of the total Hamiltonian K in Eq. (11), and z_1 is a turning point of the axial motion. The error in using formula (12) compared to the exact particle trajectory data is .34% at $z = 2$ in Fig. 1a and .97% at the z-turning point in Fig. 1b.

Of course, J (or μ for that matter) is not an adiabatic constant of the motion for particles that pass in the vicinity of the spindle point.

In fact, particles with positive p_θ have orbits that are not confined axially (see Fig. 1a), so these particles are lost through the spindle point region in an axial transit time. In a similar vein Kim and Cary[5] studied particle orbits for an elliptical z-pinch, and found two regions of the equilibrium where either J or μ was conserved, with a stochastic region in between. What we have shown is that, where it is possible to define an adiabatic invariant in current FRC equilibria, the radial action is always conserved much better than the magnetic moment.

1. R. L. Spencer and D. W. Hewett, Phys. Fluids 25, 1365 (1982).
2. D. W. Hewett and R. L. Spencer (submitted to Phys. Fluids).
3. H. E. Mynick, Phys. Fluids, 23 1897 (1980).
4. A. H. Nayfeh, Introduction to Perturbation Techniques (Wiley-Interscience, New York, 1981), p. 107.
5. J. Kim and J. R. Cary, Proceedings of 1982 Sherwood Theory Meeting in Santa Fe, New Mexico.

MODE STRUCTURE OF THE LOWER HYBRID DRIFT INSTABILITY IN A FIELD-REVERSED CONFIGURATION

A. G. Sgro and C. Lilliequist
Los Alamos National Laboratory
N. T. Gladd
Jaycor
D. W. Hewett
Massachusetts Institute of Technology

ABSTRACT

We extend previous analysis of the lower hybrid drift instability in which simulations accurately calculated the analytic linear growth rate in the low drift velocity regime to include details of spatial structure.

Anomalous transport due to the lower hybrid drift instability is thought to enhance the scattering of particles and momentum across the separatrix of field-reversed configurations, resulting in spinup, instability, and termination. We have previously compared simulations of this instabilitity with a local, linear analytic theory and found that the growth rate in the simulations agreed with that predicted by the analytic theory. In this report we make a detailed comparison of the spatial structure of the simulated instability with the predictions of a linear, nonlocal stability theory.

The simulation was done with a finite electron mass hybrid code (D. W. Hewett and C. W. Nielson, J. Comp. Phys. 29, 219 (1978)) in which the ions are kinetic and the electrons are a quasineutral fluid. This model neglects oscillations on the scale of ω_{pe}^{-1} and λ_D, which in principle permits analysis of modes having low growth rates without unreasonable expenditure of computational resources.

The linear nonlocal theory approximates the drift parameter $v_{di}(x)/v_i$ to be parabolic about its maximum. Assuming cold, magnetized electrons and hot unmagnetized ions, one finds a second order

differential equation for the eigenfunction. If m_e/m_i is neglected, this equation has the form of a Weber's equation,

$$\frac{d^2\phi}{dx^2} + (B-Cx^2)\phi = 0 \quad ,$$

whose eigenvalues and eigenfunctions, ϕ_n, are known.

We represent the fluctuations in the simulation as a linear combination of these eigenfunctions. Although ϕ_n are complete, they are not orthogonal and one must solve a set of simultaneous equations to find the amplitudes. Specifically, the y component of the fluctuating electric field, δE_y, is Fourier analysed in the y direction and the resulting Fourier coefficients are called $\alpha_l(x)$. The $\alpha_l(x)$ are in turn represented as a superposition of the Weber eigenmodes with the coefficients being given by $\beta_{n,l}$.

The equilibrium of a simulation we have analyzed is illustrated in Fig. 1. The simulated δE_y, α_l (x) , and $\beta_{n,l}$ are depicted as contour plots in Fig. 2 at $t = 120\ c/\omega_{pe}$. A mode with large amplitude at $l = 4$, $n = 1$ may be seen in the $\beta_{n,l}$ plot. In addition, we show details of this dominant mode in a plot of $\alpha_4(x)$. Note that the fluctuations in the simulation may be reasonably represented by a superposition of the first six eigenmodes. The fit is quite good in the region where the lower hybrid drift is operative ($x \sim 1.1$), but the simulation also shows evidence of edge fluctuations. These edge fluctuations may be the result of the low density and consequently the small number of particles there.

We will, in the future, extend these preliminary results and analyze the details of the instability from the linear phase until saturation.

Simulation Analyzed

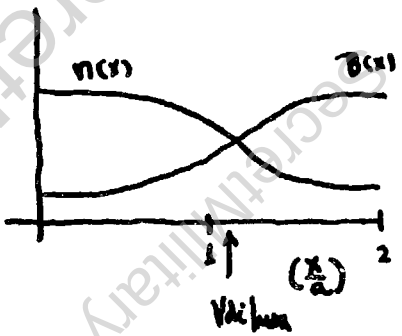

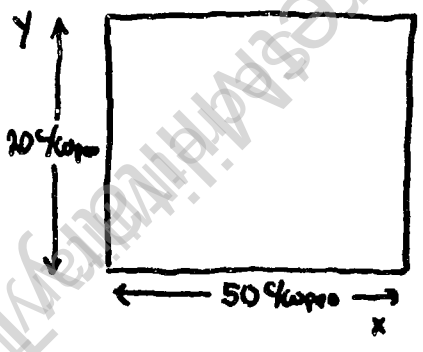

$\left.\frac{V_{di}}{V_i}\right|_{max} = 0.8$

$\left.\frac{\omega_{pe}}{\omega_{ce}}\right|_{x=0} = 10$

$\frac{T_e}{T_i} = 0.04$

$\frac{m_i}{m_e} = 100$

$\frac{\bar{V}_i}{C} = \frac{1}{10\sqrt{2}}$

51,200 PIC ions

Fluid electrons (finite electron mass)

Non radiative Darwin limit

$t = 120$

$\delta E_y(x,y)$

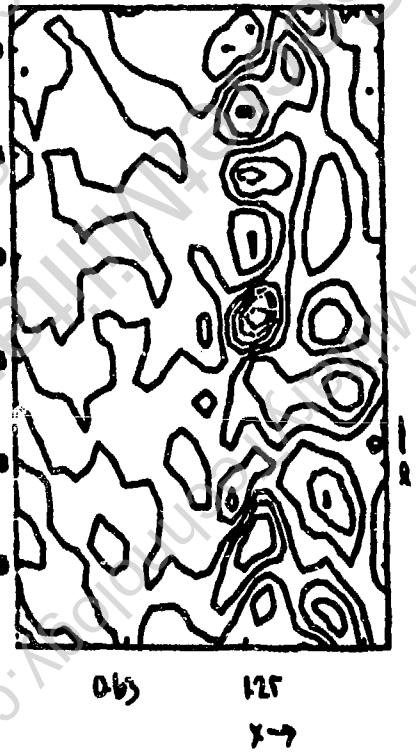

$\delta n_e(x)$

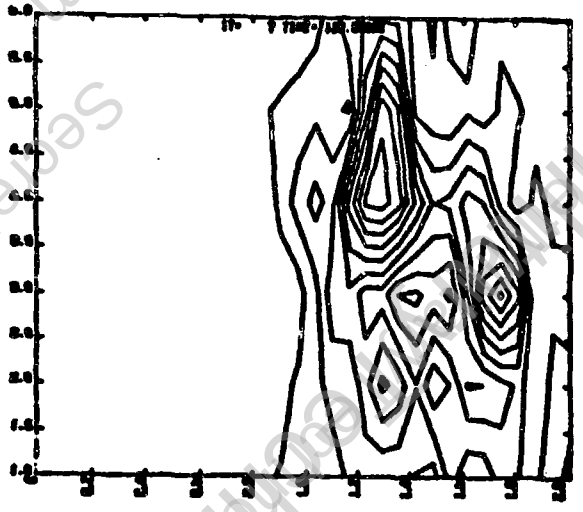

δn_i

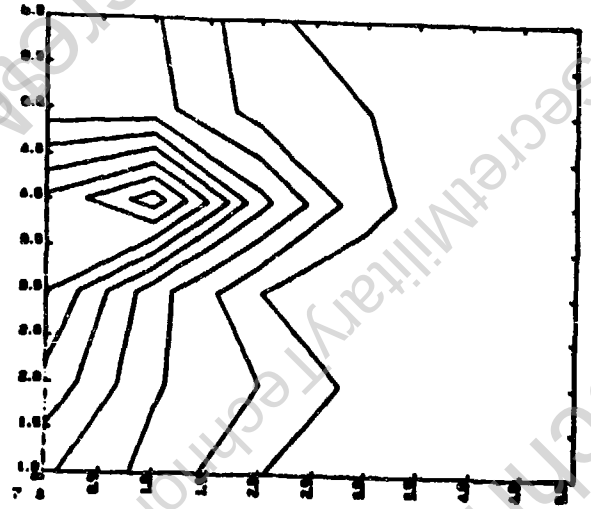

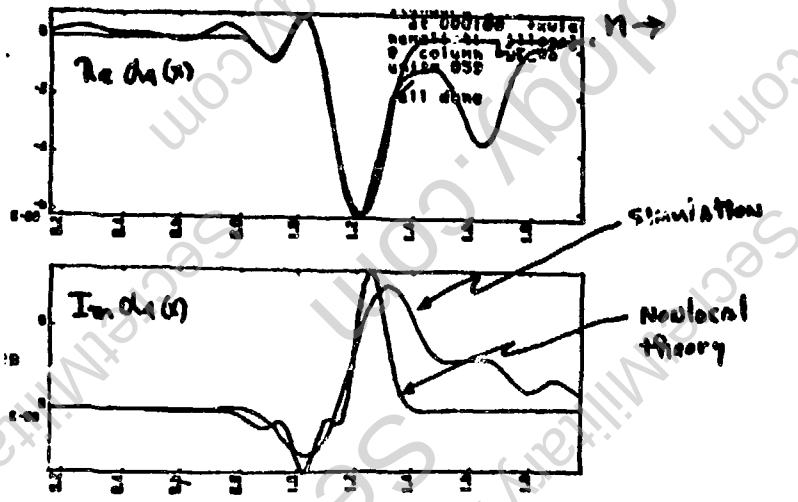

COMMENTS ON STEADY-STATE EQUILIBRIUM PROFILES IN FIELD-REVERSED CONFIGURATIONS

William K. Terry
School of Nuclear Engineering, Purdue University
West Lafayette, Indiana 47907

1. Introduction

This paper presents conclusions about the character of equilibrium profiles which may be sustained in steady state in a highly elongated ("long-thin") Field-Reversed Configuration (FRC).

Ideally, an FRC plasmoid contained in a cylindrical fusion reactor vacuum vessel would be axially elongated so that radiation and neutron fluxes on the wall and blanket would be relatively uniform and materials would be used efficiently. Fortunately, very prolate FRCs are experimentally seen to be unexpectedly stable.[1] Thus, the long-thin model of the FRC, in which the ends are ignored and the remainder is assumed axially uniform, is relevant to reactor concepts and has been adopted in numerous investigations.[2-4]

In any steady-state fusion reactor, some sort of particle source is required to make up for diffusive losses. In current Field-Reversed Theta Pinch (FRθP) experiments, which produce elongated FRCs often represented by the long-thin model, cross-field diffusion after initial formation seems to be primarily due to the lower-hybrid drift (LHD) microinstability,[2,3,5] because of the steep gradient in the magnetic field near the separatrix.[6] The particle confinement time and thermonuclear power gain in a fusion reactor would be degraded by such "anomalous diffusion"; therefore, one might hope to suppress the LHD instability, perhaps by flattening the field profile. However, it is shown in this paper that equilibria which can be sustained in a steady state in a long-thin FRC obeying classical diffusion are likely to involve relatively high fluid pressure outside the separatrix - a condition which also leads to rapid particle losses along the open field lines. Thus, suppression of microinstabilities may not actually result in better particle confinement.

2. Observations on the Steady State

A steady state requires time-invariance of the magnetic field, density, and temperature profiles. Detailed consideration of the temperature is beyond the scope of this paper. Time-invariance of the magnetic field $\vec{B}$ requires the electric field to be irrotational; in an axisymmetric FRC, this means that the azimuthal electric field is zero. Time-invariance of the density profile requires a balance between diffusion and the refueling source; this balance is discussed below.

Experiment and numerical simulations suggest that the temperature is nearly uniform within the separatrix of an FRC. In the absence of temperature variation, force-free currents, and pressure variation along $\vec{B}$, the steady-state Ohm's Law for a simple plasma is (in SI units)[7]

$$\eta_{\perp}\,\vec{j}_{\perp} = \vec{E}_{\perp} + \vec{u} \times \vec{B} - \vec{j} \times \vec{B}/en_e + \vec{\nabla}_{\perp} p_e/en_e, \qquad (1)$$

where $\vec{u}$ = fluid velocity, $p_e(n_e)$ = electron pressure (density), and $\perp$ means perpendicular to $\vec{B}$. One may solve Eq. (1) for $\vec{u}_\perp$; if the equilibrium equation $\vec{\nabla}p = \vec{j} \times \vec{B}$ is used, the result is

$$\vec{u}_\perp = \vec{E}_\perp \times \vec{B}/B^2 - \vec{\nabla}_\perp p_i \times \vec{B}/(en_eB^2) - (\eta_\perp/B^2)\,\vec{\nabla}p, \qquad (2)$$

where p_i = ion pressure and p = total pressure. If $\vec{E}_\perp$ is normal to surfaces enclosing constant magnetic flux, as required for $\partial\vec{B}/\partial t = 0$, then the first two terms in Eq. (2) are azimuthal, and the last term is the outward diffusion velocity,

$$\vec{u}_d \equiv -(\eta_\perp/B^2)\,\vec{\nabla}\,p. \qquad (3)$$

When the fluid velocity normal to magnetic flux surfaces in an FRC equals the diffusion velocity, inward diffusion and outward convection of magnetic flux cancel, so $\partial\vec{B}/\partial t = 0$. (If the normal fluid velocity differs from the diffusion velocity, the difference may be related to an induced azimuthal electric field.)

For classical resistivity ($\eta_\perp \sim T^{-3/2}$), there is a singularity in Eq. (3) at the field null ("0-point"), which implies $|\vec{u}_d| \to \infty$ for $\partial\vec{B}/\partial t = 0$ as $B \to 0$. To avoid the singularity, one must somehow provide a force to drive an azimuthal current at the null.[4,8,9] This extra force modifies Ohm's Law, and consequently the diffusion velocity. In this paper, it is assumed that the diffusion velocity differs significantly from Eq. (3) only in the vicinity of the null.

The total diffusive flow through a given flux surface can be found by integrating $n_i\vec{u}_d$ over the surface. Furthermore, the required refueling rate in the region between two flux surfaces (neglecting burnup) is just the net diffusive flow out of the region. However, if this net outflow is negative, plasma will accumulate between the two surfaces, and a physically unrealistic particle sink would be required to maintain a steady state. Hence, a steady state cannot be maintained unless

$$\frac{d}{d\Psi} \oiint_S n_i\vec{u}_d \cdot d\vec{S} \geq 0\,, \qquad (4)$$

where S denotes a flux surface, and Ψ is the magnetic flux between the field null (radius R) and the portion of S where $r > R$ (assuming $B > 0$ for $r > R$).

The next section discusses the conditions under which Eq. (4) can be satisfied.

3. Criteria for Steady-State Density Profiles

In the long-thin approximation, Eq. (4) can be applied to a unit length. If the electron and ion temperatures are equal and uniform,

and only a singly-charged ion species is present (neglect fusion product ash), then one can show that Eq. (4) leads to

$$\frac{d}{dr_2}\left\{\frac{n_i}{B^2}\,\frac{dn_i}{dr_2}\left[\frac{r_1}{dr_1/dr_2}\,(\eta_\perp)_{r_1} - r_2\,(\eta_\perp)_{r_2}\right]\right\} \geq 0, \qquad (5)$$

where r_1 and r_2 are, respectively, the radii of the inner and outer portions of a particular flux surface ($r_1 = \sqrt{2R^2 - r_2^2}$).

The equation of state, $p = 2n_i kT$, and the pressure-balance equation, $p + B^2/2\mu_0 = B_0^2/2\mu_0$ (in which B_0 is the magnetic field in the vacuum outside the FRC), may be used to eliminate n_i in favor of B. Then particular models for $\eta_\perp$ may be used in Eq. (5) to obtain restrictions on physically permissible steady-state field profiles.

Case 1: Classical Resistivity

In this case, $\eta_\perp \sim T^{-3/2}$, so resistivity can be eliminated from Eq. (5). The eventual result is

$$\frac{d^2B}{dr_2^2} - \frac{1}{r_2}\,\frac{dB}{dr_2} - \frac{(B_0^2+B^2)}{B(B_0^2-B^2)}\left(\frac{dB}{dr_2}\right)^2 \geq 0. \qquad (6)$$

This criterion must be satisfied for all r_2 between the null and the separatrix.

It was assumed in writing Eq. (4) that $B > 0$ at $r = r_2$. Clearly, then, r_2, $(B_0^2-B^2)$, $(B_0^2+B^2)$, dB/dr_2, and $(dB/dr_2)^2$ are all positive, and the left-hand side of Eq. (6) can be positive only if d^2B/dr_2^2 is both positive and large enough to dominate the other two terms.

But there must be a region where $d^2B/dr_2^2 < 0$, in order for the field to merge smoothly with B_0. If this condition occurs within the separatrix, then Eq. (6) cannot be satisfied between the separatrix and the inflection point in the field profile. Even if the inflection point occurs outside the separatrix, the third term in Eq. (6) becomes very large in magnitude just inside the separatrix if B approaches B_0 there, whereas the curvature in the field profile will be small inwards from the inflection point. Thus, Eq. (6) is unlikely to be satisfied unless B is substantially less than B_0 at the separatrix; this condition would require high pressure outside the separatrix, with excessive particle losses along the open field lines.

Even away from the separatrix, Eq. (6) is difficult to satisfy; d^2B/dr_2^2 cannot remain large over a very broad interval in r_2 without increasing dB/dr_2 enough for the other two terms to dominate. (Note that the singularity in Eq. (6) at the null is a direct consequence of the singularity in Eq. (3)).

Case 2: LHD Resistivity

If the form for LHD resistivity derived by Gary[10] is used, then Eq. (5) yields

$$\left(\frac{2R^4}{r_2^4} - \frac{2R^2}{r_2^2} + 1\right)\left[\frac{3d^2B}{dr_2^2} + \frac{4B}{(B_0^2-B^2)}\left(\frac{dB}{dr_2}\right)^2\right]$$

$$+\frac{1}{r_2}\left(1 + \frac{2R^2}{r_2^2} - \frac{6R^4}{r_2^4}\right)\frac{dB}{dr_2} \geq 0. \qquad (7)$$

Eq. (7) does not pose such severe restrictions on steady-state profiles as does Eq. (6), although Eq. (7) is not satisfied by all FRC equilibria; for example, the rigid rotor,[2,3] which is often used to model FRC behavior, does not satisfy either Eq. (6) or Eq. (7).

4. Conclusions

In a long-thin uniform-temperature FRC with one, singly charged, ion species, if the current drive mechanism significantly affects the diffusion velocity only near the field null, then equilibria which can exist in a steady state in the absence of anomalous resistivity must have relatively high fluid pressure outside the separatrix - a condition which will lead to rapid particle losses along open field lines. Hence, efforts to reduce particle losses by suppressing anomalous resistivity may not be successful unless the current drive system is made to tailor the diffusion velocity profile throughout the plasmoid. This could be a much more difficult task for the current drive system than simply sustaining field reversal at the null.

Acknowledgment. This work was supported by U.S. Department of Energy Contract No. DEAC02-79ER10044.

References

1. W.T. Armstrong, et al., Phys. Fluids 24, 2068 (1981).
2. E.H. Klevans, Proc. U.S.-Japan Joint Symposium on Compact Toruses and Energetic Particle Injection, Princeton University, p. 135 (1979).
3. M. Tuszewski and R.K. Linford, Phys. Fluids 25, 765 (1982).
4. J.H. Hammer and H.L. Berk, Nucl. Fusion 22, 89 (1982).
5. R.D. Milroy and J.U. Brackbill, Phys. Fluids 25, 775 (1982).
6. Loren Steinhauer, Phys. Fluids 21, 230 (1978).
7. S.I. Braginskii, in Reviews of Plasma Physics (Consultants Bureau, New York, 1965), M.A. Leontovich, ed., vol. 1, pp. 262-291.
8. L.D. Pearlstein, et al., Nucl. Fusion Supplement 1979 (Plasma Physics and Controlled Nuclear Fusion Research, Seventh Conf. Proc., Innsbruck, 23-30 August 1978), p. 457.
9. Steven P. Auerbach and William C. Condit, Nucl. Fusion 21, 927 (1981).
10. S.P. Gary, Phys. Fluids 23, 1193 (1980).

Spheromak Equilibrium, Stability and Lifetime

SPECTROSCOPIC STUDIES OF IMPURITY CONTROL IN COAXIAL SOURCES FOR SPHEROMAKS AT LOS ALAMOS

H. W. Hoida, Cris W. Barnes, I. Henins, T. R. Jarboe, S. O. Knox, J. Marshall, D. A. Platts, A. R. Sherwood
Los Alamos National Laboratory, Los Alamos, New Mexico 87545

ABSTRACT

Spectroscopic measurements have been made of impurity radiation from coaxial sources used to produce spheromaks at Los Alamos. Some of these measurements were viewing the interelectrode region of the source. They show Doppler shifts implying impurity transport for low-Z impurities but not for metallic impurities. In others the relative emission of various lines from the spheromak in the VUV, quartz UV, and optical spectral regions are compared for various source operating parameters. Evidence for the control of impurity production is presented, and a descriptive model is proposed which explains aspects of the transport of impurities from the source into the spheromak.

I. INTRODUCTION

A magnetized coaxial Marshall gun is used as a source to form spheromaks in CTX. Plasma from this source is injected into a close-fitting conducting shell, the flux conserver, which is used to stabilize gross MHD modes, e.g., the tilt instability. Reconnection of magnetic field lines stretched during the injection process occurs in approximately 50 μs, forming a detached spheromak. This paper reports spectroscopic measurements of impurity line radiation taken as an indication of effectiveness of various cleanup measures. Comparisons were made of impurity radiation in the vicinity of the source electrodes and in the spheromak itself as experimental parameters were changed. These parameters included the voltage applied to the source, the amount of flux in the source magnetizing field, and the presence or absence of a background hydrogen gas (the "fill") in the source and the flux conserver. All of these affected the appearance of impurities at the source electrodes as well as in the spheromak. For example, "vacuum" discharges (shots with no hydrogen fill) showed more impurity radiation at the electrodes than "fill" discharges. The initial magnetic flux applied to the source, the "source poloidal flux" was also important. A fraction of this flux returned in the the space between the electrodes, and we call the field there "the bias field." For a flux of 0.02 Wb the bias field was 2.3 kG.

II. SPECTROSCOPIC OBSERVATIONS

Spectroscopic data reported here were taken using one VUV and two quartz UV spectrometers. One quartz UV instrument measured radiation along a line of sight into the region between the coaxial electrodes. The other spectrometers observed light coming from a diameter across the midplane of the spheromak. Doppler shifts were observed in spectral lines recorded by the spectrometer viewing the source, but not in the lines of the other two instruments. The wavelength range of observations was from 525 Å to 3600 Å. Data were acquired in two modes of spectrometer operation. One was to use film to obtain time-integrated spectrograms; the other was to to measure time-resolved intensity of a single line. Table I summarizes the observations. The "High" (H), "Moderate" (M), "Low" (L) and "Very Low" (VL) refer to the relative levels of radiation in the lines of the various impurities under different operating conditions. In both of the vacuum cases shown in the table the source poloidal flux was 0.018 Wb. In the background fill case the flux was 0.025 Wb. The voltage given is that on the capacitor bank driving the source. The bank voltage was lower and the poloidal flux was higher in the fill case. A "D" is used to show when a Doppler shift (~ 10^7 cm/s) was observed by the source spectrometer. Figure 1 shows the variation of an OV line intensity in the source and in the spheromak as a function of the poloidal flux in vacuum operation. At about 0.017 Wb there is a minimum in the oxygen radiation from the source, whereas, in the spheromak the radiation decreases monotonically with increasing poloidal flux.

TABLE I.

IMPURITIES IN CTX						
	VACUUM V = 46 kV Φ = 17 mWb		VACUUM V = 40 kV Φ = 17 mWb		BACKGROUND FILL (8mT) V = 36 kV Φ = 26 mWb	
IMPURITY	SOURCE	FLUX CONS.	SOURCE	FLUX CONS.	SOURCE	FLUX CONS.
METALS	H	M	L	M-L	L	VL
SILICON	H,D	M	H,D	M	L,D	L
ALUMINUM	M-L	L	M-L	L	L	VL
OXYGEN	H,D	H	H,D	M	M,D	L
CARBON	M,D	M	M,D		L,D	L

*Qualitative observation of the level of impurity radiation in CTX. H-high, M-moderate, L-low, VL-very low. D means that Doppler shift was observed.

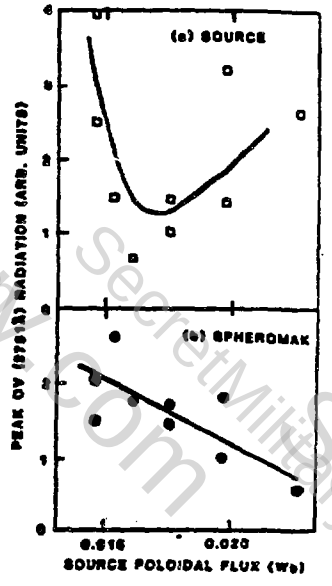

Fig. 1.
Peak OV radiation vs source poloidal flux.

High-Z impurities from the electrodes have been identified as iron, nickel, chromium, and tungsten from a plasma-sprayed coating. Medium-Z impurities such as aluminum (from the aluminum oxide insulator) and silicon (a constituent of the stainless steel electrodes) have been observed. Low-Z impurities, carbon, nitrogen, and oxygen, have also been seen in the source discharge. The origin of these impurities may be from atoms diffusing out from the electrode material or from gas originally from the flux conserver, insulator, or other regions of the vacuum system which is adsorbed on the surface. A decrease in the discharge current or voltage reduces the production of high-Z impurities in the source. The use of a background fill of H_2 reduces further the high-Z impurities and also lowers the level of medium-Z impurities; however, the amount of low-Z impurities in the source does not appear to be affected by the fill.

With an oxygen-free copper flux conserver and with tungsten-coated electrodes, rf discharge cleaning and pulse discharge cleaning in H_2 at about 7 mT pressure reduce the level of oxygen and nitrogen observed in the source. This reduction was not possible with a nickel-plated flux conserver. Carbon impurities were always reduced by discharge cleaning. Thus a combination of techniques are used to reduce the production of all categories of impurities in the source.

III. MODEL FOR TRANSPORT OF IMPURITIES FROM THE SOURCE INTO THE SPHEROMAK

The amount of flux in the spheromak depends on the values of the main bank energy and the source poloidal flux and also on the ratio of these two quantities. For low values of source poloidal flux, most of this flux is used in the spheromak formation; the flux in the spheromak is roughly proportional to the geometric mean of the volt seconds delivered by the bank and the source poloidal flux. As the source poloidal flux is increased, a monotonically decreasing fraction of the flux is used to form the spheromak. At very high source poloidal flux values the plasma is stopped in the source and no spheromak is formed. The fraction of source flux that is used in spheromak formation may be increased by increasing the bank energy. The impurities are released from the surface of the electrodes, and since the bias field inhibits their transport radially, they tend to remain on flux surfaces which were originally near the electrodes. If all the available flux is not used, the unused flux surfaces are those closest to the inner electrode (see Fig. 2), and the impurities released there are left behind. Ignoring flux mixing, the poloidal flux near the outer electrode maps into outer flux surfaces of the spheromak. Thus impurities from the outer electrode tend to end up on the outside of the spheromak where they may be more easily lost.

The amount of impurities entering the spheromak from the source can thus be dependent on the magnitude of the source poloidal flux. It can also depend on the impurity charge-to-mass ratio. Doppler shift measurements show that the medium-Z and low-Z impurities are Doppler shifted, and the high-Z (low charge-to-mass ratio) impurities are not. The magnitude of the shift is approximately one angstrom measured at 3000 Å (for OIV) corresponding to a velocity of 10^7 cm/s. The absence of a Doppler shift shows that the high-Z impurity ions are not accelerated with

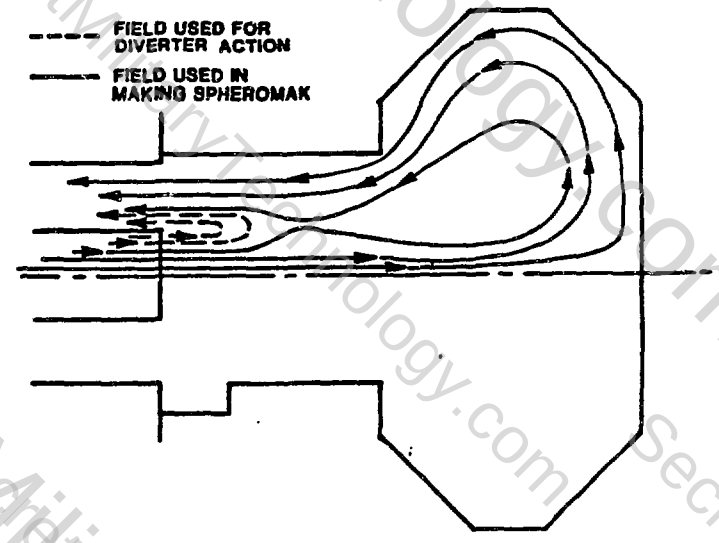

Fig. 2.
Flux surface geometry and reconnection phenomena during the formation of the spheromak.

the current sheath. These late-arriving high-Z ions are probably easily separable from the spheromak plasma after reconnection with a modest amount of source poloidal field (Fig. 3). The Doppler shifts for the medium-Z and low-Z impurities indicate that these impurities are accelerated with the current sheath. The hydrogen fill allows operation with more source poloidal flux for similar spheromak fluxes, thus utilizing a smaller fraction of the available source poloidal flux. This model explains the reduction in the levels of oxygen and iron with increasing source poloidal flux shown in Figs. 1 and 3. Figure 1a shows a minimum in the peak OV radiation vs source poloidal flux. For higher flux values the oxygen stagnates in the source causing the increase in observed radiation there, while the radiation in the spheromak is decreased as shown in Fig. 1b. For lower values the lower bias field reduces the protection of the electrodes allowing an increase in the oxygen released from them.

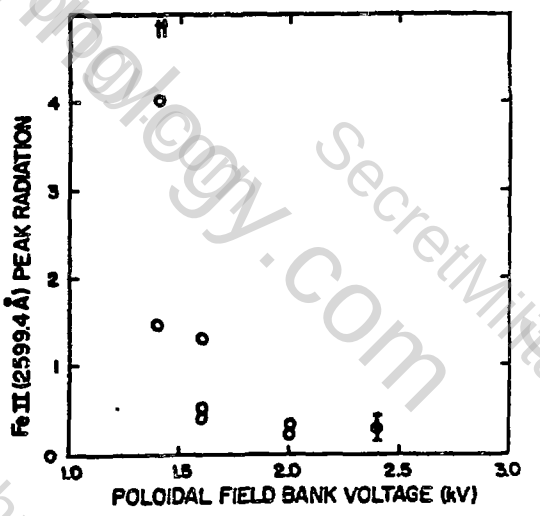

Fig. 3.
Peak FeII radiation vs source poloidal field bank voltage, in both the source and the flux conserver.

IV. DISCUSSION

The appearance of impurities and their transport into the spheromak is affected by many factors. The level of impurities in the source appears to be affected by the electrode material, the contaminants on the electrodes, the bank voltage, the amount of poloidal flux, and the presence of a gas fill. The transport of impurities into the spheromak is affected by the charge-to-mass ratio of ions and the amount of source poloidal flux, which acts as a divertor spatially and a barrier (after reconnection) temporally. The impurity level in the spheromak has been minimized by changing the electrode material to tungsten, lowering the main bank voltage, operating at as high a poloidal flux as possible, discharge cleaning to remove the contaminants, and adding a hydrogen fill.

Effects of Passive Coils on Spheromak Gross MHD Instabilities

C.Munson, A.Janos, S.Paul, F.Wysocki,
and M.Yamada

Princeton Plasma Physics Lab
Princeton, N.J. 08544

Abstract

The experimental investigation of the effectiveness of figure-8 coils in stabilizing the $n = 1$ tilting mode of spheromak plasmas in Proto S-1 A/B is extended. In addition, another coil configuration, the "saddle" coil, is examined.

Introduction

Spheromak plasmas are known, both theoretically[1., 2., 3.] and experimentally,[4., 5., 6.] to be unstable to a number of gross MHD modes, the most important being the $n = 1$ tilt, shift, and vertical instabilities. The behavior of these modes is dependent upon the plasma parameters, the position and shape of nearby conductors, and the index of the externally applied vertical field B_{V0},

$$n_i \equiv (-R_0/B_{V0})(\delta B_{V0}/\delta R).$$

Very simple estimates of this behavior may be obtained by considering a thin, rigid current ring as a model for the plasma. In the case of the $n = 1$ tilting mode this model reduces, for small tilt angles, to:

$$\Theta'' + \Theta\left(\frac{\pi |I_{pl}| B_{V0}| R_0^2}{c I_{zz}}\right)(n_i - 1) = 0,$$

where Θ = tilt angle, I_{pl} = toroidal plasma current, B_{V0} = external equilibrium field at the midplane, R_0 = plasma major radius, $I_{zz} = (M_{pl}/2)(R_0^2 + \frac{5}{4}a^2)$ = moment of inertia around the tilt axis, M_{pl} = plasma mass, a = plasma minor radius, and n_i is the field index. For typical experimental parameters (He fill of $\approx 50\mu$, $n_e \approx 10^{15}/cm^3$, $I_{pl} \approx$ 15KA, $R_0 \approx$ 7cm, $a \approx$ 4cm , $B_{V0} \approx$ 1.2KG , $B_{pol} \approx B_{tor} \approx$ 1.3KG , and $n_i \approx -0.1$), this model yields an inverse growth rate $\gamma^{-1} \approx \tau_{Alfven}$ (τ_{Alfven} defined using peak B_{tor} and a).

More sophisticated treatments of the plasma behavior may be achieved through the use of a modified version of the PESTII code,[7.] or MAGIC3C, the 3-D MHD code recently developed by Sato and co-workers at Hiroshima.[8.] Results of the modified PESTII code, scaled to simulate experimental parameters, yield a value $\gamma^{-1} \approx (2 \rightarrow 3)\tau_{Alfven}$, while the MAGIC3C code gives $\gamma^{-1} \approx 10\tau_{Alfven}$.

Experimental runs in Proto S-1 A/B produce tilt unstable plasmas with measured values of $\gamma^{-1} \approx (3 \rightarrow 6)\tau_{Alfven}$ for $n_i \leq -0.1$, or plasmas which are stable for a lifetime of $20 \rightarrow 25\mu$sec with n_i very slightly positive. The stability of these cases with $0 \leq n_i \leq 1$, which are expected to be slightly ($\gamma\tau_{Alfven} << 1$) unstable to tilting, is attributed to line-tying to the nearby flux core. The lifetime is limited by radiative energy loss and resistive decay ($L/R \approx 27 \rightarrow 50\mu$sec for $Z = 2$ and $T_e \approx 10 \rightarrow 15$ev) causing the plasma to deviate from an equilibrium configuration.

Experimental Setup

The Proto S-1 A/B device[9.,10.,11.] is composed of a cylindrical stainless steel vacuum vessel (24 inch diameter, 30 inch length, with a $\frac{3}{8}$ inch wall thickness), with eight pancake coils at each end plate providing the required equilibrium magnetic field ($B_Z \leq 1.2$KG). Either of two essentially identical flux cores (see Fig. 1) may be mounted at the midplane. Each of these flux cores contains a 3 turn Poloidal Field winding and a 40 turn Toroidal Field winding, with associated current leads, has a 15cm major radius R_C, a 3cm minor radius r_c, and is covered by a three mil stainless steel liner. At one time, pinch coils were installed to aid in the separation of the plasma from the flux core (hence the A/B designation), but were found to be unnecessary. Currents required to drive the necessary flux swings in the core are supplied by capacitor banks.

Magnetic field information is provided by a probe array composed of five sets of orthogonal coils (B_Z, B_θ, B_R) spaced 2cm apart radially (2cm $\rightarrow$ 10cm). Signals from this array are integrated and digitized at a 1 MHz rate and the resulting information stored for later use. The probe may be rotated toroidally and translated axially, providing access to the entire spheromak region. By stepping the probe along Z, and rotating by 180°, complete field information in any selected toroidal plane may be obtained.[10., 11.] Plasma reproducibility is generally good but, in order to help reduce the effects of shot-to-shot variations, several shots are fired at each probe position and the results averaged.

The figure-8 coils, a passive stabilizing configuration suggested by numerical studies of close fitting conducting shells,[12.] consist of two sets of two orthogonal coils: one above, and one below the plasma. The top set is shown in Fig. 2a. These may be positioned so that their inner edges are a specified distance from the plasma midplane. The "saddle" coils depicted in Fig. 2b are composed of four coil loops positioned around the flux core so that their inner edges are 6cm above and below the plasma midplane at a radius of 9cm. Both coil sets are designed to couple to the $n = 1$ tilting, but not to the $n = 0$ core currents.

Experimental Results

With the machine parameters adjusted to produce a tilting instability with an inverse growth rate $\gamma^{-1} \approx 5.9\mu\text{sec}$ ($\approx 6\tau_{Alfven}$), where $\gamma \equiv (d \ln \theta/dt)_t$, a comparison has been made between the figure-8 coils, with inner edges 6cm from the midplane, and the "saddle" coils. The results are shown in Fig. 3, where $T = 0\mu\text{sec}$ corresponds to the initial time when a spheromak configuration is present. Also shown in Fig. 3 is a case for which the figure-8 coils were covered with an insulating ceramic material to eliminate the possibility of line-tying effects with the coils.

A linear regression analysis applied to the cases in Fig. 3 indicates an initial tilt angle at $T = 0$ of $\Theta \approx 3°$ for the no coil case. The plasma has begun to tilt even before the spheromak configuration is completely established. Both the figure-8 and "saddle" coil cases regress to $\Theta \leq 3°$ for times later than the formation time, indicating the presence of a "stable period", i.e. growth rates reduced to such an extent that initial perturbations do not grow to $\Theta > 3°$ during this time. This stable period is $\tau_S \approx 9\mu\text{sec}$ (compared to a total plasma lifetime of $\approx 22\mu\text{sec}$) for the figure-8 coil case, and $\tau_S \approx 13\mu\text{sec}$ for the "saddle" coil case. After these times, plasma conditions apparently have changed sufficiently to reduce the effectiveness of the coils.

Fig. 4 shows, for machine parameters which give an inverse growth rate without stabilizing coils of $\gamma^{-1} \approx 7\mu\text{sec}$, and a total lifetime of $\approx 25\mu\text{sec}$, the results of systematically decreasing the distance from the edges of the insulated figure-8 coils to the midplane.

Applying the same analysis to the cases in Fig. 4 as was used for Fig. 3 yields an initial tilt angle $\Theta \approx 2.5°$ for the 20cm case, indicating that the coils at this distance are effectively decoupled from the plasma. The case with the coils 14cm from the midplane has a stable period $\tau_S \approx 17\mu\text{sec}$ ($\approx \frac{3}{4}$ the total plasma lifetime) and the case with a 12cm coil position has $\tau_S \approx 21\mu\text{sec}$. Thus it is seen that as the coils are brought closer to the plasma, the stable period increases rapidly. For times after $\approx 20\mu\text{sec}$, the resistive decay of the plasma currents has resulted in significant changes in the configuration, reducing the effectiveness of the coils. In addition, the instabilities which appear at these times may not be purely tilting modes.

Conclusions

Two different coil configurations, the figure-8 coils and the "saddle" coils, have been shown to be effective in stabilizing the tilting instability of Proto S-1 spheromak plasmas while maintaining compatibility with the formation technique.

Work supported by U. S. DOE contract no. DE-ACO2-76-CHO-3073

References

[1]M. N. Rosenbluth and M. N. Busac, Nuclear Fusion **19** (1979) pg. 489.

[2]M. Okabayashi and A. M. M. Todd, Nuclear Fusion **20** (1980) pg. 571.

[3]S. C. Jardin et al., Nuclear Fusion **21** (1981) pg. 1203.

[4]C. Munson et al. , in ***Proceedings of the Fourth Symposium on the Physics and Technology of Compact Toroids***, Lawrence Livermore National Lab (1981), pg. 149.

[5]T. R. Jarboe et al., in ***Proceedings of the U. S. -Japan Joint Symposium on Compact Toruses and Energetic Particle Injection*** , 1979, PPPL, pg. 53.

[6]H. Bruhns et al., presented at 23rd APS/DPP Meeting in New York, NY, October 12-16, 1981.

[7]F. Wysocki and R. Grimm, presented at 24th APS/DPP Meeting in New Orleans, LA, November 1-5, 1982.

[8]T. Sato et al. , in ***Proceedings of the Ninth Conference on Plasma Physics and Controlled Nuclear Fusion***, Baltimore (1982).

[9]H. P. Furth, in ***Proceedings of the U. S. -Japan Joint Symposium on Compact Toruses and Energetic Particle Injection*** , 1979, PPPL, pg. 1.
M. Okabayashi et al. , ibid pg. 166.
M. Yamada et al. , ibid pg. 171.

[10]M. Yamada et al. , Phys. Rev. Lett. **46** (1981) 188.

[11]M. Yamada et al. , in ***Third Symposium on Physics and Technology of Compact Toroids in the Magnetic Fusion Energy Program*** , Los Alamos Scientific Lab, pg. 124.

[12]S. C. Jardin and U. Christensen, ***Stabilizing Windings for the Tilting and Shifting Modes in an Inductively Formed Spheromak***, PPPL-1814, August, 1981.

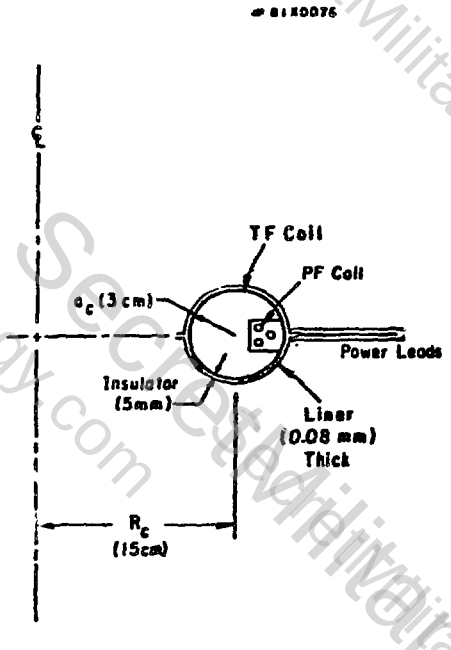

Flux Core
Figure 1

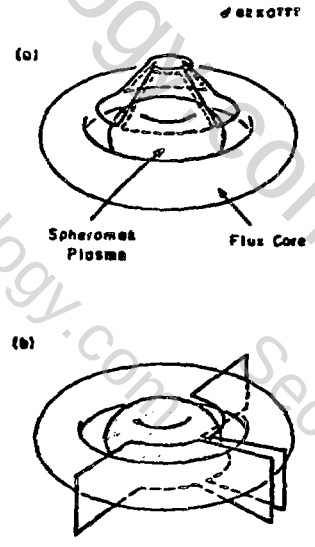

Configuration of figure-8 and saddle coils
Figure 2

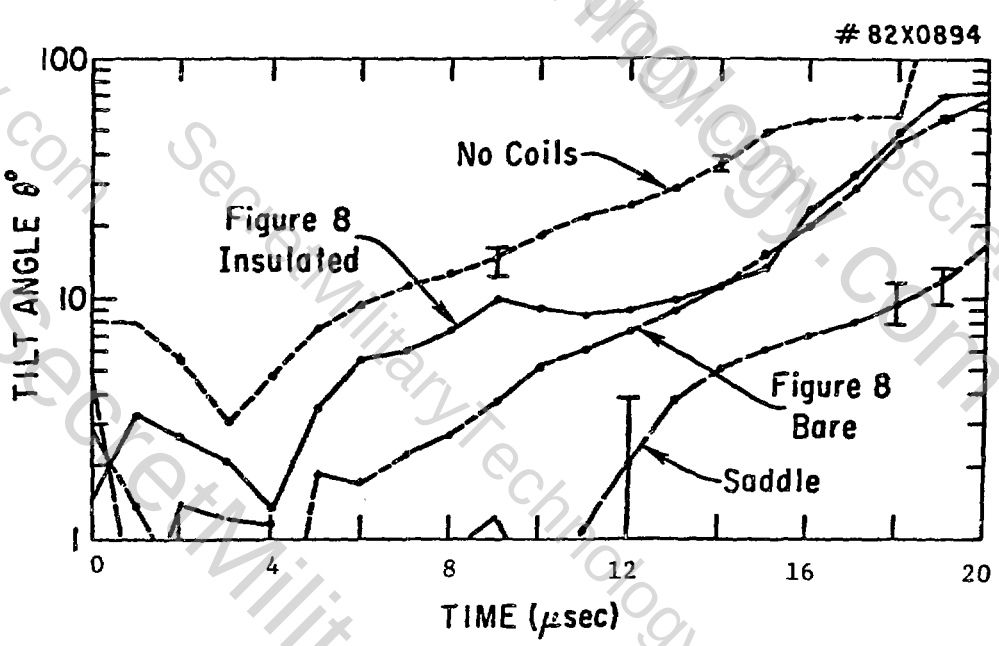

Figure 3

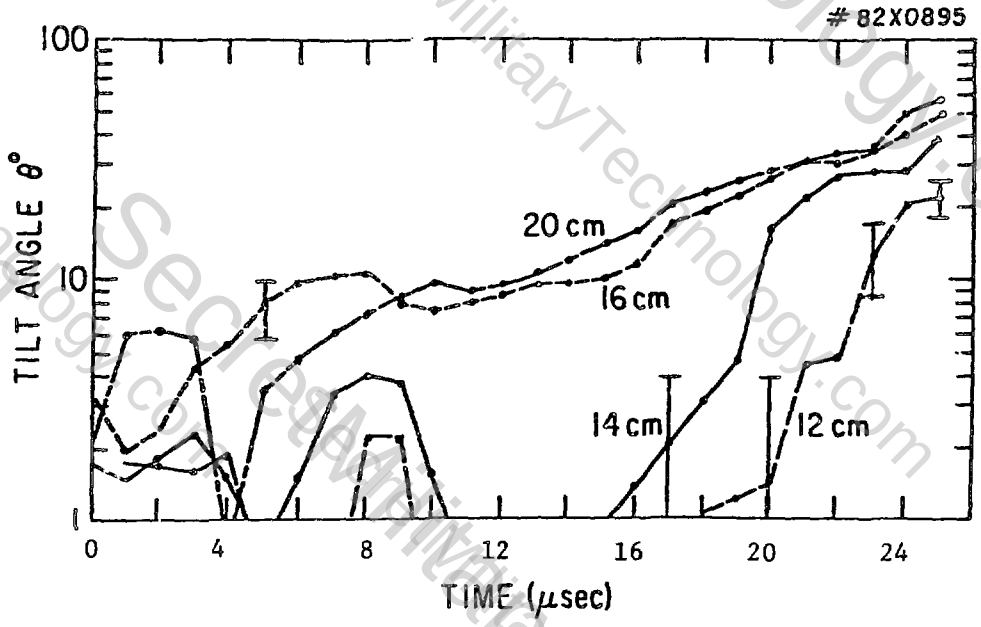
82X0895
100
10
1
TILT ANGLE θ°
20 cm
16 cm
14 cm
12 cm
0
4
8
12
16
20
24
TIME (μsec)

Figure 4

CURRENT RESULTS FROM THE LOS ALAMOS CTX SPHEROMAK

Cris W. Barnes, I. Henins, H. W. Hoida, T. R. Jarboe, S. O. Knox,
R. K. Linford, D. A. Platts, and A. R. Sherwood
Los Alamos National Laboratory, Los Alamos, NM 87545

INTRODUCTION

Continued discharge cleaning, improved vacuum practices, and optimized plasma formation operation have resulted in the Los Alamos CTX spheromak experiment achieving 1 millisecond plasma lifetimes with average temperatures of 20-40 eV. Several methods have been used to augment the cleanup of the plasma, resulting in significant reductions in the impurity radiation power loss. The major advance in operation has been the use of a constant, uniform background of 5-20 mTorr of H_2 filling the vacuum tank, flux conserver, and plasma source. This fill operation directly reduces the impurities generated in the plasma source, allows operation of the source at parameters resulting in fewer impurities, and provides a neutral particle source to maintain the density for long lifetimes. In this paper we present data on the improved operation of CTX.

NEW DIAGNOSTICS

Essential to the increased understanding of the CTX spheromak has been the addition of several new plasma diagnostics. Foremost has been a multipoint Thomson scattering system with 12-radial positions, giving radial profiles of temperature and density on a single shot. Spectroscopic measurements have been augmented by the use of a 1-m vacuum ultraviolet spectrometer for observing the power radiated in resonance transitions of low-Z impurity ions. Also, a quartz UV spectrometer has been used to view the inter-electrode region of the source.

METHODS FOR IMPURITY REDUCTION

We have continued a program of discharge cleaning the electrodes and the vacuum system after any opening to the atmosphere. Continued use of a 0.1-0.2 Hz repetitive operation of the source at low voltage (1.5-2.5 kV) results after several nights (10^4-10^5 pulses) in significant decreases in carbon and nitrogen radiation, as well as oxygen, achieving higher charge states and approaching burnthrough. During the pulse discharge cleaning we now use an rf glow discharge which is seen to be at least as effective in cleaning as a dc glow, but with far less sputtering of metal surfaces in the vacuum system.

In order to prevent arcs across the insulator of the source electrodes as the voltage reverses we now crowbar the main capacitor gaps. This has prevented the arcs from releasing aluminum and oxygen after each shot that would contaminate the electrodes for the next shot.

When using the dc glow for discharge cleaning the copper flux conserver sputtered badly, coating optical surfaces in the vacuum system. To reduce sputtering the flux conserver was nickel-plated by electroplating it in a solution of $NiSO_3NH_2$ and boric acid. However, after considerable use it was recognized that this coating was an important source of impurities in the system. The replacement of the Ni-plated flux conserver with an oxygen-free-copper one resulted in significant improvement of the discharge.

We have been heating the flux conserver to over 200 ^{0}C during discharge cleaning but as yet cannot ascribe directly any improvement to this effort. The installation of hydrogen-furnace-baked tungsten-sprayed electrodes coincided with the removal of the Ni-plated flux conserver, and again no direct improvement can be asserted.

BACKGROUND FILL OPERATION

The coaxial source has been operated in the presence of a static background of hydrogen filling the source, flux conserver and vacuum tank. This mode of operation has directly reduced the impurity production in the source compared to operation at the same voltages and bias fields injecting into a low-base-pressure vacuum. Even more importantly it has broadened the range of operating parameters to lower voltages and higher poloidal fields, further reducing the impurities in the spheromak.[1] In this mode the plasma has higher initial temperatures and slower magnetic-field-energy decay rates τ_{B2}. Figure 1 shows the magnetic field and density for one of our best shots obtained with the fill operation. The lifetime is 1 ms, with τ_{B2} exceeding 400 μs. The poloidal field on axis has bumps during its decay. Further analysis reveals that after the separated spheromak has

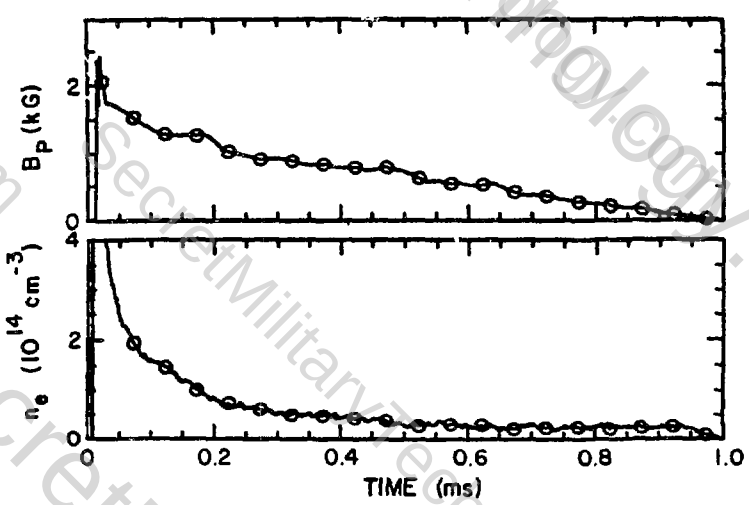

Fig. 1.
Poloidal magnetic field and line-integrated density versus time for H_2 fill operation.

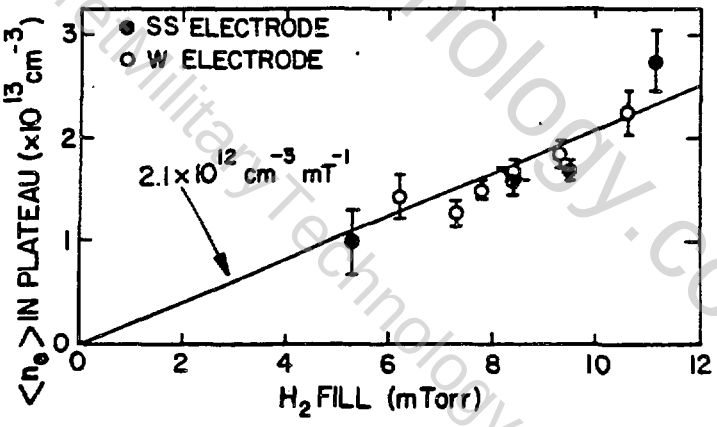

Fig. 2.
Mean electron density during the "plateau" versus the fill pressure of hydrogen. Too little gas does not protect the electrodes and results in dirty, short-lived shots. Too much gas also causes too much radiation and faster B-field decays. The optimum pressure is typically 7-9 mTorr for our experiment.

formed, these bumps in the axial component of the field are accompanied by a rotation of the transverse components on the major axis of the plasma. This fluctuation quickly saturates and does not adversely affect the stability of the plasma; rather, it seems to always accompany the longest lived discharges.

The interferometer indicates an initial density spike that precedes the observation of magnetic field in the spheromak, possibly due to an ionizing shock from the source. After the flux is injected the density decreases at a more rapid rate than the magnetic field, until it reaches a value around $2\text{-}4\times10^{13}$cm^{-3} where it remains constant. This differs from the results observed under vacuum-operation conditions where the magnetic field decays smoothly, and the density decays at about the same rate.[2] The level of the constant density "plateau" is linearly proportional to the fill pressure in the tank (Fig. 2). Changing vacuum surfaces can have a noticeable effect of the optimum amount of fill for operation.

THOMSON SCATTERING AND β PROFILES

Figure 3 shows radial density (normalized to interferometric density measurement) and temperature profiles measured on a single shot with multipoint Thomson scattering. This shot is typical of fill operation, and has a τ_{B2} of 410±100 μs. On almost all shots the density is peaked at the 28 cm position, near the expected location of the magnetic axis.[3] The temperature has a decrease or "hollowing" at the peak density. In spheromaks which are known to be very dirty (achieved by poisoning the fill gas with up to 6% argon impurity) the temperature is flat and low (≤15 eV) with a dip at the peak density. On cleaner shots the peak temperature can

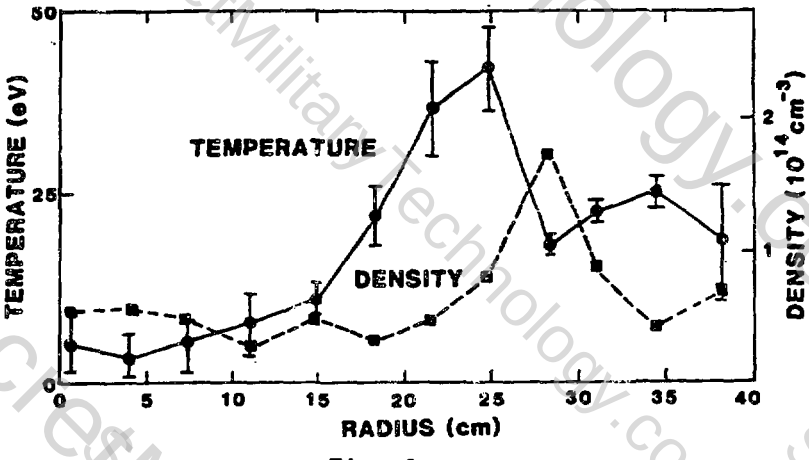

Fig. 3.
Thomson scattering temperatures (circles) and density (squares) measured on a single shot 198 μs after source injection.

be over 50 eV, and it almost always has a pronounced hollow profile. This would be expected if impurity radiation were dominating the local energy balance near the magnetic axis, because the radiation increases greatly with higher density and tends to cool the plasma locally.

Assuming a model for the magnetic field which minimizes the magnetic energy at constant helicity,[3] and normalizing the magnitude to the single point measurement on the geometric axis, local β's can be determined from the measured pressure profile. The ion density and temperature are assumed to equal the electron values. Figure 4 shows the value of β determined from the data of Fig. 3. Values of β from 10% to 30% have been observed in the clean fill operation, with an average value of typically 15±8%. For the data of Fig. 4, an energy confinement time can be estimated by assuming all the magnetic energy decay is going into input heating power. Then $\tau_E \cong 3/2 \langle\beta\rangle \tau_{\beta 2} \approx 62\pm24$ μs where the average plasma pressure normalized to the average B-field squared is about 10±3%.

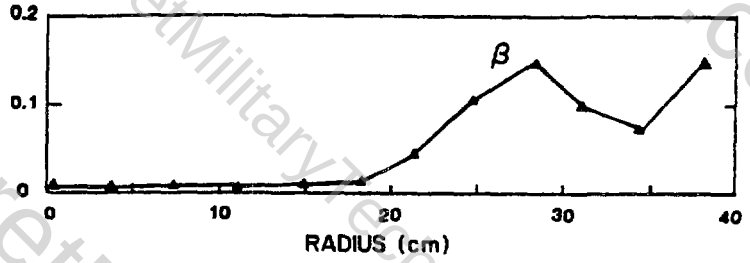

Fig. 4.
The local β obtained from the measured plasma pressure (Fig. 3) with ion density and temperature assumed equal to the electron values, and the calculated magnetic field (Ref. 3).

Finally we note that the dramatic difference in plasma behavior between the colder, radiation-dominated discharges and the hotter, fast-density decay shots provides evidence that the plasma β may be affecting the transport in the latter case.

REFERENCES

1. H. W. Hoida et al., in Proceedings of the U.S.-Japan Workshop on Compact Toroids (1982).

2. Cris W. Barnes et al., in Proceedings of the Fourth Symposium on the Physics and Technology of Compact Toroids, Livermore, CA (October 27-29, 1981) p.125.

3. J. M. Finn, W. M. Manheimer, and E. Ott, Phys. Fluids 24 (1981) 1336; A. Bondeson et al., Phys. Fluids 24 (1981) 1682.

4. Cris W. Barnes et al., Proceedings of the U.S.-Japan Workshop on Compact Toroids (October 19-20, 1982), to be published.

Ion Temperatures inferred from Newtron Measurements in TRISOPS IIX

D. R. Wells, P. Ziajka, and J. Tunstall

Department of Physics, University of Miami, Coral Gables Florida 33124

The ion temperature history of the plasma fireball in TRISOPS IIX has been measured by comparing the time resolved neutron yield from a D-D reaction and a D-T reaction. This measurement results in a reading of ion temperature that is independent of any assumptions of plasma density or fireball volume. The results verify and clarify previously reported TRISOPS parameters. In a separate set of measurements using a D-D reaction, the ion temperature rises in 5 μs to 6 KeV with a corresponding density of 10^{15} ions/cm^3. After 8 μs it falls rapidly to 1 KeV as the density rises to 10^{17} ions/cm . The 1 KeV temperature is held for about 20 s. These temperatures and densities yield an equilibration time for ions and electrons that is long compared to the duration of the experiment.

PACS numbers: 52.25 Lp, 52.55 Ke, 52.55 Pi

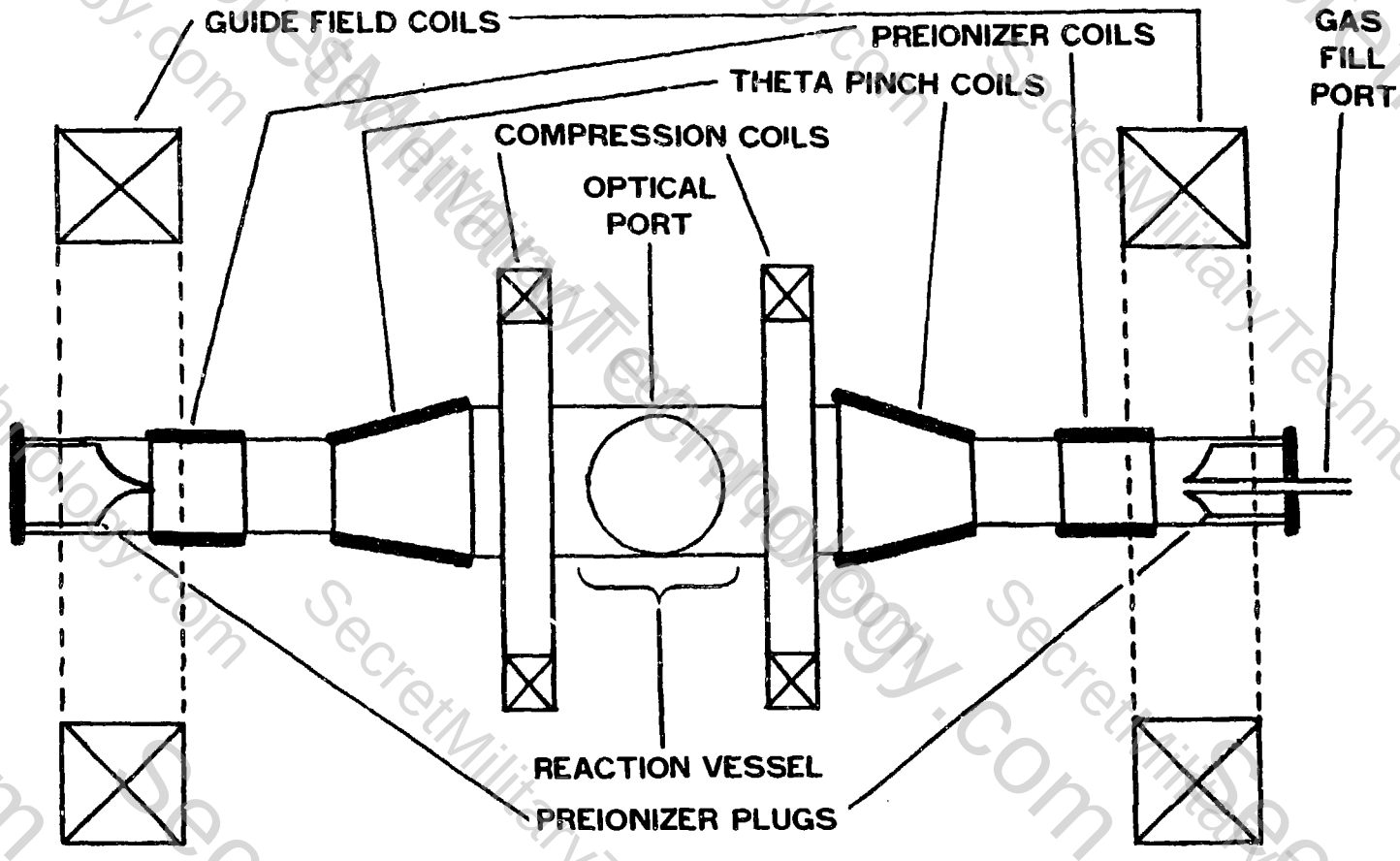
GUIDE FIELD COILS
PREIONIZER COILS
THETA PINCH COILS
GAS FILL PORT
COMPRESSION COILS
OPTICAL PORT
REACTION VESSEL
PREIONIZER PLUGS

Figure 1

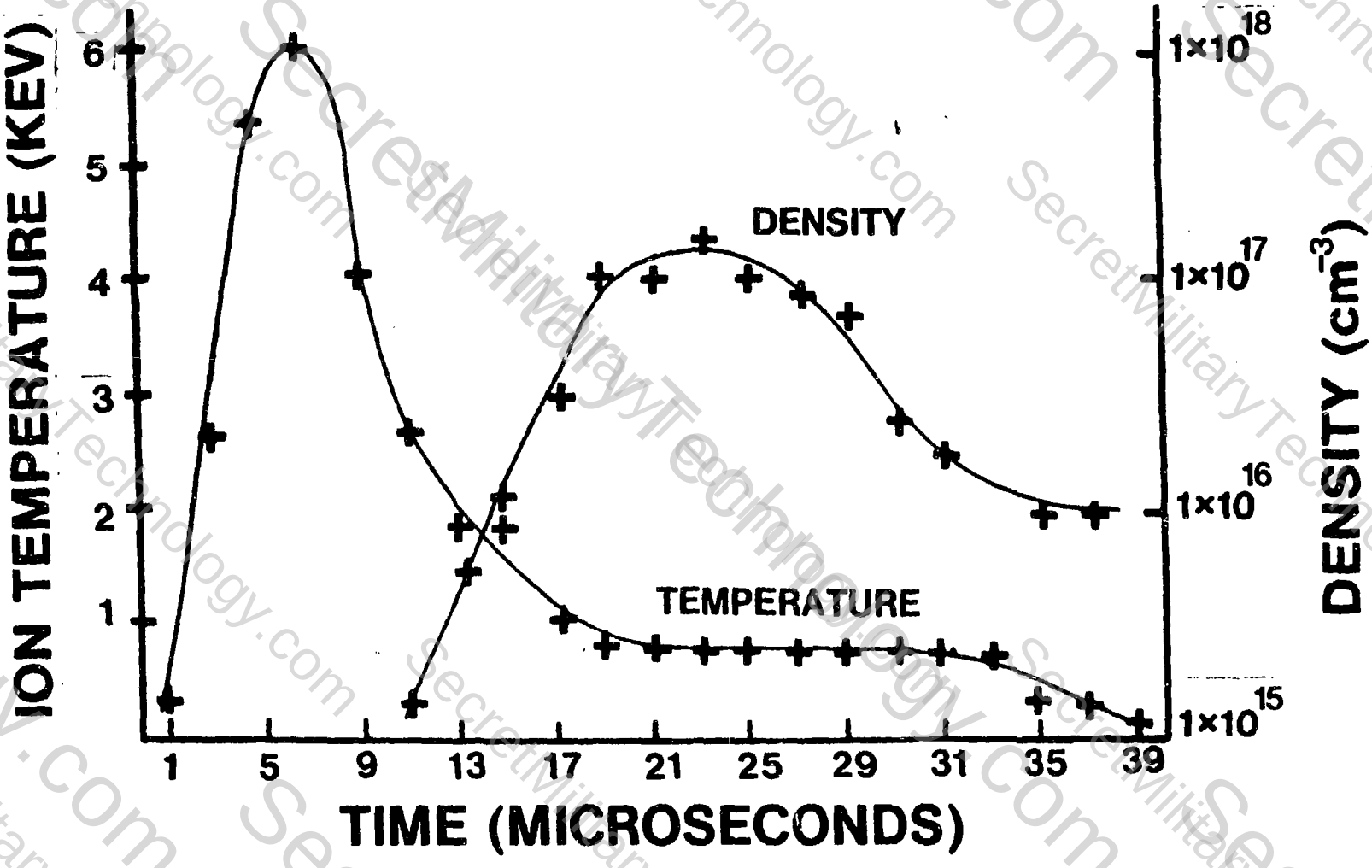
ION TEMPERATURE (KEV)
6
5
4
3
2
1
DENSITY
TEMPERATURE
1×10^18
1×10^17
1×10^16
1×10^15
DENSITY (cm^-3)
1
5
9
13
17
21
25
29
31
35
39
TIME (MICROSECONDS)

Figure 2

NEUTRON EMISSION RATE (10/μsec.)
1 2 3 4 5 6 7 8 9 10
T_i - kev
1 2 3 4 5 6
B comp., 36 kG peak
T_i
DENSITY
NEUTRON EMISSION
TIME-MICROSECONDS
1 7 10 20 30 40
10^15 10^16 10^17
ION DENSITY (particles/cc)

Figure 3

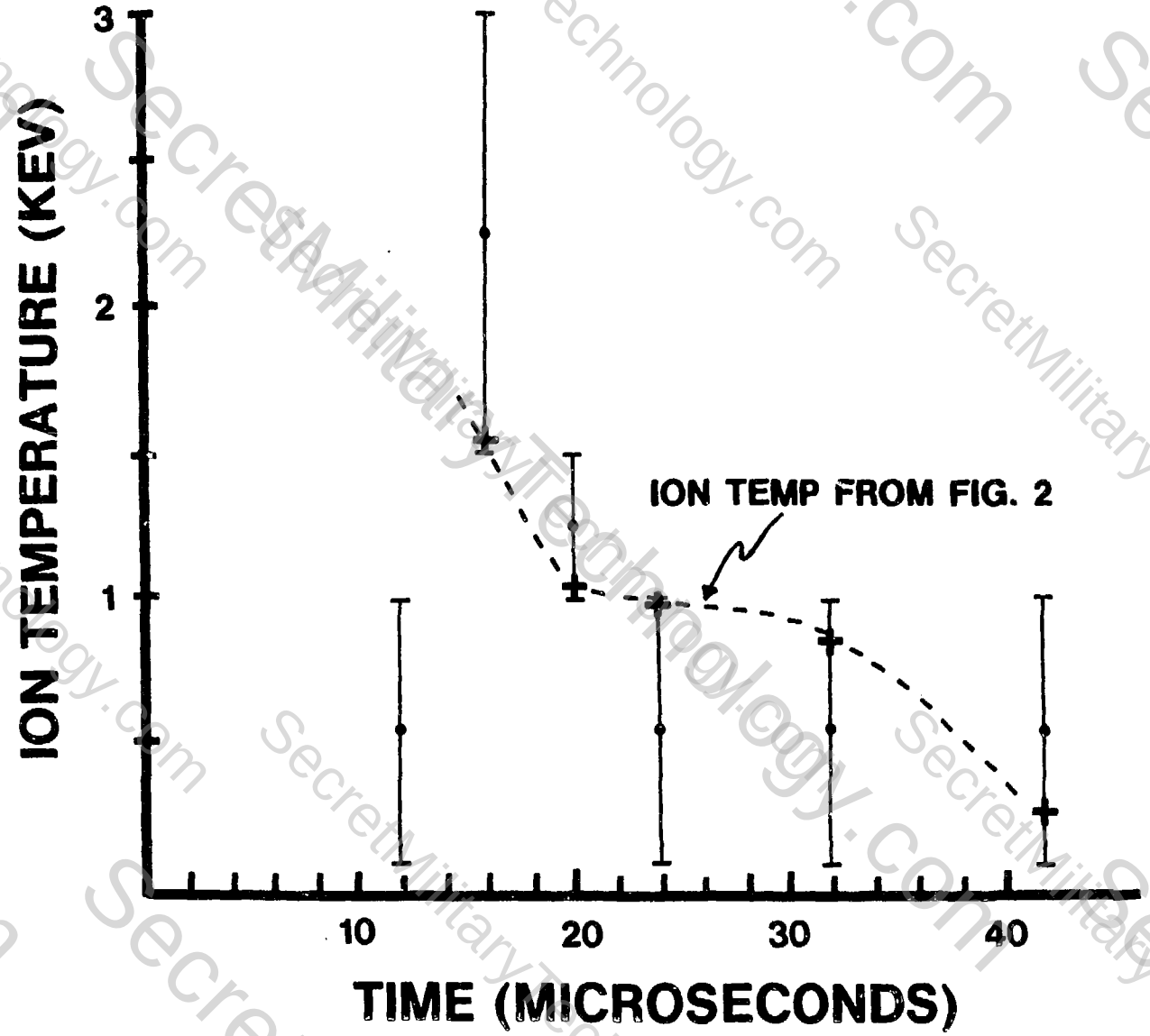

Figure 4

LINEAR and NONLINEAR STUDIES OF THE RESISTIVE INTERCHANGE MODE IN THE CYLINDRICAL SPHEROMAK.

J. DeLucia and S. C. Jardin

Plasma Physics Laboratory, Princeton University
P.O. Box 451, Princeton, New Jersey 08544

1. Linear

The growth rates for resistive instabilities in the cylindrical spheromak are computed by using two complementary methods. The first method solves the full linearized resistive MHD equations as an initial value problem, utilizing zone packing around the mode rational surface. Resolution requirements limit this to values of the magnetic Reynolds number $S < 10^7$. The second method employs boundary layer analysis and asymptotic matching,[1,2] most valid for $S \gtrsim 10^5$. The 6th order resistive inner region equations are solved numerically as an asymptotic boundary value problem. These solutions are matched onto a numerical solution of the ideal Euler equations in the outer region. The general matching condition involves even and odd parity modes with complex frequency, and includes both interchange and tearing forces. The inner region equations and matching condition have also been generalized to toroidal geometry with multiple rational surfaces.

Each of these methods has independent checks on its accuracy. The results from these two methods agree to better than 1 in 10^3 in the overlap region $10^7 > S > 10^5$. We scan the parameter space of possible spheromak configurations by computing contours of the resistive growth rates in the continuous space formed by nq_o, na/R, for several values of the central pressure p_o and the poloidal mode number m. If we take the q-profiles to be parabolic in r, the least unstable configurations have $q_oR/a \sim 0.67$. In figure 1 contours of constant growth rate in $[na/R, nq_o]$ space are plotted for $m = 1$, $S = 10^6$ and a pressure profile parameterized by the Suydamn parameter $\alpha = 0.5$. Growth rates are proportional to the integer labels. Dashed curves separate ideally stable and unstable regions. Dotted-dashed curves in the resistively unstable region mark the points where $\Delta' = 0$. It is evident in figure 1 that the Δ' criteria is not a useful measure of resistive instability

in finite pressure configurations. As the pressure is decreased the growth rate contours become increasingly parallel to the $\Delta' = 0$ curves. We expect these straight system results to be fairly insensitive to toroidal corrections, as is the case for ideal instabilities in the spheromak.[3]

2. Nonlinear

The nonlinear time development of the m = 1 resistive interchange mode in the cylindrical spheromak is studied using a fully compressible, single helicity resistive MHD code. The time advancement equations for the plasma quantities are

$$\frac{\partial}{\partial t}\chi + \vec{v}\cdot\nabla\chi = \eta[\Delta^*\chi - Mg] + c(t) ,$$

$$\frac{\partial}{\partial t}(g - M\chi) + \alpha^2\vec{v}\cdot\nabla\frac{g}{\alpha^2} + g\nabla^2\Omega = \alpha^2\vec{B}\cdot\nabla\frac{\omega}{\alpha^2} + \eta\Delta^* g - M\,c(t),$$

$$\frac{\partial}{\partial t}\omega + \vec{v}\cdot\nabla\omega = \vec{B}\cdot\nabla g ,$$

$$\frac{\partial}{\partial t}\Delta^* A + \nabla\cdot\left[\frac{(\Delta^* A - M\omega)}{\alpha^2}\vec{v}\right] = \frac{k^2}{\alpha^4}\frac{\partial}{\partial\tau}(g^2 - \omega^2) + \vec{B}\cdot\nabla\left[\frac{\Delta^*\chi - Mg}{\alpha^2}\right] ,$$

$$\frac{\partial}{\partial t}\nabla^2\Omega + \nabla^2 p + \vec{B}\cdot\nabla^2\left[\frac{\hat{e}}{\alpha}\times\nabla\chi + \frac{\hat{e}}{\alpha}g\right] = -\nabla\cdot(\vec{v}\cdot\nabla\vec{v}) - (\nabla\times\vec{B})^2 ,$$

and

$$\frac{\partial}{\partial t}p + \vec{v}\cdot\nabla p + \frac{5}{3}p\nabla^2\Omega = \frac{2}{3}\eta\,(\nabla\times\vec{B})^2 .$$

Here $\tau \equiv m\theta + kz$ is the helical coordinate, $\alpha^2 \equiv m^2 + k^2r^2$, $M \equiv 2mk/\alpha^2$, $\Delta^* \equiv \alpha^2\nabla\cdot 1/\alpha^2\nabla$ and r, θ, z are the usual cylindrical coordinates. η is the plasma resistivity and is chosen to be constant. The magnetic field is given by $\vec{B} = (\hat{e}/\alpha)\times\nabla\chi + (\hat{e}/\alpha)\,g$ and the fluid velocity is given by $\vec{v} = (\hat{e}/\alpha)\times\nabla A + \nabla\Omega + (\hat{e}/\alpha)\,\omega$, where χ, g, A, ω, Ω, and p are functions of r, τ, and time and $\hat{e}$ is a unit vector in the symmetry direction. Magnetic field perturbations due to density gradients are ignored.

The above equations have several advantages over more primative forms. First, the physically interesting incompressible resistive MHD equations are a subset of the full set of equations and are obtained by setting $\Omega = 0$ and dropping the last two equations. Qualitative differences between compressible

and incompressible calculations will be presented. The major difference is shown in figure 2 where it is seen that the island structure for the compressible case developes a large m = 2 component.

Second, by taking the divergence and curl of the momentum equation the shear Alfvèn wave motion has been removed from the quantity Ω and the fast magnetosonic wave motion has been removed from the quantities A and ω. This separation of ideal MHD wave characteristics has been shown to have dramatic effects on the accuracy and stability of the numerical solutions.[4]

The plasma variables and time advancement equations are fourier analysed in τ. The resulting equations are integrated in time using a scheme which treats the linear terms implicitly, thereby avoiding small time step restrictions. Linear terms include all resistive terms and terms which produce waves with velocities derived from the lowest harmonic of the magnetic field and pressure.

We look at effects on the mode growth due to the nonlinear modification of the equilibrium profiles. Kinetic energy saturation occurs and field growth slows down from exponential to algebraic due to the quasilinear flattening of the pressure profile in the neighborhood of the singular surface. The nonlinear growth of the field perturbations depends in a large way on whether or not the Ohmic heating term is included in the pressure equation. If the Ohmic heating term is present then neighboring islands "quickly" overlap so that ergodic field structure probably exists over a large portion of the Spheromak minor radius. If the Ohmic heating term is not included then the island growth slows down considerably.

References:

1. B. Coppi, J. Greene, and J. L. Johnson, Nucl. Fusion 6, 102 (1966).
2. A. H. Glasser, J. M. Greene, and J. L. Johnson, Phys. Fluids 18, 875 (1975).
3. S. C. Jardin, Nucl. Fusion 22 629 (1982).
4. S. C. Jardin, J. L. Johnson, J. M. Greene, and R. C. Grimm, J. Comput. Phys. 19 101 (1978).

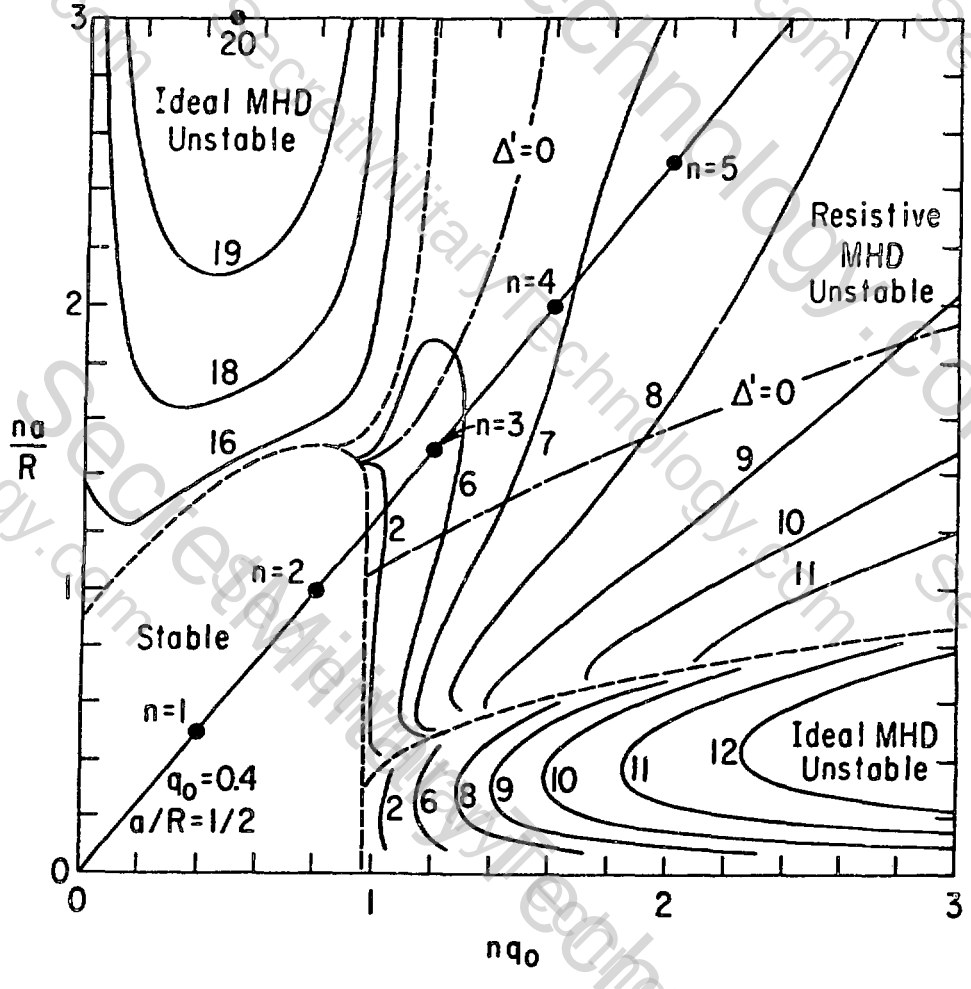

Fig. 1 Linear growth rate contours.

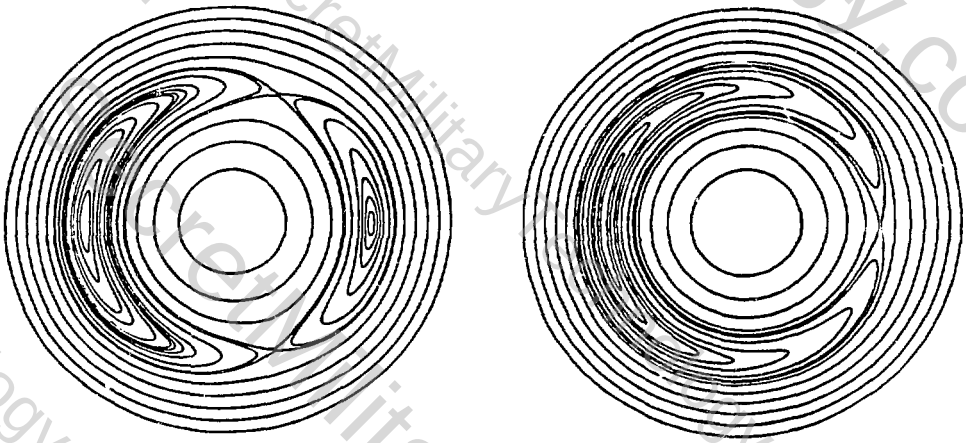

(a) Compressible (b) Incompressible

Fig. 2 Helical flux (χ) contours.

Experimental Investigation of Spheromak Configurations in Proto S-1C

S. Paul, A. Janos, D. McNeill, M. Newhouse, M. Yamada

Princeton University, Plasma Physics Laboratory

Princeton, New Jersey 08544

INTRODUCTION

The Proto S-1C device was constructed to investigate further the electrodeless, quasi-static scheme for forming a spheromak. A double-sized version of the previous spheromak experiment at PPPL,[1] the primary purpose of Proto S-1C[2] is the achievement of higher temperatures and longer lifetimes, and the study of equilibrium and stability aspects of the larger configuration. The Proto S-1C flux core is a combination of toroidal and poloidal field windings enclosed in a toroidally shaped support having a major radius of 30 cm and a minor radius of 6 cm. The core is lined with 5 mil thick stainless steel sheet, which is formed and welded to provide a vacuum seal.

The toroidal and poloidal fields are generated by 72 kG and 24 kJ capacitor banks, respectively. The rise time of the TF bank, which defines the spheromak formation time is 50 μsec. The resulting poloidal and toroidal plasma currents are 120 and 60 kA, respectively. The equilibrium field is provided in part by a steady-state field, produced by coils outside the vacuum vessel. An EF current of 1800 amp generates a mirror-like field with a strength of 2 kG. Reconnection occurs upon reversal of the poloidal field, and the plasma is pinched off the core and moved into the center of the vacuum vessel. The strength and crowbar time of the poloidal field bank determine the extent to which the plasma separates from the core and, therefore, strongly affect the stability.

PLASMA PARAMETERS

According to data from an array of magnetic field probes inside the plasma, without stabilizing conductors, spheromak configurations with typical lifetimes of 30-80 μsec have been obtained in Proto S-1C. Plasma currents and core currents generate a poloidal field of 2.2 kG. The plasma poloidal current generates a toroidal field of 1.7 kG.

Electron temperature and density were measured initially with a single channel Thomson scattering experiment consisting of a 2 Joule ruby laser and a monochromator. This has recently been improved by adding a 5-channel polychromator and fiber optic link. Measurements have been taken with both systems in hydrogen and helium plasmas with filling pressures ranging from 3 to 60 millitorr. (Figure 1) The higher fill pressure plasmas are radiation dominated with electron temperatures clamped at 10-15 eV. The densities were 2-5 $\times 10^{14}$ cm^{-3} (calibrated with Raleigh scattering in neutral nitrogen). Much higher temperatures were

obtained at lower filling pressures. Temperatures surpassing 40 eV were observed at densities of 1×10^{14} cm^{-3}. This density decrease and the accompanying temperature increase are corroborated by spectroscopic and bolometric measurements which show greatly reduced radiative emission at lower densities. The total radiated power is measured to be $\lesssim 10$ MW, enough to account for nearly all of the ohmic heating input. The source of the radiation is low-Z impurities (principally carbon and oxygen) which are introduced into the plasma primarily as a result of the interaction between the initial breakdown plasma and the metallic surface of the flux core. Because the impurity radiation scales with n_e^2 (it was found that the impurity density scales with electron density), a decrease in impurity radiation is to be expected as the radiation barrier is passed. The increased power input per particle and the decreased energy loss from carbon radiation (which peaks at approximately 13 eV)[3] combine to raise the electron temperature to 40 eV. Though the peak radiated power from oxygen occurs at 40 eV, the total combined radiated power from these two low-Z impurities peaks at 22 eV ($n_e = 4 \times 10^{14}$ cm^{-3}, $n_o/n_e = n_c/n_e = 2.5\%$, confinement time = 10 μsec). Energy losses from other processes such as neutral hydrogen influx followed by excitation, charge exchange and ionization were found to be a small fraction of radiative losses.

STABILITY OBSERVATIONS

Shifting instabilities have been observed when the equilibrium field index ($n = (-R/B)\partial B/\partial R$) is increased towards 0.1 by adjusting currents in the flux core and EF coils. In addition to magnetic field probe data, framing camera photographs of helium plasmas show an asymmetry in light emission after 50 μsec (Figure 2). The asymmetry appears as a distinct horizontal shift in the region of emission away from the center and towards the core. Growth times are observed to be comparable to the tilting instability growth times measured in Proto S-1A.[4] These are typically 10-20 times the Alfvén transit time or 1-5 μsec. That the growth times are significantly longer than the Alfvén time might be explained by "line tying", i.e., plasma flowing along poloidal field lines which wrap around the flux core. Numerical studies[5] have predicted that line tying through the vacuum vessel wall delays the onset of the tilting instability.

Evidence of line tying has been observed in framing camera photographs of hydrogen spheromaks. These photographs reveal a three-lobed structure in the plasma region, whose position corresponds directly to the three legs which support the core, but only when the plasma is not strongly pinched off. These lobes are attributed to line radiation emitted by impurities sputtered off the legs by plasma current flowing along poloidal field lines, which are wrapped around the core. In plasmas forced to pinch off more abruptly, the lobes are not visible. In addition, these plasmas are observed to have shorter lifetimes according to magnetic probe data. The line tying, made visible by the sputtered impurities, seems to have a stabilizing effect. The fully stripped hydrogen does not emit at the 20 eV

plasma temperatures, making this effect more evident. In helium plasmas, stripped fully only at higher temperatures, radiation is emitted primarily from the dominant plasma species, masking the radiation from the sputtered impurities.

The spheromak lifetime falls to less than 30 μsec when the fill pressure is reduced below 8 millitorr. Under these conditions, the plasma configuration terminates abruptly, as indicated by a sudden decrease in the magnetic field (Figure 3). The pyroelectric detectors and spectroscopic monitors observe a sudden simultaneous burst of radiation lasting 15 μsec. This abrupt termination has been eliminated by inserting a floating cylindrical "mini flux conserver" with a diameter of 8 cm (Figure 3). The lifetime was extended to over 150 μsec. As the classical resistive diffusion decay time is 430 μsec for a plasma with characteristic length = 12 cm, T_e = 20 eV, Z_{eff} = 1.5, the plasma lasts approximately 1/3 as long as the classical field lifetime. The magnetic fields were found to increase to 4 kG inside this flux conserver. Recently, the stainless steel resistive liner extension at the ends of the center column has been removed. The plasma lifetime decreased to about 130 μsec and the peak fields fell by 10%, but the plasma continued to terminate slowly.

SPECTROSCOPIC MEASUREMENTS

Visible spectroscopic measurements have been made of the CIV lines at 5801 and 5812 Å. The emission time history reveals a two-peak distribution. The first peak occurs at the beginning of the discharge and the second after 110 μsec. Because the observed intensity ratio of the 5812 and 5801 lines agreed with theory for the later peak but not for the first, we suspected that the earlier peak is not from CIV. It may be the strong hydrogen molecular line at 5812.6 Å, emitted by the relatively dense neutral gas surrounding the spheromak. This interpretation is confirmed by the disappearance of the earlier peak in helium discharges.

CV radiation has not been observed although computer simulations indicate that virtually 100% of the carbon should be helium-like in a 40 eV, 50 μsec plasma.[3] The failure to observe CV lines may be due to the fact that the excitation energies for these lines are on the order of 350 eV, quite close to the 392 eV ionization potential for CV. Although the resonance transition lines share the problem that their excitation energies are hundreds of electron volts, they have transition probabilities four orders of magnitude greater than the 2274 Å near UV line. The resonance line emission occurs in the extreme UV (for example $1s^2$-1s2p at 40 Å), and is not observable in Proto S-1C at this time.

Plans to extend visible spectroscopic measurements are proceeding in two directions. First, a gated two-dimensional SIT detector array is being constructed to provide spatial and wavelength resolution in Proto S-1C and S-1. This will be useful for single-shot survey and line ratio measurements. Second, time resolution will be probided by an 8-channel

impurity line monitoring system. 3 Å bandwidth interference filters will be used to observe, H_α, H_β, and CI-IV and OI-IV lines. The time and intensity of the line peaks will be compared with a time-dependent coronal model[3] to obtain estimates of the temperature and impurity densities.

Further experimental work on Proto S-1C includes: a single channel CO_2 interferometer to measure line averaged electron density, a multi-chord pyroelectric detector to obtain spatially resolved radiative power data, and ECR breakdown to extend the regime of reproducible, long lasting spheromaks to lower densities.

REFERENCES

1] M. Yamada, H. P. Furth, W. Hsu, A. Janos, S. Jardin, M. Okabayashi, J. Sinnis, T. H. Stix, and K. Yamazaki, Phys. Rev. Lett, 46, 188, (1980).

2] A. Janos, S. Cowley, H. Hsuan, S. Paul, C. Skinner, F. Wysocki, and M. Yamada, Proceedings of the Fourth Symposium on the Physics and Technology of Compact Toroids, Lawrence Livermore National Laboratory, Livermore, CA, CONF-811087, October 20-27, 1981, pp. 137-141.

3] C. Skinner, E. Salberta, and M. Yamada, Bull. Am. Phys. Soc. 26, 1054 (1981).

4] C. Munson, A. Janos, M. Newhouse, E. Salberta, F. Wysocki, and M. Yamada, Proceedings of the Fourth Symposium on the Physics and Technology of Compact Toroids, Lawrence Livermore National Laboratory, Livermore, CA, CONF-811087, October 20-27, 1981, pp. 149-152.

5] K. Watanabe, K. Ikegami, M. Nishikawa, A. Ozaki, N. Satomi, T. Uyama, T. Sato, S. Otsuka, K. Mishikawa, Merging Experiment and Simulation of Compact Toroids, Ninth International Conference on Plasma Physics and Controlled Nuclear Fusion Research, IAEA, Baltimore USA, 1-8 September 1982, paper M-4.

FIGURE CAPTIONS

Figure 1. Dependence of electron density, electron temperature, and total radiated power on filling pressure in hydrogen.

Figure 2. Framing camera photographs of spheromak formation and decay in 20 millitorr helium. At 10 μsec, emission occurs primarily from around the flux core. At 30 μsec the plasma is pinched off the core and lasts until 50 μsec when the emission begins to move to the left. Obvious asymmetry occurs later than 60 μsec.

Figure 3. Time evolution of the toroidal and poloidal currents in the flux core coils without a stabilizing conductor. Poloidal and toroidal magnetic fields at R = 2.5 and R = 7.5 cm as measured by magnetic pick-up coils interior to the plasma. Note the abrupt decrease in both fields. Drawing of the center conductor and stainless steel partial flux conserver. Time evolution of the magnetic fields after the installation of the center conductor.

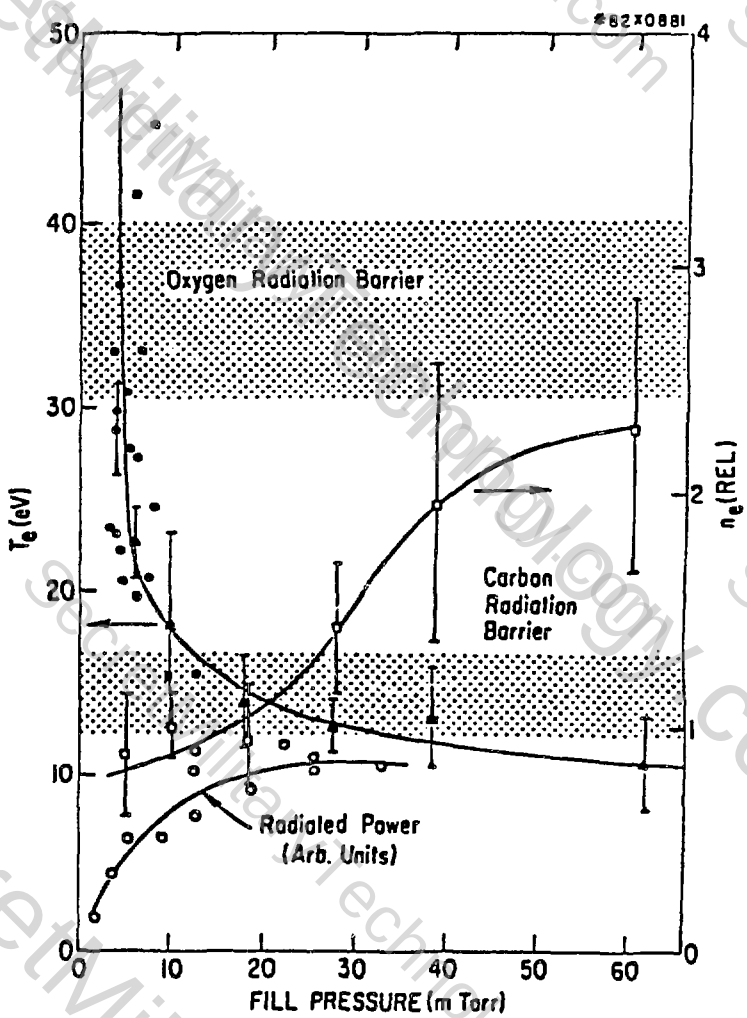

Fig. 1.

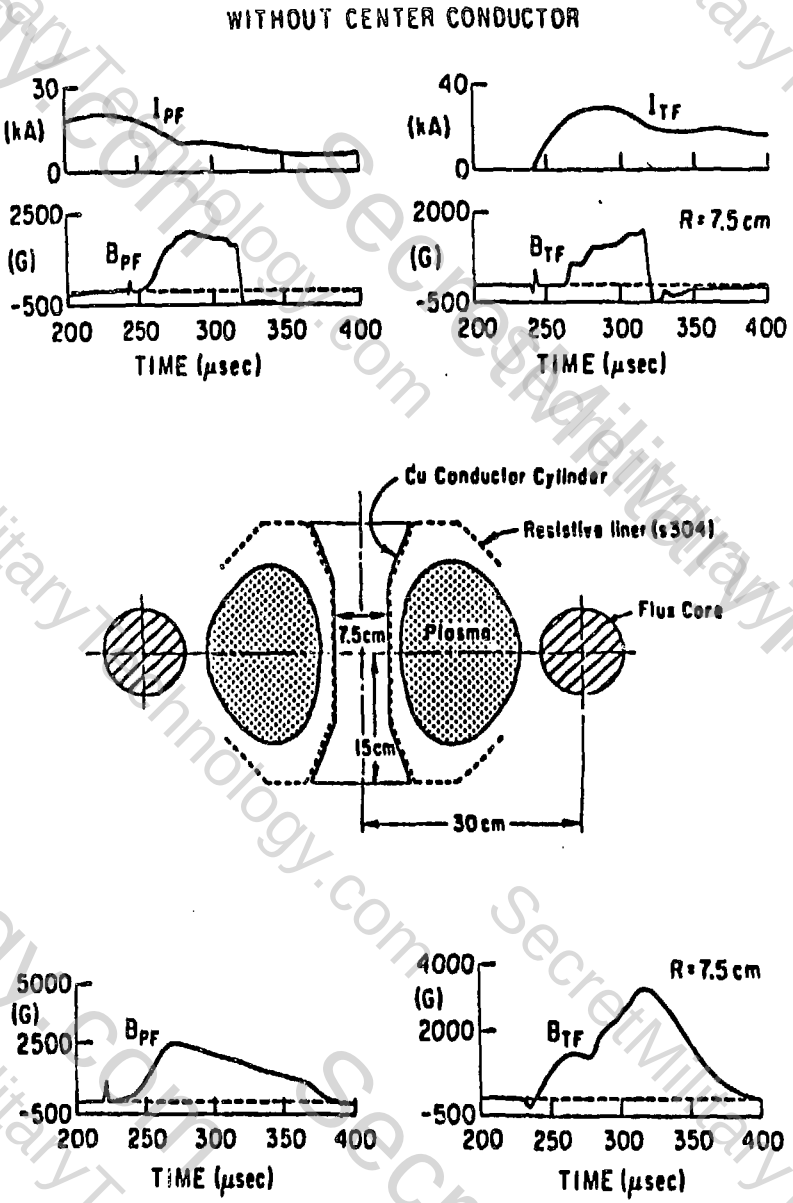
WITHOUT CENTER CONDUCTOR
30
(kA)
0
I_{PF}
40
(kA)
0
I_{TF}
2500
(G)
-500
B_{PF}
200 250 300 350 400
TIME (μsec)
2000
(G)
-500
B_{TF}
R = 7.5 cm
200 250 300 350 400
TIME (μsec)
Cu Conductor Cylinder
Resistive liner (s304)
Flux Core
7.5cm
Plasma
15cm
30cm
5000
(G)
2500
-500
B_{PF}
200 250 300 350 400
TIME (μsec)
4000
(G)
2000
-500
B_{TF}
R = 7.5 cm
200 250 300 350 400
TIME (μsec)

Fig. 3.


40 30 20 10
58 56 54 52 50
68 66 64 62 60

Fig 2.

Particle Rings

INJECTION OF AN INTENSE ION BEAM INTO A TOKAMAK

S. Robertson and J. Katzenstein
University of California, Irvine, California 92717

We describe an experiment to investigate the direct injection of an intense ion beam into a tokamak by means of the polarization drift. Confinement of 100 keV ions in the UCI tokamak (r = 15 cm, R = 60 cm, B_T = 6 kG) requires operation with a plasma current of 56 kA corresponding to q (limiter) = 2. Trapped ions are to be detected by a charge-exchange analyzer. The present status of the experiment will be discussed.

Work supported by United States Department of Energy.

Description of Experiment

This experiment has as its object the injection and trapping of an intense ion beam in a tokamak. Fig. 1 is a photograph of the experiment. An ion diode of the type developed by Humphries and Kuswa[1] is connected to the University of California, Irvine (UCI) Tokamak by a tangential port. The diode is driven by a six-stage Marx generator nominally charged to 30 kV to provide a high voltage pulse of some 150 keV. The resulting ion current is detected by a Faraday cup located some 30 cm from the anode. Fig. 2 is a voltage and current density waveform of a typical diode discharge. The peak diode current density is the order of 7.5 amp/cm^2. As can be seen at once the ion current is emitted during a time in which the diode voltage is falling so the ions are emitted with a broad spectrum of energies ranging from 50 keV to 150 keV.

A complete description with operating characteristics of the UCI Tokamak is given in another publication.[2] These characteristics are taken for a normal configuration of the machine which features two 15 x 30 cm rectangular ports diametrically opposite each other whose axes are along the local direction of the major radius. One of these ports is nominally used for the main pumping line, the other was available for general diagnostic use and for injection. The magnetic fields of the machine are inadequate to trap radially injected ions of the energy emitted by the diode. The machine was modified by substituting a sector of the torus containing one of the radial ports for a sector containing a tangential port. The toroidal windings of this sector were modified to accomodate this tangential port with minimal field perturbation.

Fig. 3A shows a current trace of the Tokamak discharge current along with traces of the ohmic heating and vertical field coil currents before and Fig. 3B after modification of the machine. It is seen at once that the duration of the current is reduced severely for the modified machine due presumably to the large toroidal field perturbations introduced by the tangential injection port. Despite this shorter current duration of only 600 - 800 μ sec, it was felt that meaningful results could be still obtained since this time is long compared to the half width of the ion

current pulse (~ 0.5 μ sec) and the ion transit time around the major circumference of the machine (~ 1.0 μ sec). It is thus reasonable to assume uniform plasma conditions during the time of injection and trapping.

The principal diagnostic instrument is an electrostatic ion energy analyzer of the type described by Eubank and Wilkerson[3]. It was attached to a 2" tangential port some 50 cm from the axis of the tangential injection port. The axis of this diagnostic port was at an angle of ~ 20° with the axis of the injection port. Thus it was not possible for ions injected into the Tokamak when the latter was under high vacuum to reach the analyzer. This was verified by injecting the intense ion beam into the Tokamak in the absence both of magnetic fields and gas and observing the response of the detector. No detectable signals were observed under these conditions.

Preliminary Results

The ion beam was injected into the Tokamak at a time corresponding approximately to peak plasma current. Fig. 4 shows a typical result. The upper trace is the photomultiplier current of the scintillation counter used to detect ions passing through the analyzer from the secondary electrons emitted from an auxiliary electrode as described in Reference 3. The lower trace is the ion diode current. Note that the waveform of Fig. 2 refers to the same shot except the time scale has been increased by a factor 5. The potential on the electrostatic ion energy analyzer was such as to accept protons of 60 keV energy. A number of records have been taken at various energy settings of the analyzer from 50 keV to 120 keV. Ion pulses with delays appropriate to the energy setting of the analyzer have been obtained in every case.

Discussion and Conclusions

The time interval between the peak of the diode current and the first pulse of the analyzer signal was found to be equal to the interpulse spacing of the analyzer signal within the accuracy of measurement and equal to 1.3 ± 0.1 μ sec. The outer limiter major radius was 72.7 cm corresponding to a circumference of 4.57 m. The transit time of a proton of 60 keV energy about this circumference is 1.35 μ sec. Thus the spacing between ion signals equals within experimental error of the transit time of ions of the energy to be accepted by the analyzer. The evidence is thus quite strong for the trapping of 60 keV ions for three transits of the major circumference of the Tokamak. The increase of the heights of successive pulses is to be expected assuming an exponential lifetime τ for the trapped particles since the escaping particles would have a 1-exp. $(-t/\tau)$ time dependence.

The direct distance from the Faraday Cup to the entrance of the ion analyzer is 2 meters, hence the direct transit time is 0.59 μ sec, which is less than the observed ion transit time by more than a factor of two. The possibility that the analyzer signal is due to directly transiting ions rather than trapped ions is quite remote.

As mentioned before no analyzer signal is observed when there is no gas fill in the Tokamak and no magnetic fields are applied. When there is no gas fill and the toroidal field alone is applied a single analyzer pulse is observed at a time appropriate to a single circumferential transit indicating that the toroidal field alone is sufficient to produce trapping for a single transit. Presumably the residual gas has sufficient conductivity to short out the polarization potential of the neutralized ion beam crossing the field.

More data will be taken at different energy settings of the analyzer and different operating conditions of the Tokamak. Every effort will be made to increase both the amplitude and duration of the plasma current until the "normal" operating conditions typified by Fig. 3A are achieved. It can be assumed that tangential injection into a Tokamak of minor diameter large compared with that of the tangential port should produce no effect on the operation of the larger machine, hence tangential injection could be accomplished under normal operating conditions.

References

1. S. Humphries, Jr., and G. W. Kuswa, Appl. Phys. Lett. 35 (1), p. 13, July 1979.

2. S. Robertson and F. Wessel, Proceedings of the Small Toroidal Plasma Device Users Meeting, Monterey, Calif., May 18, 1978.

3. H. P. Eubank and T. D. Wilkerson, Rev. Sci. Inst. 34 (1), p. 12, (1963).

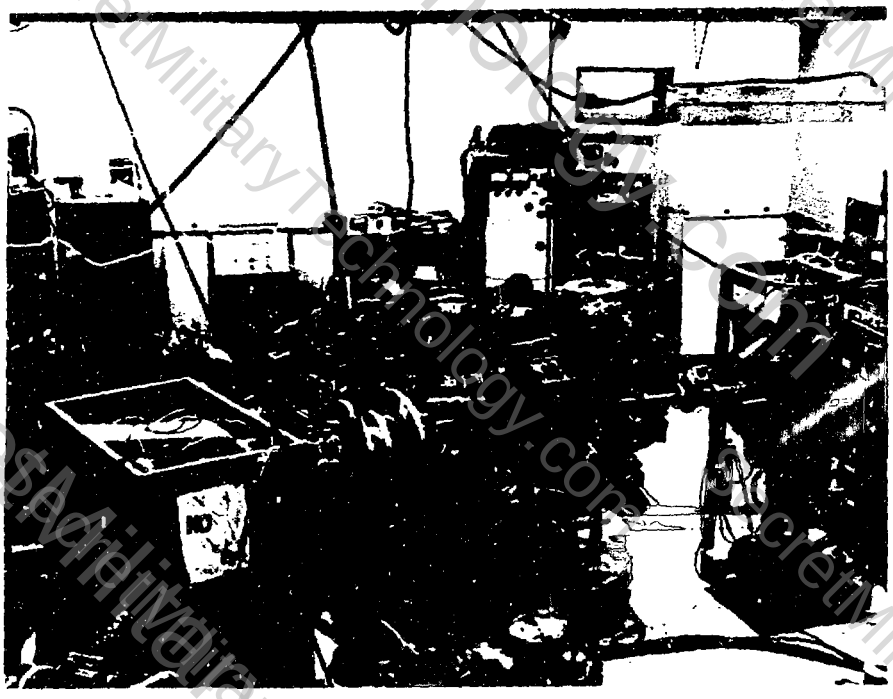

FIG. 1 - Photograph of Experimental Set-up Showing Tokamak (Center), Ion Diode and Tangential Injection Port (Left), and Electrostatic Ion Energy Analyzer (Right).

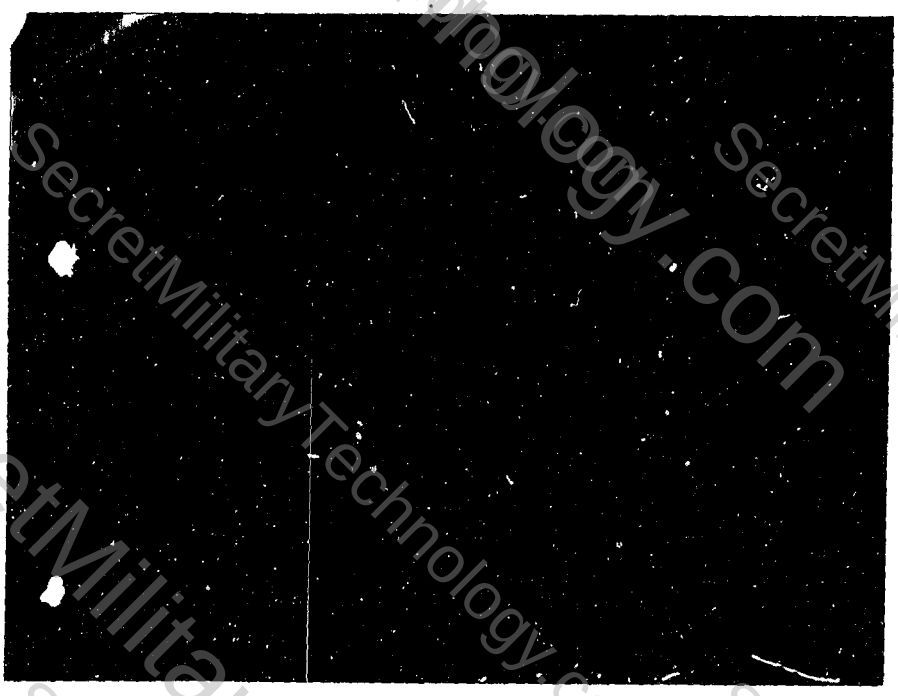

FIG. 2 - Voltage Applied to Ion Diode (Upper Trace) and Ion Current Density (Faraday Cup Signal)(Lower Trace). Time Base is 0.2 μ sec/cm.

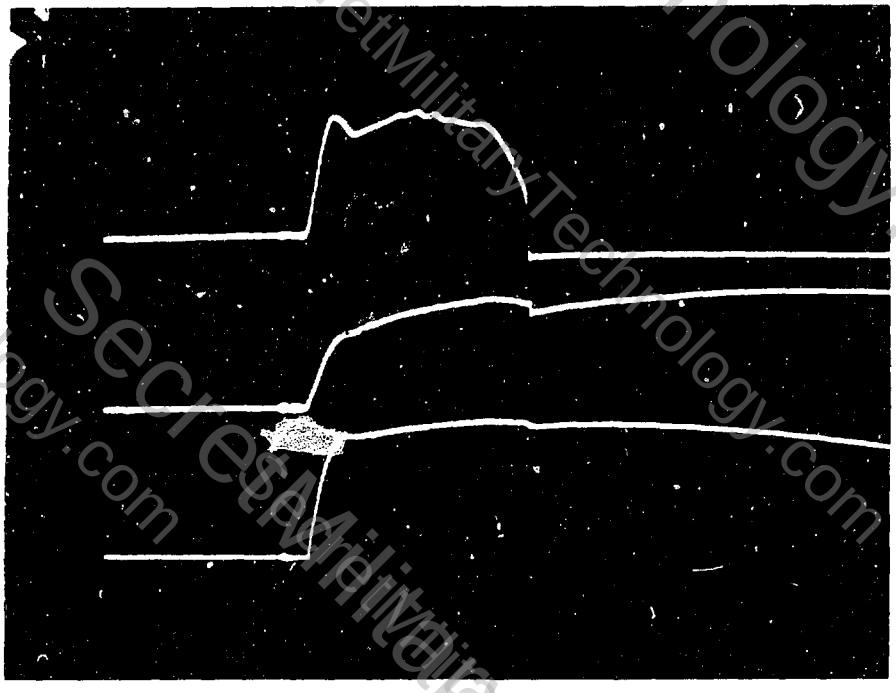

FIG. 3A - Normal Operation of UCI Tokamal Showing Plasma Current (Upper Trace) Ohmic Heating Current (Middle Trace) and Vertical Field Current (Bottom Trace). Time Base is 1 msec/cm.

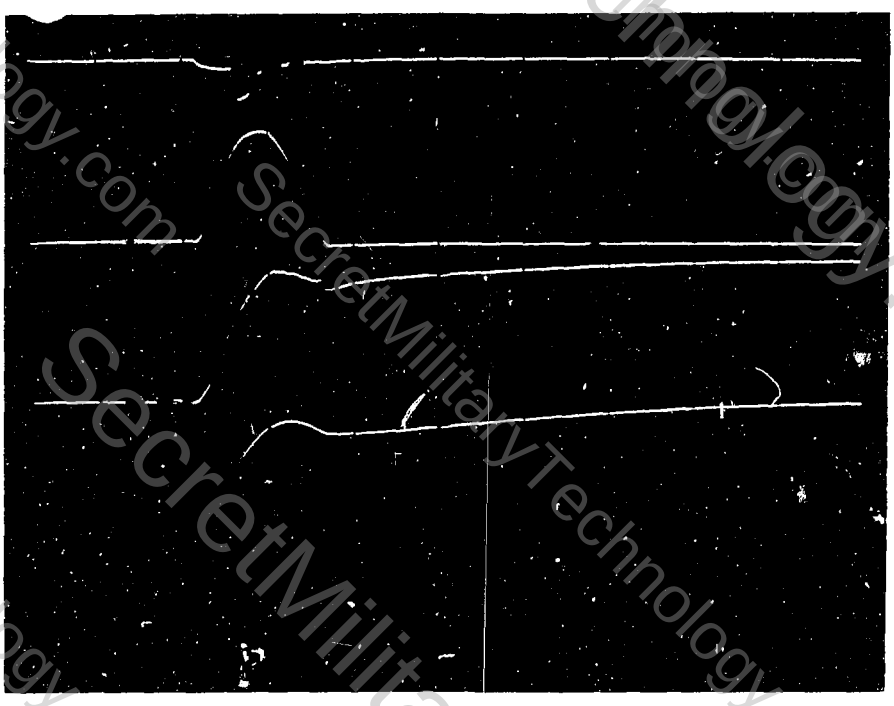

FIG. 3B - Operation of UCI Tokamak with Tangential Injection Port Installed. Traces as in 3A. Time Base is 0.5 msec/cm.

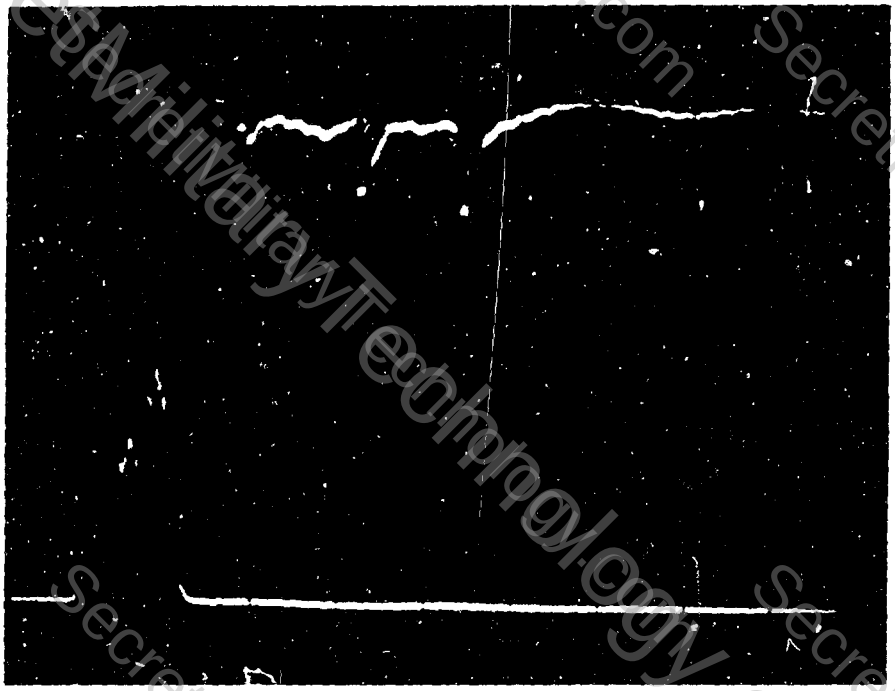

FIG. 4 - Output of Electrostatic Ion Energy Analyzer (Upper Trace) and Ion Current Density (Same Signal as Lower Trace of Fig. 2) (Lower Trace). Time Base is 1 μsec/cm.

MeV AND GeV PROSPECTS FOR PRODUCING A LARGE ION LAYER CONFIGURATION FOR FUSION POWER GENERATION AND BREEDING

J. Rand McNally, Jr.
Fusion Energy Consultant
103 Norman Lane
Oak Ridge, TN 37830

Injection of multi-MeV molecular hydrogen ions into a magnetic mirror or magnetic mirror well can lead to the production of an Ion (or proton-E) Layer with prospects for fusion power generation. This involves: 1). "slow" (exponential or Lorentz) trapping of protons from dissociation and/or ionization of H_2^+ ions; 2). electron cyclotron drive of the electronic temperature to reduce the electron stopping power; 3). production of an Ion-Layer, E-Core plasma configuration having prospects for cold fuel feed with in situ axial acceleration of say D_2^+ ions into the negative E-Core; 4). ignited advanced fuel burns in the resulting high beta plasma with excess (free) neutrons available for energy mulitplication or fissile fuel breeding; 5). development of a nuclear dynamo with fuel feed, plasma energy, and Ion-Layer current maintenance by fusion products; and 6). a natural divertor end loss of ashes with charge separation permitting a natural direct electrical conversion prospect.

The 100 mA cw H_2^+, 5-MeV FMIT-prototype and the 20/35 MeV FMIT accelerators under design and/or construction at Los Alamos National Laboratory will provide adequate H_2^+ beam power to generate small plasmas capable of demonstrating the principles of proton density buildup via the exponential process at 5-MeV and the Lorentz process at 20 or 35 MeV. For fusion reactor core evaluation a LAMPF size or larger (1 mA, 800 MeV to 10 GeV H_2^+) accelerator would be required to develop a GeV Ion-Layer of 1 to 5 m radius. Microwave power at 60–120 GHz of up to about 100/1000/10,000 kw cw for the 5/20 or 35/$\geq$ 800 MeV injection cases will be necessary to provide buildup conditions via programmed electron cyclotron heating (ECH) in magnetic fields of about 20 to 40 kG at the midplane of the 2/1 magnetic mirror.

The basic $n\tau$ conditions for ion containment against ion-ion scatter and ion-electron slowing down are for deuterons:

$$n\tau_{ii} \simeq 6 \times 10^{10}\ T_i^{3/2} \log R_{eff}$$
$$n\tau_{ie} \simeq 6K \times 10^{11}\ T_e^{3/2} / (1 - T_e/T_i),$$

with n in cm^{-3}, τ in s, T in keV, and K determined by the number of e-folds permitted in ion slowing down. Instabilities will be ameliorated by the broad velocity spectrum of the slowed down and scattered ions and their large Larmor radii; however, a magnetic well may be initially needed until beta exceeds a few percent (partial field reversal). Appropriate programming of ECH power will adjust the electron temperature and minimize the plasma potential effects as the ion density grows until an Ion-Layer is generated. During reactor core evaluation with programmed cold fuel feed into the multi-mega-Joule energy plasma, the ECH power level can be reduced and perhaps even turned off when a full scale ignition of plasma occurs. It should be noted that the 300 keV protons in the ORNL DCX-1 mirror experiment were remarkably quiescent for the spread proton population and losses were dominated by classical charge-exchange shortly after beam turn-off indicating the beam-on instability was driven by a few well-ordered, recently trapped protons.

Following generation of the Ion-Layer cold D-T or primed D–D (~1% T, ~8% ^{3}He) can be fed axially into the E-Core with D_2^+, T_2^+, DT^+, $^3He^+$, and/or $^6Li^+$ ions formed by ionization reactions being accelerated into the E-Core. Dissociation or further ionization of these ions then results in irreversible trapping of these second generation ions unless up-scattering doubles their energy in the axial direction. Coulomb and nuclear elastic scattering of fuel ions as well as fusion reactions will result in large, magnetic cross-field, radial excursions of these ions leaving the electrons behind to maintain the E-Core. The charged fusion reaction products will contribute to partial or complete sustainment of the Ion-Layer.

The poloidal pinch current will satisfy the approximate relation

$$I_p^2 \,(\ln 8R/a - 3/2) = 10\, I_p B_0 R - 200\, P\pi a^2 \Sigma n_0 T_0$$

where P is of order unity but depends on the particular plasma profiles of density and temperature, I_p is in amperes, a and R are the minor and major radii in cm, B_0 is the applied field in gauss, and $\Sigma n_0 T_0$ is the plasma energy density at the center in ergs. Since most of the plasma density will be resident in the ions ($T_i \sim 2T_e \leqslant 200$ keV at r = 0) in a fully catalyzed reacting D–D plasma core the ion pressure will drive an ion dominated current flow ($J \times B = -\nabla p$) which may replace in part the GeV injection beam requirements for sustaining the Ion-Layer. The charged fusion reaction products with initial ion energies up to about 15 MeV will provide a seed current to permit possible in situ drive of the pressure gradient driven bootstrap current.

Shafranov proposed an equilibrium ring current configuration in a magnetic field (or atmospheric pressure field) involving both toroidal and poloidal currents and associated poloidal and toroidal magnetic fields (Sov. Phys. J.E.T.P. 6, 545, 1958). Such fields (see figure), analogous to tokamak fields, will provide a loss region for ash and unburned plasma as well as some direct losses of 3 and 14 MeV protons from DD and D^{3}He reactions which may offer sufficient seed current (without severe Ohkawa back electron currents) to sustain the pressure gradient driven bootstrap currents and thus the configurational properties.

The reacting configuration will operate as a nuclear dynamo with self generation of electric and magnetic (except for external mirror coils) field provided appropriate fueling and ash removal can be performed. Electrons leaving the system axially at small radii and ions departing the system at larger radii will provide some direct electrical conversion prospects primarily as a result of the natural divertor action of the Ion-Layer, E-Core configuration.

This Ion-Layer, E-Core fusion reactor core offers an optimal magnetic fusion configuration for burning the advanced fuels (D–D, D–^{3}He, and/or D–^{6}Li) for breeding fusile (T, ^{3}He) fuels or fissile (^{233}U or ^{239}Pu) fuels, for direct electrical conversion, or for thrust prospects.

References: "Prospects of a Multi-MeV H_2^+ Injection-Accumulation Experiment", ORNL/TM-3207 (November, 1970); Nucl. Fusion 11, 191 (1971); "Fusion Chain Reaction Prospects and Problems", ORNL/TM-4575 (July, 1974); "Simplified Approach to Attaining a Proton E-Layer", ORNL/TM-4965 (July, 1975); "A Double Quantum Jump in CTR", ORNL/TM-4967 (July, 1975); "Alpha-Driven, Steady State Tokamak", ORNL/TM-6492 (August, 1978); "Physics of Fusion Fuel Cycles", Nuclear Technology/Fusion (January, 1982).

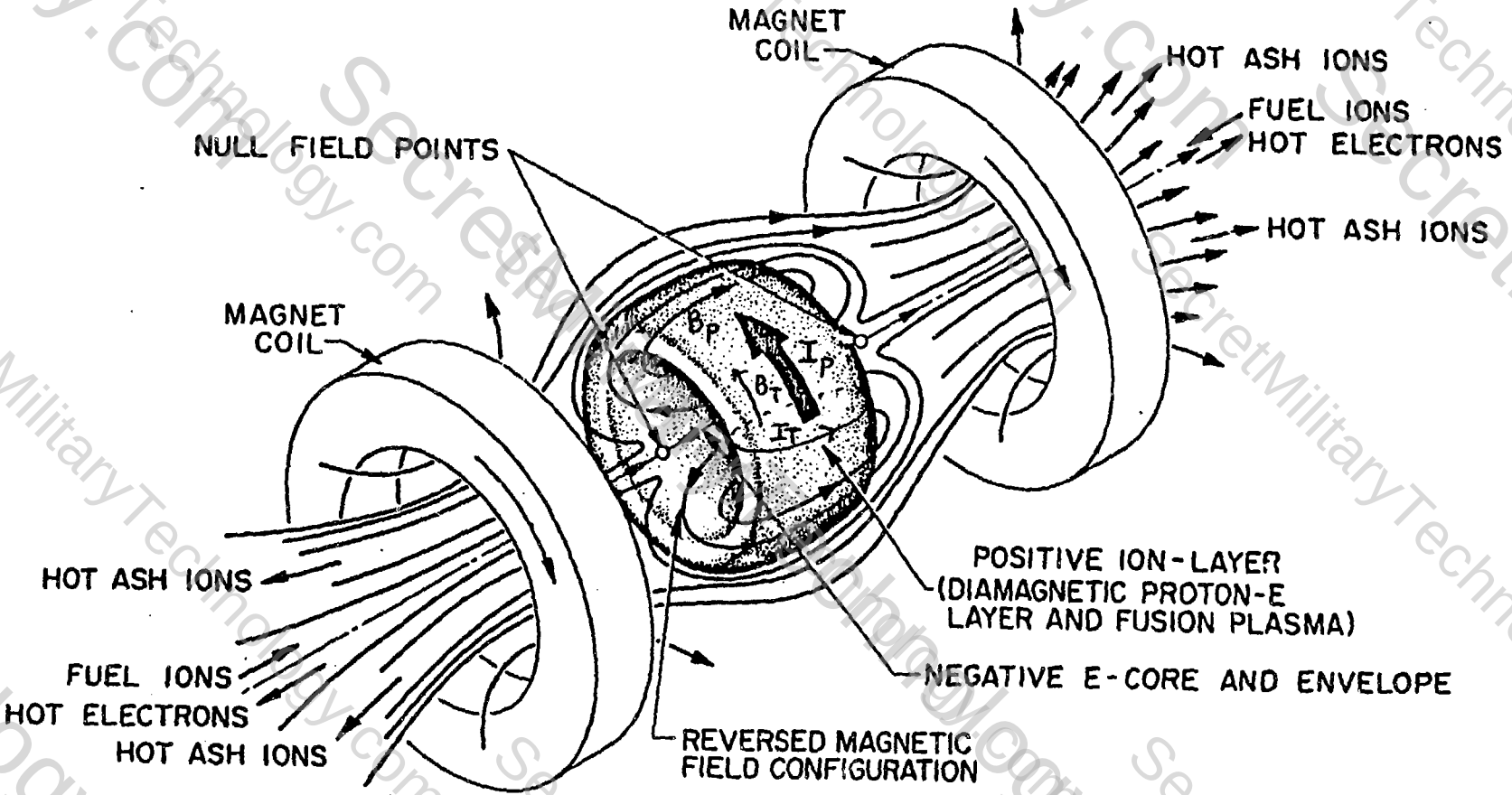

POSSIBLE ION-LAYER, ELECTRON-CORE REACTING PLASMA CONFIGURATION

D_1^+ and/or $^3He^+$ fuel ions are accelerated along field lines to negative core where change of charge to mass ratio leads to irreversible trapping of D^+ and/or $^3He^{++}$ which scatter across field lines leaving excess electrons behind to eventually escape out axis (Nuclear Fusion 12, 265, 1972). This electromagnetic configuration is somewhat analogous to a gravitational "black hole."

APPENDIX: COMMENTS ON MULTI-MeV BUILDUP STUDIES

Opponents of multi-MeV buildup studies cite the density-limited instability properties of the ORNL DCX-1 (or DCX-2) experiments to justify their position on multi-MeV studies. The following physics factors are offered for consideration:

1. ORNL DCX-1 experimenters turned to Lorentz trapping studies which grossly accentuated the negative mass instability inasmuch as this more rapid trapping put more recently-trapped, highly organized, axis-encircling proton orbits in the plasma and these drove the instability even harder.
2. The instability threshold density was significantly increased by non-concentric injection modes as well as by stochastic ion cyclotron drive of energy spreads. These stabilizing effects are predicted by the theory of the negative mass instability.
3. B. Maglich, using the migma mode (axial) injection, apparently achieved comparable densities to that achieved in DCX-1 without instabilities present. His 650 keV deuterons have about the same charge exchange cross-section as the 300 keV protons of DCX-1.
4. The DCX-1 plasma became extremely quiescent, even above the instability threshold, very shortly after beam turnoff when the highly organized proton component had decayed away.
5. Stable confinement times up to 150 seconds were attained in DCX-1 and the loss time was associated with classical charge exchange processes. It should be noted that other plasma experiments give confinement times of order 100 milliseconds or less.
6. Energy degradation of only 10% doubled the charge exchange loss cross-section in DCX-1——no such drastic sensitivity exists with multi-MeV ions at or above the exponential condition.
7. Attempts at exponential buildup (plasma trapping rate greater than charge exchange loss rate) were unsuccessful in DCX-1 although one set of experiments suggested the possibility of incipient exponentiation; however, at least two other causes may have contributed to making the density buildup time shorter than the decay time.
8. Should exponential buildup be achieved in an injection-trapping experiment the density would increase to a scatter limited density which could be several orders of magnitude higher than that of charge exchange limited density. The Stagg field fission experiment led by Fermi demonstrated an exponential buildup of the neutron rate.
9. To prevent ion-electron scatter slowing down the ions too rapidly it will be necessary to introduce electron cyclotron heating in a programmed fashion. This will permit ion-ion scatter density limits being achieved (the Coulomb cross-section varies as $1/E^2$; nuclear elastic scatter is important in GeV experiments). (The charge exchange cross-section varies as $1/E^5$).
10. Exponentiation at multi-MeV energies with programmed electron cyclotron heating should produce an Ion Layer with about 10–20 mA at 4 MeV H_2^+; the FMIT prototype accelerator will be capable of 100 mA at 5 MeV H_2^+.
11. If necessary a magnetic mirror well (e.g., quadrupole mirror) may be used to suppress the negative mass instability, flute, and precessional instability modes.

PULSED DIODE SOURCE OF POLARIZED IONS

J. Katzenstein and N. Rostoker
University of California, Irvine, California 92717

The advantages of polarized nuclei for fusion reactors have recently been described.[1] We propose a pulsed source of polarized nuclei that consists of an ion diode with a polarized anode. With magnetic resonance techniques the nuclear spins of the protons of solid NH_3 can be made about 90-95% polarized.[2] This material would be used for the anode. The diode would be pulsed with a voltage of 1-200K-volts for 1-2 μ sec. Flashover of the anode produces a surface plasma from which the polarized protons would be extracted to form a beam. Depolarization during this phase is considered. Measurement of beam polarization could be detected by comparing reaction cross sections and/or distribution of reaction products with similar results for unpolarized[1] beams.

In thermal equilibrium very large magnetic fields and very low temperatures are required for significant nuclear polarization. For example, for protons which have spin 1/2, the thermal polarization is

$$p = \frac{N_+ - N_-}{N_+ + N_-} = \tanh (g_n \mu B/2 kT)$$

$$\cong 10^{-7} (B/T) \text{ gauss}/^{o}K$$

$g_n \cong .003$, the nuclear g-factor, $\mu = .93 \times 10^{-27}$ erg/gauss, the Bohr magneton. To obtain $p = .1$ at liquid helium temperature ($1.5^{o}K$) requires $B/T = 10^6$ or $B \approx 1.5 \times 10^6$ gauss.

Dynamic nuclear orientation consists of saturation of the microwave spin resonance of electrons. Nuclear polarization is obtained through certain relaxation processes involving mutual electron and nuclear spin flips that take place through an $\underset{\sim}{I} \cdot \underset{\sim}{S}$ type of hyperfine structure coupling. $\underset{\sim}{I}$ is nuclear spin and $\underset{\sim}{S}$ is electron spin. For nuclei in crystals in weak dipolar coupling with paramagnetic ions the nuclear polarization is enhanced by the factor $g/g_n \sim 10^3$ which is the ratio of the electron to nuclear g-factor. Thus dynamic methods provide a means of producing nuclear polarizations

$$p \cong \frac{g \mu B}{2kT} \cong 10^{-4} (B/T) \text{ gauss}/^{o}K$$

For 10% polarization at $1.5^{o}K$, only 1.5×10^3 gauss is required.

There are many variants of dynamic polarization. Allowed transitions can be saturated, or forbidden transitions. In the former case,

polarization is produced indirectly by the simultaneous flipping of an electron spin and a nuclear spin involved in the relaxation process. In the latter case the spin flipping is induced directly by the applied microwave field. Either forbidden transitions can be induced,[3] or there is a transient method involving applied fields at two frequencies.[4]

Solid polarized proton targets have been developed for nuclear and high energy physics scattering experiments. They employ dynamic nuclear orientation as described above. Many forms of solid targets have been polarized such as H_2O, solid HD, solid methane CH_4, etc. For present purposes, the most interesting case is solid ammonia NH_3 for which 90-95% polarization has been obtained.[2] To accomplish this requires a temperature of about 1^oK, a static magnetic field of 50k-gauss and a 4 mm microwave generator.

The general idea of dynamic polarization involves spin pumping. This means the application of resonant radiation to a multi-level system resulting in a radical rearrangement of level populations leading to nuclear polarization. Dynamic nuclear orientation of atoms by optical pumping and spin exchange between different nuclei in binary encounters is another method for producing nuclear polarization[5] that may be developed for fusion fuel. Yet another method involves a chemical reaction[6]; the molecular recombination rate of (electron) spin polarized hydrogen is sensitive to nuclear spin. Conditions have been reported where the nuclear polarization is over 99%.

Although all of the above methods may be useful for polarizing fusion fuel, none of them have been developed for this purpose. Which method (if any) is useful will be determined by percent polarization achievable, adaptability to various fusion fuels, and special handling problems involved in fueling a reactor. In the balance of this paper we consider only spin pumping with microwaves because there are already satisfactory results for protons in solids. Large targets of polarized NH_3 have been constructed and the techniques should be applicable to solid ND_3 or NT_3. We consider an ion diode based on polarized ND_3 or NT_3; an intense beam of polarized D^+ or T^+ would be developed, neutralized and transported. The feasibility of injecting and trapping an intense ion beam in a tokamak has been studied at UCI for several years and experimental results are reported in another paper at this meeting.[7] Thus if a polarized ion diode is feasible, an entire system of fuel handling is conceivable.

Reflex[8] and magnetically insulated[9] ion diodes are illustrated schematically in Fig. 1. A schematic diagram of an experiment to polarize, generate and propagate the beam is also illustrated in Fig. 1 for the case of a reflex diode. Both types of diodes have been operated at U.C.I. at voltages of 1 - 200 k-volts to produce ion currents of average value a few kilo-amperes for 1 - 2 μ sec. The ion source is a plasma produced by flashover on the anode surface. If the anode consists of frozen ND_3 with the D-spins polarized, flashover on the surface will still produce a plasma from which mostly D^+ would be extracted. The main question of feasibility is whether or not the D^+-spins would de-polarize

during the process of plasma formation and ion extraction. Similar questions arise if polarized fuel is to be employed in a fusion reactor and they have previously been considered.[1] Kulsrud, et al., find for reactor plasma ($n = 2 \times 10^{14}$ cm^{-3} $T = 10^4$ ev) the rate of depolarization to be 2×10^{-5} sec^{-1} for T, and about 10^{-6} sec^{-1} for D. The results scale like $n\sigma_i v_{rel}$ where v_{rel} is electron velocity, n is electron density and σ_i is the appropriate cross section (spin-orbit, spin-spin interaction, etc.) For the flashover plasma of an ion diode we expect that $n \sim 10^{20}$ and $T \cong 10$ ev. Thus the depolarization rates should be .6 sec^{-1} for T and .03 sec^{-1} for D. Those rates produce negligible depolarization in a few microseconds - the pulse length of the ion diodes. A polarized nucleus of a hydrogenic atom is not depolarized by ionization, but is by recombination; the latter process is inhibited by a strong magnetic field; in a 50 k-gauss field the depolarization from recombination should be negligible.[1] We therefore conclude that it is feasible to make a high current polarized ion beam by polarizing the anode of an ion diode.

Work supported by United States Department of Energy.

References

1. R. W. Kulsrud, J.P. Furth, E.J. Valeo and M. Goldhaber, P.P.P.L. - 1912, June 1982.

2. C. D. Jeffries, UC Berkeley; private communication. See also C. D. Jeffries, Dynamic Nuclear Orientation (John Wiley & Sons, Inc.) New York) 1963.

3. C. D. Jeffries, Phys. Rev. 106, 164 (1957); 117, 1056 (1960).

4. G. Feher, Phys. Rev. 103, 500 (1956).

5. N. D. Bhaskar, W. Happer, and T. McCelland, Phys. Rev. Lett. 49, 25 (1982).

6. R. W. Cline, T. J. Greytak and D. Kleppner, Phys. Rev. Lett. 47, 1195 (1981).

7. J. Katzenstein and S. Robertson, Fifth Symposium on Compact Toroids, November 16 - 18 (1982).

8. S. Humphries, J. J. Lee and R. N. Sudan, Appl. Phys. Lett. 25, 20 (1974); J. Appl. Phys. 46, 187 (1975).

9. S. Humphries, R. N. Sudan and L. Wiley, J Appl. Phys. 47, 2382 (1976).

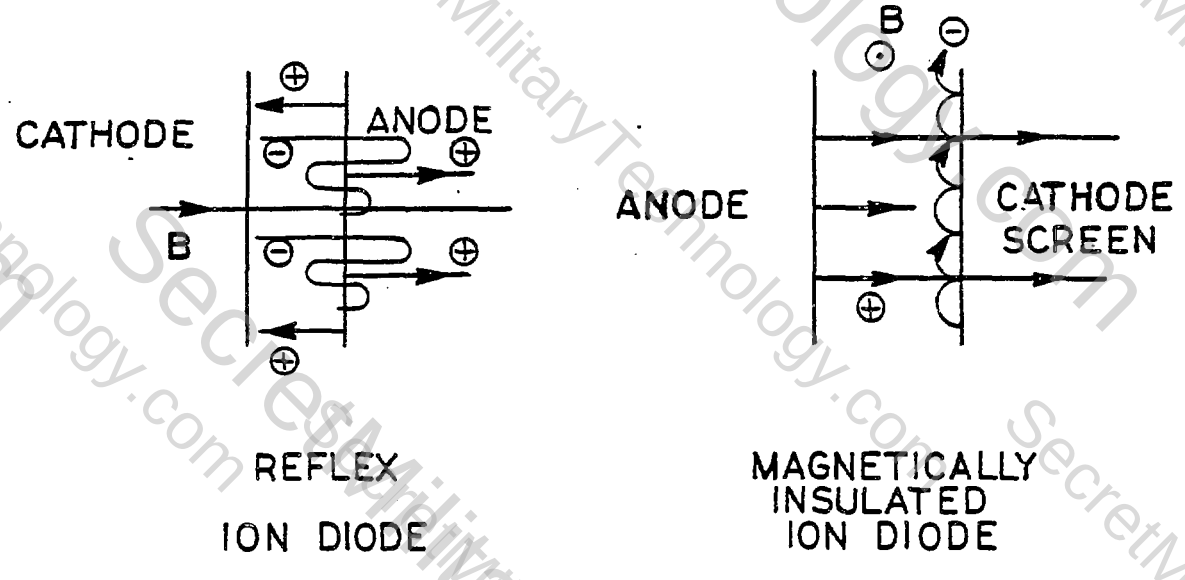

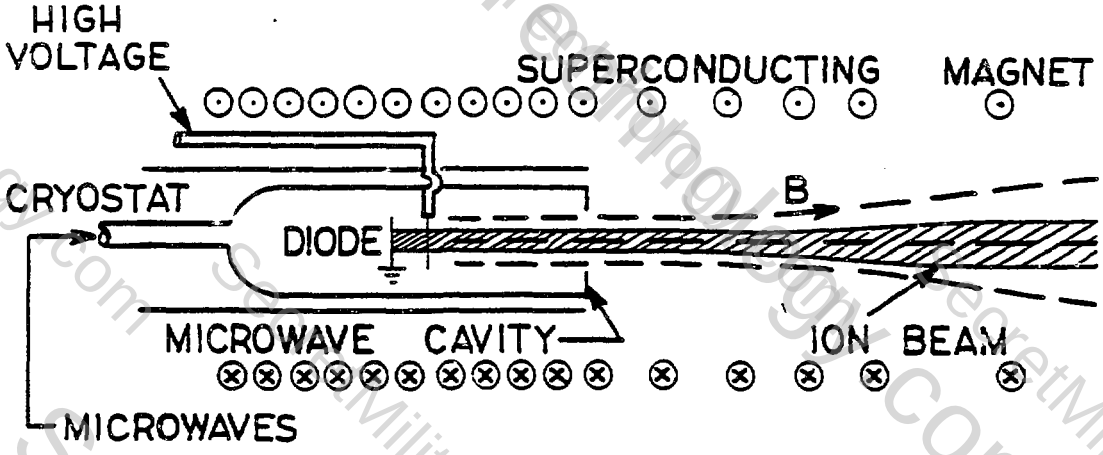

FIG. 1 SCHEMATIC DIAGRAM OF POLARIZED ION DIODES

CUSP INJECTION OF A 700 ns ROTATING R.E.B. INTO A PREFORMED PLASMA

Gary A. Saenz
University of California, Irvine, California 92717

Computer calculations indicate that in a mirror geometry with an axial current to generate a B_θ, single particles trajectories change radius as the z component of velocity changes magnitude and direction. The axisymmetric orbit can be solved analytically. This analysis may lead to new methods of trapping e-layers in a preformed plasma.

One method suggested for creating a compact torus magnetic geometry is via injection of an intense relativistic particle beam into a background magnetic guide field. Field reversals greater than 100% have been attained by injecting a beam into initially neutral gas and also into a preformed plasma. Hans Fleischmann, et al., of Cornell University have trapped field reversing rings with millisecond lifetimes in neutral gas. Unfortunately, a relatively large background pressure of several hundred millitorr of hydrogen is required for appreciable beam propagation. The cross section for production of a beam generated plasma must be sufficient to space charge neutralize the intense electron beam. This high density background serves to limit the overall lifetime of the field reversing relativistic electron layer. Injection of the e-layer into a preformed plasma will allow space charge neutralization in a particle background several orders of magnitude less dense. This suggests an increase in lifetime of these e-layers by several orders of magnitude. However, no trapping of primary (relativistic) electrons in a preformed plasma has been observed, as indicated by the absence of hard X-rays shortly after (>300 ns) the voltage pulse.

Another important difference between the two environments (neutral gas and pre-ionized plasma) is the velocity at which the beam generated magnetic fields propagate. In neutral gas these field changes propagate at c, the speed of light; whereas the beam particles always move at less than c (slower in the axial direction, depending on the pitch angle). The self fields can significantly alter the applied magnetic field in the time required for a beam particle to transit the system and return. These self fields would, and apparently do, aid in trapping of beam particles.

In contrast, return currents in a conducting plasma inhibit magnetic field changes such that beam generated magnetic fields move in the plasma at the Alfvén speed, $v_A = B/(\mu_o \rho)^{\frac{1}{2}}$, parallel to the applied field and at the magnetosonic speed, v_{MS}, in perpendicular directions. Even in particle densities as low as $10^{12}/cm^3$ and B_o on the order of 1 kG, $v_{MS} \simeq v_A = .01c$, while beam particle velocities are easily greater than 0.1c. Therefore, the background magnetic field is essentially stationary during one transit period of a beam particle. This may explain why methods used to trap field-reversing rings in neutral gas have not as yet been successful in a pre-ionized plasma.

For times much less than the Alfvén time, return currents in the plasma neutralize the magnetic field generated collectively by the beam particles. This causes high current beam particles to behave more like single particles such that their trajectories may be calculated to first order. The relativistic Lagrangian is given by

$$L = -\frac{mc^2}{\gamma} + \frac{e}{c}\vec{A}\cdot\vec{v} + e\Phi \quad , \text{(cgs)} \ ,$$

where e is the electric charge, c is the speed of light, m is the mass of the electron, γ is the relativistic factor $(1 - v^2/c^2)^{-\frac{1}{2}}$, Φ is the electric potential and $\vec{A}$ is the magnetic vector potential. In a magnetic geometry with B_r, B_θ, and B_z having axial symmetry, A is not a function of $\hat{\theta}$. This gives

$$\frac{\partial L}{\partial \theta} = 0, \text{ and } \frac{d}{dt}\frac{\partial L}{\partial \dot{\theta}} = 0, \text{ or } \frac{\partial L}{\partial \dot{\theta}} = \text{constant}.$$

The canonical momentum $\hat{P}_\theta = \frac{\partial L}{\partial \dot{\theta}} = \gamma m r^2 \dot{\theta} + \frac{e}{c} A_\theta r$ is a constant of the motion.

Computer calculations of single particle motion demonstrate a magnetic geometry which induces toroidal and poloidal currents. (See Fig. 1). This is a simple mirror field (B_z) with an axial current producing a magnetic component in the $\hat{\theta}$ direction (B_θ). The outer orbit radius for axisymmetric motion (see Fig. 1) is found analytically by

$$\frac{d}{dt}(\gamma m \vec{v}) = \frac{e}{c}(\vec{E} + \vec{v} \times \vec{B}) \quad .$$

Setting $E = 0$, $\frac{d\gamma}{dt} = 0$, $\ddot{r} = 0$, so $\vec{v} = r\dot{\theta}\hat{\theta} + \dot{z}\hat{z}$, and $\vec{B} = B_\theta\hat{\theta} + B_z\hat{z}$, gives

$$\gamma m \frac{v_\theta^2}{r} = \frac{e}{c}(v_\theta B_z - v_z B_\theta) \ ,$$

where $v_\theta = r\dot{\theta}$ is derived from initial conditions and the conservation of canonical $\hat{P}_\theta$; $\dot{z} = v_z = (v_o^2 - v_\theta^2)^{\frac{1}{2}}$; and $B_\theta = \frac{2I}{cr}$ (cgs).

Moving the particle off this magnetic surface causes oscillations about this equilibrium (see Fig. 2). Larger displacements would cause inner and outer paths to overlap. There appears to be a magnetic surface which particles of a given perpendicular and parallel energy oscillate about.

These magnetic geometries may be helpful in trapping electron layers in a preformed plasma. Present investigations involve beam injection through an asymmetric cusp. This allows the particle location r, the

perpendicular velocity v_θ, and the magnetic field components B_z and B_θ, to be adjusted independently. The beam is injected at the outer magnetic surface radius r_o, and is reflected by a large downstream mirror. The beam is expected to return at the smaller inner radius r_i, and interact with a radially localized mirror r_{rlm},

$$r_i < r_{rlm} < r_o \quad \text{(See Fig. 3)} \quad .$$

The difficulty lies in making the localized inner mirror sufficiently strong to reflect the returning beam, while producing only a negligible effect on the outer radius (the beam injection channel).

This work was supported by the Department of Energy.

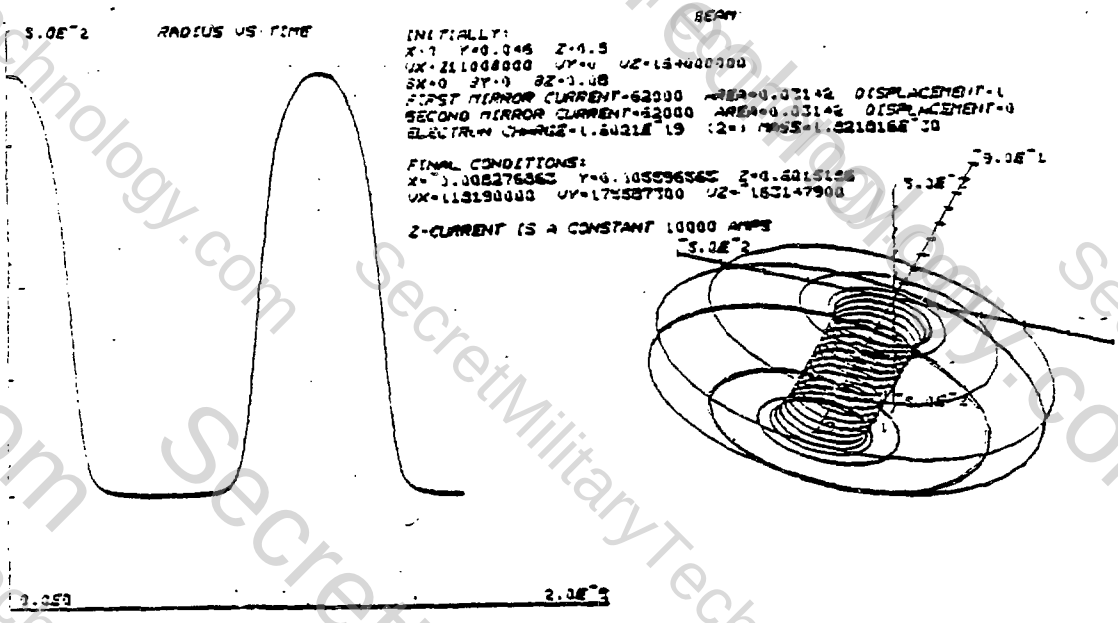

FIGURE 1

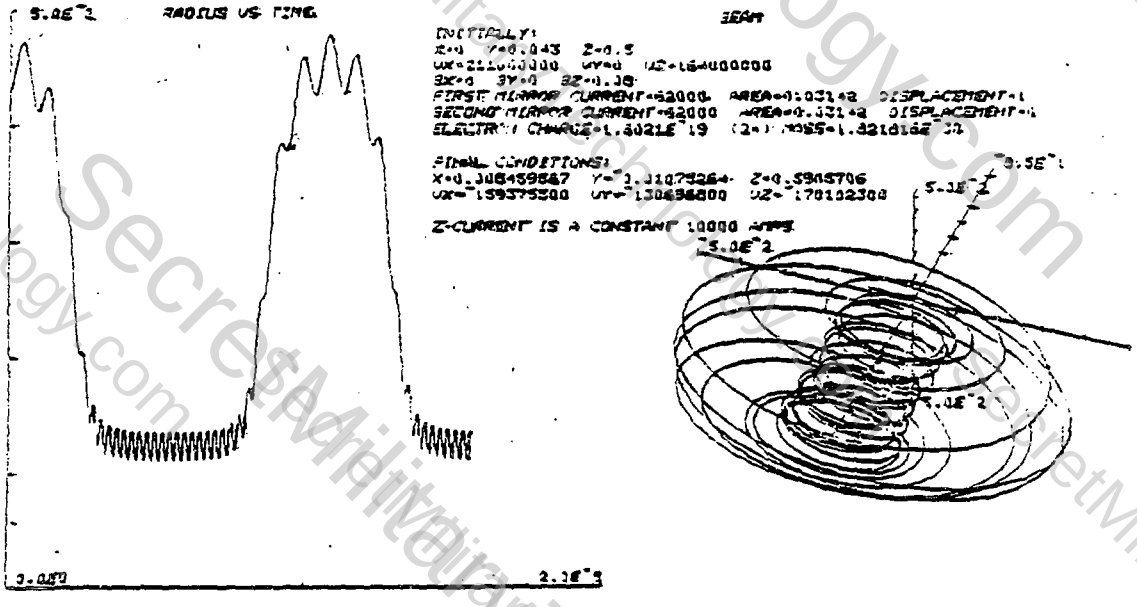

FIGURE 2

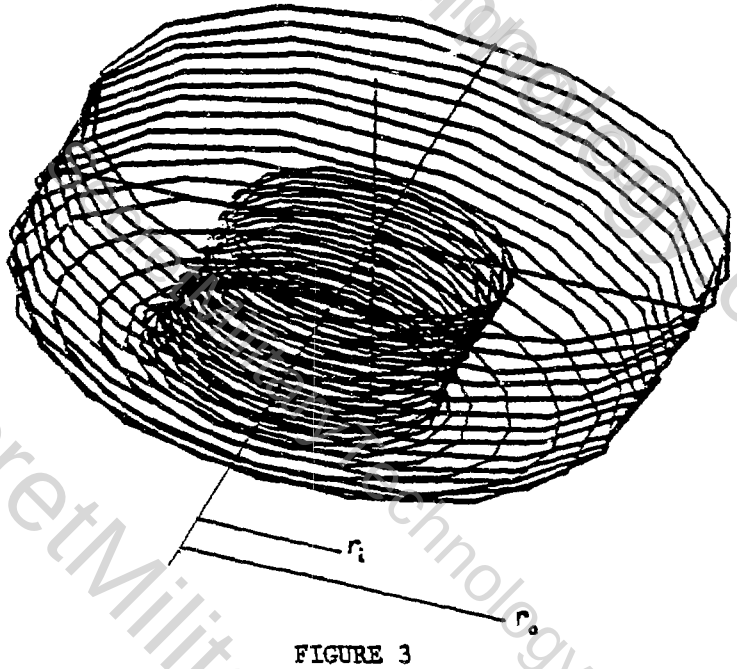

FIGURE 3

Recent Results of the RECE-Christa Experiment*

D. Taggart, M. Parker, H. Hopman, R. Jayakumar and H. H. Fleischmann
RECE-Group, Cornell University

This paper is primarily a description of recent experimental studies in the RECE-Christa(1) device on the dynamics and stability characteristics of mixed-CT configurations which are generated by inducing sizable plasma ring currents in field-reversing E-layers. Other potential CT configurations, in particular the Spheromak-type, have been projected theoretically(2) and also observed experimentally(3) to have a strong tendency towards tilt-instability except under certain circumstances which would tend to exclude potentially very interesting reactor designs. Based on the fact that this instability has never been observed in field-reversing large-orbit electron ring experiments (probably due to coupling through the large-orbit particles between the tilt motion and the internal length parameters of the rings), it has been suggested(4) that this problem may be avoided by adding large-orbit particles carrying some of the ring current to the normal Spheromak configuration. Also, recent theoretical analyses(5,6) using the angular momentum of the fast particles indicate a stabilizing tendency, although we believe this mechanism is resistively unstable. The present experiments are the first to test this situation, with the results indicating good gross stability even in cases with large plasma currents. In addition we report the generation of highly elongated E-layers and preliminary results of trapping experiments in low toroidal (B_θ) fields.

The field-reversing electron rings (lifetimes about 1.1 msec) of RECE-Christa(1) (see Fig. 1) are generated by injecting intense relativistic electron beams (typical beam pulse parameters: 2.5 MeV, 40 kA, 80 nsec) tangentially into a mirror field (B_z=300-500 Gauss) and axially translating rings into a low density surrounding (p=0.05-2 mTorr) downstream. In the present experiments,(7) toroidal plasma currents are induced in the rings through an added transformer coil (6 cm dia., 1.5 m long, 300 turns) placed along the ring axis. This coil is driven by a capacitor bank ($V_C \lesssim 6$ kV, $t_{1/4}$=160 µsec). Diagnostics include magnetic probes, line spectroscopy, framing camera and microwave interferometry.

As indicated by magnetic probes along the ring axis, very large plasma currents are induced by this arrangement. Figure 2 gives an example in which the original field-reversal strength of the pure electron ring of about 110% is enhanced to 240% by the induced plasma currents during the transformer pulse. The additional induced-current ring field (on top of the pure electron-ring generated field) rises in about 40 µsec and then decays again with the induced voltage. The indicated ring response is smooth and without any signs of gross instabilities. Some fast-electron losses are indicated by the smaller ring field after termination of the current drive. These losses appear to be consistent with enhanced wall losses due to increase of fast-electron energy and radius in the accelerating field of the heating coil. Wall probes indicate that plasma currents flow at a radius somewhat smaller than the fast-electron radius. Analysis of the combined system dynamics is complicated by the acceleration of the fast electrons and changes in the ring

*Work supported by DOE Contract DE-AS02-76ET53017

equilibrium radii due to the $\vec{j}\times\vec{B}$ force exerted by the plasma on the fast electrons. While a full analysis awaits equilibrium calculations which take this coupling into account, we presently estimate that the plasma currents and fast-particle current are approximately equal in Fig. 2.

In order to distinguish the dynamics of the mixed system (where both plasma and fast electron currents are present) from the dynamics of the fast electrons alone in the accelerating field of the on-axis transformer coil, a separate experimental series was performed in which plasma currents were suppressed by a high density background gas while the fast electrons were accelerated. The observed radius changes of an electron ring during the heating pulse were compared to a simple, single-particle model (which neglects the effect of the B_θ field as well as the self-field of the ring). The radius changes observed were less than those predicted by the model.

A new type of E-layer equilibrium has been observed in RECE-Christa. Figure 3 is an example of one of these new, highly elongated E-layers. This layer has a length to radius ratio $\Delta Z/R \approx 6$. Normal E-layers in RECE-Christa have $\Delta Z/R \sim 2$. The length of these layers is determined as the ring moves from the trapping region to the downstream field minimum at the heating coil center and again when the ring comes to rest around the magnetic probe array at the heating coil center. These measurements show that the ring length does not change during its axial translation and stationary decay lifetime. The existence of such highly elongated equilibria has been demonstrated theoretically.(8) The creation mechanism of such elongated E-layers is being investigated.

Finally, experiments are being performed in order to reduce the applied toroidal field. To date, field reversals $\delta \leq 0.7$ have been achieved in low-B_θ trapping experiments. Figure 4 is an example of an electron ring trapped in a DC hydrogen fill at a toroidal to axial field ratio of 0.25. The ring is seen to decay stably. It has also been possible to reduce the toroidal field during the lifetime of the ring by a factor of 3 with no gross instability [in contrast to the results of R. Meger(9) where such changes were accompanied by abrupt "dumps"]. Experiments at low-B_θ are continuing.

References

1. M. Tuszewski, D. J. Rej and H. H. Fleischmann, Phys. Rev. Lett. 43, 449 (1979).
2. M. N. Rosenbluth and M. N. Bussac, Nucl. Fusion 19, 489 (1979).
3. T. R. Jarboe, I. Henins, H. W. Hoida, R. K. Linford, J. Marshall, D. A. Platts and A. R. Sherwood, Phys. Rev. Lett. 45, 1264 (1980).
4. H. H. Fleischmann, Proc. US-Japan Symposium on Compact Toruses, Princeton (December 1979), p. 41.
5. A. Mohri, Jap. J. Appl. Phys. 19 L686 (1980).
6. R. N. Sudan and P. Kaw, Phys. Rev. Lett. 47, 575 (1981).
7. R. Jayakumar et al., 1982 IEEE International Conference on Plasma Studies (Ottawa), IEEE Conference Record, Paper 1E5, 14 (1982).
8. C. Ruchti and R. Lovelace, private communication.
9. R. Meger, Ph.D. Thesis, Cornell University, May 1977.

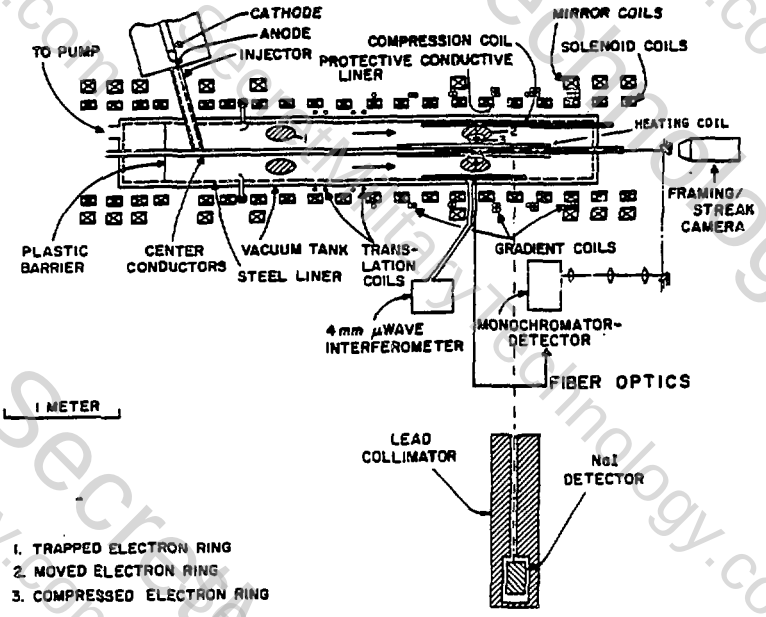

Fig. 1 - RECE Christa

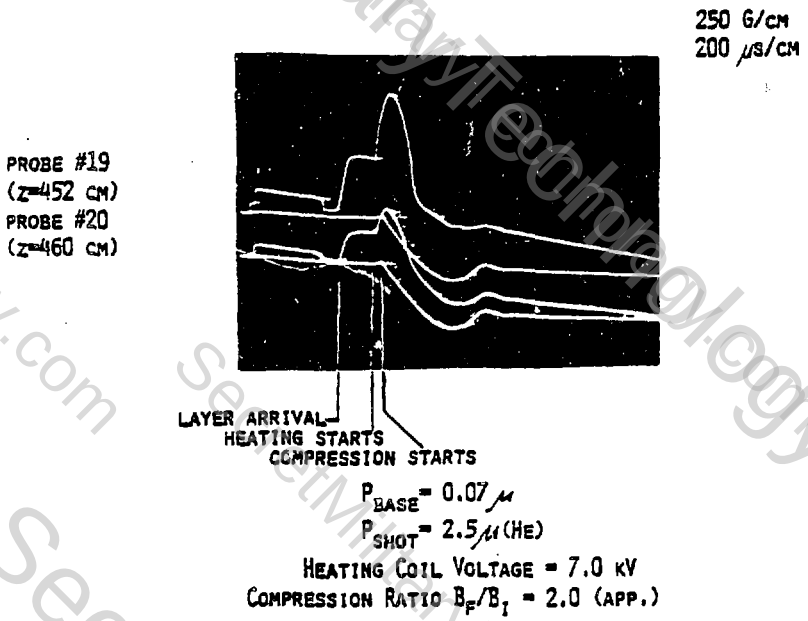

Fig. 2. Sample recordings from two axial probes for a shot with plasma currents ("heating") and compression. In addition to one baseline (without ring) each, indicating the return field of the transformer coil and the compression field, each recording shows the arrival of the ring layer and the changes in the ring field after the start of the plasma currents and compression. Field-reversal changes from 110% to about 240% with plasma currents.

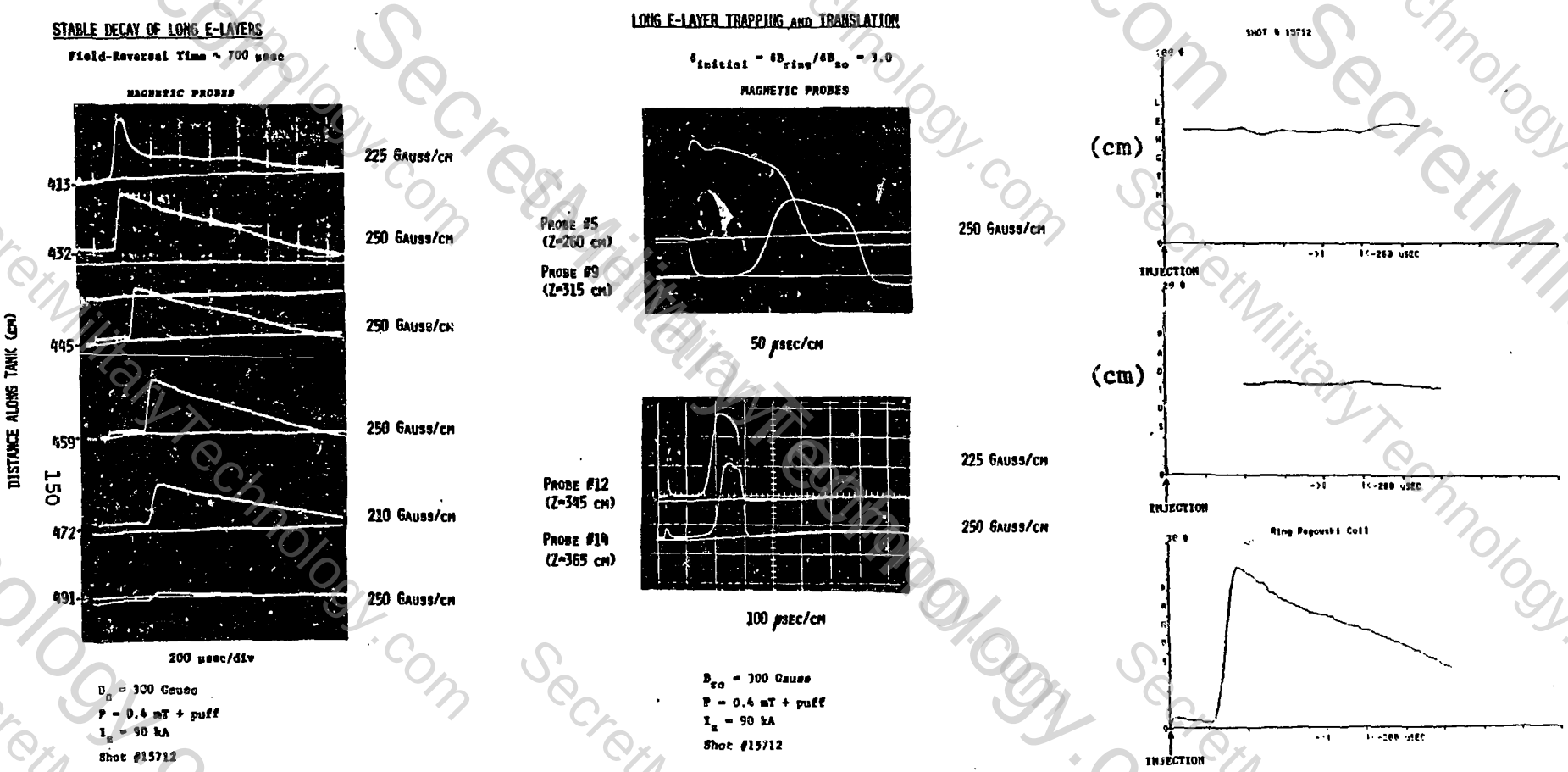

Fig. 3 - Highly elongated E-layers have been observed in RECE-Christa. On the left (above) are shown signals from an array of magnetic probes on the axis of one of these long layers as it stably decays in a DC field minimum centered on the heating coil (the layer is not moving). These same magnetic probe signals were digitized. The digitized data was then used to determine the length, radius and total current of the ring. These quantities are plotted on the right as a function of time. The ring length and radius are seen to remain constant during the ring lifetime. The layer is 60 cm long with a radius of 10 cm (z/R=6). The middle traces show the magnetic signal of the ring as it moves from the trapping region to the heating coil. These also indicate that the layer is highly elongated.

E-RING TRAPPING AT LOW TOROIDAL FIELDS

300 mT HYDROGEN FILL, SHOT 16674

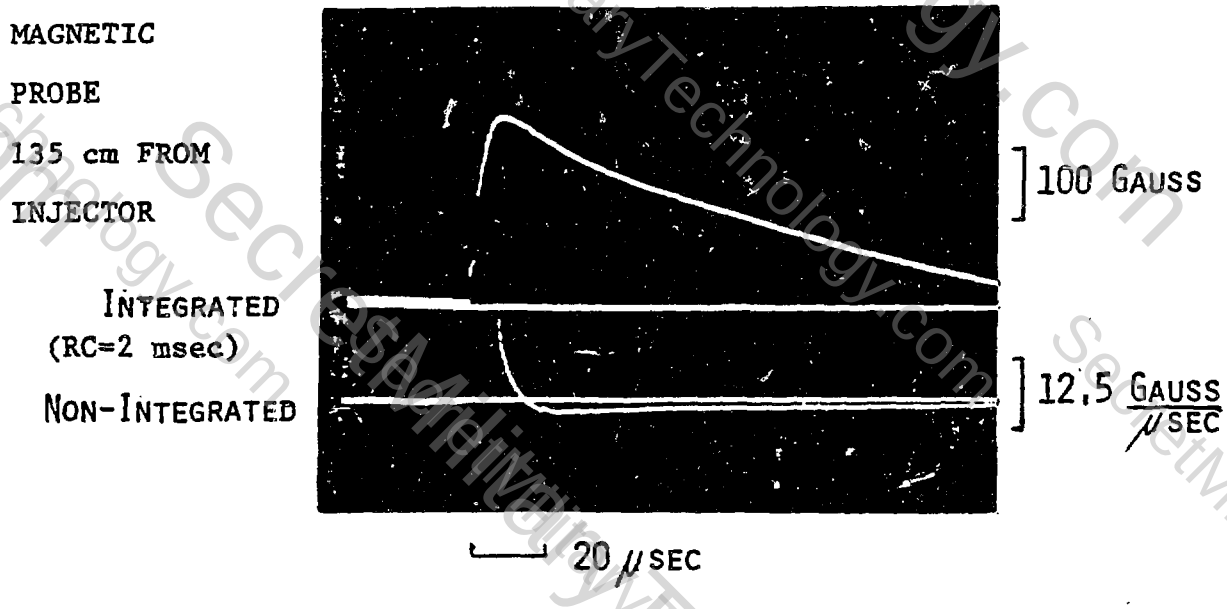

B_Z = 530 GAUSS

I_Z = 8 kAMP → $B_T / B_Z \approx 0.25$

Fig. 4 - Trapping and stable decay of an E-ring in a low toroidal field

COMPACT TOROID GENERATED WITH TWO COUNTERSTREAMING ELECTRON BEAMS

J. D. Sethian, K. A. Gerber, A. W. DeSilva,* and A. E. Robson

Naval Research Laboratory
Washington, D.C.

A Compact Toroid[1] is a magnetic confinement system comprised of a reversed axial B_z (or poloidal) field encircling the plasma, and an azimuthal B_θ (or toroidal) field trapped within the plasma. Such a device has many advantages over more conventional toroidal schemes for confining a hot plasma, including; relatively high plasma β, the absence of magnetic structures linking the plasma, small size, and a potentially simple vacuum vessel. Unfortunately, the very simplicity of the Compact Toroid makes it difficult to set up, and the various approaches being tried (plasma guns, spheromak, reversed field theta pinch) all suffer from their own peculiar disadvantages.

In this paper it is shown that a Compact Toroid can be made by a novel method using two rotating relativistic electron beams. The beams are sequentially injected into an initially field-free metal tube filled with neutral hydrogen according to the process shown schematically in Fig. 1. By adjusting the gas pressure so the plasma produced by the first beam is sufficient to neutralize the beam charge, but not the beam current, the first beam can be made to induce the fields (Fig. 1a), heat the plasma, thus "freezing in" the fields (Fig. 1b), and, upon leaving the system, induce persistent plasma currents that maintain the field configuration established during the beam pulse. This configuration, as reported elsewhere,[2] has two components: (1) a reversed B_z field (because the net axial flux through the tube must always be zero, the axial field induced inside the plasma has a corresponding antiparallel component between the plasma and wall), and (2) an external B_θ field. The latter is maintained by a continuous net axial current that returns through the walls (Fig. 1c). The configuration produced by the first beam is thus a linear reversed field pinch.

To create a compact torus, the axial current must be eliminated. This is done by injecting a second rotating beam from the opposite end of the system, after passage of the first beam, between the first beam-formed plasma and the wall. The sense of rotation is such that the axial fields are amplified, and the current is adjusted so that the net axial current is just cancelled (Fig. 1d). The B_θ field is now contained solely in the plasma, and the system is free to contract axially and produce the Compact Toroid (Fig. 1e). This contraction is expected, not only because it is energetically favorable, but because the beginnings of such a contraction have been observed[2] during the decay of the single-beam-produced open current line configuration, as in Fig. 1c.

The primary advantage in producing a Compact Toroid in this manner is the relative simplicity with which it is formed: as the beams produce both the field and plasma, no applied magnetic field or plasma source is required, and all of the electrical components are contained in the electron beam generators. Furthermore, the vacuum vessel and first wall can be made quite simple, or more importantly, can be readily configured to accept whatever post formation heating scheme, if any, is deemed necessary.

*Sachs/Freeman Associates, Inc., Bowie, MD.

A simple model has been developed to predict the behaviour of the second beam in the presence of the fields induced by the first. This model is an extension of an earlier work that has been verified for a single beam.[3] Among the conclusions drawn from this model were: (1) a first beam current pitch angle of $\alpha_1 = \arctan v_\theta/v_z \sim 55°$ is optimal, as this ensures the second beam will be well away from both the plasma and the wall (v_θ and v_z are the net azimuthal and axial velocities of the beam, respectively); (2) the current pitch angle of the second beam, $\alpha_2 = 45°$; (3) the axial flux enclosed by each beam i.e., that enclosed by the cathode emission surfaces, must be the same; and (4) the energy required of the second beam to close the current lines is less than half that required of the first beam to form the initial configuration. This model is described in Reference 4.

The experimental facility is shown in Fig. 2. The first electron beam was provided by the TRITON generator (700 kV, 60 kA, 120 nsec), which was used in all the previous single beam studies. The second beam was provided by the more powerful POSEIDON generator (1 MeV, 100 kA, 120 nsec), which was built expressly for this task. The generators injected beams into opposite ends of a 14 cm diameter 60 cm long drift tube filled with neutral hydrogen. The drift tube and gas fill system were mounted on a cart, and could be readily moved to allow access to the front end of the generators. The most complex components of the system were the two foil changers that allowed the anode foils, which rupture on each shot, to be replaced without breaking the system vacuum. Basically complex airlocks, these items were essential as it would be impossible to evacuate both generator diodes and the drift tube with the foils in place. Each rotating beam was produced with a "half cusp". In this arrangement, a flat pancake coil was placed just after the anode foil and in front of an aluminum plate located in the foil changer. When the coil was energized, the field lines emanated perpendicular to the cathode emission surface, and, because they could not penetrate the aluminum during the coil current pulse, were diverted radially outward immediately after the foil. The interaction of the axially directed beam with the radially directed field caused the beam to rotate. POSEIDON used a 10.0 cm diameter carbon cathode (annular thickness of .5 cm), whereas TRITON used a 7.6 cm diameter cathode (same thickness). The TRITON applied flux and current were set to give a beam pitch angle of 55° and a radius of 4.0 cm. Then, in accordance with the model, the POSEIDON applied flux and current were adjusted to be equal to and 50% larger than those of TRITON, respectively. The TRITON anode was made of 17.8 μm thick titanium foil. The POSEIDON anode was made of the same material, with the addition of a 7.0 cm diameter, .5 cm thick aluminum disc attached in the center. When the foil was rolled into position, this disc made an uninterrupted electrical and mechanical transition with a 7.0 cm diameter, 10 cm long aluminum cylinder which was held in place by three radial supports. This cylinder served two distinct purposes: it thoroughly decoupled the fields and particles of the two beams, and it allowed the POSEIDON beam to make a smooth transition to the TRITON configuration

Experimental verification of the two beam concept is displayed in Fig. 3, which shows the poloidal (B_z) and toridal (B_θ) fields just inside the tube wall; i.e., external to the second beam. The arrows mark the injection time of the two beams. The presence of B_z (a reversed poloidal field) in the absence of B_θ (no net axial current) after the POSEIDON beam is injected signifies that a closed field line system was produced. (Without injection of the second beam both signals would decay to zero at the same time.) Despite this verification, the configuration was not originally as anticipated. In order to achieve any current cancellation, the TRITON current had to be lowered to 20 kA (compared to the 60 kA used in previous experiments) and the hydrogen fill pressure had to be lowered from 150 mTorr, which had previously been found to be the

optimum pressure, to 85 mTorr, the lowest pressure at which the beam would still propagate. Unfortunately this was not in an optimum regime, as the lower current reduced the plasma temperature, and consequently, the configuration lifetime. Furthermore, the magnitude of the increase in B_z, over six times the initial value, could not be predicted by the model: the current cancellation was complete only within 15 cm of the POSEIDON diode; and there was virtually no evidence of the POSEIDON beam at 45 cm from the diode. All of these effects were attributed to a plasma outside the first beam. The density of this plasma was low, less than $10^{14}cm^{-3}$, (the minimum resolvable by previous Thomson scattering measurements[4]) and certainly small compared to the 6×10^{15} cm $^{-3}$ in the main channel. Nevertheless, it was sufficient to prevent the self-field at the beam head from diffusing into the plasma fast enough. This resulted in both axial retardation of the beam, which caused an increase in B_z, and partial current neutralization of the beam, which resulted in less current downstream. This hypothesis was confirmed by observing that the second beam exhibited similar propagation behavior whenever it was injected less than 400 μsec after the first beam. As previous studies with an He-Ne Interferometer[4] showed that the TRITON-formed plasma persisted for at least 350 μsec, even though the magnetic fields remained for only 20 μsec, this confirmed the cause of this behavior.

This plasma was found to be created by electrons that were produced, but not confined by, the first electron beam. The source of these electrons is postulated as follows: When the beam is injected into the tube, it represents a sudden presence of negative charge. An electric field is then set up, with the field lines extending from the beam head to the drift tube wall and even to the POSEIDON foil. The ultraviolet and X-ray radiation produced by the beam creates electron and ion pairs (i.e., a plasma) in front of, and well away from, the influence of the beam self-field. The ions are accelerated into the beam head, and their relatively large Larmor orbit allows them to penetrate the self-field. The electrons, on the other hand, are accelerated away from the beam and end on the tube wall, ionizing new atoms in the process. This is why the second beam propagated best at the lower fill pressures (less of a plasma source) and weaker first beam current (less of a plasma generator).

In conclusion, the scientific feasibility of producing a Compact Toroid with two electron beams was demonstrated. The second counterstreaming beam completely neutralized the net current of the first, and produced an amplified, longer lived axial field. However, the propagation of the second beam was hindered by plasma external to the first beam channel, resulting in an axially nonuniform configuration. This plasma is inherent to the propagation of the rotating beam and, in the current experiments, restricted the parameter range in which axial current cancellation could be achieved to lower fill pressures and reduced first beam current. This was a regime in which the first beam propagation was not optimal. Nevertheless, it may be possible to achieve complete axial uniformity at optimum conditions through the use of a more powerful generator to supply the second beam. The result would be a relatively simple method of producing a Compact Toroid.

The authors are grateful for the competent technical expertise of D. R. Evenson and W. D. Webster, and for the engineering work of F. Mora, M. Sy and J. Chow. This work was supported by the Office of Naval Research and the U.S. Department of Energy.

REFERENCES

1. See, for example "Proceedings of the Fourth Symposium on the Physics and Technology of Compact Toroids," Lawrence Livermore Laboratory, 1981, and references therein.

2. J.D. Sethian, K.A. Gerber, D.N. Spector and A.E. Robson, Phys. Rev. Lett **41** 798 (1978).

3. J.D. Sethian, K.A. Gerber, D.N. Spector and A.E. Robson, Phys. Fluids 23, 1880 (1980).

4. J.D. Sethian, K.A. Gerber, A.W. DeSilva and A.E. Robson, NRL Memorandum Report No. 4932.

5. J.D. Sethian, D.A. Hammer, K.A. Gerber, D.N. Spector, A.E. Robson and G.C. Goldenbaum, Phys. Fluids **21**, 1227 (1978).

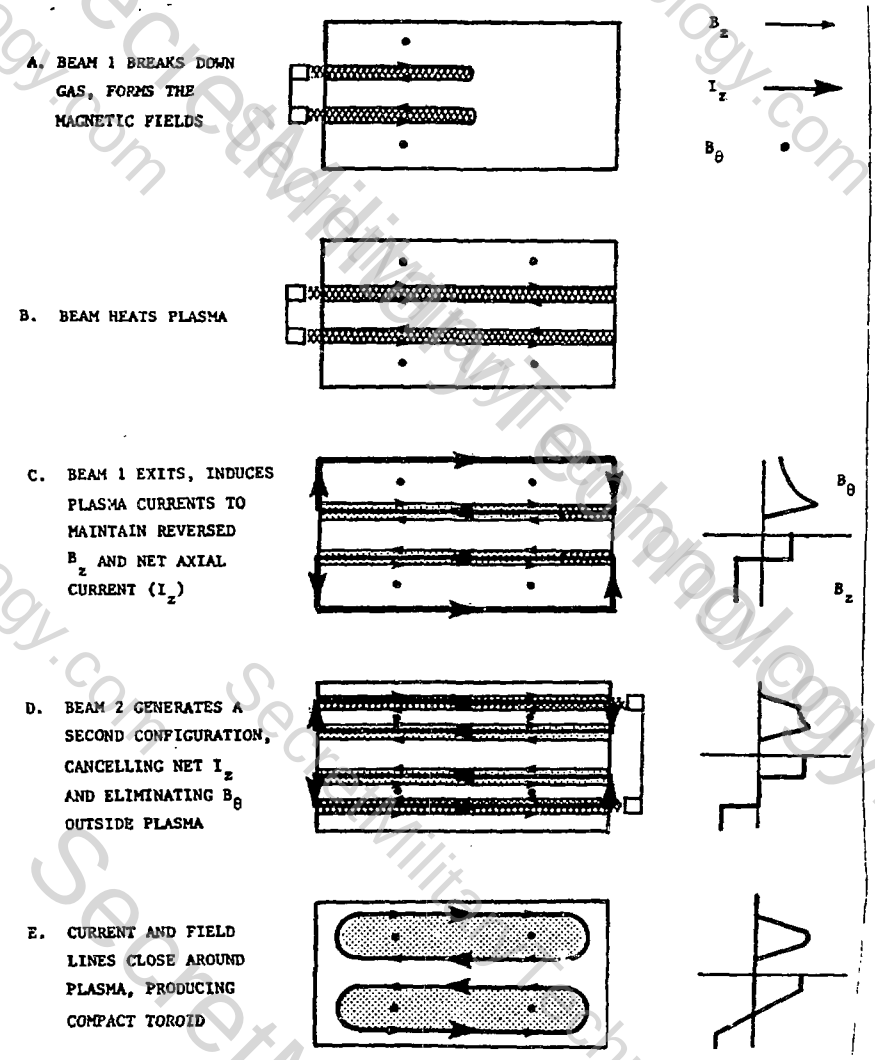

Fig. 1 — Formation of a compact toriod with electron beams

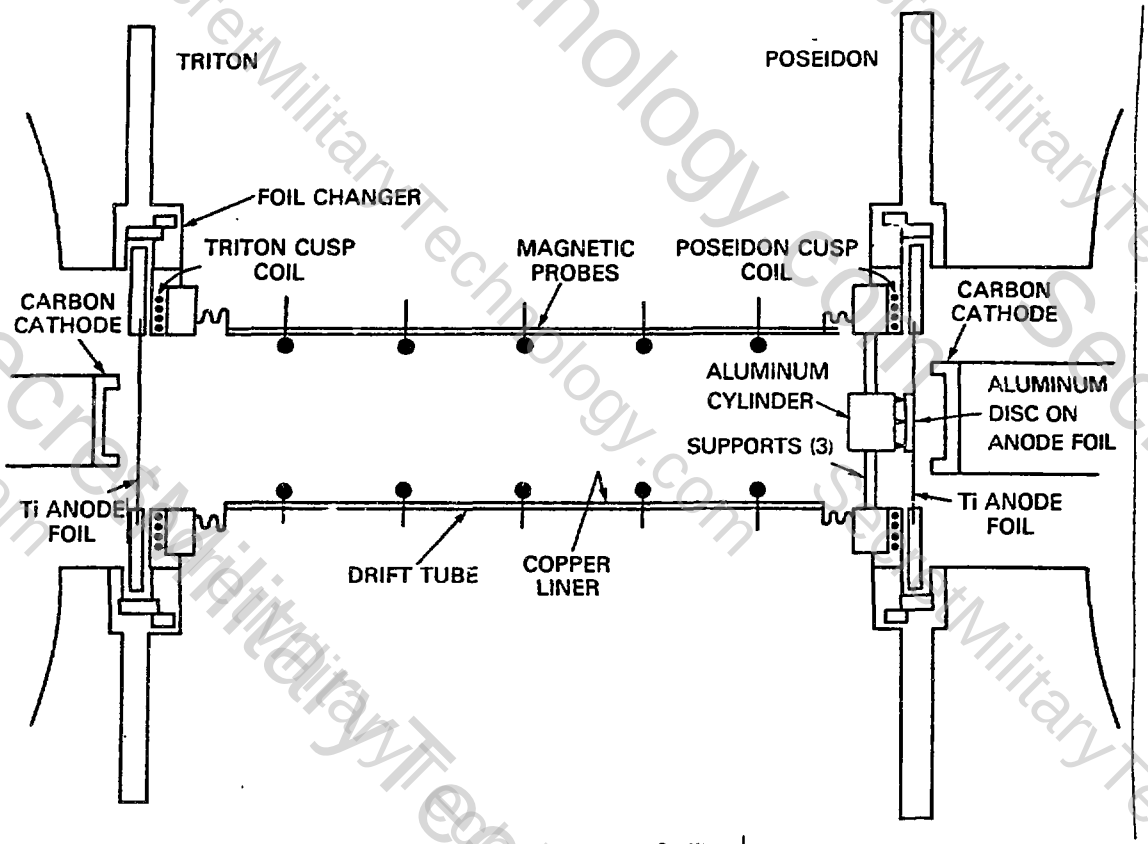

Fig. 2 — The experimental facility

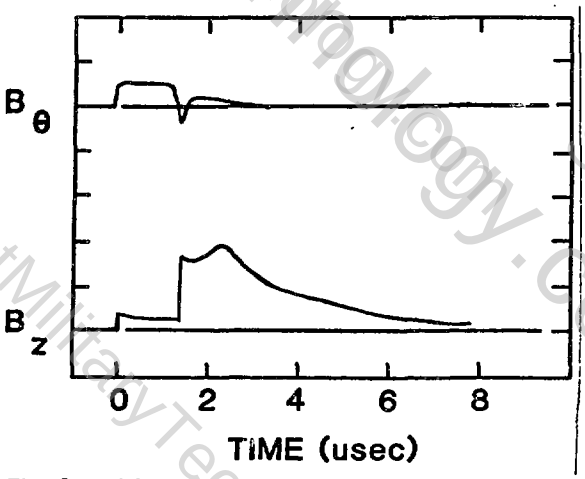

Fig. 3 — Magnetic signals from probes located at a radius of 6.3 cm (r_w = 7.3 cm) and axial position 10 cm from the POSEIDON diode

REACTOR SCENARIOS FOR COMPACT TOROIDS*

Randy L. Hagenson, Technology International Incorporated, Ames, Iowa 50010-6789

Several reactor studies have been performed for compact toroid (CT) plasmas, generally defined as a toroidal plasma configuration in which no magnet coils or structural walls extend through the center of the torus. These studies include: The Field-Reversed Theta-Pinch (FRΘP) reactor (CTOR)[1]; the Trigger-Reconnected Adiabatically-Compressed Torus (TRACT)[2]; The Slowly-Imploding Liner (LINUS)[3]; Field-Reversed Mirror (FRM)[4]; Translating[5-7] and Stationary[7,8] Spheromaks; the Ion-Ring Compressor (IRC)[9]; and the Moving-Ring Reactor (MRR)[10]. Plasmoids without toroidal field are classified as Field-Reversed Configurations (FRC) and are typically produced by a FRΘP, whereas systems containing toroidal field are termed spheromaks.

The CT reactor system may be categorized according to Figure 1 as using either a steady-state or pulsed plasmoid. The key questions that must be addressed for each approach are also shown in terms of startup, stability/equilibrium and plasma engineering. Methods of building steady-state CT reactors with *in situ* plasma production have recently been identified[8], although definitive work needs to be done in this area. Crucial equilibria/stability questions must be addressed for these steady-state configurations, requiring the imposition of a number of stabilization techniques including a conducting shell, axis-encircling particles (AEP), finite-Larmor- radius (FLR) effects, multipole fields and quite probably an active feedback system. Upon achieving a stable configuration, additional plasma engineering problems, including fueling, heating, impurity/ash control, flux drive and profile control, must be overcome to maintain a steady-state system.

Reactor designs are further categorized in Table I according to type of CT plasma with key parameters listed in Table II. The field-reversed theta-pinch (FRΘP) is typically used to generate the FRC. Equilibrium of these plasmas requires a highly-prolate structure, $\ell/r_s \sim 6$, where ℓ is the total plasmoid length and the separatrix radius is r_s. Another crucial parameter in the FRΘP plasma is the ratio of r_s to conducting shell radius, r_c, $x_s = r_s/r_c \gtrsim 0.5$ due to the beta relationship $\langle\beta\rangle = 1 - x_s^2/2$. Small values of x_s dictate high-beta values and sharp gradients leading to rapid transport. The CTOR design uses a FRΘP source (∼50 MJ), a traveling-wave compression network (∼200 MJ) and a linear burn section. The tapered burn section allows alpha-particle expansion work to force the CT through the chamber assuring continuous presence of a conducting shell. This normally unstable translation is stabilized by a thin first-wall shell providing a drag force proportional to ring speed in addition to the primary conducting shell outside the blanket. The TRACT and LINUS reactors envisage a stationary plasma within an engineering system that uniquely combines many reactor functions. The TRACT approach integrates a shock-heating plasma source within the reactor burn section. This device introduces stability/equilibrium questions when attempting to use *in situ* shock heating and compression to ignition temperatures while maintaining $x_s \gtrsim 0.5$ if a 0.9 s burn is stabilized by a conducting shell. Efficiency of the axial shock heating, effect of the barrier coil during startup and engineering problems of high-voltage in a neutron environment

*Work performed under the auspices of the U. S. Department of Energy and the Los Alamos National Laboratory.

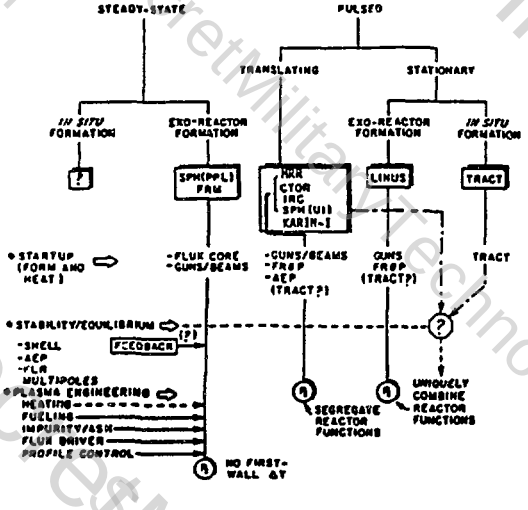

Figure 1. Categorization of CT reactor studies.[1]

TABLE I. COMPACT TOROID STABILITY/EQUILIBRIUM

	PULSED /S.S.	TRANS /STAT.	COND. SHELL	FLR $S=a/\rho_i$	AEP (MEV)	MULTI-POLES	FEED-BACK	T_i (keV)	SHAPE L/r_s	B_ϕ	$\langle\beta\rangle$
FRCP									PROLATE		
CTOR	P	T	THICK	30	---	---	---	15	~7	0	~0.8
TRACT	P	S	?	20-25	---	BARRIER (STARTUP)	---	12-35	~6	0	~0.8
LINUS	P	S	THICK	100	---	---	---	35-20	~90	0	0.5-0.6
FRM	S.S.	S	THIN	5-15	?	IOFFE	?	50-70	~2	0	~1.0
SPHEROMAK									OBLATE		
SPHEROMAK (PPPL, UI)	P	T	THIN	50-150	---	---	---	15	1.0	$\sim B_\theta$	0.17-0.34
KARIN-I	P	T	THICK (?)	100	---	---	---	10	0.5	$\sim B_\theta$	0.36
SPHEROMAK (PPPL)	S.S.	S	THIN	150	---	---	?	15	1.0	$\sim B_\theta$	0.17
HIGH-ENERGY RING											
IRC	P	T	?	1	300	---	---	20	OBLATE (~1)	0	$\gtrsim$0.5
HYBRID											
MOVING-RING	P	T	NONE	22-34	20 (20% of Current)	YES	---	75	PROLATE (2)	$\sim\frac{B_\theta}{2}$	0.67

TABLE II. KEY PARAMETERS OF COMPACT TOROID REACTORS

	TRACT (INIT-FINAL)	CTOR (INLET-OUTLET)	FRM (STEADY STATE)	LINUS (INIT-COMP)	SPH (PPPL) (STATIONARY)	SPH (UI) (TRANSLATING)	KARIN-I	MOVING-RING (INLET-OUTLET)	IRC
FIRST-WALL RADIUS (m)	0.68	1.2-1.6	0.73	1.4-0.11	3.2	1.4	2.0	1.25	4.5
BURNER LENGTH (m)	10	40	22	10	6	8.5	50	18	20-25
SHELL RADIUS (m)	0.7(?)	1.7-2.1	---	1.4-0.11	3.2	1.4 (?)	2.0 (?)	NONE	4.5
SEPARATRIX RADIUS (m)	0.39-0.55	0.85-1.05	0.23	1.4	3	1.05	2.0	0.39-0.57	4.0
PLASMOID LENGTH (m)	2.1-3.0	5.0-8.0	0.42	10.0	3	0.7	1.0	0.8-1.14	4.5
BURN/SWELL TIME (s)	0.9/0.2	2.0/5.8	---	0.001/0.5	---	~6.5/5	10/1	5.9/2	5/1
PLASMA DENSITY ($10^{20}/m^3$)	20	25-5	6.5	8.2-1900	2.1	~3	6.8	5	0.6
PLASMA TEMP (keV) (PRECOMP/COMP/FINAL)	4.4/12/37	1.5/8/12	96	0.5/20/20	15	15	1.6/9.3/9.3	/3/75	low/20
ENERGY CONF. TIME (s)	~0.9	~0.1	~0.5	~0.001	1.4	~1.0	~1.0	~1.8	~5
BURN MAGNETIC FIELD (T)	4.7	4.1-2.0	4.1	0.6-60	4.0	5.0	2.88	6.5	1.4
RING SPEED (m/s)	---	38-10	---	---	---	~1	5	STEPPED	5
FIRST-WALL LOAD (MW/m^2) (AVE/PEAK)	7.46/38	2.0/5.8	1.8	1/260	4.0/	7.8/	2.4/	1.9/4.0	2.3/7
PEAK SURFACE FLUX (MW/m^2)	1.3	~0.4	---	---	?	?	?	0.3	?
BURN-SECTION POWER DENSITY (MWc/m^3)	1	0.5	0.4	~20	1.3	~1	0.7	0.20	0.4
NET/GROSS POWER	0.68	0.85	0.54	0.78	---	~0.75	0.74	0.77	~0.7
NET ELECTRIC (MWe)	99	310	74	900	1000 (thermal)	200	647	99	~450

(SiC first wall) must be addressed. The LINUS reactor uses a rotating-liquid metal liner (first wall) to compress and contain plasma, introducing problems of evaporated liner material, flux diffusion into the liner, design of the liner drive mechanism and liner reversibility. Finally, problems of CT equilibrium, have led the FRM configurations to evolve into the MRR system where equilibrium is provided by energetic ion rings as discussed below.

Several potential spheromak reactors have been defined although most involve translating the oblate configurations. Recent experimental evidence has underlined the need for a relatively close fitting conducting shell which may have large penetrations, however, translating these plasmoids through a long-linear burn chamber will not maintain an equilibrium. Reactor configurations utilizing stationary spheromak plasmas are considered the most promising with refluxing being a major concern. Experimental results suggest a minimum-energy state as predicted by the Reversed-Field Pinch (RFP) experiments[11]. Flux may be transferred from poloidal-to-toroidal circuits or *vice versa* by the plasma, allowing external steady-state refluxing either by beams or direct DC current drive[8] through electrodes. This reactor scheme is particularly interesting due to recent RFP reactor studies[11] work. High-efficiency, high-power density reactor systems using normal conducting magnet coils to ohmically heat to ignition, require poloidal betas of ∿10-20% and energy transport of ∿0.1 s. Similar beta values have already been achieved in spheromak experiments.

Reactor embodiments using high-energy rings to heat and confine the plasma were among the first to be suggested. Areas of concern for the ion-ring (IRC) machine include beam requirements and trapping efficiency, plasma power balance and the resultant reactor energy balance. The moving-ring reactor (MRR) combines the plasma characteristics of the FRΘP/Spheromak/IRC, attempting to produce a stable plasma in a translating geometry with no conducting shell present. The characteristics of this CT must be experimentally defined including production, compression and maintenance. This reactor study concentrated on minimizing nuclear related problems leading to hands on maintenance wherever possible and eliminating meltdown if a loss of coolant occurred. The price for achieving these characteristics included a low-power density and large SiC structures.

In summary, the highly-prolate FRC lends itself to a translating pulsed-reactor configuration; segregating key reactor functions, allowing the continuous presence of a thick-conducting shell and leading to small unit sizes. Development of a slow plasma source which can be powered by a rotating machine and optimizing the plasma transport properties by increasing x_s, (smoothing the profile) which minimizes the CT size are the most crucial experimental tasks for a reactor configuration. Equilibrium constraints leads to stationary spheromak reactors surrounded by a loosely fitted conducting shell. Translating these oblate configurations is deemed very difficult. Reactor studies for the CRFPR are directly applicable indicating very attractive machines operating at betas already experimentally achieved, ohmic heating to ignition and normal conducting magnet coils. Steady-state refluxing methods have also been proposed. Finally, questions of beam requirements, equilibrium/stability, and energy balance must be experimentally addressed for the high-energy beam reactors. For all CT systems the principle advantages of a natural divertor, small unit size and the segregation of key reactor functions are typically realized.

REFERENCES

1. R.L. Hagenson and R.A. Krakowski, "A Compact-Toroid Fusion Reactor Based on the Field-Reversed Theta Pinch," Los Alamos National Laboratory Report LA-8748-MS (1981).
2. H.J. Willenberg, Project Leader, "Definition and Conceptual Design of a Small Fusion Reactor," Mathematical Sciences Northwest, Inc. Report MSNW 1159 (1982).
3. R.L. Miller and R.A. Krakowski, "Assessment of the Slowly-Imploding Liner (LINUS) Fusion Reactor Concept," Proc. 4th ANS Topical Meeting on the Technology of Controlled Nuclear Fusion, King of Prussia, PA. (1980).
4. G.A. Carlson, W.C. Condit, R.S. Devoto, J.H. Fink, J.D. Hanson, W.E. Neef, and A.C. Smith, Jr., "Conceptual Design of the Field-Reversed Mirror Reactor," Lawrence Livermore Laboratory Report UCRL-52467 (1978).
5. Working Group on KARIN-I, "Conceptual Design of Moving Ring Reactor: KARIN-I," 9th IAEA Conf. on Plasma Physics, Baltimore IAEA-CN-41/O-2-1 (1982).
6. A.M.M. Todd, R.E. Olson, J.G. Gilligan and G.H. Miley, "The Spheromak Fusion Reactor," Proc. 15th Intersoc. Energy Conversion Eng. Conf., 3, 2229-2236 (August 18-22, 1980).
7. M. Katsurai and M. Yamada, "Conceptual Design Study of Spheromak Reactors," Princeton Physics Laboratory Report PPPL-1614 (1980).
8. T.R. Jarboe, "Steady State Spheromak," Fifth Sym. on Physics and Tech. of Compact Toroids, Bellevue, WA (1981).
9. H.H. Fleischmann and T. Kammash, "System Analysis of the Ion-Ring Compressor Approach to Fusion," Nucl. Fus., 15, 1143-1155 (1975).
10. A.C. Smith, Jr., Project Leader, "Conceptual Design of a Moving-Ring Reactor," 9th IAEA Conf. on Plasma Physics, Baltimore, IAEA-CN-41/O-2-2 (1982).
11. R.L. Hagenson and R.A. Krakowski, "Compact Reversed-Field Pinch Reactors (CRFPR): Sensitivity Study and Design-Point Determination," Los Alamos National Laboratory Report LA-9389-MS (1982).

APPLICATIONS OF ACCELERATED COMPACT TOROIDS*

J. H. Hammer and C. W. Hartman

Lawrence Livermore National Laboratory
Livermore, California 94550

It has recently been suggested[1] that magnetic acceleration of low-β plasma rings, similar to those produced in existing experiments, could fill some of the wide gap in parameter space that lies between the extremes of conventional particle acceleration and magnetic acceleration of metallic slugs or magnetized pellets. Many applications can be conceived that exploit the newly-accessible regimes, some of which also make use of the special magnetic or confinement properties of the rings. Listed below are some of the possible applications, ordered in increasing energy (but not necessarily decreasing credibility). Low energy is defined as U = input energy $\gtrsim U_M$ = initial magnetic energy. Medium energy is $U > U_M$ and high energy is $U \gg U_M$. We invite the reader to add to the list.

LOW ENERGY: Magnetic fusion applications dominate the low energy uses.

1) Current drive. Most toroidal confinement devices employ parallel current, giving a net helicity to the fields. The additive property of helicity allows for current maintenance through providing an external helicity source, i.e., plasma rings, to match the ohmic losses. High values of Q are estimated for current drive by plasma ring injection although the resulting disturbance of magnetic surfaces may cause unacceptable heat loss.

*Work performed under the auspices of the U.S. Department of Energy by the Lawrence Livermore National Laboratory under contract number W-7405-ENG-48.

2) Fueling and heating. Dense rings moving faster than their internal Alfvén speed but slower than the Alfvén speed of the fusion reactor medium should cross field lines readily. The ultimate annihilation of rings by tilting and reconnection deposits a "cargo" of energetic particles or fuel.

MEDIUM ENERGY:

1.) Neutron Source. Accelerated rings can be focussed radially (e.g., by conducting cones) causing an increase in the field intensity and adiabatic heating. If the rings are designed to reach fusion temperatures they can provide a high fluence (due to the high density) pulsed neutron source.

2.) High field moving ring reactor. More stringent conditions on the rings, e.g., larger values of I, the circulating current, can lead to net power production. Small rings ($R \sim 20$ cm) operating near stress limits ($B_{wall} \sim 500$ kG) can have reasonable Q's and lower energy/ring than traditional fusion schemes ($\sim 5 \times 10^7$ Joules). The price paid is a high peak wall loading, although the duration of the peak at any location can be controlled by the ring velocity. The simple topology (a hollow conducting tube surrounded by tritium breeding material), the absence of nearby coils, and the small diminsions may make frequent replacement acceptable.

HIGH ENERGY:

1.) Fast switching/power amplification. Energy stored in a relatively slow medium, e.g., highly capacitive or inductive capacitor banks and high-explosive generators, can be converted at high efficiency into either inductively stored energy behind the ring or kinetic/magnetic energy of the ring itself. The energy is switched to a load in a time of

order L/V (L = length of ring, V = velocity of ring). Rings compressed to dimensions less than a centimeter appear possible with speeds a significant fraction of c, giving switching times of a fraction of a nanosecond. If the energy is stored in the ring itself, then the deposition time is also of order L/V.

2.) Inertial fusion driver. Given the power amplification feature mentioned above, the use of accelerated rings as efficient drivers for inertial fusion is a possibility. Rings moving $\sim 10^8$ cm/sec with dimensions < 1 cm and kinetic energies $\sim$ 10 megajoules would match the power requirements for inertial fusion. The compactness of the accelerator (lengths $\sim$ 10 m) is an advantage in addition to the efficiency, making this a reasonable candidate for fusion powered rocket propulsion.

3.) Synthesis of trans-uranic elements. A low mass ring containing $\sim$ 1 coulomb of protons and salted with a few percent of high mass nuclei could be accelerated to a kinetic energy $\sim$ 10 megajoules with about 10 MeV/nucleon. Such rings would be suitable for transuranic elements synthesis at a much higher particle flux than obtainable from conventional accelerators.

4.) High flux ion source. A ring with $\sim$ 1 MeV/nucleon could serve as a high flux source of ions for an accelerator. A small fraction of the ions released by the destructive deceleration of the ring could be collimated then accelerated by conventional means to high energies.

5.) Attainment of super-high magnetic fields. An interesting feature of moving rings undergoing focusing in a conducting channel is that the extent to which the magnetic field penetrates the wall is a function of velocity, Δ = skin depth = $\sqrt{\eta L/V}$ where η is the resistivity.

Even if the fields [which scale as $(R_0/R)^2$] are strong enough to modify the wall resistivity by ohmic heating (B > 1 MG) the velocity can be chosen large enough to give negligible wall penetration. At fields high above the stress limits (B > 10 MG), the passage of the rings launches a radial shock wave at a velocity $u \sim B/\sqrt{4\pi\rho_{wall}}$. Again, at high ring velocity, V >> u, the ring outraces the receding wall and continues to focus. The limit may be reached when the wall is shocked to plasma temperatures and the resulting radiation precedes the ring and destroys the tube (B ~ several hundred MG). Further focusing may be possible by passing the ring through material of increasing density. The dynamic pressure following the resulting bow shock is matched by magnetic pressure in the ring leading to field strengths $\sim 10^9$ Gauss.

6.) Inertial fusion by sudden ring deceleration. If very high magnetic fields are obtainable, the ring density, ρ, (proportional to B^2 for fixed T, β) becomes high, eventually exceeding solid densities. The ring itself is then suitable as a "target" for inertial fusion. The ring is ignited by sudden deceleration in a dense medium, launching an internal shock wave that heats the ring to fusion temperatures. The advantage of this method is that the energy input required for a given Q decreases with increasing density. Energies per pulse as low as 1 megajoule may be possible at reasonable Q's.

References

[1] C. W. Hartman, J. H. Hammer, Physical Review Letters 48, 929 (1982).

ACCELERATION OF MAGNETIZED PLASMA RINGS*

Charles Hartman, J. Eddleman,** J.H. Hammer

Lawrence Livermore National Laboratory

University of California

Livermore, California 94550

Introduction

In an earlier publication[1] we considered acceleration of plasma rings (Compact Torus). Several possible accelerator configurations were suggested and the possibility of focussing the accelerated rings was discussed. In this paper we consider one scheme, acceleration of a ring between coaxial electrodes by a B_θ field as in a coaxial rail-gun. If the electrodes are conical, a ring accelerated towards the apex of the cone undergoes self-similar compression (focussing) during acceleration. Because the allowable acceleration force[1] $F_a = \kappa U_m/R$ ($\kappa < 1$) increases as R^{-2}, the accelerating distance for conical electrodes is considerably shortened over tnat required for coaxial electrodes. In either case however, since the accelerating flux can expand as the ring moves, most of the accelerating field energy can be converted into kinetic energy of the ring leading to high efficiency.

* Work performed under the auspices of the U.S. Department of Energy by the Lawrence Livermore National Laboratory under Contract No. W-7405-ENG-48.

** Consultant S. Levy Inc., Campbell, California.

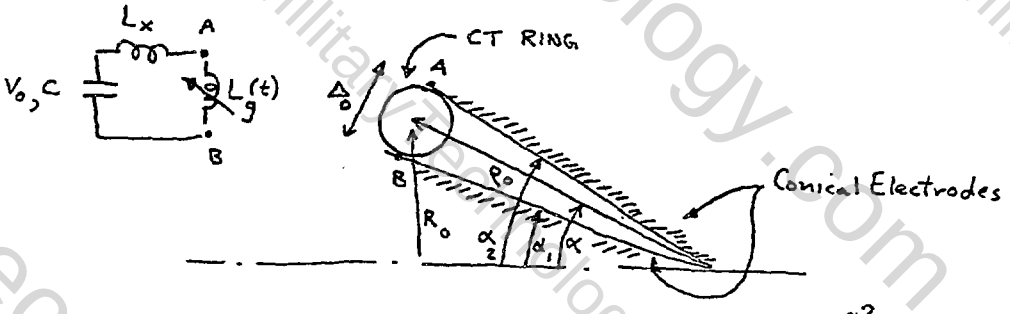

FIGURE 1: Geometry and Circuit. Here $L_g = \frac{\mu_o}{2\pi} \ln \left[\frac{\tan \frac{\alpha 2}{2}}{\tan \frac{\alpha 1}{2}}\right] (\rho_o - \rho)$.

Equations of Motion

We consider a ring between electrodes as shown in Fig. 1. Since the ring approximately conserves flux ψ_p, ψ_T during acceleration, and since $p << B^2/2\mu_o$, so that $B_T \simeq B_p$, it is readily seen that the aspect ratio a/R remains constant as R changes. We note that the net accelerating force on the ring is due to the B_θ field behind the ring, $F_{B\theta} = (dL_g/d\rho)\ (I^2/2)$ and the component of the equilibrium force along the cone, $\bar{F}_{eq} \cdot \hat{\rho} \simeq U_m/\rho$. The ring motion is given by,

$$M_r \ddot{\rho} - F_{drag} = U_m/\rho - L'_g\ I^2/2 \qquad (1)$$

where U_m and M_r are the ring's magnetic energy and mass respectively. F_{drag} is computed from the eddy current dissipation in the electrode surfaces. Approximately, $F_{drag} = (2\delta/\Delta^2)U_m$ where δ is the skin depth allowing for velocity-dependent and diffusive penetration of the ring fields. The electrode resistively η used to compute δ is corrected for nonlinear diffusion.[2]

Equation (1), the driving circuit equation,

$$V_o - \int \frac{I\,dt}{c} = \frac{d}{dt}\left[(L_x + L_g)\,I\right] \qquad (2)$$

and the energy equation,

$$\dot{U}_m = \dot{U}_m\Big|_{\text{compression}} - \dot{U}_m\Big|_{\text{skin loss}} - \dot{U}_m\Big|_{\text{plasma resistance}}$$

are solved numerically for the ring motion.

Results and Summary

A number of problems have been studied using parameters approximating CT rings which have been produced by plasma guns, and using parameters appropriate to various high-energy, high power electromagnetic pulse sources (Python, SHIVA-STAR, etc.). Here we summarize one case, a ring accelerated in two phases by the SHIVA STAR capacitor bank.[3] Phase I consists of adiabatically compressing the ring in an $\alpha = 90^0$ cone. Phase II allows the compressed ring to turn the corner and accelerate along an attached small-angle cone thus converting the stored magnetic energy into ring kinetic energy. The results are given in the table.

If the ring at the maximum kinetic energy (4.4 MJ) were allowed to stike a target, the deposition power would be roughly 1.2×10^{16} watts ($\tau \simeq .3$ nsec) with a power density of 5.3×10^{15} watts/cm^2. Only the ring mass is specified here, the choice of ion species being left to further optimization.

TABLE

Phase I Initial State

t = o

L_x	Δ_o	R_o	M_r	U_{mo}	T_e	B_{ave}	U_{cap}
nH	cm	cm	gm	10^5 joules	eV	MG	10^5j
40	15	50	1(-4)	0.4	10	1.3(-2)	93.3

Phase I Final State

t = 10.0 μsec

R	L	I	U_{cap}	U_L	U_m	U_{mlost}	B_{ave}
cm	nH	DMA=10^7A	10^5j	10^5j	10^5j	10^5j	MG.
5.7	66.7	1.4	19.5	69.2	1.9	1.2	0.77

Phase II Maximum Kinetic Energy State

t = 10.58 μsec

R	U_m	U_k	V_{ring}	E_k	Δ	B_{ave}	L_{acc}
cm	10^5j	10^5j	cm/μsec	eV/nucleon	cm	MG	cm
1.1	9.2	44.0	930.0	4.4×10^6	0.33	20.0	400

References

1. P.R. Lett., V. 48, No. 14, April 5, 1982, p. 929.
2. "Pulsed High Magnetic Fields", H. Knoepfel, N. Holland Pub. Co. 1970, p. 73.
3. SHIVA-STAR is a 9.3 MJ Upgrade of SHIVA-II see; W. Baker, et al., paper ID5-6 Proc. 1982 IEEE Int. Conf. on Plasma Science, May 1982, Ottawa, Canada.

STEADY STATE SPHEROMAK

T. R. Jarboe
Los Alamos National Laboratory, Los Alamos, NM 87545

I. INTRODUCTION

A major effort is being made in the national program to make the operation of axisymmetric, toroidal confinement systems steady state by the application of expensive rf current drive. Described here is a method by which such a confinement system, the spheromak, can be refluxed indefinitely through the application of dc power.

Presently, spheromaks are generated by pulsed techniques. For coaxial source produced spheromaks the generation process, gross behavior, and magnetic field profiles are in qualitative agreement with Taylor's minimum energy principle.[1] This principle states that a plasma-laden magnetic field configuration enclosed within a flux-conserving boundary will go to the minimum energy state allowed by the boundary conditions subject to the constraint that the magnetic helicity is conserved. Helicity has the dimensions of magnetic flux squared and is a measure of linkage of flux with flux.[2] This minimum energy principle was applied by J. B. Taylor to explain the remarkable phenomenon of self-reversal of the toroidal field in the Zeta reversed field pinch experiment.

In order to maintain a spheromak continuously both its toroidal and poloidal flux must be maintained against resistive diffusion. An important consequence of the Taylor principle is that the boundary conditions imposed by the geometry and the amount of helicity present determine the magnetic field profiles. Thus, if the boundary conditions are chosen properly and a dc source of helicity is provided, continuously refluxed spheromaks should be possible. Guided by ideal MHD theory, sufficient boundary conditions have been determined from experience with pulse-generated spheromaks.

When dc power is used to sustain a spheromak the source of power must be applied by electrodes. The electrodes must be configured so that the toroidal flux coming from the electrodes ($\dot{\phi}_t = V$) links some poloidal flux ϕ_p (See Fig. 1.), where V is the voltage applied to the electrodes. The helicity is supplied at a rate of $2 V\phi_p$.[2]

II. SLOW SOURCE MODE

Four important time scales in the formation and sustainment of a spheromak are the Alfvén time τ_A, the resistive tearing or reconnection time τ_t, the magnetic decay time τ_B, and the system impurity cleanup time τ_C. In most of our results reported to date, the spheromak is generated with a power application time comparable to τ_A (~ 2 μs). However, Figure 2 shows some results of generating a spheromak using a power application time of about the reconnection time τ_t in CTX. The voltages at the gun are about an order lower and the generation time (~ 60 μs) is over an order longer than in the fast τ_A generation time. The spheromaks generated on

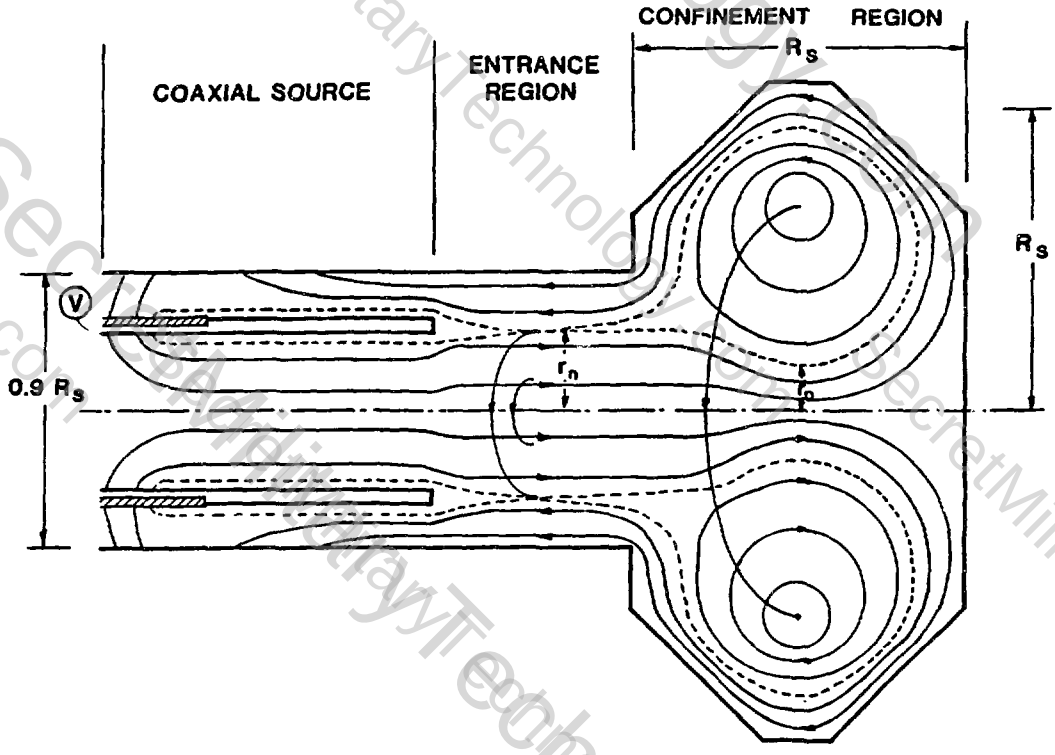

Fig. 1.
Schematic of steady state spheromak.

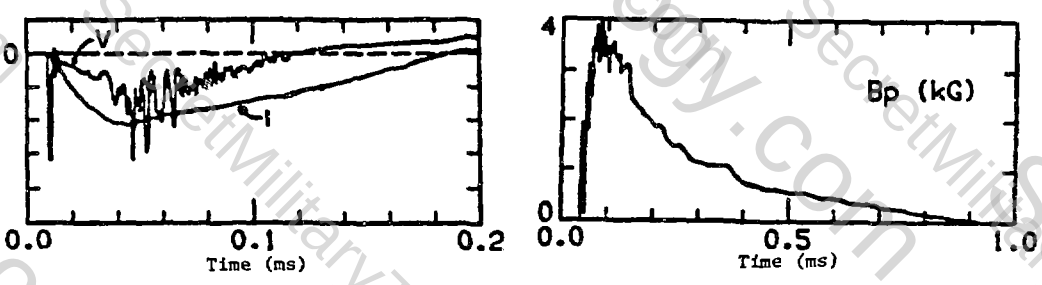

Fig. 2. Slow source formation.
The current and voltage vs time of the source and the poloidal field (B_p) vs time of the spheromak. The scales for I and V are 500 kA full scale and 10 kV full scale.

the τ_t time scale are similar to the ones generated on the faster time scales and have total lifetimes of about 1 ms. The obvious next experiment is to lengthen the power application time to a few τ_B (~ 1 ms). This should test the concept of dc sustainment. Increasing the power

application time scale to τ_t and then to τ_B may not help the impurity situation and could even be detrimental because of the longer time for impurity transport from the source. However, if metalic impurities can be controlled a real gain in cleanliness will probably be realized when the spheromaks are sustained for times long compared to τ_C. The time for this clean up effect has been observed on the Elmo Bumpy Torus to be about 5 minutes.

III. IMPURITY CONSIDERATIONS

In pulsed discharges where electrodes are used impurities can be a problem. In the past, impurity problems from such discharges were important factors in the demise of many concepts utilizing electrodes. The application of modern cleaning techniques and vacuum technology can substantially reduce these problems as we have seen during the history of the coaxial source generated spheromaks. However, when electrodes are used continuously, such as in vacuum tubes, Q-machines, and MPD arcs, impurities become less of a problem.

The hollow cathode MPD arc[3] has a geometry similar to the coaxial helicity generator shown in Fig. 1. A rule of thumb for the MPD arc is that the input gas supplied must provide the charge carriers for the input current. MPD arcs of a few centimeters size have operated several tens of hours (passing thousands of moles of gas) showing little erosion (a small fraction of a mole). This demonstrates that the erosion problems have been controlled at least to the point where electrode material contamination is negligible. Also, the large volume of gas flowing through the system will rapidly remove any other contaminants provided a clean pumping system is used. Thus, if the erosion problems can be solved, as they have been with MPD arcs, the plasma from the source should be pure. The high gas flow rates associated with this type of source should tend to maintain a clean gas blanket around the spheromak, providing a clean source for recycling of particles.

IV. EFFICIENCY OF DC SUSTAINMENT

There are two sources of inefficiency considered in this section: the mismatch of the source with the spheromak and the energy loss due to ohmic heating of the source and entrance region. In the first subsection the mismatch loss will be treated. The second subsection will add heat loss based on classical resistivity and thermal conductivity.

A. Match Efficiency

Helicity is transferred with high efficiency (assumed 100%) from the source to the spheromak. Energy flows from the source with the helicity. When the helicity is absorbed by the spheromak the energy of the spheromak is increased. The Taylor minimum energy principle dictates that the energy gained by the spheromak is less than that flowing from the source. Thus there is a loss of magnetic energy in the process. A very useful concept in considering this process is the ratio of the helicity to magnetic energy. This ratio has the units of inductance. The magnetic field

profiles for the Taylor minimum energy state of an oblate spheromak (in a right circular cylinder of radius R_s and length ℓ) are well known.[4] These profiles yield a helicity per unit energy of $L_{HE} = 2\,\mu_o/\sqrt{K_{rs}^2 + K_z^2}$, where $K_{rs} = 3.83/R_s$, $K_z = \pi/\ell$, and μ_o is the magnetic permeability of free space. The match efficiency then is simply the L_{HE} of the source divided by that of the spheromak. To estimate this loss I will assume that the field profiles in the entrance region adjacent to the source are those given by the Taylor principle for a segment of an infinitely prolate spheromak. The source L_{HE} then has the same form as that of the spheromak with ℓ going to ∞ and R_s going to R_w. R_w is the radius of the entrance region. Thus the efficiency is $\varepsilon_m = \sqrt{(K_{rs}^2 + K_z^2)/K_{rw}^2}$. For the geometry of Fig. 1 $\varepsilon_m = 0.6$. This value is insensitive to the profile assumed in the entrance region.

B. Adding Ohmic Losses

Efficient current drive, by this method, means that the ηj^2 losses in the entrance region must be smaller than the ηj^2 losses in the spheromak. One advantage of this method of steady state sustainment over the Bumpy Z-Pinch[5] is that a larger fraction of the inevitable power loss from the spheromak will be diverted to heat the entrance region (and lower its resistance) since the driven layer surrounds the entire spheromak. The value of j^2 in the entrance region relative to that of the spheromak scales as $(r_o/r_n)^4$. (See Fig. 1.) This effect and the temperature of the spheromak dominate the efficiency. The efficiency has a weaker dependence on the amount of diverted power and the length of the entrance region.

Acceptable (Eff ≈ 50%) maximum values for r_o/r_n can be found by solving the parallel heat flow problem with classical resistivity and heat conductivity. These types of estimates show that r_o/r_n must be less than about 1/10 for a reactor ($B_{wall} \approx 5$ T, $T_e \approx 5000$ eV) and less than about 1/3 for an interesting experiment ($B \approx 0.2$ T, $T_e \approx 100$ eV). Whether or not these values are large enough for sustainment depend on the absorption rates for the helicity. The amount of local excess helicity near the outside available for absorption compared to the amount the spheromak has is proportional to $(r_o/R_s)^4$. Thus r_o must be large enough for sustainment yet small enough so that the sustainment is efficient. The existence of an operating window needs to be shown experimentally. The smallness of r_o will be a good measure of success for dc current drive.

V. SUMMARY

As a step towards steady state sustainment we have operated the present CTX source in the slow source mode with a longer power application time (~ 0.1 ms) and successfully generated long-lived spheromaks. Steady state operation should be very clean if the erosion of the electrodes can be controlled as well as it is with MPD arcs. Steady state sustainment can be very efficient if only a small fraction (10% for an experiment) of the poloidal flux of the spheromak connects to the source. However, the amount of connecting flux that is necessary for sustainment needs to be determined experimentally.

REFERENCES

1. J. B. Taylor, Phys. Rev. Lett. 33 (1974).

2. H. K. Moffatt, Magnetic Field Generation in Electrically Conducting Fluids, (Cambridge University Press, Cambridge, 1978), pp.14-15.

3. D. B. Fradkin, A. W. Blackstock, D. J. Roehling, T. F. Stratton, M. Williams, and K. W. Liewer, AIAA Journal 8, 886 (1970).

4. J. M. Finn, W. M. Manheimer, and E. Ott, Physics of Fluids, 24 1336 (1981).

5. T. H. Jensen, M. S. Chu, J. Plasma Physics 25, Part 3, 459 (1981).

A CLASS OF STEADY STATE COMPACT TORI

by
Torkil H. Jensen and Ming S. Chu
GA Technologies, Inc, San Diego, CA

In the search for magnetic configurations for confinement of plasmas, it may be a prudent strategy to search in the neighborhood of absolutely stable (MHD-sense) configurations. Two classes of absolutely stable states are known, namely the vacuum field and the Taylor state.[1] A configuration may also be classified according to its topology, singly or doubly connected. The singly connected configuration based on the vacuum field is the mirror while the doubly connected is the stellarator. The class of singly connected configurations based on Taylor states includes the spheromak[2] and many yet unnamed configurations while that of doubly connected configurations includes tokamaks, RFP's and OHTE's[3]. The class of configurations considered here is that of singly connected configurations based on Taylor states. The problem of steady current drive is particularly emphasized.

Configurations based on Taylor states are more complicated than those based on vacuum fields, but they also provide more possibilities. Specifically, singly connected Taylor states may be closed configurations while singly connected vacuum fields are open. The attraction of singly connected configurations stems from the potential hardware simplicity. The complications of configurations based on Taylor states arise from the need to provide means for current drive, the associated problems of current driven instabilities, as well as the problem of how much pressure may be added before pressure driven instabilities become intolerable. Only the last of these problems is shared with configurations based on the vacuum field.

One may consider the current driving mechanism "ideal" if an electric field, $\bar{E}$, is established, so that $\bar{E} = \eta \bar{J}_T$, where $\bar{J}_T$ is the current density of the Taylor state and η is the resistivity. Inductive current drive in tokamaks may be almost "ideal" in this sense. Inductive drive in RFP's is not "ideal"; based on experimental evidence, it is believed that transport associated with mild turbulence, sometimes called "dynamo effect"[4], causes the current density to be near that of the Taylor state. It is assumed here that this "dynamo effect" is in operation so that it is sufficient to inject helicity in order to accomplish current drive.

From Ohm's law for a single fluid and Maxwell's equations one gets for the transport of helicity, $K \equiv \bar{A} \cdot \bar{B}$

$$\frac{\partial K}{\partial t} + \bar{\nabla} \cdot \bar{Q} = -2\eta \, \bar{J} \cdot \bar{B} \qquad (1)$$

$$\bar{Q} \equiv 2 \phi \bar{B} + \bar{A} \times \frac{\partial \bar{A}}{\partial t} \qquad (2)$$

Here, $\bar{Q}$ may be interpreted as helicity flow, analogous to Poynting's vector for energy density flow. One sees from (1) that helicity is consumed through finite resistivity. The rate of helicity injection is

$$\frac{d\mathcal{K}}{dt} \equiv \int \bar{Q} \cdot d\bar{s} = \int \phi B_{\perp} ds + \int \bar{A} \times \frac{\partial \bar{A}}{\partial t} \cdot d\bar{s} \qquad (3)$$

where the integrations are performed around the surface, S, of the plasma. The first of the terms on the r.h.s. of (3) may be utilized for helicity injection when the configuration is not completely closed ($B_{\perp} \neq 0$) by establishing appropriate potentials, ϕ, at the surface. This means of injection of helicity may be continuous. For singly connected equilibria the second term on the r.h.s. of (3) (inductive drive) is not attractive since $\bar{A}$ on the surface is small (unlike doubly connected configurations such as tokamaks).

A Taylor state has been defined as one which satisfies

$$\bar{\nabla} \times \bar{\nabla} \times \bar{A} + \mu \bar{\nabla} \times \bar{A} = 0 \qquad (4)$$

with the vector potential, $\bar{A}_B$, given on the boundary, and with the constant, μ, given. One may gain insight into the properties of solutions to (4) using the solutions to the eigenvalue problem

$$\bar{\nabla} \times \bar{\nabla} \times \bar{a}_{\nu} + \lambda_{\nu} \bar{\nabla} \times \bar{a}_{\nu} = 0 \qquad (5)$$

with $\bar{a}_{\nu}$ vanishing on the boundary. It is easy to see that the solutions are orthogonal and can be normalized so that

$$\int \bar{a}_{\nu} \cdot \bar{\nabla} \times \bar{a}_{\mu} \, dV = \delta_{\mu\nu} \quad . \qquad (6)$$

A solution to (4) can then be written

$$\bar{A} = \bar{A}_I + \sum_{\nu} \alpha_{\nu} \bar{a}_{\nu} \qquad (7)$$

here, the inhomogeneous part, $\bar{A}_I$, satisfies the boundary conditions, $\bar{A}_{IB} = \bar{A}_B$, and $\bar{\nabla} \times \bar{\nabla} \times \bar{A}_I = 0$ in the interior. One finds re dily for the expansion coefficients

$$\alpha_{\nu} = \frac{\mu}{\lambda_{\nu} - \mu} \int \bar{a}_{\nu} \cdot \bar{\nabla} \times \bar{A}_I \, dV \qquad (8)$$

One sees from (8) that μ must fall between zero and the lowest eigenvalue, λ_o. The quantity μ is determined from the ratio of the current density imposed externally at the wall (electrode current) and the "seed" field, $B_{\perp}$, at the wall. Alternatively, μ is determined from the total helicity of the volume. One sees that when μ approaches λ_o, the field in the interior approaches infinity so that the voltage necessary to drive the

external current must approach infinity also. This may be exploited to accomplish high impedance drive rather than the usual low impedance drive of plasma devices. Also, in the limit where μ approaches λ_0, the configuration approaches one of closed field lines only.

The concept of helicity injection as exemplified by (3) may also be useful for cases where μ is not constant over the whole volume. For example, for gun produced spheromaks[5,6] μ is numerically larger for the plasma in the gun barrel or guide tube than in the cavity where the spheromak is coming to rest. The transition zone between regions of different μ may be similar to that of a shock. These concepts may be valid whether a gun is operated in pulsed fashion or whether a steady current[7] is provided.

Within the concepts of this paper, the Princeton method[8] of establishing a spheromak relies in the initial phase on inductive drive, which is practical because the plasma is doubly connected, followed by an irreversible transition to the spheromak.

Up until now, the spheromak is the only member of the singly connected Taylor state class which has been investigated in some detail[2]. In the framework of the concepts of this paper the current driven instabilities such as "tilt" and "shift" do not exist. The "tilt instability" appears when the shape of the boundary is such that the solution of (5) associated with the lowest eigenvalue is not axisymmetric. Studies of beta limits have yielded encouraging results as one might expect since the connection length is short. There exist however many other possible configurations and one may guess that still undiscovered configurations may be more attractive than the spheromak. In order to invent a new configuration, one just has to specify the shape of a boundary and find the solution $\bar{a}_0$ to (5) with the lowest eigenvalue[9]; next, one finds a vacuum field, $\bar{A}_I$, such that the coupling integral of $\bar{a}_0$ and A_I given in (8) is nonvanishing, and finally an electric gap is cut in the boundary so that helicity injection may be accomplished by application of proper electrostatic potentials to parts of the boundary separated by the electric gap. Alternatively, one may inject helicity using a guide tube for helicity injection[6].

In order to realize the potential for fusion of singly connected Taylor states one must investigate the validity of the key assumption of this paper, namely the benign, spontaneous approach to the Taylor state. At this time analytic and numerical approaches to this problem seem very difficult. Experimentally, the assumption seems valid for RFP's and OHTE's (although it is not known if the fluctuations are acceptable from an energy confinement point of view) while it may be argued that the major disruption of tokamaks is an example of an unacceptable approach to the Taylor state.

The simplest experiment we can imagine, which may shed light on this question, involves an attempt to drive a spheromak continuously. The basic idea is that of the Bumpy-Z-Pinch[10]. It is schematically illustrated in Fig. 1. The hardware is intended axisymmetric about the z-axis. The rectangular cross section of the vacuum chamber is chosen for

ease of manufacture and the relative dimensions are chosen to insure that the solution of (5) with the lowest eigenvalue is axisymmetric ("tilt stable"). In Fig. 2 are shown magnetic field line topologies for a low value of μ (a), for maximum μ (c) and for an intermediate value of μ (b). It is believed that the intended experiments require only a primitive plasma with a density of the order of 10^{14} cm^{-3}, current densities ~ 10^6 A/m^2 and temperatures about 10eV, mainly limited by radiation. With a chamber length of 30 cm, the ratio between the resistive time and the Alfvén time is of order 10^3. The necessary experimental time is about 1 msec.

It is felt essential that the question of continuous current drive for singly connected Taylor configurations be addressed. As argued above, in the approximation of single fluid MHD, essentially only one possibility, namely that involving electrostatic potentials (electrodes) exists. In other approximations there are of course other possibilities such as RF and neutral beam drive. The electrostatic drive may however, if viable, be the most attractive.

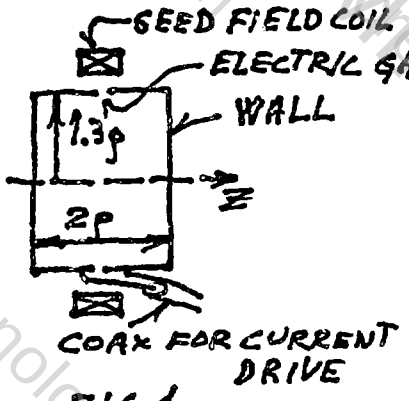

FIG 1.

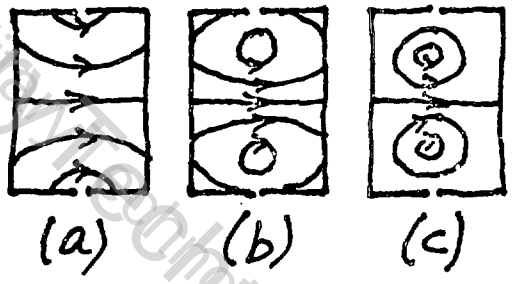

FIG 2.

References

1. Taylor, J. B., Phys. Rev. Lett. 33 1119 (1974)
2. Bussac, M. N., et al in Plasma Physics and Controlled Nuclear Fusion Research (Proc. 7th Int. Conf. Innbruck, 1978, Vol. 3, IAEA, Vienna (1979) 249.
3. Ohkawa, T.; Chu, M.; Chu, C.; Schaffer, M., Nuclear Fusion 20 (1980) 1464
4. Bunting, C. A., et al, p.79, Vol. 1, Proc. of the 8th Conf. on Contr. Fusion and Plasma Physics (Prague 1979)
5. Jarboe, T. R., et al, Phys. Rev. Lett. 45, 1264 (1980)
   Turner, W. C., et al, in Proc. of Third Symposium on Physics and Technology of Compact Toroids, Los Alamos Scientific Laboratory, Dec. 1980, LASL, Rep. No. LA-8700-C, p. 113
6. Hartman, C. W. & Hammer, J. H., Phys. Rev. Lett. 48, 929 (1982)
7. Jarboe, T. R., Bull. of APS 27, P. 930 (1982)
8. Yamada, M., et al, Phys. Rev. Lett. 46 188 (1981)
9. Chu, M. S., Jensen, T. H., and Dy, B., Phys. of Fluids 25 1611 (1982)
10. Jensen, T. H. and Chu, M. S., J. of Plamsa Phys. 25 459 (1981)

A COMPARISON OF SPHEROMAKS AND FRCS

George C. Vlases
Mathematical Sciences Northwest, Inc.

I. INTRODUCTION

Within the past year there have been dramatic advances in both the "Spheromak" and "FRC" branches of the Compact Toroid (CT) research program. The long-troublesome n=2 rotational instability has been controlled in FRC experiments at Osaka University and MSNW, while improved impurity control techniques have lead to the extension of spheromak configurational lifetimes to the 1 ms range at LANL and Osaka. It thus seems appropriate, on the occasion of this 5th CT Symposium, to compare the two approaches with respect to present status and potential for extrapolation to reactors and critical research needs.

II. SUMMARY OF PHYSICS CHARACTERISTICS

Although FRCs and spheromaks might appear to be very similar entities, at first glance, they differ significantly with respect to both their physics properties and their technologies. Figure 1 shows a schematic of an FRC and a spheromak contained in a flux conserving shell. All FRCs are currently produced using field reversed θ-pinch technology with varying degrees of sophistication with respect to control of reconnection. Spheromaks have been made in at least four different ways ranging from purely inductive to purely electrode-produced discharges.

The most distinguishing feature about an FRC is its very high $\langle\beta\rangle_{sep}$, which is required by the profile-independent 2-D global equilibrium condition given first by Barnes:[1]

$$\langle\beta\rangle_{sep} = 1 - \frac{1}{2}\left[\frac{r_s}{r_c}\right]^2 . \qquad [1]$$

In present experiments, $r_s/r_c \lesssim 0.6$, so that $\langle\beta\rangle \gtrsim 0.8$. This leads to very steep pressure and field gradients at the separatrix with a flat pressure profile and very low field value in the interior. It is important to note that, contrary to intuition based on earlier work with non-reversed linear θ-pinches, these steep gradients do not relax as time progresses; the configuration contracts axially to maintain the condition set by Eq. [1]. Because of the low value of $|B|$ in the interior, which

General

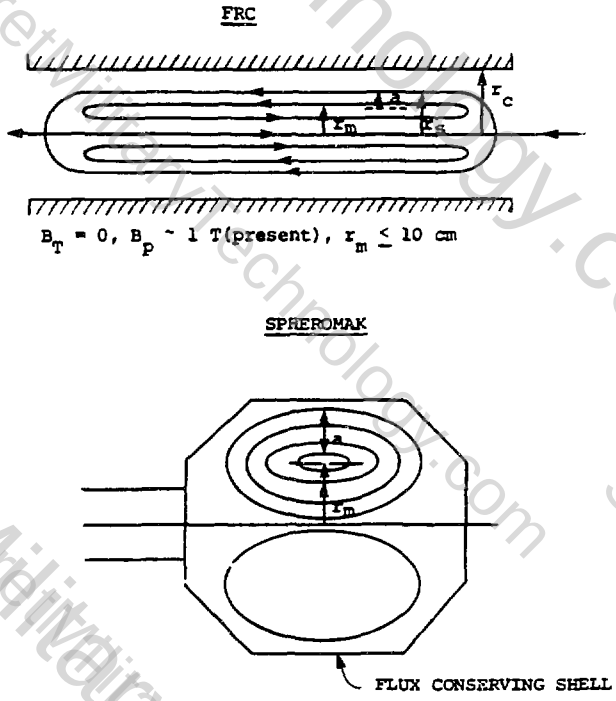

Figure 1. Schematic Illustration of FRCs and Spheromaks.

passes through zero at the magnetic axis ($r_m = r_s/\sqrt{2}$), the interior particles have very large "orbits", and many of the physics phenomena are described neither by guiding center theory or simple fluid theories. Transport in the interior is very rapid while transport at the edge is also enhanced many times over classical by what is believed to be the LHD instability resulting from the steep gradients and consequent high drift velocities. Experiments appear to indicate relatively good agreement with a heuristic model based on LHD theory.[2]

By way of contrast, stable spheromak configurations have a toroidal field roughly comparable to the poloidal, arranged in a nearly force-free configuration consistent with Taylor's prediction. The particles, consequently, tend to have orbit sizes small compared with the configuration dimensions $[(\rho_i/r_s)^2 << 1]$, so that neo-classical transport can be calculated in principle, and is expected to be more "tokamak-like" than the LHD-dominated FRCs.

With respect to stability, both FRCs and spheromaks are theoretically predicted to be tilt-unstable. In FRC experiments, tilting is not seen as long as the axial contraction is not violent enough to produce too small an elongation. In spheromaks, tilting is seen but can be controlled by either external conductors placed close to the separatrix or by a passive center conductor.

FRCs are observed to rotate and, although several theories for the rotation have been advanced, the origin of rotation and its connection with transport have not yet been experimentally clarified. However, it has been demonstrated, experimentally and theoretically, that the n=2 instability normally associated with rotation can be suppressed by the addition of multipole fields. The saturated rotating state may even be beneficial and account for some unexpected favorable FRC stability properties.

One unsolved problem in spheromaks is that of understanding and controlling "sudden termination" of the configuration, which is observed occasionally in all spheromak experiments. Further work needs to be done in this area.

In summary, both FRCs and spheromaks have demonstrated relatively good stability properties, albeit not yet for reactor-grade plasmas. The effects of high R/ρ_i in FRCs, leading to reduction of FLR effects, and of high temperature in spheromaks, are yet to be determined.

III. STATUS OF EXPERIMENTS

Table I lists relevant parameters of two FRC experiments and two spheromak experiments. These experiments were selected as representative of the field; other important experiments in various universities and in Japan have been omitted for brevity. Details can be found in other papers within these proceedings. Also included, for comparison, is data from the ASDEX tokamak without auxiliary heating.

From Table I, it can be seen that plasma properties in FRCs are quite far advanced, with relatively high temperatures, high densities and with $n\tau$ products, in very small devices that are within a factor of 3 of those most presently operating tokamaks. In spheromaks, densities are relatively low, as are temperatures, due to either radiation barriers and/or β-limits. However, configuration lifetimes are longer than FRCs

TABLE I

	FRCs		Spheromaks		Tokamak
	FRX-C (LANL)	TRX-1 (MSNW)	CTX (LANL)	Pr.S-1C (PPPL)	ASDEX
R, cm	8	4.5	23	11.5	165
a, cm	3.3	1.9	15	8	40
n_e, cm^{-3}	3.5×10^{15}	3×10^{15}	3×10^{13}	1×10^{14}	3×10^{13}
T_e, eV	130	110	30	20	1000
T_i, eV	250	250	-	-	1000
$\|B\|$, typical (kG)	10	10	2	2	22
τ_ϕ, μsec	200	80			
τ_{B^2}, μsec			400	100	
τ_p, μsec	150	70	100	(?)	
τ_E, μsec	100	40	60	10	4×10^3
$n_e\tau_E$, sec cm^{-3}	3.5×10^{11}	1.2×10^{11}	2×10^9	1×10^9	1.2×10^{12}
$n_e\tau/a^2$, sec cm^{-5}	3.2×10^{10}	3.3×10^{10}	4.5×10^6	1.5×10^7	7×10^8
$\langle\beta\rangle_{sep}$	0.87	0.85	0.15	0.10	0.01
$\tau_{formation}$ μsec	4	3	≤50	40	10^6

due to the availability of a large amount of magnetic energy (a consequence of smaller β's) to resupply losses by means of Ohmic dissipation; it is nevertheless quite remarkable that such long stable times have been achieved. In all of these CT experiments the demonstrated β values considerably exceed those of tokamaks.

IV. EXTRAPOLATION TO A REACTOR

Because of differing plasma properties, it appears that FRCs and spheromaks may have significantly different reactor embodiments. FRCs appear to be well suited to devices where the plasmoids are formed, heated to ignition, and then translated through a long cylindrical burn chamber without refluxing and without the need for active stabilizing magnets in the burn chamber. Spheromaks, because of problems with tilt, will probably be injected into a burn chamber where they remain stationary, held by feedback stabilization. Schemes for refluxing and refueling, in order to achieve steady or quasi-steady state operation, have been proposed using both continuous and pulsed techniques.

In both cases, a central issue in extrapolation to reactor-like devices is that of the amount of energy which must be supplied to form the plasmoid and bring it to ignition, and of the timescale on which this energy must be supplied. In order to make a simple estimate, assume a Lawson product, $n_e\tau_e = 5 \times 10^{14}$ cm^{-3}sec is required. If $\tau_e = \alpha a^2$, then $a^2 = 5 \times 10^{14}/n_e\alpha$. The plasma thermal energy is the $W_{plasma} = 2n_e kT \cdot V_p$, where V_p is the plasma volume and the total required energy investment is approximately $W_T = W_p(1 + 1/\beta_e)$, where β_e is the engineering β, defined as $W_p / (B^2/2\mu)\, dV_M$, with the integral taken over the entire field region. Table II shows a and W_T for various choices of α, which corresponds to choosing a particular transport law. In both cases, we choose $B_{wall} = 5$ T, kT = 10 keV.

TABLE II

FRC (Elongated)	Spheromak
$\langle\beta\rangle_{sep} \simeq 0.6$ $(x_s \simeq 0.9)$	$\langle\beta\rangle_{sep} = 0.1$
"Alcator": a = 7 cm, W_T = 200 kJ	Alcator: a = 70 cm, W_T = 100 MJ
LHD Scaling: a = 40 cm, W_T = 150 MJ	1/10 Alcator: a = 210 cm, W_T = 3 GJ

There is no reason to expect that Alcator scaling would be valid for FRCs with entirely non-tokamak-like transport so the Alcator entry in the table is crossed out. LHD scaling requires $W_T = 150$ MJ; therefore it is conceivable that the transport would be less rapid, and the energy investment correspondingly less. Alcator scaling for spheromaks results in an energy investment roughly corresponding to that for FRCs. Although spheromaks might be expected to follow an Alcator-like law, this has not yet been demonstrated, nor has a theoretical study of neoclassical or enhanced transport for spheromaks been published.

Although the required energy investment appears roughly equal for spheromaks and FRCs, the timescales, at least based on presently investigated formation techniques, are significantly different. In both cases, the initial bias flux can be invested arbitrarily slowly. In the case of spheromaks, such as the S-1 device at Princeton, for example, the field lines are always closed, and the critical field reversal phase can be done on a resistive timescale (Figure 2a). This probably permits the

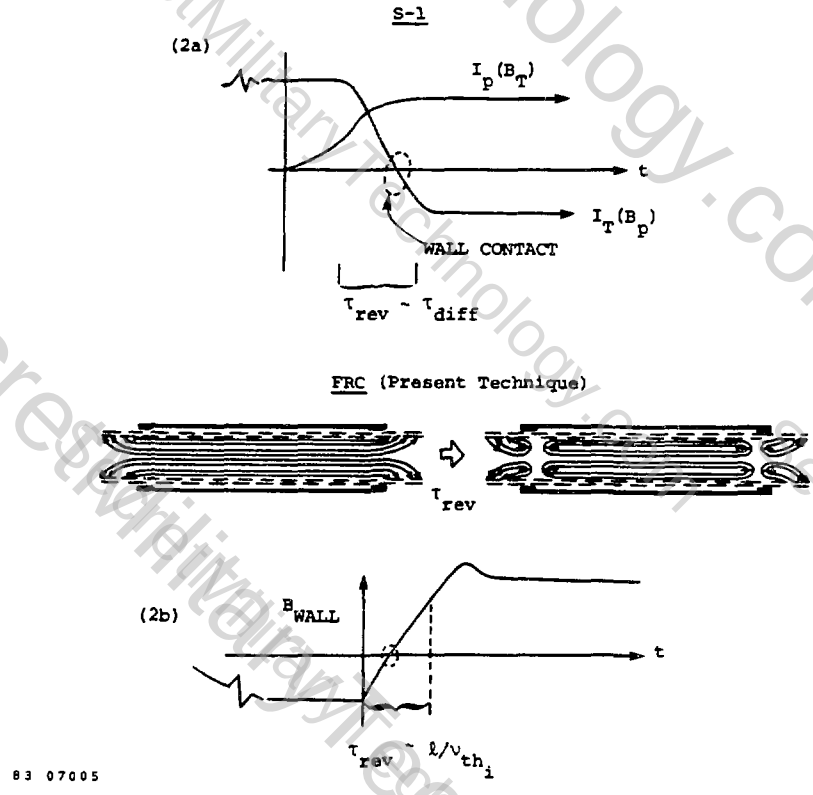

Figure 2. Illustration of Reversed Timescales.

use of rotating machinery. In FRCs based on field reversed theta pinch technology, once the plasma has been formed by some sort of preionization technique, the field reversed phase must be completed on a longitudinal Alfven timescale, typically a few tens of microseconds (Figure 2b). The energy required is only a small fraction of the total but will require "fast" technology such as capacitor banks. An intensive search is underway for ways to circumvent this problem.

In both FRCs and spheromaks, it will probably be necessary to use some form of auxiliary heating to get to ignition. In spheromaks, RF techniques used on tokamaks can probably be adapted. In the FRC, on the other hand, different techniques such as magneto-acoustic pumping or "rotomak" drive may be necessary. It will probably also be necessary, at least in spheromaks, to do some refluxing. This may also occur through RF current drive, or through a more direct scheme such as merging spheromaks or direct current drive through electrodes.

V. CONCLUSIONS

The relatively new set of alternate fusion concepts known collectively as Compact Toroids has recently made remarkable progress with gross stability leading to long lifetimes having been demonstrated. For spheromaks, critical research areas appear to be to increase temperatures and fields while maintaining plasma purity, as well as to develop reactor-relevant stabilization configurations. Critical problem areas with FRCs center on the development of slow formation techniques and methods for reducing the gradients near the separatrix in order to minimize anomalous transport. Stability at high R/ρ_i remains to be demonstrated. In both approaches, auxiliary heating techniques have received only cursory examination; clearly more work needs to be done here.

VI. ACKNOWLEDGEMENTS

The author wishes to thank Alan Hoffman for several stimulating discussions.

REFERENCES

1. D. Barnes, Proceedings of Second Compact Toroid Symposium, Princeton (1979).

2. M. Tuszewski and R. Linford, Physis of Fluids 25, 765 (1982).